Dipole-Forbidden Vibrational Transitions in Molecular Ions

A novel route to precision spectroscopy and studying effects of interest to fundamental physics

Inauguraldissertation

zur

Erlangung der Würde eines Doktors der Philosophie

vorgelegt der

Philosophisch-Naturwissenschaftlichen Fakultät

der Universität Basel

von

Matthias Germann

aus

Zürich und Jonschwil SG

Zürich, 2016

Genehmigt von der Philosophisch-Naturwissenschaftlichen Fakultät

auf Antrag von

Prof. Dr. Stefan Willitsch und Prof. Dr. Frédéric Merkt

Basel, den 22. März 2016

Prof. Dr. Jörg Schibler
Dekan

Abstract

Homonuclear diatomic molecules, such as H_2 or N_2, are usually not expected to show a vibrational spectrum. Although this is true within the electric-dipole approximation, higher-order terms in the interaction of matter and radiation give rise to very weak spectroscopic transitions. These "electric-dipole-forbidden" transitions are spectrally extremely narrow and thus of interest to precision spectroscopy and tests of fundamental physical theories by high-precision measurements.

Until recently, such forbidden transitions have only been observed in neutral molecules, but not in molecular ions. In this thesis, we report the observation of electric-quadrupole rotation-vibration transitions in the molecular nitrogen cation N_2^+—to our knowledge the first observation of a dipole-forbidden vibrational transition in a molecular ion.

For this observation, N_2^+ ions produced state-selectively by photoionization of neutral N_2 molecules were trapped in a radio-frequency ion trap (linear Paul trap) and cooled to millikelvin temperatures through interaction with cotrapped, laser-cooled atomic Ca^+ ions (sympathetic cooling). Vibrational excitation of N_2^+ was achieved with high-intensity mid-infrared radiation from a frequency-stabilized quantum cascade laser. Vibrationally excited ions were detected through a state-dependent charge-transfer reaction of N_2^+ with Ar atoms.

Addressing these extremely narrow transitions in a molecular ion enables the application of techniques developed for manipulation and control of atomic ions that exploit the long-range Coulomb interaction of charged particles, such as trapping, sympathetic cooling and non-destructive state detection through mapping of the quantum state to a cotrapped, experimentally more easily accessible ion (quantum logic spectroscopy).

Besides reporting the observation of electric-quadrupole rotation-vibration transitions in a molecular ion, this thesis gives a detailed description of the mechanism underlying these transitions and a derivation of their line strengths in fine- and hyperfine-resolved spectra based on spherical tensor algebra.

Moreover, a model for fine- and hyperfine-structure effects in molecular photoionization, an essential method for production of molecular ions, is presented. The model was successfully applied to analyze photoelectron spectra from the literature and is used to study future hyperfine-state-selective molecular photoionization schemes.

Finally, a quantum-logic state-detection method for molecular ions is discussed. The method is based on state-dependent optical dipole forces acting on a hybrid molecular-atomic two-ion system. By inducing a geometric quantum phase, these forces map the state of the molecular ion onto the atomic one, from which it may be detected through interrogation of a closed optical cycling transition. Here, feasibility of this method for the N_2^+-Ca^+ system is positively assessed by estimating the relevant experimental parameters.

Our observation and the theoretical framework developed here might considerably increase the precision and accuracy of molecular spectroscopy and therefore open up a new route to study fundamental scientific questions by means of high-precision molecular spectroscopy, such as a possible variation of fundamental physical constants or the search for yet unknown fundamental interactions.

Felix, qui potuit rerum cognoscere causas.
Lucky who was able to understand the causes of things.
(Publius Vergilius Maro)

Contents

Chapter 1

Introduction

Understanding nature

The goal of science is to understand the causes behind the phenomena observed in nature. Understanding, in physics means to describe these phenomena with mathematical models. Such models are regarded correct, when they properly predict the results of quantitative observations, or measurements.

In the endeavour to achieve ever deeper insights, new models are tested that have been suggested to incorporate new observations or observations so far not described by a unified model. The previous models are not wrong—they have been proven correct by observation—but they may not be applicable in regimes they were not tested for and where discrepancies between predictions and measurements hence were not noticed. Moreover, even in the regime in which a model was tested discrepancies between measurements and predictions of the model could also have been too small for having been discovered at the uncertainty of the measurements done as tests.

We may, e.g., use the model of classical mechanics to describe mechanical phenomena of our everyday life, say, the dynamics of a bicycle. This means, predictions of that model will closely reproduce observations. However, we know that classical mechanics is not the whole truth. At speeds much higher than reached with a bicycle, we would notice deviations between measurements and predictions. So, we had to replace the model of classical mechanics by relativistic mechanics. The former is not wrong, but just not applicable for such high velocities. We would notice the same, if we were to study phenomena at everyday-life velocities with classical mechanics, but measure physical quantities with uttermost precision: we would encounter discrepancies between theory and observations not noticed previously and hence not covered by the model of classical mechanics.

So, to test established physical models for deviations between predictions and observations and to search for more fundamental models, we may either perform experiments in a regime not yet or hardly examined or we may increase the precision of our measurements to unveil discrepancies so far obscured by measurement uncertainties. A situation similar to the one described here, prevails currently at the level of fundamental models in physics.

The present view on the world in physics

The two big pillars our most fundamental understanding of the world in terms of physics lies on are the standard model of particle physics and the general theory of relativity. According to the standard model, matter consists of fundamental particles, quarks and leptons. Quarks make up hadrons and as such protons and neutrons in atomic nuclei that form together with the electron, a lepton, the matter around us [1]. Between these particles, four fundamental interactions are observed, the electromagnetic, the "weak" and the "strong" interaction as well as gravity. The former three are covered by the standard model, the latter is described by the general theory of relativity [2]. These models have been proven correct in numerous observations.

This picture, however, is challenged by astrophysics and cosmology as well as theoretical considerations. For example, the nature of the "dark matter", introduced in cosmological models to account for the dynamics of visible matter, as well as the one of "dark energy", proposed to describe the accelerated expansion of the universe, are unknown [3, 4]. Concerning gravity, a generally accepted model unifying gravity with the other three fundamental forces has not yet been found [2, 5].

Furthermore, the "fundamental constants", meaning the free parameters used to fit the predictions of these models to experimental results, cannot be predicted within these models. Hence, rationalizing their values by a more fundamental description is desirable. Also, the values of these constants, or more precisely their low-energy limits, are assumed to be the same—or "constant"—everywhere and at every moment in time—an assumption that might be questioned given that we live in a changing, steadily expanding universe.

Therefore, theories beyond these established models involving additional particles, presently unknown forces or extra dimensions have been developed. Hence, experimental data to test such theories are desired.

Following the scheme described above, such tests may either be done by searching for new phenomena in a regime established models were not tested for, say, at very high, so far hardly explored or unreached interaction energies—the approach followed in elementary particle physics—or by increasing the precision of measurements in well studied regimes to search for signatures of phenomena so far concealed by measurement uncertainties. The latter approach is the one followed in high-precision atomic and molecular spectroscopy. Effects beyond the standard model are expected to manifest in the low-energy limit probed by spectroscopic experiments as tiny changes in the frequencies of spectroscopic transitions. Although these deviations are tiny, the overwhelming precision and accuracy achieved in spectroscopy and frequency metrology over the last decades might enable their detection and renders these techniques promising ways to search for such "new physics".

Among the phenomena studied by high-precision experiments and particularly among those benefitting from the properties of high-precision molecular spectroscopy are investigations of possible variations of fundamental constants and the search for yet unknown fundamental interactions.

Many cosmological models and models unifying gravity with the other fundamental interactions predict a change of fundamental constants over the evolution of the universe. Among others, variations of the fine-structure constant α or the proton-to-electron mass ratio $\mu = m_\mathrm{p}/m_\mathrm{e}$ are claimed. Indeed, data from quasar absorption spectra, from the Oklo natural nuclear reactor as well as other observations suggest values for these constants over the evolution of the universe and during the history of earth

different from their present-day figures. However, no conclusive evidence has been found so far [6, 7, 8, 9].

Variations in both of these constants, α and μ, have been investigated using high-precision spectroscopic experiments (recent measurements include [10, 11, 12]). Molecular experiments are particularly suited to search for possible variations in μ, since the frequencies of molecular rotation and vibration transitions show a more prominent dependence on the mass ratio μ than transitions in atoms. Hence, molecules have been proposed as probes for μ-variation already four decades ago [13] and have been employed in various astrophysical studies (see [14, 15] for two recent investigations). High-precision laboratory studies with molecules are hence promising [16, 17, 18].[1]

Certain extensions of the standard model suggest additional fundamental interactions, known as a "fifth force" [20, 21]. Thus, searches for unknown forces are an interesting route to look for new physics. High-precision spectroscopy on simple systems, such as the hydrogen or the helium atom, treatable with ab-initio quantum-electrodynamics (QED) calculations may provide a test for such unknown forces. If existing, they might manifest as deviations of the measured transition frequencies from ab-initio predictions. Whereas the H and He atom provide a test ground for unknown hadron-lepton and lepton-lepton interactions, respectively, simple molecules also treatable with ab-initio QED such as the hydrogen molecule H_2 and the molecular hydrogen cation H_2^+ as well as their deuterated cousins HD, HD^+ and D_2, D_2^+ may be used as probes to search for unknown hadron-hadron interactions [20].

Contributions of high-precision molecular spectroscopy to fundamental science besides these two examples include measurements of the electric-dipole moment of the electron [22, 23, 24] or the search for signs of parity violation in stereoisomers due to the weak interaction [25], whose parity-violating character is well-known from nuclear and elementary particle physics [26, 27]. Considerable interest in this effect exists because of a possible link to the homochirality of biomolecules [28].

Spectroscopy: Allowed and forbidden transitions

For high-precision measurements, the atomic or molecular transitions examined need to be spectrally narrow, i.e., they must exhibit a small natural linewidth. This is only possible for "weak" transitions, meaning transitions hardly excited by electromagnetic radiation—in the language of quantum mechanics, transitions with a small transition matrix element.[2]

The excitation of spectroscopic transitions by electromagnetic radiation occurs via the coupling of the charges in an atom or a molecule to the electromagnetic radiation field. Usual transitions are driven by the coupling of the system to the field via the quantum mechanical electric-dipole operator. These "electric-dipole-allowed" transitions are often "too strong" for high-precision studies, meaning their linewidths are too large. Therefore, high-precision measurements rely on transitions with either an exceptionally low or even a vanishing electric-dipole transition matrix element. The latter are known

[1] Strictly speaking, measurements of rotational-vibrational transition frequencies in most molecules do not probe the proton-to-electron mass ratio directly, but rather the ratio of some effective mass of the molecule, depending on the masses of the nuclei in the molecule, to the mass of the electron. In general, it is assumed that the neutron mass follows the same behaviour as the one of the proton and that no effects depending on quark structure persist such that molecular rotational-vibrational frequencies may be used to probe the proton-to-electron mass ratio [19].

[2] The transition matrix element is in general a complex quantity and "small" thus refers to its absolute value.

as “electric-dipole-forbidden” transitions. Though dubbed “forbidden”, these transitions do occur due to the coupling of the charges to the electromagnetic field via higher-order terms in the respective multipole expansion, most prominently via the magnetic-dipole and the electric-quadrupole term. However, forbidden transitions are very weak. Typical transition rates are several orders of magnitude lower than those of electric-dipole-allowed transitions.

Although their low intensity renders these forbidden transitions challenging to observe, they also exhibit natural linewidths orders of magnitude smaller than those of allowed ones, rendering them well suited for high-precision measurements. Indeed, spectroscopic experiments aimed at fundamental effects largely rely on such forbidden transitions. For example, measurements of forbidden transitions in atomic ions have been used to search for a variation in the fine-structure constant α [11, 12].

Electric-quadrupole rotation-vibration transitions

The mechanism of forbidden transitions is particularly well conceivable in the case of vibrational transitions in diatomic molecules. According to the usual tenet of molecular spectroscopy, a diatomic molecule may only exhibit a vibrational spectrum, if the molecular electric-dipole moment changes as a function of the internuclear separation. For homonuclear diatomic molecules, such as H_2, N_2, etc., the electric-dipole moment vanishes due to symmetry reasons for all internuclear distances. Consequently, it does not change with distance and thus vibrational transitions are not supposed to occur.

This reasoning, however, is only valid within the electric-dipole approximation. Higher-order terms in the multipole expansion of the charge distribution of homonuclear diatomics, such as the electric-quadrupole term do exist and couple to electromagnetic radiation. This coupling may excite vibrational transitions. However, the intensities of these transitions are reduced by roughly a factor 10^{-8} compared to dipole-allowed transitions [29, 30].

The first observation of electric-quadrupole vibrational transitions, or “lines” in the jargon of spectroscopy, dates back over half a century to an absorption experiment of H_2 done by Herzberg [31]. Because of the extreme weakness of electric-quadrupole lines, an equivalent absorption path length of several kilometres was needed for this measurement. Later on, electric-quadrupole rotation-vibration spectra of other species such as O_2 and N_2 have been reported [32, 33]. Recently, such experiments attracted renewed interest in view of precision studies. With the technique of cavity ring-down spectroscopy, spectra of electric-quadrupole rotation-vibration lines were recorded with high precision [34, 35, 36, 37, 38]—some of them subsequently being interpreted in terms of fifth-force searches [20].

Advantages of ions: trapping, shielding, cooling, detection

For high-precision spectroscopy, the narrow forbidden lines must also not be impaired by additional broadening mechanisms such as thermal motion (Doppler broadening) or collisions (pressure broadening). These effects are reduced by observation in a well controlled, shielded, collision-free environment at low temperatures.

Ions, and particularly molecular ions, offer a couple of advantages to achieve this control compared to their neutral counterparts. Because of their charge, ions may be electrically trapped, allowing for long interrogation times in the largely collision-free environment of an ultra-high vacuum. The Coulomb interaction between ions also allows "sympathetic cooling": the ions to be investigated, known as the "spectroscopy ions", are cooled via the exchange of kinetic energy with nearby, laser-cooled ions of another species, known as the "refrigerator ions". Since laser cooling is a well-established technique for atomic ions but—apart from a very few exceptions—is not applicable to molecules, sympathetic cooling of molecular spectroscopy ions with atomic refrigerator ions offers a method to significantly reduce Doppler broadening of molecular transitions and as such represents an important technique for high-precision molecular spectroscopy.

Finally, the Coulomb interaction between a pair of trapped ions may be used for indirect state-detection schemes. In such schemes, the quantum state of a spectroscopy ion is mapped to another ion, known as the "logic ion", which is more easily accessible for state detection. This technique is known as "quantum logic spectroscopy", since it is based on techniques borrowed from trapped-ion quantum information processing experiments. Concerning molecular spectroscopy, the method allows to detect the quantum state of a molecular ion in a non-destructive way, which is otherwise prevented by the lack of closed optical cycling transitions used for state detection in atomic ions [39, 40, 41, 42, 43, 44].

Because of these advantages, some of the most precise measurements in physics have been achieved with electric-dipole-forbidden transitions in trapped atomic ions [11, 12].

Forbidden transitions in molecular ions

Concerning molecular ions, however, no electric-dipole forbidden rotation-vibration spectra have been observed until recently. The advantages of ions have thus not fully been exploited in precision molecular spectroscopy. For example, the above-mentioned studies on a possible time variation of the proton-to-electron mass ratio have been carried out either with weak, electric-dipole-allowed transitions or have been restricted to neutral species.

In this thesis, we show that electric-dipole-forbidden rotation-vibration transitions in a molecular ion may be addressed. More precisely, we report the observation of electric-quadrupole infrared fundamental lines in trapped and cooled molecular nitrogen cations N_2^+. To the best of our knowledge, this is the first observation of an electric-dipole-forbidden vibrational transition in a molecular ion.

On the basis of our measurement as well as theoretical estimates based on ab-initio calculations from the literature [45], we estimated the natural linewidth of the observed transitions to reach down to the nanohertz range. Correspondingly, lifetimes of the vibrationally excited states of several months are expected.

Therefore, our measurements open the way to study fundamental questions such as those mentioned above with a novel, promising approach. Indeed, dipole-forbidden rotation-vibration transitions have been proposed as molecular clocks and to search for variations in the proton-to-electron mass ratio μ [46, 47]. In particular, transitions in N_2^+ have been shown promising for such studies based on estimates for the sensitivity of transition frequencies on spurious electromagnetic fields [16, 48] and given that N_2^+ ions are well suited for sympathetic cooling by Ca^+ ions.

As usual for a new observation, our findings not only open up new opportunities, but also raise new questions: how can we understand the measured spectrum, particularly its fine and hyperfine structure? Which effects of our experimental approach do we need to take into account when analyzing our data? Do we, e.g., understand the details of our ion production method? Which new tools do we need for further experiments to exploit the full potential of our discovery?

Apart from reporting the first observation of electric-dipole-forbidden rotation-vibration transitions in a molecular ion, the goal of this thesis is to provide the theoretical framework for discussing these questions and to explore possible routes for future experiments fully exploiting the potential of these narrow transitions—with the goal of opening up a new route for investigating questions of fundamental physics.

Outline of this thesis

The points just mentioned already give an overview of the contents of this thesis. In the following chapter, the general theory of spectroscopic transitions and in particular of electric-quadrupole, rotation-vibration transitions in diatomic molecules is developed. There, the ideas outlined above about the "weakness" of electric-quadrupole transitions are formulated in an exact way. In Ch. 3, this theory is applied to the N_2^+ molecular cation and extended to cover the fine and hyperfine structure of this species. The experimental setup for the observation of electric-quadrupole rotation-vibration transitions in N_2^+ is described in Ch. 4. The results of the measurements with this setup are presented and critically discussed. In Ch. 5, a model for the photoionization of diatomic molecules covering fine- and hyperfine-structure effects is developed. In view of open questions raised in the analysis of the experimental results in the previous chapter as well as of future high-precision experiments, this model provides essential insights into molecular photoionization. In Ch. 6, a non-destructive state-detection method, a form of quantum logic spectroscopy, for molecular ions is presented. Finally, the findings of this thesis are summarized and discussed as well as an outlook on a possible continuation of the experiments is given.

Chapter 2

Theory of rotation-vibration transitions in diatomic molecules

2.1 Introduction

In the introductory chapter, we have already mentioned electric-dipole and electric-quadrupole transitions and emphasized the weakness of the latter. In this chapter, these concepts are discussed rigorously by working out the fundamental principles of spectroscopic transitions.

First, the theory of spectroscopic transitions is developed for a generic single-particle system. Essential concepts and the corresponding terminology, such as the formulation of the interaction of matter and radiation in a series expansion, which leads to the classification of spectroscopic transitions in electric-dipole lines, magnetic-dipole lines, electric-quadrupole lines, etc., are introduced. The corresponding transition rates are calculated for excitation by a plane electromagnetic wave as well as by isotropic radiation. Based on the latter, the Einstein rate coefficients are worked out leading to a phenomenological treatment of spontaneous emission. We deduce these concepts in a clean and consistent way based on time-dependent quantum mechanical perturbation theory as an underlying principle. After having developed this theory for a single-particle system, we apply it in an appropriately extended form to spectroscopic transitions in diatomic molecules, particularly rotation-vibration transitions.

Obviously, this theory has not been developed originally in this thesis but rather has been around for quite some time already. However, it seems that a complete and consistent text treating electric-dipole-forbidden rotation-vibration transitions in molecules is hardly readily available. Even though forbidden transitions are discussed in a couple of textbooks on atomic spectroscopy (among others [49, 50, 51]), these treatments are not directly applicable to molecular spectroscopy. Textbooks on molecular spectroscopy, on the other hand, present forbidden transitions usually only in a brief way—if at all. In the theory and review articles available on the subject (e.g., [52, 53, 54]), the results presented are not derived from first principles, which hinders a profound understanding of the underlying physical concepts and comprises the risk of applying expressions wrongly for lack of understanding of the underlying definitions and assumptions. Furthermore, many of the texts mentioned above were published several decades ago—some of them even less than a decade after the advent of quantum physics in its present form—which does not ease accessibility. Therefore, we give here a clear and consistent description of these concepts as a theoretical basis of this thesis.

2.2 Interaction of a quantum mechanical system with electromagnetic radiation

2.2.1 The quantum mechanical system

In spectroscopic experiments, the reaction of a quantum mechanical system (an atom, a molecule, a crystal, a quantum dot, etc.) exposed to electromagnetic radiation is studied. On one hand, the system may influence the radiation field, as by absorption of radiation or inducing a phase shift, on the other hand, the radiation may change the population of the different quantum states of the system as well as affect the relative quantum phases between them. States not populated prior to exposition to radiation can, e.g., get populated. This change can be detected, e.g. by the fluorescence when the population in such an excited state decays to a lower state or—as in the experiment described in Ch. 4—by a change in the chemical reactivity of the system. In the following, the dynamics of the simplest quantum mechanical system exhibiting these effects, a two-level single-particle system, under the influence of an external perturbation will be studied.[1]

We begin with a two-level quantum mechanical system governed by a time-independent Hamiltonian $\hat{H}^0$ with two known eigenstates, the energetically lower one $|\psi_\mathrm{a}\rangle$ and the energetically higher one $|\psi_\mathrm{b}\rangle$. They are solutions of the time-independent Schrödinger equation of the system with the corresponding energies E_a and E_b (with $E_\mathrm{b} > E_\mathrm{a}$),

$$\hat{H}^0 |\psi_\mathrm{a}\rangle = E_\mathrm{a} |\psi_\mathrm{a}\rangle , \tag{2.1a}$$

$$\hat{H}^0 |\psi_\mathrm{b}\rangle = E_\mathrm{b} |\psi_\mathrm{b}\rangle . \tag{2.1b}$$

As noted above, we are interested in the reaction of the system when affected by an external time-dependent perturbation described by the Hamiltonian $\hat{H}'(t)$ with t denoting the time variable. The total Hamiltonian (system and perturbation) thus reads,

$$\hat{H}(t) = \hat{H}^0 + \hat{H}'(t), \tag{2.2}$$

and we would like to find a solution $|\Psi(t)\rangle$ for the Schrödinger equation,

$$\hat{H}(t) |\Psi(t)\rangle = i\hbar \frac{\partial}{\partial t} |\Psi(t)\rangle . \tag{2.3}$$

Because the states $|\psi_\mathrm{a}\rangle$ and $|\psi_\mathrm{b}\rangle$ form a basis of the relevant Hilbert space, we may express the solution as a linear combination of them with time-dependent coefficients and use the ansatz:

$$|\Psi(t)\rangle = c_\mathrm{a}(t) |\psi_\mathrm{a}\rangle \exp(-iE_\mathrm{a}t/\hbar) + c_\mathrm{b}(t) |\psi_\mathrm{b}\rangle \exp(-iE_\mathrm{b}t/\hbar). \tag{2.4}$$

The solution is thus obtained when having found expressions for the coefficients $c_\mathrm{a}(t)$ and $c_\mathrm{b}(t)$. In particular, the populations in the lower and upper state $P_\mathrm{a}(t)$ and $P_\mathrm{b}(t)$ are given by these coefficients as $P_\mathrm{a(b)}(t) = |c_\mathrm{a(b)}(t)|^2$.

This problem is discussed in many physics and spectroscopy textbooks (see, e.g., [55]) and is thus not

[1] The following treatment is mainly based on the texts by Griffiths [55] and by Park [56] as well as to a minor extent on the one by Bransden and Joachain [57].

reproduced here. With the abbreviation $H'_{ij} = \langle\psi_i|\hat{H}'|\psi_j\rangle$ for $i, j = \mathrm{a}, \mathrm{b}$ and the additional assumption of vanishing diagonal elements of the perturbing Hamiltonian[2] ($H'_{\mathrm{aa}} = H'_{\mathrm{bb}} = 0$), the solution is given in the form of two coupled, first-order differential equations as,

$$\dot{c}_{\mathrm{a}}(t) = -\frac{i}{\hbar} H'_{\mathrm{ab}} \exp(-i\omega_{\mathrm{ba}} t) c_{\mathrm{b}}(t), \tag{2.5a}$$

$$\dot{c}_{\mathrm{b}}(t) = -\frac{i}{\hbar} H'_{\mathrm{ba}} \exp(i\omega_{\mathrm{ba}} t) c_{\mathrm{a}}(t), \tag{2.5b}$$

with $\omega_{\mathrm{ba}} = (E_{\mathrm{b}} - E_{\mathrm{a}})/\hbar$ and dotted symbols ($\dot{}$) denoting the respective temporal derivatives.

As for every temporal differential equation, initial conditions are needed to solve equation (2.5). They are assumed here as $c_{\mathrm{a}}(0) = 1$ and $c_{\mathrm{b}}(0) = 0$, meaning that the system is in the lower state at $t = 0$. For a vanishing perturbation ($\hat{H}' = 0$), this state would be preserved forever. We obtain an approximate solution for equation (2.5), within first-order perturbation theory (known as the "weak field solution"), when substituting this "zeroth-order" result into the right-hand side of equation (2.5). Integration then yields,

$$c_{\mathrm{b}}(t) = -\frac{i}{\hbar} \int_0^t H'_{\mathrm{ba}}(t') \exp(i\omega_{\mathrm{ba}} t') \mathrm{d}t'. \tag{2.6}$$

Within first-order perturbation theory, the whole dynamics of the system is described by this coefficient.

2.2.2 The radiation field

So far the physical meaning of the perturbing Hamiltonian $\hat{H}'$ has not been specified. It could represent any effect influencing the system. In spectroscopic experiments, this perturbation is usually caused by electromagnetic radiation. Here, this radiation is treated as a classical electromagnetic field. Although this treatment fails in describing phenomena involving few-photon effects and restricts our treatment of spontaneous emission to a phenomenological one, it is appropriate for describing many spectroscopic experiments.

The electromagnetic field is therefore governed by Maxwell's equations, which read in free space,

$$\nabla \cdot \mathbf{E} = 0, \tag{2.7a}$$

$$\nabla \cdot \mathbf{B} = 0, \tag{2.7b}$$

$$\nabla \times \mathbf{E} = -\frac{\partial \mathbf{B}}{\partial t}, \tag{2.7c}$$

$$\nabla \times \mathbf{B} = \frac{1}{c^2} \frac{\partial \mathbf{E}}{\partial t}, \tag{2.7d}$$

with $\mathbf{E}$ and $\mathbf{B}$ the electric and magnetic field respectively, c the speed of light in vacuum and ∇ the nabla operator.

Solutions for these equations can be given in terms of a vector potential $\mathbf{A}$ and a scalar potential V

[2] If this condition is not met, the solution retains a similar form but with additional phase factors [55]. For simplicity, here, this assumption is assumed to hold.

according to:

$$\mathbf{B} = \nabla \times \mathbf{A}, \tag{2.8a}$$

$$\mathbf{E} = -\nabla V - \frac{\partial \mathbf{A}}{\partial t}. \tag{2.8b}$$

In the experiments described in Ch. 4, the electromagnetic field used to study the system (a molecular ion) is the electromagnetic field of a laser beam. For a region of the size of a molecule, the electromagnetic field in such a beam is described to a good approximation by a plane electromagnetic wave.[3] The vector potential $\mathbf{A}$ of a linearly polarized plane wave may be written as,

$$\mathbf{A}(\mathbf{r}, t) = A_0 \mathbf{e}_0 \cos(\mathbf{k} \cdot \mathbf{r} - \omega t), \tag{2.9}$$

and the scalar potential is chosen to vanish ($V = 0$). Here, the independent variable $\mathbf{r}$ represents the position vector, A_0 is the amplitude of the field and $\mathbf{e}_0$ a unit vector describing the direction of polarization. Moreover, $\mathbf{k}$ is the wavevector that points in direction of propagation and is perpendicular to the polarization vector ($\mathbf{e}_0 \cdot \mathbf{k} = 0$). Finally, ω is the angular frequency of the wave and is related to $\mathbf{k}$ by $|\mathbf{k}| = k = \omega/c$. The vector potential given above is divergence free, i.e., $\nabla \cdot \mathbf{A} = 0$.

The electric field corresponding to this vector potential is,

$$\mathbf{E}(\mathbf{r}, t) = -\frac{\partial \mathbf{A}(\mathbf{r}, t)}{\partial t} = E_0 \mathbf{e}_0 \sin(\mathbf{k} \cdot \mathbf{r} - \omega t), \tag{2.10}$$

with $E_0 = -A_0\omega$ and the magnetic field is,

$$\mathbf{B}(\mathbf{r}, t) = \nabla \times \mathbf{A}(\mathbf{r}, t) = \mathbf{B}_0 \sin(\mathbf{k} \cdot \mathbf{r} - \omega t), \tag{2.11}$$

with $\mathbf{B}_0 = A_0 \mathbf{e}_0 \times \mathbf{k}$.

2.2.3 Interaction of matter and radiation

After having found the general dynamics of a quantum mechanical system affected by an external perturbation as well as the description of the electromagnetic field generating this perturbation, we may set up the interaction Hamiltonian and study the dynamics of the system in this particular case.

The interaction Hamiltonian of a single charged particle in an electromagnetic field is given by [56],

$$\hat{H} = \frac{1}{2m} \left[\hat{\mathbf{p}} - q\mathbf{A}\right]^2 + qV(\hat{\mathbf{r}}). \tag{2.12}$$

Here, m and q are the mass and the charge of the particle, $\hat{\mathbf{p}}$ represents the momentum operator, $\mathbf{A}$ designates the vector potential introduced in the last section and $V(\hat{\mathbf{r}})$ is the potential appearing in $\hat{H}^0$, i.e., the potential of the quantum mechanical system of its own (if, e.g., the system studied is the electron of a hydrogen atom, $V(\hat{\mathbf{r}})$ would be the Coulomb potential of the proton). This potential is

[3] In a more accurate (but yet idealized) model, the laser beam could, e.g., be described as a "Gaussian beam" [58]. In such a description, the wavefronts are curved (instead of plane) and the intensity of the radiation varies over space. However, as these effects are taking place on length scales much larger than the size of an atom or molecule, it is sufficient to describe the electromagnetic radiation as a plane wave with the intensity of the beam at the relevant position.

not to be confused with the scalar potential V from the last section, which has been set to zero. As the scalar potential of the last section will no more appear below, no confusion should arise.

Expanding the Hamiltonian yields:

$$\hat{H} = \frac{1}{2m}\left[\hat{\mathbf{p}}^2 - q\hat{\mathbf{p}}\cdot\mathbf{A} - q\mathbf{A}\cdot\hat{\mathbf{p}} + q^2\mathbf{A}^2\right] + qV(\hat{\mathbf{r}}) \tag{2.13}$$

$$\approx \hat{H}^0 + \hat{H}'(t). \tag{2.14}$$

The term $q^2\mathbf{A}^2$ may be neglected as it is small for usual radiation intensities [56].[4] The Hamiltonian then has the form of equation (2.2) with the Hamiltonian of the unperturbed system,

$$\hat{H}^0 = \frac{\hat{\mathbf{p}}^2}{2m} + qV(\hat{\mathbf{r}}), \tag{2.15}$$

and the perturbing Hamiltonian,

$$\hat{H}'(t) = -\frac{q}{2m}\left[\hat{\mathbf{p}}\cdot\mathbf{A}(\hat{\mathbf{r}},t) + \mathbf{A}(\hat{\mathbf{r}},t)\cdot\hat{\mathbf{p}}\right]. \tag{2.16}$$

The matrix element of $\hat{H}'$ for the two states of the two-level system is given by:

$$\left\langle \psi_\mathrm{b}\,\middle|\,\hat{H}'(t)\,\middle|\,\psi_\mathrm{a}\right\rangle = -\frac{q}{2m}\int \psi_\mathrm{b}^*(\mathbf{r})[\hat{\mathbf{p}}\cdot\mathbf{A}(\mathbf{r},t) + \mathbf{A}(\mathbf{r},t)\cdot\hat{\mathbf{p}}]\psi_\mathrm{a}(\mathbf{r})\mathrm{d}^3\mathbf{r}, \tag{2.17}$$

with $\psi_\mathrm{a}(\mathbf{r}) = \langle\mathbf{r}\,|\,\psi_\mathrm{a}\rangle$ and $\psi_\mathrm{b}(\mathbf{r}) = \langle\mathbf{r}\,|\,\psi_\mathrm{b}\rangle$ the wavefunctions belonging to the states $|\psi_\mathrm{a}\rangle$ and $|\psi_\mathrm{b}\rangle$, respectively, and the integral extending over the entire space. The term in brackets in (2.17) can be simplified when using $\hat{\mathbf{p}} = -i\hbar\nabla$ and that $\mathbf{A}$ is divergence free ($\nabla\cdot\mathbf{A} = 0$), yielding:

$$\left\langle \psi_\mathrm{b}\,\middle|\,\hat{H}'(t)\,\middle|\,\psi_\mathrm{a}\right\rangle = -\frac{q}{m}\int \psi_\mathrm{b}^*(\mathbf{r})\mathbf{A}(\mathbf{r},t)\cdot\hat{\mathbf{p}}\psi_\mathrm{a}(\mathbf{r})\mathrm{d}^3\mathbf{r}. \tag{2.18}$$

Inserting this expression into equation (2.6), we obtain the coefficient $c_b(t)$ that contains the complete description of the dynamics of the system within first-order perturbation theory:

$$c_\mathrm{b}(t) = -\frac{i}{\hbar}\int_0^t H'_\mathrm{ba}(t')\exp(i\omega_\mathrm{ba}t')\mathrm{d}t' \tag{2.19}$$

$$= -\frac{i}{\hbar}\int_0^t \langle\psi_\mathrm{b}\,|\,H'(t')\,|\,\psi_\mathrm{a}\rangle\exp(i\omega_\mathrm{ba}t')\mathrm{d}t' \tag{2.20}$$

$$= \frac{iq}{m\hbar}\int_0^t\int \psi_\mathrm{b}^*(\mathbf{r})\mathbf{A}(\mathbf{r},t')\cdot\hat{\mathbf{p}}\psi_\mathrm{a}(\mathbf{r})\mathrm{d}^3\mathbf{r}\exp(i\omega_\mathrm{ba}t')\mathrm{d}t' \tag{2.21}$$

$$= \frac{iqA_0}{m\hbar}\int_0^t\int \psi_\mathrm{b}^*(\mathbf{r})\mathbf{e}_0\cdot\hat{\mathbf{p}}\cos(\mathbf{k}\cdot\mathbf{r} - \omega t')\psi_\mathrm{a}(\mathbf{r})\mathrm{d}^3\mathbf{r}\exp(i\omega_\mathrm{ba}t')\mathrm{d}t' \tag{2.22}$$

$$= \frac{iqA_0}{2m\hbar}\left[\langle\psi_\mathrm{b}\,|\,\mathbf{e}_0\cdot\hat{\mathbf{p}}\exp(i\mathbf{k}\cdot\hat{\mathbf{r}})\,|\,\psi_\mathrm{a}\rangle\int_0^t\exp(i(\omega_\mathrm{ba}-\omega)t')\mathrm{d}t'\right.$$
$$\left. + \langle\psi_\mathrm{b}\,|\,\mathbf{e}_0\cdot\hat{\mathbf{p}}\exp(-i\mathbf{k}\cdot\hat{\mathbf{r}})\,|\,\psi_\mathrm{a}\rangle\int_0^t\exp(i(\omega_\mathrm{ba}+\omega)t')\mathrm{d}t'\right]. \tag{2.23}$$

As shown above, the spatial and temporal integrals can be separated and the former has been written

[4] At high intensities, this term may give rise to "two-photon transitions", see [50], p. 76 and 95.

in bra-ket notation as,

$$\langle \psi_\mathrm{b} \,|\, \mathbf{e}_0 \cdot \hat{\mathbf{p}} \exp(\pm i\mathbf{k}\cdot\hat{\mathbf{r}}) \,|\, \psi_\mathrm{a}\rangle = \int \psi_\mathrm{b}^*(\mathbf{r}) \mathbf{e}_0 \cdot \hat{\mathbf{p}} \exp(\pm i\mathbf{k}\cdot\mathbf{r}) \psi_\mathrm{a}(\mathbf{r}) \mathrm{d}^3\mathbf{r}. \tag{2.24}$$

Moreover, the temporal integral can be given explicitly,

$$\int_0^t \exp(i(\omega_\mathrm{ba} \pm \omega)t')\mathrm{d}t' = \frac{\exp(i(\omega_\mathrm{ba} \pm \omega)t) - 1}{i(\omega_\mathrm{ba} \pm \omega)}, \tag{2.25}$$

such that we arrive at:

$$\begin{aligned} c_\mathrm{b}(t) = & \frac{qA_0}{2m\hbar} \left[\langle \psi_\mathrm{b} \,|\, \mathbf{e}_0 \cdot \hat{\mathbf{p}} \exp(i\mathbf{k}\cdot\hat{\mathbf{r}}) \,|\, \psi_\mathrm{a}\rangle \frac{\exp(i(\omega_\mathrm{ba} - \omega)t) - 1}{\omega_\mathrm{ba} - \omega} \right. \\ & \left. + \langle \psi_\mathrm{b} \,|\, \mathbf{e}_0 \cdot \hat{\mathbf{p}} \exp(-i\mathbf{k}\cdot\hat{\mathbf{r}}) \,|\, \psi_\mathrm{a}\rangle \frac{\exp(i(\omega_\mathrm{ba} + \omega)t) - 1}{\omega_\mathrm{ba} + \omega} \right]. \end{aligned} \tag{2.26}$$

In spectroscopic experiments, the frequency ω of the radiation lies typically close to the resonance frequency ω_ba. In this case, the expression above is dominated by the first summand and the second one may be neglected. In this "rotating wave approximation" we get:

$$c_\mathrm{b}(t) = \frac{iqA_0}{m\hbar} \langle \psi_\mathrm{b} \,|\, \mathbf{e}_0 \cdot \hat{\mathbf{p}} \exp(i\mathbf{k}\cdot\hat{\mathbf{r}}) \,|\, \psi_\mathrm{a}\rangle \frac{\sin[(\omega_\mathrm{ba} - \omega)t/2]}{\omega_\mathrm{ba} - \omega} \exp[i(\omega_\mathrm{ba} - \omega)t/2]. \tag{2.27}$$

The population in the upper state at time t is hence given as,

$$P_\mathrm{b}(t) = |c_\mathrm{b}(t)|^2 = \frac{q^2A_0^2}{m^2\hbar^2} |\langle \psi_\mathrm{b} \,|\, \mathbf{e}_0 \cdot \hat{\mathbf{p}} \exp(i\mathbf{k}\cdot\hat{\mathbf{r}}) \,|\, \psi_\mathrm{a}\rangle|^2 \frac{\sin^2[(\omega_\mathrm{ba} - \omega)t/2]}{(\omega_\mathrm{ba} - \omega)^2}. \tag{2.28}$$

In principle, equation (2.27) describes the whole dynamics of a single-particle two-level system in a single-photon spectroscopic experiment within first-order perturbation theory. However, for evaluating it, the actual spatial forms of the wavefunctions $\psi_\mathrm{a}(\mathbf{r})$ and $\psi_\mathrm{b}(\mathbf{r})$ are needed. A simpler treatment, providing also more physical insight, is obtained when expanding the exponential function in (2.27) in a Taylor series around the origin, i.e.,

$$\exp(i\mathbf{k}\cdot\hat{\mathbf{r}}) = 1 + i\mathbf{k}\cdot\hat{\mathbf{r}} - \frac{1}{2}(\mathbf{k}\cdot\hat{\mathbf{r}})^2 - \frac{i}{6}(\mathbf{k}\cdot\hat{\mathbf{r}})^3 + \ldots \tag{2.29}$$

The wavelength λ of electromagnetic radiation at a frequency close to resonance with a usual transition in a quantum mechanical system, such as an atom or a molecule, is much larger than the size of such a system. The extent of an electronic orbital in an atom, e.g., is on the order of a few Å (1 Å = 10^{-10} m). The radiation inducing electronic transitions is usually in the optical or ultraviolet part of the electromagnetic spectrum, i.e., the wavelength is $\gtrsim$ 100 nm = 10^{-7}m. Therefore, the wavelength accounts for $\approx$ 1000 times the size of the system. In molecular vibrational spectroscopy, the length of typical bonds being vibrationally excited, is also on the order of a few Å and the radiation at resonance with vibrational transitions typically lies in the infrared spectral region with wavelengths $\gtrsim 1\,\mu$m. Thus, the wavelength of the radiation is about 10000 times the size of the system.

Saying that the size of the system is considerably smaller than the wavelength λ of the radiation means, in a quantum mechanical description, that the absolute values of the wavefunctions $\psi_\mathrm{a}(\mathbf{r})$ and $\psi_\mathrm{b}(\mathbf{r})$ appearing in the integral in (2.24) (and in bra-ket notation in (2.27) and (2.28)) differ only

significantly from zero in a region, which is small compared to the wavelength λ (and essentially vanish outside of this region). This means there exists some length scale $r_{\max}$ characterizing the extent of that region with $r_{\max} \ll \lambda$.

When choosing the origin of the coordinate system at the position of the quantum mechanical system, we may thus restrict the integral (2.24) to a cube around the origin with edge length $2r_{\max}$:

$$\begin{aligned}
&\int \psi_{\mathrm{b}}^*(\mathbf{r})\mathbf{e}_0 \cdot \hat{\mathbf{p}} \exp(\pm i\mathbf{k}\cdot\mathbf{r})\psi_{\mathrm{a}}(\mathbf{r})\mathrm{d}^3\mathbf{r} \\
&= \int_{-\infty}^{\infty}\int_{-\infty}^{\infty}\int_{-\infty}^{\infty} \psi_{\mathrm{b}}^*(\mathbf{r})\mathbf{e}_0 \cdot \hat{\mathbf{p}} \exp(\pm i\mathbf{k}\cdot\mathbf{r})\psi_{\mathrm{a}}(\mathbf{r})\mathrm{d}r_x\mathrm{d}r_y\mathrm{d}r_z \qquad (2.30)\\
&\approx \int_{-r_{\max}}^{r_{\max}}\int_{-r_{\max}}^{r_{\max}}\int_{-r_{\max}}^{r_{\max}} \psi_{\mathrm{b}}^*(\mathbf{r})\mathbf{e}_0 \cdot \hat{\mathbf{p}} \exp(\pm i\mathbf{k}\cdot\mathbf{r})\psi_{\mathrm{a}}(\mathbf{r})\mathrm{d}r_x\mathrm{d}r_y\mathrm{d}r_z. \qquad (2.31)
\end{aligned}$$

Because the magnitude of the wavevector k is proportional to $1/\lambda$ and because[5] $|\mathbf{r}| \leq \sqrt{3}r_{\max} \ll \lambda$ for all possible values of $\mathbf{r}$ in the integral (2.31), the scalar product $\mathbf{k}\cdot\mathbf{r}$ in (2.31) is much smaller than 1. Therefore, only the first few terms of the Taylor series (2.29) contribute significantly to this integral and each following term in (2.29) is significantly smaller than the previous one for values of $\mathbf{r}$ relevant for this integral.

If, e.g., we assume the maximal length of $\mathbf{r}$ relevant for the integral in (2.24) to be 1 Å and $\lambda = 100\,\mathrm{nm}$, we obtain $\mathbf{k}\cdot\mathbf{r} < 6.3 \cdot 10^{-3}$. Therefore, each term in (2.29) only amounts for less than a fraction of about $6 \cdot 10^{-3}$ of the previous one. A rather accurate value for the integral in (2.24) can thus be obtained by just considering the first few terms of this expansion.[6]

2.2.4 Electric-dipole approximation

For the description of many spectroscopic experiments, it is even sufficient to just consider the first term of the Taylor series in (2.29). Physically, this means that the whole spatial dependence of the electromagnetic wave is neglected and that it is simply regarded as a spatially constant, oscillating field. This is the well-known "electric-dipole approximation".

Applying it, we obtain the matrix element in (2.27) approximately as,

$$\langle \psi_{\mathrm{b}} \,|\, \mathbf{e}_0 \cdot \hat{\mathbf{p}} \exp(i\mathbf{k}\cdot\hat{\mathbf{r}}) \,|\, \psi_{\mathrm{a}} \rangle \approx \langle \psi_{\mathrm{b}} \,|\, \mathbf{e}_0 \cdot \hat{\mathbf{p}} \,|\, \psi_{\mathrm{a}} \rangle \,. \qquad (2.32)$$

For further simplification, we would like to take advantage of $|\psi_{\mathrm{a}}\rangle$ and $|\psi_{\mathrm{b}}\rangle$ being eigenstates of the Hamiltonian $\hat{H}^0$ of the unperturbed system. This is achieved by expressing the momentum operator in terms of the commutator of $\hat{H}^0$ with the position operator $\hat{\mathbf{r}}$ as [56],

$$\hat{\mathbf{p}} = \frac{im}{\hbar}[\hat{H}^0, \hat{\mathbf{r}}]. \qquad (2.33)$$

Thus, we get,

$$\mathbf{e}_0 \cdot \hat{\mathbf{p}} = \frac{im}{\hbar}\left(\hat{H}^0\hat{\mathbf{r}}\cdot\mathbf{e}_0 - \hat{\mathbf{r}}\cdot\mathbf{e}_0\hat{H}^0\right), \qquad (2.34)$$

[5] The factor $\sqrt{3}$ stems from the space diagonal of the cube and is not relevant for our reasoning.

[6] This argument can be formulated analytically for hydrogen-atom-like systems. The expansion (2.29) then corresponds to an expansion in powers of the fine-structure constant $\alpha \approx 1/137$ (see [59, 56]).

and, when using that $|\psi_\mathrm{a}\rangle$ and $|\psi_\mathrm{b}\rangle$ are eigenstates of $\hat{H}^0$,

$$\langle\psi_\mathrm{b}\,|\,\mathbf{e}_0\cdot\hat{\mathbf{p}}\,|\,\psi_\mathrm{a}\rangle = im\frac{E_\mathrm{b}-E_\mathrm{a}}{\hbar}\,\langle\psi_\mathrm{b}\,|\,\mathbf{e}_0\cdot\hat{\mathbf{r}}\,|\,\psi_\mathrm{a}\rangle = im\omega_\mathrm{ba}\,\langle\psi_\mathrm{b}\,|\,\mathbf{e}_0\cdot\hat{\mathbf{r}}\,|\,\psi_\mathrm{a}\rangle\,. \tag{2.35}$$

Substituting this result into (2.27) and using the label "E1" for electric-dipole transitions, we obtain:

$$c_\mathrm{b}^{(\mathrm{E1})}(t) = -\frac{A_0}{\hbar}\frac{\omega_\mathrm{ba}}{\omega_\mathrm{ba}-\omega}q\,\langle\psi_\mathrm{b}\,|\,\mathbf{e}_0\cdot\hat{\mathbf{r}}\,|\,\psi_\mathrm{a}\rangle\,\sin[(\omega_\mathrm{ba}-\omega)t/2]\exp[i(\omega_\mathrm{ba}-\omega)t/2] \tag{2.36}$$

$$= -\frac{A_0}{\hbar}\frac{\omega_\mathrm{ba}}{\omega_\mathrm{ba}-\omega}\mathbf{e}_0\cdot\langle\psi_\mathrm{b}\,|\,\hat{\boldsymbol{\mu}}\,|\,\psi_\mathrm{a}\rangle\,\sin[(\omega_\mathrm{ba}-\omega)t/2]\exp[i(\omega_\mathrm{ba}-\omega)t/2] \tag{2.37}$$

$$= -\frac{A_0}{\hbar}\frac{\omega_\mathrm{ba}}{\omega_\mathrm{ba}-\omega}\mathbf{e}_0\cdot\boldsymbol{\mu}_\mathrm{ba}\,\sin[(\omega_\mathrm{ba}-\omega)t/2]\exp[i(\omega_\mathrm{ba}-\omega)t/2]. \tag{2.38}$$

Here, we have used the "electric-dipole operator" defined as,[7]

$$\hat{\boldsymbol{\mu}} = q\hat{\mathbf{r}}, \tag{2.39}$$

and its matrix element for the states $|\psi_\mathrm{b}\rangle$ and $|\psi_\mathrm{a}\rangle$, the "electric-dipole transition matrix element" given by:

$$\boldsymbol{\mu}_\mathrm{ba} = \langle\psi_\mathrm{b}\,|\,\hat{\boldsymbol{\mu}}\,|\,\psi_\mathrm{a}\rangle\,. \tag{2.40}$$

In the electric-dipole approximation, the population in the upper state at time t is obtained as:

$$P_\mathrm{b}^{(\mathrm{E1})}(t) = |c_\mathrm{b}^{(\mathrm{E1})}(t)|^2 = \frac{A_0^2\omega_\mathrm{ba}^2}{\hbar^2}|\mathbf{e}_0\cdot\boldsymbol{\mu}_\mathrm{ba}|^2\frac{\sin^2[(\omega_\mathrm{ba}-\omega)t/2]}{(\omega_\mathrm{ba}-\omega)^2}. \tag{2.41}$$

The amplitude of the vector potential A_0 used here to specify the "strength" of the radiation field is not a quantity usually measured in the laboratory or widely used in spectroscopy, it is thus worth replacing it by the time-averaged spatial energy density u given as [55],

$$u = \frac{1}{2}\varepsilon_0 E_0^2 = \frac{1}{2}\varepsilon_0\omega^2 A_0^2, \tag{2.42}$$

with ε_0 the vacuum permittivity. We then get the upper-state population as:

$$P_\mathrm{b}^{(\mathrm{E1})}(t) = \frac{2u\omega_\mathrm{ba}^2}{\varepsilon_0\hbar^2\omega^2}\,|\mathbf{e}_0\cdot\boldsymbol{\mu}_\mathrm{ba}|^2\,\frac{\sin^2[(\omega_\mathrm{ba}-\omega)t/2]}{(\omega_\mathrm{ba}-\omega)^2}. \tag{2.43}$$

Until now, it has been assumed that the electromagnetic wave is purely monochromatic. In reality, electromagnetic radiation is never completely monochromatic, but rather shows a non-vanishing spectral (and spatial) energy density $\rho(\omega)$ for some range of angular frequencies ω. Therefore, we replace the spatial energy density of a monochromatic wave u with $\rho(\omega)\mathrm{d}\omega$ and integrate over the whole spectrum. The population in the upper state is then:

$$P_\mathrm{b}^{(\mathrm{E1})}(t) = \frac{2\omega_\mathrm{ba}^2}{\varepsilon_0\hbar^2}\,|\mathbf{e}_0\cdot\boldsymbol{\mu}_\mathrm{ba}|^2\int_0^\infty\frac{\rho(\omega)}{\omega^2}\frac{\sin^2[(\omega_\mathrm{ba}-\omega)t/2]}{(\omega_\mathrm{ba}-\omega)^2}\mathrm{d}\omega. \tag{2.44}$$

[7] From here on, the Greek, small letter μ (in several typographical variations) is used for the electric-dipole moment (operator) instead of for the proton-to-electron mass ratio as in Ch. 1. As we will no more refer to the latter, no confusion should arise.

The second factor in the integral above exhibits a narrow peak at $\omega \approx \omega_{\mathrm{ba}}$, whereas the term $\rho(\omega)/\omega^2$ does not change much over this narrow frequency interval. We may thus replace ω by the constant ω_{ba} in the first factor and take this factor out of the integral. By the same argument we may also extend the lower limit of the integral to $-\infty$ such that it may be given in analytical form (namely as $t\pi/2$), i.e,

$$P_{\mathrm{b}}^{(\mathrm{E1})}(t) \approx \frac{2}{\varepsilon_0 \hbar^2} \left|\mathbf{e}_0 \cdot \boldsymbol{\mu}_{\mathrm{ba}}\right|^2 \rho(\omega_{\mathrm{ba}}) \int_0^\infty \frac{\sin^2[(\omega_{\mathrm{ba}} - \omega)t/2]}{(\omega_{\mathrm{ba}} - \omega)^2} \mathrm{d}\omega \tag{2.45}$$

$$\approx \frac{2}{\varepsilon_0 \hbar^2} \left|\mathbf{e}_0 \cdot \boldsymbol{\mu}_{\mathrm{ba}}\right|^2 \rho(\omega_{\mathrm{ba}}) \int_{-\infty}^\infty \frac{\sin^2[(\omega_{\mathrm{ba}} - \omega)t/2]}{(\omega_{\mathrm{ba}} - \omega)^2} \mathrm{d}\omega \tag{2.46}$$

$$= \frac{t\pi}{\varepsilon_0 \hbar^2} \left|\mathbf{e}_0 \cdot \boldsymbol{\mu}_{\mathrm{ba}}\right|^2 \rho(\omega_{\mathrm{ba}}). \tag{2.47}$$

The transition rate is given by the derivative of the population with respect to time, i.e.,

$$R_{\mathrm{a}\to\mathrm{b}}^{(\mathrm{E1})} = \frac{\mathrm{d}P_{\mathrm{b}}^{(\mathrm{E1})}}{\mathrm{d}t} \approx \frac{\pi}{\varepsilon_0 \hbar^2} \left|\mathbf{e}_0 \cdot \boldsymbol{\mu}_{\mathrm{ba}}\right|^2 \rho(\omega_{\mathrm{ba}}). \tag{2.48}$$

2.2.5 Electric-dipole-forbidden transitions

As seen in the previous section, every term in the series expansion of $\exp(i\mathbf{k}\cdot\hat{\mathbf{r}})$ is considerably smaller than the previous one, and it is thus sufficient to just take into account the first (constant) term of this expansion for the description of many spectroscopic experiments, i.e., to use the electric-dipole approximation.

However, if the transition moment calculated within the electric-dipole approximation vanishes, the next-higher-order term in (2.29), the term $i\mathbf{k}\cdot\hat{\mathbf{r}}$, gets important, as this term may give rise to a non-vanishing transition moment. Such transitions are called "forbidden transitions" or more precisely "electric-dipole-forbidden" transitions. As mentioned in Ch. 1, they may be observed, but their transition rates are several orders of magnitude lower than those of electric-dipole-allowed transitions (i.e., those with a non-vanishing transition moment in the electric-dipole approximation).

In the following, such dipole-forbidden transitions are studied. Hence, we assume the transition moment due to first term in the expansion (2.29), the electric-dipole term, to vanish and study only the effect of the second term in this expansion. We obtain for the transition matrix element:

$$\langle \psi_{\mathrm{b}} \,|\, \mathbf{e}_0 \cdot \hat{\mathbf{p}} \exp(i\mathbf{k}\cdot\hat{\mathbf{r}}) \,|\, \psi_{\mathrm{a}} \rangle \approx i \,\langle \psi_{\mathrm{b}} \,|\, (\mathbf{e}_0 \cdot \hat{\mathbf{p}})(\mathbf{k}\cdot\hat{\mathbf{r}}) \,|\, \psi_{\mathrm{a}} \rangle \,. \tag{2.49}$$

Substituting this expression into (2.27) yields:

$$c_{\mathrm{b}}(t) = -\frac{qA_0}{m\hbar} \,\langle \psi_{\mathrm{b}} \,|\, (\mathbf{e}_0 \cdot \hat{\mathbf{p}})(\mathbf{k}\cdot\hat{\mathbf{r}}) \,|\, \psi_{\mathrm{a}} \rangle \, \frac{\sin[(\omega_{\mathrm{ba}} - \omega)t/2]}{\omega_{\mathrm{ba}} - \omega} \exp[i(\omega_{\mathrm{ba}} - \omega)t/2]. \tag{2.50}$$

We want again take advantage of $|\psi_{\mathrm{a}}\rangle$ and $|\psi_{\mathrm{b}}\rangle$ being eigenstates of the Hamiltonian $\hat{H}^0$. To this end, we express the transition operator in a similar way as we did for the dipole operator using the commutator with $\hat{H}^0$. This can be achieved with the two relations [56],

$$\frac{im}{\hbar}[\hat{H}^0, (\mathbf{e}_0 \cdot \hat{\mathbf{r}})(\mathbf{k}\cdot\hat{\mathbf{r}})] = (\mathbf{e}_0 \cdot \hat{\mathbf{p}})(\mathbf{k}\cdot\hat{\mathbf{r}}) + (\mathbf{k}\cdot\hat{\mathbf{p}})(\mathbf{e}_0 \cdot \hat{\mathbf{r}}), \tag{2.51}$$

and,

$$\mathbf{k} \times \mathbf{e}_0 \cdot \hat{\mathscr{L}} = (\mathbf{e}_0 \cdot \hat{\mathbf{p}})(\mathbf{k} \cdot \hat{\mathbf{r}}) - (\mathbf{k} \cdot \hat{\mathbf{p}})(\mathbf{e}_0 \cdot \hat{\mathbf{r}}), \tag{2.52}$$

where $\hat{\mathscr{L}} \coloneqq \hat{\mathbf{r}} \times \hat{\mathbf{p}}$.

Adding (2.51) and (2.52), we obtain,

$$(\mathbf{e}_0 \cdot \hat{\mathbf{p}})(\mathbf{k} \cdot \hat{\mathbf{r}}) = \frac{1}{2}\left(\mathbf{k} \times \mathbf{e}_0 \cdot \hat{\mathscr{L}} + \frac{im}{\hbar}[\hat{H}^0, (\mathbf{e}_0 \cdot \hat{\mathbf{r}})(\mathbf{k} \cdot \hat{\mathbf{r}})]\right), \tag{2.53}$$

and thus for the transition matrix element (with $\hat{\mathscr{L}} = \hbar\hat{\mathbf{L}}$)

$$\langle \psi_\mathrm{b} \,|\, (\mathbf{e}_0 \cdot \hat{\mathbf{p}})(\mathbf{k} \cdot \hat{\mathbf{r}}) \,|\, \psi_\mathrm{a} \rangle = \frac{1}{2}\left(\hbar\mathbf{k} \times \mathbf{e}_0 \cdot \langle \psi_\mathrm{b}|\hat{\mathbf{L}}|\psi_\mathrm{a}\rangle + \frac{im}{\hbar}\langle \psi_\mathrm{b}|[\hat{H}^0, (\mathbf{e}_0 \cdot \hat{\mathbf{r}})(\mathbf{k} \cdot \hat{\mathbf{r}})]|\psi_\mathrm{a}\rangle\right) \tag{2.54}$$

$$= \frac{1}{2}\left(\hbar\mathbf{k} \times \mathbf{e}_0 \cdot \langle \psi_\mathrm{b}|\hat{\mathbf{L}}|\psi_\mathrm{a}\rangle + \frac{im}{\hbar}(E_\mathrm{b} - E_\mathrm{a})\langle \psi_\mathrm{b}|(\mathbf{e}_0 \cdot \hat{\mathbf{r}})(\mathbf{k} \cdot \hat{\mathbf{r}})|\psi_\mathrm{a}\rangle\right) \tag{2.55}$$

$$= \frac{1}{2}\left(\hbar\mathbf{k} \times \mathbf{e}_0 \cdot \langle \psi_\mathrm{b}|\hat{\mathbf{L}}|\psi_\mathrm{a}\rangle + im\omega_\mathrm{ba}\langle \psi_\mathrm{b}|(\mathbf{e}_0 \cdot \hat{\mathbf{r}})(\mathbf{k} \cdot \hat{\mathbf{r}})|\psi_\mathrm{a}\rangle\right). \tag{2.56}$$

When inserting this expression for the transition matrix element into (2.50), we obtain,

$$c_\mathrm{b}(t) = -\frac{qA_0}{2m\hbar}\left[\hbar\mathbf{k} \times \mathbf{e}_0 \cdot \langle \psi_\mathrm{b}|\hat{\mathbf{L}}|\psi_\mathrm{a}\rangle + im\omega_\mathrm{ba}\langle \psi_\mathrm{b}|(\mathbf{e}_0 \cdot \hat{\mathbf{r}})(\mathbf{k} \cdot \hat{\mathbf{r}})|\psi_\mathrm{a}\rangle\right] \frac{\sin[(\omega_\mathrm{ba} - \omega)t/2]}{\omega_\mathrm{ba} - \omega} \exp[i(\omega_\mathrm{ba} - \omega)t/2]. \tag{2.57}$$

The second term in brackets is treated in a componentwise notation. Denoting the Cartesian components of $\mathbf{e}_0$, $\mathbf{k}$ and $\hat{\mathbf{r}}$ with Greek letter indices α and β (where $\alpha, \beta = x, y, z$), we may write,

$$(\mathbf{e}_0 \cdot \hat{\mathbf{r}})(\mathbf{k} \cdot \hat{\mathbf{r}}) = \left(\sum_\alpha e_{0,\alpha}\hat{r}_\alpha\right)\left(\sum_\beta k_\beta \hat{r}_\beta\right) = \sum_\alpha \sum_\beta e_{0,\alpha}k_\beta \hat{r}_\alpha \hat{r}_\beta \tag{2.58}$$

$$= k\sum_\alpha \sum_\beta e_{0,\alpha}\kappa_\beta \hat{r}_\alpha \hat{r}_\beta = \frac{\omega}{c}\sum_\alpha \sum_\beta e_{0,\alpha}\kappa_\beta \hat{r}_\alpha \hat{r}_\beta, \tag{2.59}$$

where in the second line a unit vector $\boldsymbol{\kappa}$ in direction of $\mathbf{k}$ was introduced such that $\mathbf{k} = k\boldsymbol{\kappa} = \frac{\omega}{c}\boldsymbol{\kappa}$. We thus obtain for the second matrix element appearing in (2.57),

$$\langle \psi_\mathrm{b}|q(\mathbf{e}_0 \cdot \hat{\mathbf{r}})(\mathbf{k} \cdot \hat{\mathbf{r}})|\psi_\mathrm{a}\rangle = \frac{\omega}{c}\sum_\alpha \sum_\beta e_{0,\alpha}\kappa_\beta \langle \psi_\mathrm{b}|q\hat{r}_\alpha \hat{r}_\beta|\psi_\mathrm{a}\rangle \tag{2.60}$$

$$= \frac{\omega}{c}\sum_\alpha \sum_\beta \epsilon_{\alpha\beta}\langle \psi_\mathrm{b}|\widetilde{Q}_{\alpha\beta}|\psi_\mathrm{a}\rangle. \tag{2.61}$$

Here, the two symbols $\epsilon_{\alpha\beta}$ and $\widetilde{Q}_{\alpha\beta}$ defined as $\epsilon_{\alpha\beta} \coloneqq e_{0,\alpha}\kappa_\beta$ and $\widetilde{Q}_{\alpha\beta} \coloneqq q\hat{r}_\alpha \hat{r}_\beta$ have been introduced. They are components of the two Cartesian tensors (matrices) $\boldsymbol{\varepsilon}$ and $\widetilde{\mathsf{Q}}$, respectively.[8]

The tensor $\boldsymbol{\varepsilon}$ describes the direction of the variation of the electric-field in space. It is related to the

[8] In this text, Cartesian tensors are typeset in bold upright symbols, their components in italic symbols with Greek small letter indices.

Jacobian matrix of the electric field (loosely speaking, the electric-field gradient)[9] by the relation,

$$\frac{\mathrm{d}\mathbf{E}}{\mathrm{d}\mathbf{r}} = \boldsymbol{\varepsilon}\frac{E_0\omega}{c}\cos(\mathbf{k}\cdot\mathbf{r}-\omega t), \tag{2.62}$$

which reads in a componentwise notation:

$$\frac{\partial E_\alpha}{\partial r_\beta} = \epsilon_{\alpha\beta}\frac{E_0\omega}{c}\cos(\mathbf{k}\cdot\mathbf{r}-\omega t). \tag{2.63}$$

Equation (2.62) for the electric-field "gradient" corresponds to equation (2.10) for the electric field itself: both of these equations consist of a scalar factor for the "strength" of these two quantities (E_0 in (2.10) and $E_0\omega/c$ in (2.62)), a directional factor ($\mathbf{e}_0$ and $\boldsymbol{\varepsilon}$, respectively) and finally a factor expressing the time-dependence.

As suggested by the notation, $\widetilde{Q}_{\alpha\beta}$ is related to the electric-quadrupole tensor operator. However, the calculations below are simplified by defining the quadrupole tensor in a traceless form. Because the polarization vector of an electromagnetic wave in free space is always perpendicular to the direction of propagation, we have:

$$\mathbf{k}\cdot\mathbf{e}_0 = k\boldsymbol{\kappa}\cdot\mathbf{e}_0 = k\sum_\alpha \kappa_\alpha e_{0,\alpha} = 0. \tag{2.64}$$

We may thus add an arbitrary operator $\hat{f}$ to the diagonal elements of $\widetilde{Q}_{\alpha\beta}$ without changing the sum in (2.61), i.e., using the Kronecker delta $\delta_{\alpha\beta}$, we may write:

$$\sum_\alpha\sum_\beta \epsilon_{\alpha\beta}\left\langle\psi_\mathrm{b}|\widetilde{Q}_{\alpha\beta}|\psi_\mathrm{a}\right\rangle = \sum_\alpha\sum_\beta \epsilon_{\alpha\beta}\left\langle\psi_\mathrm{b}|\widetilde{Q}_{\alpha\beta}+\delta_{\alpha\beta}\hat{f}|\psi_\mathrm{a}\right\rangle. \tag{2.65}$$

Making use of this freedom, we define the electric-quadrupole tensor operator $\hat{\mathsf{Q}}$ with the components $\hat{Q}_{\alpha\beta}$ as:[10]

$$\hat{Q}_{\alpha\beta} \coloneqq q\left(\hat{r}_\alpha\hat{r}_\beta - \delta_{\alpha\beta}\frac{\hat{r}^2}{3}\right), \tag{2.66}$$

with $\hat{r}^2 = \hat{r}_x^2+\hat{r}_y^2+\hat{r}_z^2$. This tensor is traceless, meaning that

$$\operatorname{tr}\hat{\mathsf{Q}} = \sum_\alpha \hat{Q}_{\alpha\alpha} = 0. \tag{2.67}$$

Furthermore, $\hat{\mathsf{Q}}$ is symmetric: $\hat{Q}_{\alpha\beta} = \hat{Q}_{\beta\alpha}$.

Using this definition for the electric-quadrupole operator, the matrix element in (2.61) is given as

$$\left\langle\psi_\mathrm{b}|q(\mathbf{e}_0\cdot\hat{\mathbf{r}})(\mathbf{k}\cdot\hat{\mathbf{r}})|\psi_\mathrm{a}\right\rangle = \frac{\omega}{c}\sum_\alpha\sum_\beta \epsilon_{\alpha\beta}\left\langle\psi_\mathrm{b}|\hat{Q}_{\alpha\beta}|\psi_\mathrm{a}\right\rangle. \tag{2.68}$$

Substituting this expression into (2.57) and also using the relation $\mathbf{B}_0 = A_0\mathbf{e}_0\times\mathbf{k}$ between the vector

[9] Mathematically, the gradient of a vector field is not defined and we should rather speak of the Jacobian matrix. Physically, however, "gradient" might give a better picture of what is meant.

[10] Several definitions for the electric-quadrupole tensor are used in the literature differing by constant factors and whether or not they are given in traceless form. Relations between different definitions are discussed in Appendix A.1.

potential $\mathbf{A}$ and the magnetic field amplitude $\mathbf{B}_0$, we obtain the coefficient $c_\mathrm{b}(t)$ as,

$$c_\mathrm{b}(t) = \frac{1}{2m}\left[q\mathbf{B}_0 \cdot \langle\psi_\mathrm{b}|\hat{\mathbf{L}}|\psi_\mathrm{a}\rangle - \frac{iA_0 m\omega_\mathrm{ba}\omega}{\hbar c}\sum_\alpha\sum_\beta \epsilon_{\alpha\beta}\langle\psi_\mathrm{b}|\hat{Q}_{\alpha\beta}|\psi_\mathrm{a}\rangle\right] \frac{\sin[(\omega_\mathrm{ba}-\omega)t/2]}{\omega_\mathrm{ba}-\omega}\exp[i(\omega_\mathrm{ba}-\omega)t/2], \tag{2.69}$$

and the population in the upper state as,

$$P_\mathrm{b}(t) = \frac{1}{4m^2}\left|q\mathbf{B}_0 \cdot \langle\psi_\mathrm{b}|\hat{\mathbf{L}}|\psi_\mathrm{a}\rangle - \frac{iA_0 m\omega_\mathrm{ba}\omega}{\hbar c}\sum_\alpha\sum_\beta \epsilon_{\alpha\beta}\langle\psi_\mathrm{b}|\hat{Q}_{\alpha\beta}|\psi_\mathrm{a}\rangle\right|^2 \frac{\sin^2[(\omega_\mathrm{ba}-\omega)t/2]}{(\omega_\mathrm{ba}-\omega)^2}. \tag{2.70}$$

The first term within the absolute value in this equation describes the interaction of the quantum mechanical system with the magnetic field (a first-rank tensor) of the electromagnetic wave. It gives rise to the "magnetic-dipole" transitions. The second term describes the interaction of the system with the "gradient" of the electric-field at the position of the system (represented by the second-rank tensor $\epsilon_{\alpha\beta}$). This term entails the "electric-quadrupole" transitions. In the frame of this thesis, the electric-quadrupole transitions are primarily of interest and we will in the following only study those. Since these two kind of transitions are due to different radiative processes, no interference term between them exists [56] and we may simply omit the magnetic-dipole term. We get for the population excited to the upper state due to an electric-quadrupole transition (labelled as "E2"):

$$P_\mathrm{b}^{(\mathrm{E2})}(t) = \frac{A_0^2\omega_\mathrm{ba}^2\omega^2}{4\hbar^2c^2}\left|\sum_\alpha\sum_\beta \epsilon_{\alpha\beta}\langle\psi_\mathrm{b}|\hat{Q}_{\alpha\beta}|\psi_\mathrm{a}\rangle\right|^2 \frac{\sin^2[(\omega_\mathrm{ba}-\omega)t/2]}{(\omega_\mathrm{ba}-\omega)^2} \tag{2.71}$$

$$= \frac{A_0^2\omega_\mathrm{ba}^2\omega^2}{4\hbar^2c^2}\left|\sum_\alpha\sum_\beta \epsilon_{\alpha\beta}Q_{\mathrm{ba},\alpha\beta}\right|^2 \frac{\sin^2[(\omega_\mathrm{ba}-\omega)t/2]}{(\omega_\mathrm{ba}-\omega)^2}. \tag{2.72}$$

Here, the symbol $Q_{\mathrm{ba},\alpha\beta}$ denotes the electric-quadrupole transition matrix element for the states $|\psi_\mathrm{b}\rangle$ and $|\psi_\mathrm{a}\rangle$, i.e.,

$$Q_{\mathrm{ba},\alpha\beta} = \langle\psi_\mathrm{b}|\hat{Q}_{\alpha\beta}|\psi_\mathrm{a}\rangle\,. \tag{2.73}$$

Upon substituting the amplitude A_0 of the vector potential $\mathbf{A}$ with the spatial energy density u (see equation (2.42)), we obtain,

$$P_\mathrm{b}^{(\mathrm{E2})}(t) = \frac{u\omega_\mathrm{ba}^2}{2\varepsilon_0\hbar^2c^2}\left|\sum_\alpha\sum_\beta \epsilon_{\alpha\beta}\langle\psi_\mathrm{b}|\hat{Q}_{\alpha\beta}|\psi_\mathrm{a}\rangle\right|^2 \frac{\sin^2[(\omega_\mathrm{ba}-\omega)t/2]}{(\omega_\mathrm{ba}-\omega)^2}. \tag{2.74}$$

Likewise as for electric-dipole transitions, we are again interested in the reaction of the system to a radiation field with a certain spectral profile instead of an (unphysical) monochromatic wave. Thus we replace u by $\rho(\omega)\mathrm{d}\omega$ and integrate over the whole spectrum. Once more, we make use of $\rho(\omega)$ varying slowly with the angular frequency ω, whereas the other frequency-dependent term shows a steep peak around $\omega \approx \omega_\mathrm{ba}$. Therefore, $\rho(\omega)$ may be substituted by $\rho(\omega_\mathrm{ba})$ and taken out of the integral. By the same argument, the lower limit of the integral is again extended to $-\infty$ such that it can be given in

an analytical form:

$$P_{\mathrm{b}}^{(\mathrm{E2})}(t) = \frac{\omega_{\mathrm{ba}}^2}{2\varepsilon_0\hbar^2c^2}\left|\sum_\alpha\sum_\beta \epsilon_{\alpha\beta}\,\langle\psi_{\mathrm{b}}|\hat{Q}_{\alpha\beta}|\psi_{\mathrm{a}}\rangle\right|^2 \int_0^\infty \rho(\omega)\frac{\sin^2[(\omega_{\mathrm{ba}}-\omega)t/2]}{(\omega_{\mathrm{ba}}-\omega)^2}\mathrm{d}\omega \tag{2.75}$$

$$\approx \frac{\omega_{\mathrm{ba}}^2}{2\varepsilon_0\hbar^2c^2}\left|\sum_\alpha\sum_\beta \epsilon_{\alpha\beta}\,\langle\psi_{\mathrm{b}}|\hat{Q}_{\alpha\beta}|\psi_{\mathrm{a}}\rangle\right|^2 \rho(\omega_{\mathrm{ba}})\int_{-\infty}^\infty \frac{\sin^2[(\omega_{\mathrm{ba}}-\omega)t/2]}{(\omega_{\mathrm{ba}}-\omega)^2}\mathrm{d}\omega \tag{2.76}$$

$$= \frac{t\pi\omega_{\mathrm{ba}}^2}{4\varepsilon_0\hbar^2c^2}\left|\sum_\alpha\sum_\beta \epsilon_{\alpha\beta}\,\langle\psi_{\mathrm{b}}|\hat{Q}_{\alpha\beta}|\psi_{\mathrm{a}}\rangle\right|^2 \rho(\omega_{\mathrm{ba}}). \tag{2.77}$$

The transition rate is obtained, as before, by the derivative of the upper-state population with respect to time:

$$R_{\mathrm{a}\to\mathrm{b}}^{(\mathrm{E2})} = \frac{\mathrm{d}P_{\mathrm{b}}^{(\mathrm{E2})}}{\mathrm{d}t} \approx \frac{\pi\omega_{\mathrm{ba}}^2}{4\varepsilon_0\hbar^2c^2}\left|\sum_\alpha\sum_\beta \epsilon_{\alpha\beta}\,\langle\psi_{\mathrm{b}}|\hat{Q}_{\alpha\beta}|\psi_{\mathrm{a}}\rangle\right|^2 \rho(\omega_{\mathrm{ba}}). \tag{2.78}$$

2.2.6 Excitation by isotropic radiation and spherical tensor formalism

Until now, we have assumed the transitions to be induced by an electromagnetic field described by a vector potential $\mathbf{A}$ pointing into one particular direction $\mathbf{e}_0$, in other words, by a plane-polarized electromagnetic wave. Now we are considering a system in an isotropic radiation field. To this end, the expression for the excitation rate is averaged over all possible orientations of the vector $\mathbf{e}_0$ with respect to the transition matrix element.

Below, we will show this averaging separately for electric-dipole and electric-quadrupole transitions. At the same time, we will introduce the spherical tensor formalism—a very useful tool for the description of spectroscopic transitions in molecules, particularly when several angular momenta are involved, as we will see in Sec. 2.3 and Ch. 3.

Electric-dipole transitions

For an electric-dipole transition, we need to average the expression,

$$R_{\mathrm{a}\to\mathrm{b}}^{(\mathrm{E1})} = \frac{\pi}{\varepsilon_0\hbar^2}\,|\mathbf{e}_0\cdot\boldsymbol{\mu}_{\mathrm{ba}}|^2\,\rho(\omega_{\mathrm{ba}}), \tag{2.79}$$

for all possible orientations of $\boldsymbol{\mu}_{\mathrm{ba}}$ relative to $\mathbf{e}_0$. This is done below using the spherical tensor formalism.

In general, for every Cartesian vector $\mathbf{v}$ a first-rank spherical tensor $\mathrm{T}_p^1[\mathbf{v}]$ (where $p = 0, \pm1$) can be defined as [60]:

$$\mathrm{T}_0^1[\mathbf{v}] = v_z, \tag{2.80a}$$

$$\mathrm{T}_{\pm1}^1[\mathbf{v}] = \mp\frac{1}{\sqrt{2}}(v_x \pm iv_y). \tag{2.80b}$$

These spherical tensors behave with respect to rotations exactly as quantum mechanical angular momentum states $|j,m\rangle$ with the angular momentum quantum number j, which describes the magnitude

of the angular momentum, corresponding to the rank of the spherical tensor, here 1, and the projection angular momentum quantum number m corresponding to p.

The scalar product of two Cartesian vectors $\mathbf{v}$ and $\mathbf{w}$ is written in spherical tensor notation as,

$$\mathbf{v}\cdot\mathbf{w} = \sum_{\alpha=x,y,z} v_\alpha w_\alpha = \sum_{p=-1}^{1} (-1)^p \mathrm{T}^1_{-p}[\mathbf{v}]\,\mathrm{T}^1_p[\mathbf{w}]\,. \tag{2.81}$$

Using this relation, the transition rate for an electric-dipole transition is

$$R^{(\mathrm{E1})}_{\mathrm{a}\to\mathrm{b}} = \frac{\pi}{\varepsilon_0\hbar^2}\left|\sum_{p=-1}^{1}(-1)^p \mathrm{T}^1_{-p}[\mathbf{e}_0]\,\mathrm{T}^1_p[\boldsymbol{\mu}_{\mathrm{ba}}]\right|^2 \rho(\omega_{\mathrm{ba}}). \tag{2.82}$$

In the following, we assume the polarization vector $\mathbf{e}_0$ to be aligned along z-axis of the coordinate system, i.e., $\mathbf{e}_0 = (0,0,1)$, and the normalized wavevector $\boldsymbol{\kappa}$ along the x-axis, i.e., $\boldsymbol{\kappa} = (1,0,0)$. As we will average over all possible orientations, this assumption does not imply any loss of generality. We then have $\mathrm{T}^1_0[\mathbf{e}_0] = 1$ and $\mathrm{T}^1_{\pm1}[\mathbf{e}_0] = 0$.

Additional to the frame of reference (x,y,z) used so far, whose orientation is chosen such that the electromagnetic field adopts a simple form, we now introduce an additional frame of reference (x',y',z') with an origin coinciding with the that one of the previously used frame of reference, but which is oriented such that the vector of the transition dipole matrix element is oriented along the z'-axis. Denoting the triple of the components of this vector in the primed coordinate system as $\boldsymbol{\mu}'_{\mathrm{ba}}$, we thus have

$$\boldsymbol{\mu}'_{\mathrm{ba}} = (0,0,\mu_{\mathrm{ba}}). \tag{2.83}$$

In spherical tensor notation, this implies $\mathrm{T}^1_q[\boldsymbol{\mu}'_{\mathrm{ba}}] = 0$ for $q = \pm1$ and $\mathrm{T}^1_0[\boldsymbol{\mu}'_{\mathrm{ba}}] = \mu_{\mathrm{ba}}$.

Here, we have assumed $\boldsymbol{\mu}_{\mathrm{ba}}$ to be real. This is true for the vibrational transitions in molecules of prime interest here that are discussed further below. In the general case of complex $\boldsymbol{\mu}_{\mathrm{ba}}$, the calculation may be separated into a real and a complex part as shown in [55].

The components of the dipole transition matrix element in spherical tensor notation in the original coordinate system are expressed in terms of the respective ones in the primed system by a Wigner rotation matrix $\mathscr{D}^{(1)}_{pq}(\phi,\theta,\chi)$, with the Euler angles[11] ϕ, θ, χ describing the relative orientation of the two frames of reference [60, 61], as:

$$\mathrm{T}^1_p[\boldsymbol{\mu}_{\mathrm{ba}}] = \sum_{q=-1}^{1}\left[\mathscr{D}^{(1)}_{pq}(\phi,\theta,\chi)\right]^* \mathrm{T}^1_q[\boldsymbol{\mu}'_{\mathrm{ba}}] \tag{2.84}$$

$$= \left[\mathscr{D}^{(1)}_{p0}(\phi,\theta,\chi)\right]^* \mathrm{T}^1_0[\boldsymbol{\mu}'_{\mathrm{ba}}] \tag{2.85}$$

$$= \left[\mathscr{D}^{(1)}_{p0}(\phi,\theta,\chi)\right]^* \mu_{\mathrm{ba}}. \tag{2.86}$$

[11] The third Euler angle χ is not defined due to the symmetry. As we integrate over all values for the Euler angles this does not pose any difficulties.

Using the above results, the scalar product relevant for the transition rate is,

$$\mathbf{e}_0 \cdot \boldsymbol{\mu}_{\mathrm{ba}} = \sum_{p=-1}^{1} (-1)^p \mathrm{T}^1_{-p}\left[\mathbf{e}_0\right] \left[\mathscr{D}^{(1)}_{p\,0}(\phi,\theta,\chi)\right]^* \mu_{\mathrm{ba}} = \left[\mathscr{D}^{(1)}_{0\,0}(\phi,\theta,\chi)\right]^* \mu_{\mathrm{ba}}. \tag{2.87}$$

To obtain the orientation-averaged transition rate, we need to calculate the average of the squared absolute magnitude of this term. This is done by integrating over all Euler angles and normalizing accordingly. Indicating this orientational average by a bar, we have,

$$\overline{|\mathbf{e}_0 \cdot \boldsymbol{\mu}_{\mathrm{ba}}|^2} = \frac{\int_0^{2\pi}\int_0^{2\pi}\int_0^{\pi} |\mathbf{e}_0 \cdot \boldsymbol{\mu}_{\mathrm{ba}}|^2 \sin\theta \mathrm{d}\theta\mathrm{d}\phi\mathrm{d}\chi}{\int_0^{2\pi}\int_0^{2\pi}\int_0^{\pi} \sin\theta \mathrm{d}\theta\mathrm{d}\phi\mathrm{d}\chi}. \tag{2.88}$$

These integrals are readily calculated when making use of the properties of the Wigner rotation matrices [62, 60] or by just noting that $\mathscr{D}^{(1)}_{0\,0}(\phi,\theta,\chi) = \cos\theta$. They yield:

$$\overline{|\mathbf{e}_0 \cdot \boldsymbol{\mu}_{\mathrm{ba}}|^2} = \frac{\frac{8\pi^2}{3}{\mu_{\mathrm{ba}}}^2}{8\pi^2}. \tag{2.89}$$

The transition rate for an electric-dipole transition driven by isotropic radiation is therefore:

$$R^{(\mathrm{E1,\ iso.})}_{\mathrm{a}\to\mathrm{b}} = \frac{\pi}{3\varepsilon_0\hbar^2} |\boldsymbol{\mu}_{\mathrm{ba}}|^2 \rho(\omega_{\mathrm{ba}}). \tag{2.90}$$

Here, the z'-component of the transition dipole matrix element has been replaced by the norm of this vector and the absolute magnitude has been taken to allow for complex transition matrix elements.

Electric-quadrupole transitions

For an electric-quadrupole transition, the averaging of the transition rate over all possible orientations of the polarization vector $\mathbf{e}_0$ relative to the quadrupole-transition moment is done along the same lines as for an electric-dipole transition. However, as the quadrupole tensor is a second-rank tensor, the calculations tend to be more involved.

The transition rate to be averaged is:

$$R^{(\mathrm{E2})}_{\mathrm{a}\to\mathrm{b}} = \frac{\pi\omega^2_{\mathrm{ba}}}{4\varepsilon_0\hbar^2c^2} \left| \sum_\alpha \sum_\beta \epsilon_{\alpha\beta} \langle\psi_{\mathrm{b}}|\hat{Q}_{\alpha\beta}|\psi_{\mathrm{a}}\rangle \right|^2 \rho(\omega_{\mathrm{ba}}) \tag{2.91}$$

$$= \frac{\pi\omega^2_{\mathrm{ba}}}{4\varepsilon_0\hbar^2c^2} \left| \sum_\alpha \sum_\beta \epsilon_{\alpha\beta} Q_{\mathrm{ba},\alpha\beta} \right|^2 \rho(\omega_{\mathrm{ba}}). \tag{2.92}$$

Here, we have used the symbol $Q_{\mathrm{ba},\alpha\beta}$ for the $\alpha\beta$-component of the transition matrix element of the corresponding component of quadrupole operator $\hat{Q}_{\alpha\beta}$ for the particular states $|\psi_{\mathrm{b}}\rangle$ and$|\psi_{\mathrm{a}}\rangle$. Likewise as for the quadrupole operator, the quadrupole transition matrix element[12] $Q_{\mathrm{ba},\alpha\beta}$ is the $\alpha\beta$-component of the Cartesian tensor Q_{ba}.

[12] In this context the term "matrix element" refers to the value of a quantum mechanical operator "sandwiched" in between a bra and a ket. It does *not* refer to the component of a Cartesian tensor for some particular indices α and β.

As before, we use spherical tensor notation to orientationally average equation (2.92). Generally, for a second-rank Cartesian tensor A (a matrix) with Cartesian components $A_{\alpha\beta}$ for $\alpha, \beta = x, y, z$, spherical tensors of zeroth, first and second rank are defined as [60]:

$$\mathrm{T}^0_0\left[\mathsf{A}\right] = -\frac{1}{\sqrt{3}}\left(A_{xx} + A_{yy} + A_{zz}\right), \tag{2.93a}$$

$$\mathrm{T}^1_0\left[\mathsf{A}\right] = \frac{i}{\sqrt{2}}\left(A_{xy} - A_{yx}\right), \tag{2.93b}$$

$$\mathrm{T}^1_{\pm1}\left[\mathsf{A}\right] = \mp\frac{i}{2}\left(A_{yz} - A_{zy} \pm i(A_{zx} - A_{xz})\right), \tag{2.93c}$$

$$\mathrm{T}^2_0\left[\mathsf{A}\right] = \frac{1}{\sqrt{6}}\left(2A_{zz} - A_{xx} - A_{yy}\right), \tag{2.93d}$$

$$\mathrm{T}^2_{\pm1}\left[\mathsf{A}\right] = \mp\frac{1}{2}\left(A_{xz} + A_{zx} \pm i(A_{yz} + A_{zy})\right), \tag{2.93e}$$

$$\mathrm{T}^2_{\pm2}\left[\mathsf{A}\right] = \frac{1}{2}\left(A_{xx} - A_{yy} \pm i(A_{xy} - A_{yx})\right). \tag{2.93f}$$

For two second-rank Cartesian tensors A and B with Cartesian components $A_{\alpha\beta}$ and $B_{\alpha\beta}$ (with $\alpha, \beta = x, y, z$), respectively, the sum of all products of their components[13] is obtained in spherical tensor notation as,

$$\sum_{\alpha=x,y,z}\sum_{\beta=x,y,z} A_{\alpha\beta}B_{\alpha\beta} = \sum_{u=0}^{2}\sum_{p=-u}^{u}(-1)^{u-p}\mathrm{T}^u_{-p}\left[\mathsf{A}\right]\mathrm{T}^u_p\left[\mathsf{B}\right]. \tag{2.94}$$

With this relation, the sum appearing in (2.92) may be written as,

$$\sum_{\alpha}\sum_{\beta}\epsilon_{\alpha\beta}Q_{\mathrm{ba},\alpha\beta} = \sum_{u=0}^{2}\sum_{p=-u}^{u}(-1)^{u-p}\mathrm{T}^u_{-p}\left[\boldsymbol{\varepsilon}\right]\mathrm{T}^u_p\left[\mathsf{Q}_{\mathrm{ba}}\right] = \sum_{p=-2}^{2}(-1)^{p}\mathrm{T}^2_{-p}\left[\boldsymbol{\varepsilon}\right]\mathrm{T}^2_p\left[\mathsf{Q}_{\mathrm{ba}}\right]. \tag{2.95}$$

As the quadrupole tensor Q_{ba} is traceless, the zeroth-rank spherical tensor defined by (2.93a) vanishes: $\mathrm{T}^0_0\left[\mathsf{Q}_{\mathrm{ba}}\right] = 0$. Since it is also symmetric, the first-rank spherical tensors defined by (2.93b) and (2.93c) vanish, too: $\mathrm{T}^1_{0,\pm1}\left[\mathsf{Q}_{\mathrm{ba}}\right] = 0$. The double sum in (2.95) is therefore equal to a single one.

Substitution of this result into (2.92) yields the electric-quadrupole transition rate in spherical tensor notation:

$$R^{(\mathrm{E2})}_{\mathrm{a}\to\mathrm{b}} = \frac{\pi\omega^2_{\mathrm{ba}}}{4\varepsilon_0\hbar^2c^2}\left|\sum_{p=-2}^{2}(-1)^{p}\mathrm{T}^2_{-p}\left[\boldsymbol{\varepsilon}\right]\mathrm{T}^2_p\left[\mathsf{Q}_{\mathrm{ba}}\right]\right|^2\rho(\omega_{\mathrm{ba}}). \tag{2.96}$$

The term to be orientationally averaged in order to obtain the excitation rate in an isotropic radiation field is the sum given in (2.95). With the assumption $\mathbf{e}_0 = (0, 0, 1)$ and $\boldsymbol{\kappa} = (1, 0, 0)$, we get for the components of the Cartesian electric field tensor,

$$\epsilon_{\alpha\beta} = 1 \quad \text{for} \quad \alpha = z \text{ and } \beta = x, \tag{2.97a}$$

$$\epsilon_{\alpha\beta} = 0 \quad \text{else.} \tag{2.97b}$$

[13] This expression is known as the "Frobenius product" of A and B and written as $\langle\mathsf{A},\mathsf{B}\rangle_{\mathrm{F}}$ or $\mathsf{A}:\mathsf{B}$ (see, e.g., [63]).

In spherical tensor notation, this implies:

$$\mathrm{T}^2_0\left[\boldsymbol{\varepsilon}\right] = 0, \tag{2.98a}$$

$$\mathrm{T}^2_{\pm1}\left[\boldsymbol{\varepsilon}\right] = \mp\frac{1}{2}, \tag{2.98b}$$

$$\mathrm{T}^2_{\pm2}\left[\boldsymbol{\varepsilon}\right] = 0. \tag{2.98c}$$

Equation (2.95) then becomes,

$$\sum_\alpha \sum_\beta \epsilon_{\alpha\beta} Q_{\mathrm{ba},\alpha\beta} = \frac{1}{2}\left(\mathrm{T}^2_{-1}\left[\mathsf{Q}_{\mathrm{ba}}\right] - \mathrm{T}^2_1\left[\mathsf{Q}_{\mathrm{ba}}\right]\right). \tag{2.99}$$

If we proceed in the same way as for electric-dipole transitions and assume that Q_{ba} is real (or, if not, can be separated into a real and an imaginary part that may be treated separately), we have $\mathrm{T}^2_{-1}\left[\mathsf{Q}_{\mathrm{ba}}\right] = -\left(\mathrm{T}^2_1\left[\mathsf{Q}_{\mathrm{ba}}\right]\right)^*$ and hence,

$$\sum_\alpha \sum_\beta \epsilon_{\alpha\beta} Q_{\mathrm{ba},\alpha\beta} = -\frac{1}{2}\left[\left(\mathrm{T}^2_1\left[\mathsf{Q}_{\mathrm{ba}}\right]\right)^* + \mathrm{T}^2_1\left[\mathsf{Q}_{\mathrm{ba}}\right]\right]. \tag{2.100}$$

Again we introduce a new coordinate system (x',y',z') aligned such that Q_{ba} takes a simple form. As Q_{ba} is a real, symmetric matrix, a coordinate system can be found (the system of eigenvectors), in which it yields a diagonal form, i.e.,

$$\mathsf{Q}'_{\mathrm{ba}} = \begin{bmatrix} Q'_{\mathrm{ba},x'x'} & 0 & 0 \\ 0 & Q'_{\mathrm{ba},y'y'} & 0 \\ 0 & 0 & Q'_{\mathrm{ba},z'z'} \end{bmatrix}. \tag{2.101}$$

In spherical tensor notation this implies: $\mathrm{T}^2_{\pm1}\left[\mathsf{Q}'_{\mathrm{ba}}\right] = 0$. To obtain the transition matrix element in the original coordinate system, we again use a Wigner rotation matrix with the Euler angles describing the relative orientation of the two systems. Using the properties just worked out, we get:

$$\mathrm{T}^2_p\left[\mathsf{Q}_{\mathrm{ba}}\right] = \sum_{q=-2}^{2}\left[\mathscr{D}^{(2)}_{pq}(\phi,\theta,\chi)\right]^* \mathrm{T}^2_q\left[\mathsf{Q}'_{\mathrm{ba}}\right] \tag{2.102}$$

$$= \sum_{q=-2,0,2}\left[\mathscr{D}^{(2)}_{pq}(\phi,\theta,\chi)\right]^* \mathrm{T}^2_q\left[\mathsf{Q}'_{\mathrm{ba}}\right]. \tag{2.103}$$

Substituting this result into equation (2.100) yields:

$$\sum_\alpha \sum_\beta \epsilon_{\alpha\beta} Q_{\mathrm{ba},\alpha\beta} = -\frac{1}{2}\sum_{q=-2,0,2}\left(\mathscr{D}^{(2)}_{1q}(\phi,\theta,\chi)\left[\mathrm{T}^2_q\left[\mathsf{Q}'_{\mathrm{ba}}\right]\right]^* + \left[\mathscr{D}^{(2)}_{1q}(\phi,\theta,\chi)\right]^* \mathrm{T}^2_q\left[\mathsf{Q}'_{\mathrm{ba}}\right]\right). \tag{2.104}$$

To obtain the transition rate in an isotropic radiation field, the squared absolute magnitude of this expression is integrated over the Euler angles and normalized accordingly. The integral is once more

calculated using the properties of the Wigner rotation matrices [62]. The result is:

$$\overline{\left|\sum_\alpha\sum_\beta \epsilon_{\alpha\beta}Q_{\mathrm{ba},\alpha\beta}\right|^2} = \frac{\int_0^{2\pi}\int_0^{2\pi}\int_0^{\pi}|\sum_\alpha\sum_\beta \epsilon_{\alpha\beta}Q_{\mathrm{ba},\alpha\beta}|^2\sin\theta\mathrm{d}\theta\mathrm{d}\phi\mathrm{d}\chi}{\int_0^{2\pi}\int_0^{2\pi}\int_0^{\pi}\sin\theta\mathrm{d}\theta\mathrm{d}\phi\mathrm{d}\chi} \tag{2.105}$$

$$= \frac{\frac{4\pi^2}{5}(|\mathrm{T}^2_{-2}\left[\mathsf{Q}'_{\mathrm{ba}}\right]|^2 + |\mathrm{T}^2_0\left[\mathsf{Q}'_{\mathrm{ba}}\right]|^2 + |\mathrm{T}^2_2\left[\mathsf{Q}'_{\mathrm{ba}}\right]|^2)}{8\pi^2} \tag{2.106}$$

$$= \frac{1}{10}\left(|\mathrm{T}^2_{-2}\left[\mathsf{Q}'_{\mathrm{ba}}\right]|^2 + |\mathrm{T}^2_0\left[\mathsf{Q}'_{\mathrm{ba}}\right]|^2 + |\mathrm{T}^2_2\left[\mathsf{Q}'_{\mathrm{ba}}\right]|^2\right) \tag{2.107}$$

$$= \frac{1}{10}\left(|Q'_{\mathrm{ba},x'x'}|^2 + |Q'_{\mathrm{ba},y'y'}|^2 + |Q'_{\mathrm{ba},z'z'}|^2\right) \tag{2.108}$$

$$= \frac{1}{10}\overline{\mathsf{Q}_{\mathrm{ba}}}, \tag{2.109}$$

where the sum of the squared absolute magnitude of the diagonal elements of $\mathsf{Q}'_{\mathrm{ba}}$, i.e., of the eigenvalues of the matrix Q_{ba}, has been denoted $\overline{\mathsf{Q}_{\mathrm{ba}}}$.

The excitation rate for an electric-quadrupole transition driven by isotropic radiation is therefore:

$$R^{(\mathrm{E2,\ iso.})}_{\mathrm{a}\to\mathrm{b}} = \frac{\pi\omega^2_{\mathrm{ba}}}{40\varepsilon_0\hbar^2c^2}\overline{\mathsf{Q}_{\mathrm{ba}}}\rho(\omega_{\mathrm{ba}}). \tag{2.110}$$

2.2.7 Einstein coefficients and spectroscopic line strength

A neat way to express the "strength" of a spectroscopic line is the Einstein A-coefficient of spontaneous emission. Stemming from a model presented by Einstein in 1916 [64], this coefficient describes the interaction of a large number of two-level quantum mechanical systems such as the one discussed above. When we let N_{a} and N_{b} be the number of systems in the lower and upper state, respectively, the change of N_{b} is given in this model as (see, e.g., [55]):

$$\frac{\mathrm{d}N_{\mathrm{b}}}{\mathrm{d}t} = -N_{\mathrm{b}}A_{\mathrm{ba}} - N_{\mathrm{b}}B_{\mathrm{ba}}\rho(\omega_{\mathrm{ba}}) + N_{\mathrm{a}}B_{\mathrm{ab}}\rho(\omega_{\mathrm{ba}}). \tag{2.111}$$

Here, $\rho(\omega_{\mathrm{ba}})$ is the spectral and spatial energy density at the angular frequency ω_{ba}, B_{ab} the Einstein coefficient of stimulated (or induced) absorption, B_{ba} the coefficient of stimulated (or induced) emission and A_{ba} the coefficient of spontaneous emission. Even though a causal understanding of spontaneous emission is beyond the semiclassical model used here, this coefficient can be determined in a phenomenological treatment.

As the quantum mechanical systems are supposed to be in thermal equilibrium with the radiation field, the number of systems in the upper state is constant: $\mathrm{d}N_{\mathrm{b}}/\mathrm{d}t = 0$. Furthermore, the ratio of the number of systems in the lower and upper state is given by a Boltzmann factor,

$$\frac{N_{\mathrm{a}}}{N_{\mathrm{b}}} = \frac{\exp(-E_{\mathrm{a}}/k_{\mathrm{B}}T)}{\exp(-E_{\mathrm{b}}/k_{\mathrm{B}}T)} = \exp(\hbar\omega_{\mathrm{ba}}/k_{\mathrm{B}}T), \tag{2.112}$$

and the energy density by Planck's law,

$$\rho(\omega) = \frac{\hbar}{\pi^2c^3}\frac{\omega^3}{\exp(\hbar\omega/k_{\mathrm{B}}T) - 1}, \tag{2.113}$$

with T the absolute temperature of the system and the radiation field and k_{B} the Boltzmann con-

stant.

From (2.111), (2.112) and (2.113) the following relations can be deduced (see, e.g., [55]):

$$B_{\mathrm{ab}} = B_{\mathrm{ba}}, \tag{2.114}$$

$$A_{\mathrm{ba}} = \frac{\hbar\omega_{\mathrm{ba}}^3}{\pi^2 c^3} B_{\mathrm{ba}}. \tag{2.115}$$

The Einstein B_{ba}-coefficient can be readily obtained from the result for the excitation rate in an isotropic radiation field. For an electric-dipole transition it is according to equation (2.90):

$$B_{\mathrm{ba}}^{(\mathrm{E1})} = \frac{\pi}{3\varepsilon_0\hbar^2}|\boldsymbol{\mu}_{\mathrm{ba}}|^2. \tag{2.116}$$

Hence, the Einstein A_{ba}-coefficient for an electric-dipole transition is:

$$A_{\mathrm{ba}}^{(\mathrm{E1})} = \frac{\omega_{\mathrm{ba}}^3}{3\pi\varepsilon_0\hbar c^3}|\boldsymbol{\mu}_{\mathrm{ba}}|^2. \tag{2.117}$$

Likewise, the Einstein B_{ba}-coefficient for an electric-quadrupole line is obtained from equation (2.110) as,

$$B_{\mathrm{ba}}^{(\mathrm{E2})} = \frac{\pi\omega_{\mathrm{ba}}^2}{40\varepsilon_0\hbar^2 c^2}\overline{\mathsf{Q}'_{\mathrm{ba}}}, \tag{2.118}$$

and the Einstein A_{ba}-coefficient is:

$$A_{\mathrm{ba}}^{(\mathrm{E2})} = \frac{\omega_{\mathrm{ba}}^5}{40\pi\varepsilon_0\hbar c^5}\overline{\mathsf{Q}'_{\mathrm{ba}}}. \tag{2.119}$$

For the calculation above, the energy levels of the two-level system studied (i.e., of the Hamiltonian $\hat{H}^0$) with energies E_{a} and E_{b} have been assumed to be non-degenerate. In general, these levels are degenerate and characterized by some statistical weights g_{a} and g_{b}. The states $|\psi_{\mathrm{a}}\rangle$ and $|\psi_{\mathrm{b}}\rangle$ are thus replaced by the states $|\psi_{\mathrm{a}}, m_{\mathrm{a}}\rangle$ and $|\psi_{\mathrm{b}}, m_{\mathrm{b}}\rangle$ with m_{a} and m_{b} quantum numbers distinguishing between the several degenerate states.

In this case, the relation between the two Einstein B-coefficients is [65]:

$$B_{\mathrm{ab}} = \frac{g_{\mathrm{b}}}{g_{\mathrm{a}}} B_{\mathrm{ba}}. \tag{2.120}$$

A system in a particular upper state $|\psi_{\mathrm{b}}, m_{\mathrm{b}}\rangle$ may decay into any of the lower states $|\psi_{\mathrm{a}}, m_{\mathrm{a}}\rangle$. The total decay rate is therefore obtained as the sum of these individual rates and is in the case of an electric-dipole transition,

$$A_{\mathrm{ba}}^{(\mathrm{E1})} = \frac{\omega_{\mathrm{ba}}^3}{3\pi\varepsilon_0\hbar c^3} \sum_{m_{\mathrm{a}}} \left|\boldsymbol{\mu}_{\mathrm{b},\mathrm{m_b},\mathrm{a},\mathrm{m_a}}\right|^2, \tag{2.121}$$

with the transition matrix element,

$$\boldsymbol{\mu}_{\mathrm{b},\mathrm{m_b},\mathrm{a},\mathrm{m_a}} = \langle \psi_{\mathrm{b}}, m_{\mathrm{b}} \,|\, \hat{\boldsymbol{\mu}} \,|\, \psi_{\mathrm{a}}, m_{\mathrm{a}} \rangle \,. \tag{2.122}$$

The expression (2.121) must be independent of the quantum number m_{b} as the lifetime of degenerate states must be equal in an isotropic environment [65]. Thus, it may be written in a more symmetric

form as,

$$A_{\mathrm{ba}}^{(\mathrm{E1})} = \frac{\omega_{\mathrm{ba}}^3}{3\pi\varepsilon_0\hbar c^3}\frac{1}{g_{\mathrm{b}}}\sum_{m_{\mathrm{a}},\,m_{\mathrm{b}}}\left|\boldsymbol{\mu}_{\mathrm{b},\mathrm{m_b},\mathrm{a},\mathrm{m_a}}\right|^2 \tag{2.123}$$

$$= \frac{\omega_{\mathrm{ba}}^3}{3\pi\varepsilon_0\hbar c^3}\frac{1}{g_{\mathrm{b}}}S_{\mathrm{ba}}^{(\mathrm{E1})}. \tag{2.124}$$

The double sum appearing above is known as the "line strength" $S_{\mathrm{ba}}^{(\mathrm{E1})}$ of the transition. In spherical tensor notation, it may be given as,

$$S_{\mathrm{ba}}^{(\mathrm{E1})} = \sum_{m_{\mathrm{a}},\,m_{\mathrm{b}}}\sum_{p=-1}^{1}\left|\mathrm{T}_p^1\left[\boldsymbol{\mu}_{\mathrm{b},\mathrm{m_b},\mathrm{a},\mathrm{m_a}}\right]\right|^2. \tag{2.125}$$

When substituting the angular frequency ω_{ba} by the corresponding wavelength λ_{ba}, we get,

$$A_{\mathrm{ba}}^{(\mathrm{E1})} = \frac{16\pi^3}{3\varepsilon_0 h\lambda_{\mathrm{ba}}^3 g_{\mathrm{b}}}S_{\mathrm{ba}}^{(\mathrm{E1})}, \tag{2.126}$$

as found, e.g., in [66].

Likewise as shown above for an electric-dipole transition, the Einstein A-coefficient for an electric-quadrupole transition between degenerate levels is:

$$A_{\mathrm{ba}}^{(\mathrm{E2})} = \frac{\omega_{\mathrm{ba}}^5}{40\pi\varepsilon_0\hbar c^5}\frac{1}{g_{\mathrm{b}}}\sum_{m_{\mathrm{a}},\,m_{\mathrm{b}}}\overline{\mathsf{Q}_{\mathrm{b},\mathrm{m_b},\mathrm{a},\mathrm{m_a}}} \tag{2.127}$$

$$= \frac{\omega_{\mathrm{ba}}^5}{40\pi\varepsilon_0\hbar c^5}\frac{1}{g_{\mathrm{b}}}\sum_{m_{\mathrm{a}},\,m_{\mathrm{b}}}\left|Q'_{\mathrm{b},\mathrm{m_b},\mathrm{a},\mathrm{m_a},x'x'}\right|^2 + \left|Q'_{\mathrm{b},\mathrm{m_b},\mathrm{a},\mathrm{m_a},y'y'}\right|^2 + \left|Q'_{\mathrm{b},\mathrm{m_b},\mathrm{a},\mathrm{m_a},z'z'}\right|^2 \tag{2.128}$$

$$= \frac{\omega_{\mathrm{ba}}^5}{40\pi\varepsilon_0\hbar c^5}\frac{1}{g_{\mathrm{b}}}S_{\mathrm{ba}}^{(\mathrm{E2})}. \tag{2.129}$$

Here, $S_{\mathrm{ba}}^{(\mathrm{E2})}$ denotes the line strength of the electric-quadrupole transition, which may be written in spherical tensor notation as,

$$S_{\mathrm{ba}}^{(\mathrm{E2})} = \sum_{m_{\mathrm{a}},\,m_{\mathrm{b}}}\sum_{p=-2}^{2}\left|\mathrm{T}_p^2\left[\mathsf{Q}_{\mathrm{b},\mathrm{m_b},\mathrm{a},\mathrm{m_a}}\right]\right|^2. \tag{2.130}$$

In terms of the transition wavelength λ_{ba}, we get for the Einstein A-coefficient,

$$A_{\mathrm{ba}}^{(\mathrm{E2})} = \frac{8\pi^5}{5\varepsilon_0 h\lambda_{\mathrm{ab}}^5}\frac{1}{g_{\mathrm{b}}}S_{\mathrm{ba}}^{(\mathrm{E2})}, \tag{2.131}$$

the value for the Einstein A-coefficient of an electric-quadrupole line given in [66] or, in CGS units, in [49], for which, however, a clear, quantum mechanical derivation seems hardly available in the literature. The Einstein A-coefficient of an electric-quadrupole line scales with $1/\lambda^5$, whereas the one of an electric-dipole line scales only with $1/\lambda^3$. This is due to the fact that electric-quadrupole transitions are driven by the "gradient" of the electric field rather than just the field strength. For a smaller wavelength, this gradient increases as evident from the factor $\omega/c = 2\pi/\lambda$ in equation (2.62).

2.3 Rotation-vibration transitions in diatomic molecules

In the last section, the interaction of a single-particle quantum mechanical system with electromagnetic radiation was studied. We have shown that this radiation might induce transitions between the eigenstates $|\psi_\mathrm{a}\rangle$ and $|\psi_\mathrm{b}\rangle$ of the unperturbed system and that these transitions are governed by the matrix element $\langle\psi_\mathrm{b}\,|\,(\mathbf{e}_0\cdot\mathbf{p})\exp(i\mathbf{k}\cdot\mathbf{r})\,|\,\psi_\mathrm{a}\rangle$. Furthermore, we have found that this matrix element can be expanded in a Taylor series with terms of rapidly decreasing magnitude, since the wavelength of the radiation is typically several orders of magnitude larger than the extent of the wavefunction of the particle and thus $\mathbf{k}\cdot\mathbf{r}$ is considerably smaller than one in the relevant range. Therefore, our discussion was restricted to only the first and second term of this Taylor expansion, corresponding to electric-dipole and electric-quadrupole transitions, respectively.

Here, we will apply these findings to rotation-vibration transitions in diatomic molecules. As a diatomic molecule is a many-particle system, both the states $|\psi_\mathrm{a}\rangle$ and $|\psi_\mathrm{b}\rangle$ as well as the electric-multipole operators $\hat{\boldsymbol{\mu}}$ and $\hat{\mathsf{Q}}$ will involve many degrees of freedom. However, it can be shown that the problem might be described approximately by only a few independent variables. In the first part of this section, approximate expressions for the quantum states of a diatomic molecule when not perturbed by external electromagnetic radiation will be developed. They represent the molecular counterparts to the single-particle states $|\psi_\mathrm{a}\rangle$ and $|\psi_\mathrm{b}\rangle$ from the last section. Thereafter, we will study how transitions between these states are driven by the interaction with electromagnetic radiation. In particular, rotation-vibration transitions will be studied. In order to work out similarities as well as differences between the electric-dipole-forbidden transitions that are at the focus of this work and ordinary electric-dipole-allowed transitions, the theory of the latter is developed along with that one of the former.

2.3.1 Quantum states of a diatomic molecule

The Hamiltonian of a molecule with two nuclei, 1 and 2, at positions $\mathbf{R}_1^{(\mathrm{a})}$ and $\mathbf{R}_2^{(\mathrm{a})}$, with masses M_1 and M_2 and charges $q_1 = Z_1 e$ and $q_2 = Z_2 e$ as well as N electrons at $\mathbf{r}_1^{(\mathrm{a})}, \mathbf{r}_2^{(\mathrm{a})}, ..., \mathbf{r}_N^{(\mathrm{a})}$ with charge $-e$ and mass m is given in position representation and without spin interactions in an arbitrary (hence the superscript $^{(\mathrm{a})}$) inertial frame of reference as:

$$\hat{H}_\mathrm{tot} = -\frac{\hbar^2}{2m}\sum_{j=1}^{N}\nabla^2_{\mathbf{r}_j^{(\mathrm{a})}} - \frac{\hbar^2}{2M_1}\nabla^2_{\mathbf{R}_1^{(\mathrm{a})}} - \frac{\hbar^2}{2M_2}\nabla^2_{\mathbf{R}_2^{(\mathrm{a})}} + V^{(\mathrm{a})}\left(\mathbf{R}_1^{(\mathrm{a})}, \mathbf{R}_2^{(\mathrm{a})}, \mathbf{r}_1^{(\mathrm{a})}, \mathbf{r}_2^{(\mathrm{a})}, ..., \mathbf{r}_N^{(\mathrm{a})}\right), \tag{2.132}$$

with the potential energy:

$$\begin{aligned} V^{(\mathrm{a})}\left(\mathbf{R}_1^{(\mathrm{a})}, \mathbf{R}_2^{(\mathrm{a})}, \mathbf{r}_1^{(\mathrm{a})}, \mathbf{r}_2^{(\mathrm{a})}, ..., \mathbf{r}_N^{(\mathrm{a})}\right) = &-\frac{1}{4\pi\varepsilon_0}\sum_{j=1}^{N}\left(\frac{Z_1 e^2}{|\mathbf{r}_j^{(\mathrm{a})} - \mathbf{R}_1^{(\mathrm{a})}|} + \frac{Z_2 e^2}{|\mathbf{r}_j^{(\mathrm{a})} - \mathbf{R}_2^{(\mathrm{a})}|}\right) \\ &+ \frac{Z_1 Z_2 e^2}{4\pi\varepsilon_0 |\mathbf{R}_1^{(\mathrm{a})} - \mathbf{R}_2^{(\mathrm{a})}|} + \frac{1}{4\pi\varepsilon_0}\sum_{j=1}^{N}\sum_{l=j}^{N}\frac{e^2}{|\mathbf{r}_j^{(\mathrm{a})} - \mathbf{r}_l^{(\mathrm{a})}|}. \end{aligned} \tag{2.133}$$

This Hamiltonian is too complex to be solved analytically and even if a solution could be found numerically, it would probably be hard to gain physical insight from it because of its complexity. Therefore, we need to find approximate solutions. To this end, several coordinate transformations and approximations are made, which separate the Hamiltonian in several terms, whose mutual couplings are

small and can be neglected for an approximate treatment. These transformations and approximations are rather involved in all their details. Here, we only describe them in a shortened and simplified way. Particularly, all effects of electron and nuclear spin are neglected and the orbital angular momentum of the electrons is also treated in a simplified manner, i.e., only molecules in $^1\Sigma$ states are considered. A complete treatment can be found in several textbooks [67, 68, 60, 69]. For the discussion below, the texts by Levine [70], Bransden and Joachain [57] and Bunker [68] have served as a basis.

First, we separate the translational motion of the molecule as a whole from the relative motion of its constituents by expressing all coordinates relative to the center of mass of the molecule. This means we define $\mathbf{R}_1 = \mathbf{R}_1^{(\mathrm{a})} - \mathbf{R}_{\mathrm{cm}}$, $\mathbf{R}_2 = \mathbf{R}_2^{(\mathrm{a})} - \mathbf{R}_{\mathrm{cm}}$ and $\mathbf{r}_1 = \mathbf{r}_1^{(\mathrm{a})} - \mathbf{R}_{\mathrm{cm}}$, $\mathbf{r}_2 = \mathbf{r}_2^{(\mathrm{a})} - \mathbf{R}_{\mathrm{cm}}$, ..., $\mathbf{r}_N = \mathbf{r}_N^{(\mathrm{a})} - \mathbf{R}_{\mathrm{cm}}$ with $\mathbf{R}_{\mathrm{cm}}$ the center-of-mass position. If we follow the treatment in [57] and neglect the influence of the electrons, $\mathbf{R}_{\mathrm{cm}}$ is given approximately as,

$$\mathbf{R}_{\mathrm{cm}} \approx \frac{M_1 \mathbf{R}_1^{(\mathrm{a})} + M_2 \mathbf{R}_2^{(\mathrm{a})}}{M_1 + M_2}, \tag{2.134}$$

and the positions of the two nuclei are given by,

$$\mathbf{R}_1 \approx \mathbf{R}_{\mathrm{cm}} + \frac{M_2}{M_1 + M_2}\mathbf{R}, \tag{2.135a}$$

$$\mathbf{R}_2 \approx \mathbf{R}_{\mathrm{cm}} - \frac{M_1}{M_1 + M_2}\mathbf{R}, \tag{2.135b}$$

with $\mathbf{R} = \mathbf{R}_2^{(\mathrm{a})} - \mathbf{R}_1^{(\mathrm{a})} = \mathbf{R}_2 - \mathbf{R}_1$ their relative position vector.

As a quantum mechanical description of the translational motion of the molecule is usually not needed in spectroscopy,[14] $\mathbf{R}_{\mathrm{cm}}$ is set equal to zero by switching to a frame of reference moving with the molecule in a way that the molecular center of mass remains always at the origin. This moving (but not rotating) frame is called the "space-fixed" or "laboratory-fixed" frame. The total internal molecular Hamiltonian $\hat{H}_{\mathrm{int}}$ (i.e., the Hamiltonian without translation[15]) can be approximately[16] written as a sum of the electronic kinetic energy operator, the nuclear kinetic energy operator and the potential energy function,

$$\hat{H}_{\mathrm{int}} = \hat{T}_{\mathrm{elec}} + \hat{T}_{\mathrm{nucl}} + V(\mathbf{R}, \mathbf{r}_1, \mathbf{r}_2, ..., \mathbf{r}_N), \tag{2.136}$$

with

$$\hat{T}_{\mathrm{elec}} = -\frac{\hbar^2}{2m}\sum_{j=1}^{N} \nabla_{\mathbf{r}_j}^2, \tag{2.137}$$

$$\hat{T}_{\mathrm{nucl}} = -\frac{\hbar^2}{2M_{\mathrm{eff}}}\nabla_{\mathbf{R}}^2, \tag{2.138}$$

[14] The translational motion causes the Doppler broadening of spectral lines and is thus important, but this effect is usually treated by a classical description of the translational motion. A situation, in which a quantum mechanical description of the translational degrees of freedom is needed, is, e.g., a spectroscopic experiment with a trapped ion cooled close to the absolute motional ground state such that the coupling of the motional and the internal states can be observed as "side-band transitions".

[15] Here, "internal" refers to all degrees of freedom but the translational ones and thus includes also the rotational ones. Strictly speaking, the latter could be understood as external, but because of their coupling to the electronic and nuclear spin considered in the following chapter, it seems reasonable to regard them as internal here.

[16] In a more detailed treatment (see, e.g., [68, 67, 60]) small additional terms appear. They are neglected here for brevity and comprehensibility.

$$V(\mathbf{R},\mathbf{r}_1,\mathbf{r}_2,...,\mathbf{r}_N) = -\frac{1}{4\pi\varepsilon_0}\sum_{j=1}^{N}\left(\frac{Z_1e^2}{|\mathbf{r}_j-\mathbf{R}_1|}+\frac{Z_2e^2}{|\mathbf{r}_j-\mathbf{R}_2|}\right) + \frac{Z_1Z_2e^2}{4\pi\varepsilon_0 R}+\frac{1}{4\pi\varepsilon_0}\sum_{j=1}^{N}\sum_{l=j}^{N}\frac{e^2}{|\mathbf{r}_j-\mathbf{r}_l|}, \tag{2.139}$$

and $M_{\text{eff}} = M_1M_2/(M_1+M_2)$ the "effective" or "reduced" mass of the two nuclei.[17]

The corresponding internal Schrödinger equation is:

$$\hat{H}_{\text{int}}\psi_{\text{int}}(\mathbf{R},\mathbf{r}_1,\mathbf{r}_2,...,\mathbf{r}_N) = E_{\text{int}}\psi_{\text{int}}(\mathbf{R},\mathbf{r}_1,\mathbf{r}_2,...,\mathbf{r}_N). \tag{2.140}$$

To solve this equation, we use the ansatz $\psi_{\text{int}}(\mathbf{R},\mathbf{r}_1,\mathbf{r}_2,...,\mathbf{r}_N) = \psi_{\text{elec}}(\mathbf{R},\mathbf{r}_1,\mathbf{r}_2,...,\mathbf{r}_N)\psi_{\text{nucl}}(\mathbf{R})$. When this ansatz is inserted into (2.140), $\hat{T}_{\text{nucl}}$ operates on both, ψ_{nucl} as well as ψ_{elec}. However, because the factor $1/M_{\text{eff}}$ in $\hat{T}_{\text{nucl}}$ is considerably smaller than the factor $1/m$ in $\hat{T}_{\text{elec}}$, we may neglect the former at first such that we arrive at the purely electronic Schrödinger equation,

$$\left[\hat{T}_{\text{elec}} + V(\mathbf{R},\mathbf{r}_1,\mathbf{r}_2,...,\mathbf{r}_N)\right]\psi_{\text{elec},n}(\mathbf{R},\mathbf{r}_1,\mathbf{r}_2,...,\mathbf{r}_N) = E_{\text{elec},n}\psi_{\text{elec},n}(\mathbf{R},\mathbf{r}_1,\mathbf{r}_2,...,\mathbf{r}_N). \tag{2.141}$$

Here, we have added the index n to distinguish between the different solutions of this equation. In equation (2.141) no operator acting on R appears, hence R can be regarded as a mere parameter, meaning that there is a different solution for each value of R.

Supposed we have found a solution for the electronic Schrödinger equation (2.141), we substitute it into (2.140). By the aforementioned approximation of neglecting the effect of $\hat{T}_{\text{nucl}}$ on ψ_{elec}, we get the following purely nuclear Schrödinger equation:

$$\left[\hat{T}_{\text{nucl}} + E_{\text{elec},n}(R)\right]\psi_{\text{nucl}}(\mathbf{R}) = E_{\text{int}}\psi_{\text{nucl},n}(\mathbf{R}). \tag{2.142}$$

In this equation the electronic energy $E_{\text{elec},n}(R)$, i.e., the eigenvalue appearing in (2.141) for an eigenfunction $\psi_{\text{elec},n}$ and a given value of the parameter R, plays the role of an effective potential for the motion of the nuclei. Neglecting the effect of $\hat{T}_{\text{nucl}}$ on ψ_{elec} means that the electrons will—due to their low mass—always immediately follow the motion of the nuclei. This is the well-known Born-Oppenheimer approximation [71]. For studying energetically low-lying vibrational states of a stable molecule in its electronic ground state, this is a reasonable approximation.

In order to solve the nuclear equation (2.142), we will express $\mathbf{R}$ in spherical coordinates (R,θ,ϕ) with θ and ϕ its polar and azimuthal angle, respectively, and write $\hat{T}_{\text{nucl}}$ as a sum of a radial, i.e., vibrational, part $\hat{T}_{\text{vib}}$ and an angular, i.e. rotational, part $\hat{T}_{\text{rot}}$ according to $\hat{T}_{\text{nucl}} = \hat{T}_{\text{vib}} + \hat{T}_{\text{rot}}$ with

$$\hat{T}_{\text{vib}} = -\frac{\hbar^2}{2M_{\text{eff}}R^2}\frac{\partial}{\partial R}\left(R^2\frac{\partial}{\partial R}\right), \tag{2.143}$$

$$\hat{T}_{\text{rot}} = -\frac{\hbar^2}{2M_{\text{eff}}R^2}\left[\frac{1}{\sin^2\theta}\frac{\partial^2}{\partial\phi^2}+\frac{1}{\sin\theta}\frac{\partial}{\partial\theta}\left(\sin\theta\frac{\partial}{\partial\theta}\right)\right] \tag{2.144}$$

$$\approx -\frac{\hbar^2}{2M_{\text{eff}}{R_{\text{e}}}^2}\left[\frac{1}{\sin^2\theta}\frac{\partial^2}{\partial\phi^2}+\frac{1}{\sin\theta}\frac{\partial}{\partial\theta}\left(\sin\theta\frac{\partial}{\partial\theta}\right)\right]. \tag{2.145}$$

[17] We use the symbol M_{eff} for the effective mass instead of μ, as often found in the literature, in order to avoid confusion with the electric-dipole moment.

Besides switching to spherical coordinates, we have also replaced the variable R in $\hat{T}_{\mathrm{rot}}$ by the constant R_{e}. The meaning of R_{e} will be explained below where this approximation will also be justified.

Correspondingly, we express the nuclear wavefunction in spherical coordinates and use an ansatz for $\psi_{\mathrm{nucl}}(R,\theta,\phi)$ as a product of a radial, i.e, vibrational, and an angular, i.e., rotational, function:

$$\psi_{\mathrm{nucl}}(R,\theta,\phi) = \frac{1}{R}\psi_{\mathrm{vib}}(R)Y_{JM}(\theta,\phi), \tag{2.146}$$

with $Y_{JM}(\theta,\phi)$ a spherical harmonic.

Upon substituting (2.143), (2.145) and (2.146) into (2.142), we arrive at the vibrational Schrödinger equation,

$$\left[-\frac{\hbar^2}{2M_{\mathrm{eff}}R^2}\frac{\partial^2}{\partial R^2} + \frac{\hbar^2 J(J+1)}{2M_{\mathrm{eff}}{R_{\mathrm{e}}}^2} + E_{\mathrm{elec},n}(R)\right]\psi_{\mathrm{vib}}(R) = E_{\mathrm{vib}}(R)\psi_{\mathrm{vib}}(R). \tag{2.147}$$

The solution of this equation depends on the form of $E_{\mathrm{elec},n}(R)$, the "potential curve" or "potential surface" of the particular electronic state n. However, for a bound state of a stable molecule $E_{\mathrm{elec},n}(R)$ has a minimum at some value R_{e} for R and only the shape of the potential curve in vicinity of this minimum is relevant. This can be understood in a classical picture by realizing that the amplitude of the vibrational motion of the nuclei around this "equilibrium" position accounts for just a small fraction of R_{e}. Quantum mechanically speaking, the vibrational wavefunction exhibits values significantly different from zero only for $R \approx R_{\mathrm{e}}$. The potential curve $E_{\mathrm{elec},n}(R)$ can thus be expanded into a Taylor series around R_{e}:

$$E_{\mathrm{elec},n}(R) \approx E_{\mathrm{elec},n}(R_{\mathrm{e}}) + (R-R_{\mathrm{e}})\left.\frac{\partial E_{\mathrm{elec},n}}{\partial R}\right|_{R=R_{\mathrm{e}}} + \frac{1}{2}(R-R_{\mathrm{e}})^2\left.\frac{\partial^2 E_{\mathrm{elec},n}}{\partial R^2}\right|_{R=R_{\mathrm{e}}} \tag{2.148}$$

$$= E_{\mathrm{elec},n}(R_{\mathrm{e}}) + \frac{1}{2}k_n\zeta^2, \tag{2.149}$$

where we have used that $E_{\mathrm{elec}}(R)$ has a minimum at $R = R_{\mathrm{e}}$, i.e., its first derivative vanishes, as well as the definitions $\zeta = R - R_{\mathrm{e}}$, the displacement from the equilibrium position, and $k_n = \partial^2 E_{\mathrm{elec}}/\partial R^2|_{R=R_{\mathrm{e}}}$, the "force constant" of the chemical bond formed by the two nuclei.

Based on the same argument, namely that R deviates only sightly from R_{e}, we have also replaced R in (2.144) by R_{e} and thus treat the diatomic molecule as a rigid rotating object ("rigid rotor approximation").

By defining a shifted vibrational function $\widetilde{\psi}_{\mathrm{vib}}$ according to $\psi_{\mathrm{vib}}(R) = \widetilde{\psi}_{\mathrm{vib}}(R-R_{\mathrm{e}})$ and the variable,

$$W = E_{\mathrm{int}} - E_{\mathrm{elec},n}(R_{\mathrm{e}}) - \frac{\hbar^2 J(J+1)}{2M_{\mathrm{eff}}{R_{\mathrm{e}}}^2}, \tag{2.150}$$

we get the following vibrational equation:

$$\left[-\frac{\hbar^2}{2M_{\mathrm{eff}}}\frac{\partial^2}{\partial\zeta^2} + \frac{1}{2}k_n\zeta^2\right]\widetilde{\psi}_{\mathrm{vib}}(\zeta) = W\widetilde{\psi}_{\mathrm{vib}}(\zeta). \tag{2.151}$$

This is the Schrödinger equation of a harmonic oscillator with the solutions (see, e.g., [72, 70]):

$$\widetilde{\psi}_{\mathrm{vib},v}(\zeta) = \left(\frac{\xi^2}{\pi}\right)^{1/4}\frac{1}{(2^v v!)^{1/2}}H_v(\xi\zeta)\exp\left(-\frac{\xi^2\zeta^2}{2}\right), \tag{2.152}$$

where the "vibrational quantum number" $v = 0, 1, 2, \ldots$ has been introduced to label the different solutions.[18] H_v denotes the Hermite polynomial [72] of order v and ξ is,

$$\xi = \sqrt{\frac{M_{\text{eff}}\omega_{\text{e},n}}{\hbar}}, \tag{2.153}$$

with the (angular) vibration frequency,

$$\omega_{\text{e},n} = \sqrt{\frac{k_n}{M_{\text{eff}}}}. \tag{2.154}$$

Collecting these results, we may conclude that the internal quantum state of a diatomic molecule in a $^1\Sigma$ electronic state can be approximately represented by the wavefunction,

$$\psi_{\text{int}}(\mathbf{R}, \mathbf{r}_1, \mathbf{r}_2, ..., \mathbf{r}_N) = \psi_{\text{elec},n}(\mathbf{R}, \mathbf{r}_1, \mathbf{r}_2, ..., \mathbf{r}_N)\frac{1}{R}\psi_{\text{vib},v}(R)Y_{JM}(\theta, \phi) \tag{2.155}$$

with θ and ϕ the polar and azimuthal angles of $\mathbf{R}$ when expressed in spherical coordinates and ψ_{vib} a (shifted) harmonic oscillator wavefunction.

2.3.2 Rotation-vibration transitions due to the electric-dipole operator

Having found suitable approximate internal quantum states for a diatomic molecule, we can now study transitions between these states due to the interaction with electromagnetic radiation. The separation of the different degrees of freedom of a diatomic molecule—rotational, vibrational and electronic—turns out to be very fruitful and will considerably simplify the description of such transitions. In particular, we will study here rotation-vibration transitions. First, electric-dipole transitions will be treated, thereafter transitions due to the electric-quadrupole operator.

To describe electric-dipole transitions in a molecule, the single-particle electric-dipole operator $\hat{\boldsymbol{\mu}}$ introduced in Sec. 2.2.4 needs to be replaced by a many-particle operator, which is given by the sum of the single-particle position operators multiplied with the corresponding charges. For a diatomic molecule, this many-particle electric-dipole operator can be written (using the notation from above) as,

$$\hat{\boldsymbol{\mu}}^{(\text{s})} = -e\sum_{j=1}^{N}\hat{\mathbf{r}}_j + q_1\hat{\mathbf{R}}_1 + q_2\hat{\mathbf{R}}_2. \tag{2.156}$$

The superscript $^{(\text{s})}$ has been added to make clear that this definition is given in the space-fixed coordinate system.

The states of the unperturbed molecule, i.e., the counterparts of the states $|\psi_\text{a}\rangle$ and $|\psi_\text{b}\rangle$ from Sec. 2.2.1,

[18] Strictly speaking, the vibrational equation for a diatomic molecule differs from the one-dimensional harmonic-oscillator equation by the boundary conditions. For the latter, the wavefunction is supposed to vanish for $\pm\infty$, whereas for the former this should be the case for 0 (i.e., both nuclei are at the same position) and $+\infty$ (nuclei at infinite distance). Since the harmonic approximation is only applicable to energetically low-lying vibrational states and as their wavefunctions decrease quickly in magnitude unless $R \approx R_\text{e}$, this does not pose a problem (see also [70]).

are given by the internal molecular wavefunction just determined, i.e.,

$$\langle \mathbf{R}, \mathbf{r}_1, \mathbf{r}_2, ..., \mathbf{r}_N \,|\, \psi_\mathrm{a} \rangle = \psi_{\mathrm{elec},n}(\mathbf{R}, \mathbf{r}_1, \mathbf{r}_2, ..., \mathbf{r}_N) R^{-1} \psi_{\mathrm{vib},v''}(R) Y_{J''M''}(\theta, \phi) \tag{2.157a}$$

$$\langle \mathbf{R}, \mathbf{r}_1, \mathbf{r}_2, ..., \mathbf{r}_N \,|\, \psi_\mathrm{b} \rangle = \psi_{\mathrm{elec},n}(\mathbf{R}, \mathbf{r}_1, \mathbf{r}_2, ..., \mathbf{r}_N) R^{-1} \psi_{\mathrm{vib},v'}(R) Y_{J'M'}(\theta, \phi), \tag{2.157b}$$

where the angles $\theta = \theta(\mathbf{R})$ and $\phi = \phi(\mathbf{R})$ are understood as functions of $\mathbf{R}$. The labels "a" and "b" stand now for the two tuples of quantum numbers (n, v'', J'', M'') and (n, v', J', M'), where we have adopted the common spectroscopic notation with double primed ($''$) and single primed ($'$) symbols for the lower and upper quantum state, respectively. Transitions between these states due to the electric-dipole operator are given by the transition matrix element that takes the form of a multiple integral over the full space of all nuclear and electronic coordinates,

$$\begin{aligned}\left\langle \psi_\mathrm{b} \,\middle|\, \hat{\boldsymbol{\mu}}^{(\mathrm{s})} \,\middle|\, \psi_\mathrm{a} \right\rangle = \int \int_{...} \int \psi^*_{\mathrm{elec},n}(\mathbf{R}, \mathbf{r}_1, \mathbf{r}_2, ..., \mathbf{r}_N) R^{-1} \psi^*_{\mathrm{vib},v'}(R) Y^*_{J'M'}(\theta, \phi) \hat{\boldsymbol{\mu}}^{(\mathrm{s})} \\ \psi_{\mathrm{elec},n}(\mathbf{R}, \mathbf{r}_1, \mathbf{r}_2, ..., \mathbf{r}_N) R^{-1} \psi_{\mathrm{vib},v''}(R) Y_{J''M''}(\theta, \phi) \,\mathrm{d}^3\mathbf{r}_1 \,\mathrm{d}^3\mathbf{r}_2 ... \,\mathrm{d}^3\mathbf{r}_N \,\mathrm{d}^3\mathbf{R},\end{aligned} \tag{2.158}$$

where again the angles $\theta = \theta(\mathbf{R})$ and $\phi = \phi(\mathbf{R})$ depend on $\mathbf{R}$. The transition matrix element can be simplified when collecting the electronic terms:

$$\begin{aligned}\left\langle \psi_\mathrm{b} \,\middle|\, \hat{\boldsymbol{\mu}}^{(\mathrm{s})} \,\middle|\, \psi_\mathrm{a} \right\rangle = \int R^{-1} \psi^*_{\mathrm{vib},v'}(R) Y^*_{J'M'}(\theta, \phi) \\ \left[\int_{...} \int \psi^*_{\mathrm{elec},n}(\mathbf{R}, \mathbf{r}_1, \mathbf{r}_2, ..., \mathbf{r}_N) \hat{\boldsymbol{\mu}}^{(\mathrm{s})} \psi_{\mathrm{elec},n}(\mathbf{R}, \mathbf{r}_1, \mathbf{r}_2, ..., \mathbf{r}_N) \,\mathrm{d}^3\mathbf{r}_1 \,\mathrm{d}^3\mathbf{r}_2 ... \,\mathrm{d}^3\mathbf{r}_N \right] \\ R^{-1} \psi_{\mathrm{vib},v''}(R) Y_{J''M''}(\theta, \phi) \,\mathrm{d}^3\mathbf{R}.\end{aligned} \tag{2.159}$$

Because the electronic state n is equal for the lower and the upper state of a rotation-vibration transition, the term in brackets is exactly the dipole moment of the molecule in the electronic state n or, more precisely, the expectation value of the dipole operator in the electronic state n at a certain value for $\mathbf{R}$. Thus we get for the transition matrix element,

$$\left\langle \psi_\mathrm{b} \,\middle|\, \hat{\boldsymbol{\mu}}^{(\mathrm{s})} \,\middle|\, \psi_\mathrm{a} \right\rangle = \int R^{-1} \psi^*_{\mathrm{vib},v'}(R) Y^*_{J'M'}(\theta, \phi) \boldsymbol{\mu}^{(\mathrm{s})}_n(\mathbf{R}) R^{-1} \psi_{\mathrm{vib},v''}(R) Y_{J''M''}(\theta, \phi) \,\mathrm{d}^3\mathbf{R}, \tag{2.160}$$

with the expectation value,

$$\boldsymbol{\mu}^{(\mathrm{s})}_n(\mathbf{R}) = \left\langle \psi_{\mathrm{elec},n}(\mathbf{R}) \,\middle|\, \hat{\boldsymbol{\mu}}^{(\mathrm{s})} \,\middle|\, \psi_{\mathrm{elec},n}(\mathbf{R}) \right\rangle \tag{2.161}$$

$$= \int_{...} \int \psi^*_{\mathrm{elec},n}(\mathbf{R}, \mathbf{r}_1, \mathbf{r}_2, ..., \mathbf{r}_N) \hat{\boldsymbol{\mu}}^{(\mathrm{s})} \psi_{\mathrm{elec},n}(\mathbf{R}, \mathbf{r}_1, \mathbf{r}_2, ..., \mathbf{r}_N) \,\mathrm{d}^3\mathbf{r}_1 \,\mathrm{d}^3\mathbf{r}_2 ... \,\mathrm{d}^3\mathbf{r}_N. \tag{2.162}$$

Because $\mathbf{R}$ is treated as a parameter in the electronic states, we replace in the dipole operator from equation (2.156) the position operators of the nuclei $\hat{\mathbf{R}}_1$ and $\hat{\mathbf{R}}_2$ by the corresponding vectors $\mathbf{R}_1$ and

$\mathbf{R}_2$ multiplied with the identity operator on the electronic coordinates $\hat{\mathbf{I}}_{\text{elec}}$, i.e., we redefine[19]

$$\hat{\boldsymbol{\mu}}^{(\text{s})} = -e\sum_{j=1}^{N}\hat{\mathbf{r}}_j + \hat{\mathbf{I}}_{\text{elec}}q_1\mathbf{R}_1 + \hat{\mathbf{I}}_{\text{elec}}q_2\mathbf{R}_2 \tag{2.163}$$

$$= -e\sum_{j=1}^{N}\hat{\mathbf{r}}_j + \hat{\mathbf{I}}_{\text{elec}}\mathbf{R}\left(q_1\frac{M_2}{M_1+M_2} - q_2\frac{M_1}{M_1+M_2}\right), \tag{2.164}$$

where $\mathbf{R}_1$ and $\mathbf{R}_2$ have been substituted using equation (2.135).

To exploit the symmetry of a diatomic molecule, we switch to a coordinate system with the z-axis aligned with the internuclear axis of the molecule. This is known as the "molecule-fixed" system. In this system the dipole operator is given as,

$$\hat{\boldsymbol{\mu}}^{(\text{m})} = \hat{\boldsymbol{\mu}}^{(\text{m})}_{\text{elec}} + \hat{\mathbf{I}}_{\text{elec}}R\mathbf{e}^{(\text{m})}_{\text{z}}\left(q_1\frac{M_2}{M_1+M_2} - q_2\frac{M_1}{M_1+M_2}\right), \tag{2.165}$$

with $\mathbf{e}^{(\text{m})}_{\text{z}}$ a unit vector along the z-axis and the purely electronic dipole operator given by,

$$\hat{\boldsymbol{\mu}}^{(\text{m})}_{\text{elec}} = -e\sum_{j=1}^{N}\hat{\mathbf{r}}^{(\text{m})}_j, \tag{2.166}$$

where $\hat{\mathbf{r}}^{(\text{m})}_j$ denote the position operators of the electrons in the molecule-fixed system.

The electronic contribution to the dipole moment is given by the expectation value of the electronic dipole operator, namely:

$$\boldsymbol{\mu}^{(\text{m})}_{\text{elec},n}(R) = \left\langle \psi^{(\text{m})}_{\text{elec},n}(R)\,\middle|\,\hat{\boldsymbol{\mu}}^{(\text{m})}_{\text{elec}}\,\middle|\,\psi^{(\text{m})}_{\text{elec},n}(R)\right\rangle \tag{2.167}$$

$$= \int_{\dots}\int \psi^{(\text{m})*}_{\text{elec},n}(R,\mathbf{r}^{(\text{m})}_1,\mathbf{r}^{(\text{m})}_2,\dots,\mathbf{r}^{(\text{m})}_N)\hat{\boldsymbol{\mu}}^{(\text{m})}_{\text{elec}}\psi^{(\text{m})}_{\text{elec},n}(R,\mathbf{r}^{(\text{m})}_1,\mathbf{r}^{(\text{m})}_2,\dots,\mathbf{r}^{(\text{m})}_N)\,\mathrm{d}^3\mathbf{r}^{(\text{m})}_1\,\mathrm{d}^3\mathbf{r}^{(\text{m})}_2\dots\,\mathrm{d}^3\mathbf{r}^{(\text{m})}_N. \tag{2.168}$$

Here, we have omitted the explicit vector notation of the internuclear vector because it is always aligned with the z-axis in the molecule-fixed system.

Because the dipole operator is a sum of position operators and because the position operators in a position basis merely appear as a multiplication by the corresponding position vectors, the above expression is just a sum of integrals of the squared absolute value of the electronic wavefunction multiplied by the electronic position vectors. As the absolute value of a many-particle wavefunction does not change upon permutation of its arguments, this expression may be rewritten in a more compact and easier comprehensible form using the particle density of the electrons $\rho(\mathbf{r})$. This density is given by the square of the absolute value of the many-particle wavefunction integrated over all but

[19] We adopt the usual convention that in single-particle operators acting in a many-particle tensor product Hilbert space, identity operators are understood for all but the explicitly mentioned particles (see, e.g., [72], pp. 135ff.). Therefore, the electron position operators $\hat{\mathbf{r}}_j$ implicitly embody identity operators for all electrons with indices $\neq j$ as well as for the nuclear coordinates. However, due to the Born-Oppenheimer approximation, no quantum mechanical operators appear in the middle and the right most summand in (2.163), therefore the identity operator for the electronic coordinates has been written explicitly in these terms.

one of the single-particle position vectors [73, 74]:

$$\rho(R,\mathbf{r}^{(\mathrm{m})}) = N\int_{\dots}\int \psi^{(\mathrm{m})*}_{\mathrm{elec},n}(R,\mathbf{r}^{(\mathrm{m})},\mathbf{r}^{(\mathrm{m})}_2,\dots,\mathbf{r}^{(\mathrm{m})}_N)\psi^{(\mathrm{m})}_{\mathrm{elec},n}(R,\mathbf{r}^{(\mathrm{m})},\mathbf{r}^{(\mathrm{m})}_2,\dots,\mathbf{r}^{(\mathrm{m})}_N)\,\mathrm{d}^3\mathbf{r}^{(\mathrm{m})}_2\,\mathrm{d}^3\mathbf{r}^{(\mathrm{m})}_3\dots\mathrm{d}^3\mathbf{r}^{(\mathrm{m})}_N. \tag{2.169}$$

Using this definition, the electronic contribution to the dipole moment is calculated as,

$$\boldsymbol{\mu}^{(\mathrm{m})}_{\mathrm{elec},n}(R) = -e\int \mathbf{r}^{(\mathrm{m})}\rho(R,\mathbf{r}^{(\mathrm{m})})\,\mathrm{d}^3\mathbf{r}^{(\mathrm{m})}, \tag{2.170}$$

and the total dipole moment takes on the form:

$$\boldsymbol{\mu}^{(\mathrm{m})}_{n}(R) = -e\int \mathbf{r}^{(\mathrm{m})}\rho(R,\mathbf{r}^{(\mathrm{m})})\,\mathrm{d}^3\mathbf{r}^{(\mathrm{m})} + R\mathbf{e}^{(\mathrm{m})}_{\mathrm{z}}\left(q_1\frac{M_2}{M_1+M_2} - q_2\frac{M_1}{M_1+M_2}\right). \tag{2.171}$$

Molecular dipole moments are usually calculated in this form, see, e.g., [75].

For a diatomic molecule, the charge density in molecule-fixed coordinates is invariant under an inversion of the coordinates perpendicular to the internuclear axis:

$$\rho(R,(r^{(\mathrm{m})}_x,r^{(\mathrm{m})}_y,r^{(\mathrm{m})}_z)) = \rho(R,(-r^{(\mathrm{m})}_x,r^{(\mathrm{m})}_y,r^{(\mathrm{m})}_z)) = \rho(R,(r^{(\mathrm{m})}_x,-r^{(\mathrm{m})}_y,r^{(\mathrm{m})}_z)). \tag{2.172}$$

In other words, the electron density is an even function with respect to the x- and y-argument. As the position vector $\mathbf{r}^{(\mathrm{m})}$ is an odd function, the integrals for the x- and y-components of $\boldsymbol{\mu}^{(\mathrm{m})}_{\mathrm{elec},n}$ vanish. Because the nuclear part of the dipole moment, too, only exhibits a z-component, the total dipole moment does also only posses a z-component, the x- and y-component vanish.

Expressed in spherical tensor notation, this means that all but the zero component of the dipole moment in molecule-fixed coordinates vanish, whereas the former is equal to the z-component in Cartesian coordinates, i.e.,

$$\mathrm{T}^1_{\pm1}\left[\boldsymbol{\mu}^{(\mathrm{m})}_n(R)\right] = 0, \tag{2.173a}$$

$$\mathrm{T}^1_0\left[\boldsymbol{\mu}^{(\mathrm{m})}_n(R)\right] = \mu^{(\mathrm{m})}_{z,n}(R). \tag{2.173b}$$

For the subsequent calculation, the dipole moment must be expressed in space-fixed coordinates because the radiation field driving spectroscopic transitions is described in this frame of reference. This is accomplished by a Wigner rotation matrix $\mathscr{D}$ with the two Euler angles ϕ and θ [67, 60, 61]

$$\mathrm{T}^1_p\left[\boldsymbol{\mu}^{(\mathrm{s})}_n(R)\right] = \sum_{q=-1}^{1}\left[\mathscr{D}^{(1)}_{pq}(\phi,\theta,0)\right]^*\mathrm{T}^1_q\left[\boldsymbol{\mu}^{(\mathrm{m})}(R)\right] \tag{2.174}$$

$$= \left[\mathscr{D}^{(1)}_{p0}(\phi,\theta,0)\right]^*\mathrm{T}^1_0\left[\boldsymbol{\mu}^{(\mathrm{m})}(R)\right] \tag{2.175}$$

$$= \sqrt{\frac{4\pi}{3}}Y_{1\,p}(\theta,\phi)\mu^{(\mathrm{m})}_{z,n}(R). \tag{2.176}$$

The third Euler angle is of no relevance due to symmetry and is thus set to zero. The Wigner rotation matrix is therefore proportional to a spherical harmonic.

If we substitute this result into equation (2.160), adopt spherical tensor notation and use spherical coordinates for the integration ($\mathrm{d}^3\mathbf{R} = R^2\sin\theta\,\mathrm{d}\theta\,\mathrm{d}\phi\,\mathrm{d}R$), we get the following expression for the

electric-dipole transition matrix element:

$$\left\langle \psi_\mathrm{b} \left| \, \mathrm{T}^1_p \left[\hat{\boldsymbol{\mu}}^{(\mathrm{s})} \right] \right| \psi_\mathrm{a} \right\rangle = \sqrt{\frac{4\pi}{3}} \int_0^\infty \int_0^{2\pi} \int_0^\pi R^{-2} \, \psi^*_{\mathrm{vib},v'} \, \mu^{(\mathrm{m})}_{z,n}(R) \, \psi_{\mathrm{vib},v''}(R) \\ Y^*_{J'M'}(\theta,\phi) Y_{1p}(\theta,\phi) Y_{J''M''}(\theta,\phi) \, R^2 \sin\theta \, \mathrm{d}\theta \, \mathrm{d}\phi \, \mathrm{d}R \tag{2.177}$$

$$= \mathscr{A}(J', M', J'', M'', p) \, \mathscr{R}(v', v''). \tag{2.178}$$

As indicated above, this expression factorizes into an angular (rotational) term

$$\mathscr{A}(J', M', J'', M'', p) = \sqrt{\frac{4\pi}{3}} \int_0^{2\pi} \int_0^\pi Y^*_{J'M'}(\theta,\phi) Y_{1p}(\theta,\phi) Y_{J''M''}(\theta,\phi) \sin\theta \, \mathrm{d}\theta \, \mathrm{d}\phi \tag{2.179}$$

and a radial (vibrational) term

$$\mathscr{R}(v', v'') = \int_0^\infty \psi^*_{\mathrm{vib},v'}(R) \, \mu^{(\mathrm{m})}_{z,n}(R) \, \psi_{\mathrm{vib},v''}(R) \, \mathrm{d}R. \tag{2.180}$$

The angular term can be conveniently calculated with the Wigner-Eckart theorem [61, 62, 76]. Using this theorem together with the particular value of $\mathscr{A}$ for vanishing projection quantum numbers,

$$\mathscr{A}(J', 0, J'', 0, 0) = \sqrt{2J'+1}\sqrt{2J''+1} \begin{pmatrix} J' & 1 & J'' \\ 0 & 0 & 0 \end{pmatrix}^2, \tag{2.181}$$

to get the reduced matrix element, we obtain the result:

$$\mathscr{A}(J', M', J'', M'', p) = (-1)^{M'} \sqrt{2J'+1}\sqrt{2J''+1} \begin{pmatrix} J' & 1 & J'' \\ -M' & p & M'' \end{pmatrix} \begin{pmatrix} J' & 1 & J'' \\ 0 & 0 & 0 \end{pmatrix}. \tag{2.182}$$

Here, the double-row symbols in parentheses are Wigner 3j-symbols [77, 61, 62, 76]. Based on their properties, we obtain the angular momentum selection rules for an electric-dipole rotation-vibration transition within an electronic $^1\Sigma$ state. The 3j-symbols vanish if their upper row does not fulfill the "triangle condition" or if the sum of the lower row is not equal to zero. We thus get the following well-known selection rules for the change in the magnitude of the angular momentum $\Delta J = J' - J''$ and its projection on the space-fixed z-axis $\Delta M = M' - M''$:

$$\Delta J = \pm 1, \tag{2.183}$$

$$\Delta M = 0, \pm 1. \tag{2.184}$$

In order to calculate the radial term, we need to know the electric-dipole moment as a function of the internuclear separation R. For an approximate treatment, however, we may proceed in a similar way as we have done for the potential energy curve in the last section and make use of R being normally restricted to values close to R_e. Thus, we expand the dipole moment in a Taylor series up to linear order around R_e:

$$\mu^{(\mathrm{m})}_{z,n}(R) \approx \mu^{(\mathrm{m})}_{z,n}(R_\mathrm{e}) + (R - R_\mathrm{e}) \left. \frac{\mathrm{d}\mu^{(\mathrm{m})}_{z,n}}{\mathrm{d}R} \right|_{R=R_\mathrm{e}}. \tag{2.185}$$

In this approximation, we get:

$$\mathscr{R}(v', v'') = \mu_{z,n}^{(\mathrm{m})}(R_\mathrm{e}) \int_0^\infty \psi_{\mathrm{vib},v'}^*(R)\psi_{\mathrm{vib},v''}(R)\,\mathrm{d}R + \left.\frac{\mathrm{d}\mu_{z,n}^{(\mathrm{m})}}{\mathrm{d}R}\right|_{R=R_\mathrm{e}} \int_0^\infty \psi_{\mathrm{vib},v'}^*(R)\,(R-R_\mathrm{e})\,\psi_{\mathrm{vib},v''}(R)\,\mathrm{d}R. \tag{2.186}$$

The first integral in this expression vanishes because vibrational wavefunctions with $v' \neq v''$ (which is given by definition in a vibrational transition) are orthogonal to each other. The second integral can be approximated using the harmonic vibrational states introduced in the last section. With the variable $\zeta = R - R_\mathrm{e}$ and the corresponding position operator $\hat{\zeta}$ we obtain

$$\int_0^\infty \psi_{\mathrm{vib},v'}^*(R)\,(R-R_\mathrm{e})\,\psi_{\mathrm{vib},v''}(R)\,\mathrm{d}R = \int_{-R_\mathrm{e}}^\infty \widetilde{\psi}_{\mathrm{vib},v'}^*(\zeta)\,\zeta\,\widetilde{\psi}_{\mathrm{vib},v''}(\zeta)\,\mathrm{d}\zeta \tag{2.187}$$

$$\approx \int_{-\infty}^\infty \widetilde{\psi}_{\mathrm{vib},v'}^*(\zeta)\,\zeta\,\widetilde{\psi}_{\mathrm{vib},v''}(\zeta)\,\mathrm{d}\zeta \tag{2.188}$$

$$= \left\langle \widetilde{\psi}_{\mathrm{vib},v'} \,\middle|\, \hat{\zeta} \,\middle|\, \widetilde{\psi}_{\mathrm{vib},v''} \right\rangle, \tag{2.189}$$

where we have used that the vibrational wavefunction rapidly decreases in magnitude for $|R - R_\mathrm{e}| = |\zeta| \gg 0$ such that the integral may be extended to $-\infty$. The radial integral is thus approximated as,

$$\mathscr{R}(v', v'') \approx \left.\frac{\mathrm{d}\mu_{\mathrm{z,n}}^{(\mathrm{m})}}{\mathrm{d}R}\right|_{R=R_\mathrm{e}} \left\langle \widetilde{\psi}_{\mathrm{vib},v'} \,\middle|\, \hat{\zeta} \,\middle|\, \widetilde{\psi}_{\mathrm{vib},v''} \right\rangle. \tag{2.190}$$

The position operator $\hat{\zeta}$ may be written with the raising and lowering operators, $\hat{a}^\dagger$ and $\hat{a}$, and the constant ξ from (2.153) as [72]:

$$\hat{\zeta} = \frac{1}{\sqrt{2}\xi}\left(\hat{a}^\dagger + \hat{a}\right). \tag{2.191}$$

Because the raising and lowering operators $\hat{a}^\dagger$ and $\hat{a}$ change the vibrational quantum number v by ± 1, the following selection rule for the change in the vibrational quantum number $\Delta v = v' - v''$ for an electric-dipole rotation-vibration transition is obtained:

$$\Delta v = \pm 1. \tag{2.192}$$

Note that this selection rule is only valid within the so-called "double-harmonic approximation", meaning that we have assumed harmonic oscillator states for the vibrational states ("mechanical harmonicity") and have neglected all terms higher in order than the linear one in the Taylor expansion of the dipole moment ("electrical harmonicity") [78, 79, 30].

The line strength for an electric-dipole rotation-vibration transition is given, as for a single-particle system discussed in Sec. 2.2.7, by the squared absolute magnitude of the transition matrix element summed over all spherical tensor components and all degenerate states in the upper and lower level,

i.e.,

$$S_{\mathrm{ba}}^{(\mathrm{E1})} = \sum_{M'=-J'}^{J'} \sum_{M''=-J''}^{J''} \sum_{p=-1}^{1} \left| \left\langle \psi_{\mathrm{b}} \left| \, \mathrm{T}_p^1 \left[\hat{\boldsymbol{\mu}}^{(\mathrm{s})} \right] \right| \psi_{\mathrm{a}} \right\rangle \right|^2 \tag{2.193}$$

$$= \sum_{M'=-J'}^{J'} \sum_{M''=-J''}^{J''} \sum_{p=-1}^{1} \left| \mathscr{A}(J', M', J'', M'', p) \right|^2 \left| \mathscr{R}(v', v'') \right|^2 \tag{2.194}$$

$$= (2J'+1)(2J''+1) \begin{pmatrix} J' & 1 & J'' \\ 0 & 0 & 0 \end{pmatrix}^2 \left| \mathscr{R}(v', v'') \right|^2 . \tag{2.195}$$

To derive the last equation, the orthogonality properties of the 3j-symbols have been used.

Concluding, we have shown that a rotation-vibration transition in a diatomic molecule within a certain electronic state can only be induced by the electric-dipole operator, if the dipole moment (meaning the expectation value of the dipole operator in that particular electronic state) does change as a function of the internuclear separation (see equation (2.186)).

For a homonuclear diatomic molecule, an additional symmetry, besides those discussed above, exists: the electron density is not only invariant under an inversion of the coordinates perpendicular to the molecular axis (x- and y-coordinates), but also for the coordinate along the internuclear axis (z-coordinate), i.e. $\rho(R, (r_x^{(\mathrm{m})}, r_y^{(\mathrm{m})}, r_z^{(\mathrm{m})})) = \rho(R, (r_x^{(\mathrm{m})}, r_y^{(\mathrm{m})}, -r_z^{(\mathrm{m})}))$. In the same way as shown above for the x- and y-components, the electronic contribution to the z-component of the dipole moment thus vanishes, too. Furthermore, the nuclear contribution to the dipole moment vanishes as well because we have in the homonuclear case, $M_1 = M_2$ and $q_1 = q_2$ in (2.171), i.e., the *total* molecular dipole moment vanishes.

As this argument holds for all possible internuclear separations, the dipole moment does also not change as a function of the internuclear distance. We thus arrive at the tenet mentioned in Ch. 1, saying that a diatomic molecule does not show rotation-vibration transitions within the electric-dipole approximation. However, as we have discussed further above, the electric-dipole operator represents just the first term in a series expansion of the Hamiltonian describing the interaction between matter and radiation, thus a discussion of the next-higher-order term is of interest.

2.3.3 Rotation-vibration transitions due to the electric-quadrupole operator

After having described how the interaction of the electromagnetic radiation with the charged particles in a diatomic molecule mediated by the electric-dipole operator may induce rotation-vibration transitions in this molecule, we now show, how such transitions may also be driven by the electric-quadrupole operator. Again, the separation of the many-particle wavefunction of a molecule into a rotational, a vibrational and an electronic function considerably simplifies the treatment—and justifies the terminology used. Also the symmetry of the molecule, once more, substantially simplifies the transition operator. The crucial result of this section is that the quadrupole operator may induce rotation-vibration transitions even in homonuclear, diatomic molecules where they do not occur due to the electric-dipole operator as we have shown in the last section.

Similar to the electric-dipole operator, the single-particle electric-quadrupole operator introduced in Sec. 2.2.5 needs to be replaced by the corresponding many-particle operator to describe electric-

quadrupole transitions in a molecule. When we use the same notation as above, the electric-quadrupole operator for a diatomic molecule reads:

$$\hat{Q}_{\alpha\beta} = -e\sum_{j=1}^{N}\left(\hat{r}_{j,\alpha}\hat{r}_{j,\beta} - \delta_{\alpha\beta}\frac{\hat{r}_j^2}{3}\right) + q_1\left(\hat{R}_{1,\alpha}\hat{R}_{1,\beta} - \delta_{\alpha\beta}\frac{\hat{R}_1^2}{3}\right) + q_2\left(\hat{R}_{2,\alpha}\hat{R}_{2,\beta} - \delta_{\alpha\beta}\frac{\hat{R}_2^2}{3}\right). \quad (2.196)$$

In contrast to the last section, where the dipole-operator was treated as a vector operator, a componentwise notation is adopted here, i.e., the transition matrix element of one particular component of the quadrupole tensor operator $\hat{Q}_{\alpha\beta}$ (with $\alpha, \beta = x, y, z$) is studied.

The matrix element of this operator for a transition between the molecular rovibronic quantum states $|\psi_\mathrm{a}\rangle$ and $|\psi_\mathrm{b}\rangle$ from (2.157) is given by,

$$\left\langle \psi_\mathrm{b} \middle| \hat{Q}_{\alpha\beta} \middle| \psi_\mathrm{a} \right\rangle = \int\!\!\int_{...}\!\!\int \psi^*_{\mathrm{elec},n}(\mathbf{R}, \mathbf{r}_1, \mathbf{r}_2, ..., \mathbf{r}_N) R^{-1} \psi^*_{\mathrm{vib},v'}(R) Y^*_{J'M'}(\theta,\phi)\, \hat{Q}_{\alpha\beta}$$
$$\psi_{\mathrm{elec},n}(\mathbf{R}, \mathbf{r}_1, \mathbf{r}_2, ..., \mathbf{r}_N) R^{-1} \psi_{\mathrm{vib},v''}(R) Y_{J''M''}(\theta,\phi)\, \mathrm{d}^3\mathbf{r}_1\, \mathrm{d}^3\mathbf{r}_2 \ldots \mathrm{d}^3\mathbf{r}_N\, \mathrm{d}^3\mathbf{R}, \quad (2.197)$$

where the angles $\theta = \theta(\mathbf{R})$ and $\phi = \phi(\mathbf{R})$ are understood as functions of $\mathbf{R}$.

The terms involving the electronic coordinates may again be collected into a separate integral. Because we are interested in rotation-vibration transitions within the same electronic state, this integral represents the electric-quadrupole moment of the molecule in the electronic state n, or, more precisely, the expectation value of the electric-quadrupole operator in the electronic state n. Doing so, the transition matrix element reads,

$$\left\langle \psi_\mathrm{b} \middle| \hat{Q}_{\alpha\beta} \middle| \psi_\mathrm{a} \right\rangle = \int R^{-1} \psi^*_{\mathrm{vib},v'}(R) Y^*_{J'M'}(\theta,\phi)\, Q_{\alpha\beta,n}(\mathbf{R})\, R^{-1} \psi_{\mathrm{vib},v''}(R) Y_{J''M''}(\theta,\phi)\, \mathrm{d}^3\mathbf{R}, \quad (2.198)$$

with the electric-quadrupole moment in the electronic state n given by:

$$Q_{\alpha\beta,n}(\mathbf{R}) = \left\langle \psi_{\mathrm{elec},n}(\mathbf{R}) \middle| \hat{Q}_{\alpha\beta} \middle| \psi_{\mathrm{elec},n}(\mathbf{R}) \right\rangle \quad (2.199)$$
$$= \int\!\!\int_{...}\!\!\int \psi^*_{\mathrm{elec},n}(\mathbf{R}, \mathbf{r}_1, \mathbf{r}_2, ..., \mathbf{r}_N)\, \hat{Q}_{\alpha\beta}\, \psi_{\mathrm{elec},n}(\mathbf{R}, \mathbf{r}_1, \mathbf{r}_2, ..., \mathbf{r}_N)\, \mathrm{d}^3\mathbf{r}_1\, \mathrm{d}^3\mathbf{r}_2 \ldots \mathrm{d}^3\mathbf{r}_N. \quad (2.200)$$

Similar as in the case of the electric-dipole moment, the electric-quadrupole moment, too, is a function of the internuclear vector $\mathbf{R}$, since both, the contribution to the quadrupole moment due to the nuclei as well as the one due to the electrons (via the dependence of the electronic wavefunctions), depend on $\mathbf{R}$. As $\mathbf{R}$ appears as a parameter in the electronic wavefunction, we treat the position operators $\hat{\mathbf{R}}_1$ and $\hat{\mathbf{R}}_2$ in the quadrupole operator in the same way as we did for the dipole operator in the last section, i.e., we replace them by the corresponding vectors $\mathbf{R}_1$ and $\mathbf{R}_2$ multiplied with the identity operator for the electronic coordinates $\hat{I}_\mathrm{elec}$. Hence we rewrite the electric-quadrupole operator as:

$$\hat{Q}_{\alpha\beta} = -e\sum_{j=1}^{N}\left(\hat{r}_{j,\alpha}\hat{r}_{j,\beta} - \delta_{\alpha\beta}\frac{\hat{r}_j^2}{3}\right)$$
$$+ \hat{I}_\mathrm{elec} q_1\left(R_{1,\alpha}R_{1,\beta} - \delta_{\alpha\beta}\frac{R_1^2}{3}\right) + \hat{I}_\mathrm{elec} q_2\left(R_{2,\alpha}R_{2,\beta} - \delta_{\alpha\beta}\frac{R_2^2}{3}\right). \quad (2.201)$$

Substituting, $\mathbf{R}_1$ and $\mathbf{R}_2$ by equation (2.135) we obtain:

$$\begin{aligned}\hat{Q}_{\alpha\beta} =& -e\sum_{j=1}^{N}\left(\hat{r}_{j,\alpha}\hat{r}_{j,\beta}-\delta_{\alpha\beta}\frac{\hat{r}_j^2}{3}\right)\\ &+\hat{I}_{\text{elec}}\left(R_\alpha R_\beta-\delta_{\alpha\beta}\frac{R^2}{3}\right)\left(q_1\frac{M_2}{M_1+M_2}+q_2\frac{M_1}{M_1+M_2}\right).\end{aligned} \tag{2.202}$$

In order to take advantage of the symmetry of diatomic molecules, we again switch to molecule-fixed coordinates and separate the quadrupole operator into an electronic and a nuclear part,

$$\hat{Q}^{(\mathrm{m})}_{\alpha\beta} = \hat{Q}^{(\mathrm{m})}_{\text{elec},\alpha\beta} + \hat{Q}^{(\mathrm{m})}_{\text{nucl},\alpha\beta}. \tag{2.203}$$

Since the nuclei are located along the molecule-fixed z-axis, the nuclear part can be simplified, yielding

$$\hat{Q}^{(\mathrm{m})}_{\text{nucl},\alpha\beta} = \hat{I}_{\text{elec}}R^2\delta_{\alpha\beta}\left(\delta_{\alpha z}-\frac{1}{3}\right)\left(q_1\frac{M_2}{M_1+M_2}+q_2\frac{M_1}{M_1+M_2}\right). \tag{2.204}$$

As indicated by the Kronecker delta $\delta_{\alpha\beta}$, the nuclear part of the electric-quadrupole operator exhibits only diagonal Cartesian components in molecule-fixed coordinates. Furthermore, the xx- and yy-components are equal: $\hat{Q}^{(\mathrm{m})}_{\text{nucl},xx} = \hat{Q}^{(\mathrm{m})}_{\text{nucl},yy}$.

The electronic part of the electric-quadrupole operator is given by,

$$\hat{Q}^{(\mathrm{m})}_{\text{elec},\alpha\beta} = -e\sum_{j=1}^{N}\left(\hat{r}_{j,\alpha}\hat{r}_{j,\beta}-\delta_{\alpha\beta}\frac{\hat{r}_j^2}{3}\right), \tag{2.205}$$

and the electronic quadrupole *moment* is obtained as the expectation value of this operator in the electronic state n, i.e.,

$$Q^{(\mathrm{m})}_{\text{elec},n,\alpha\beta}(R) = \left\langle \psi^{(\mathrm{m})}_{\text{elec},n}(R)\,\middle|\,\hat{Q}^{(\mathrm{m})}_{\text{elec},\alpha\beta}\,\middle|\,\psi^{(\mathrm{m})}_{\text{elec},n}(R)\right\rangle \tag{2.206}$$

$$\begin{aligned}&= \int_{\dots}\int \psi^{(\mathrm{m})*}_{\text{elec},n}(R,\mathbf{r}^{(\mathrm{m})}_1,\mathbf{r}^{(\mathrm{m})}_2,\dots,\mathbf{r}^{(\mathrm{m})}_N)\,\hat{Q}^{(\mathrm{m})}_{\text{elec},\alpha\beta}\\ &\quad \psi^{(\mathrm{m})}_{\text{elec},n}(R,\mathbf{r}^{(\mathrm{m})}_1,\mathbf{r}^{(\mathrm{m})}_2,\dots,\mathbf{r}^{(\mathrm{m})}_N)\,\mathrm{d}^3\mathbf{r}^{(\mathrm{m})}_1\,\mathrm{d}^3\mathbf{r}^{(\mathrm{m})}_2\dots\mathrm{d}^3\mathbf{r}^{(\mathrm{m})}_N.\end{aligned} \tag{2.207}$$

This expectation value can be expressed in terms of the electron density in a similar manner as we have done for the electric-dipole moment, namely as:

$$Q^{(\mathrm{m})}_{\text{elec},n,\alpha\beta}(R) = -e\int\left(r^{(\mathrm{m})}_\alpha r^{(\mathrm{m})}_\beta-\delta_{\alpha\beta}\frac{\left(r^{(\mathrm{m})}\right)^2}{3}\right)\rho(R,\mathbf{r}^{(\mathrm{m})})\,\mathrm{d}^3\mathbf{r}^{(\mathrm{m})} \tag{2.208}$$

Again, we can make use of the symmetries of the electron density in molecule-fixed coordinates. Doing so, we notice that the off-diagonal Cartesian components of the electronic part of the quadrupole moment tensor, i.e., $Q^{(\mathrm{m})}_{\text{elec},n,\alpha\beta}$ with $\alpha\neq\beta$, vanish: as $\rho(R,\mathbf{r}^{(\mathrm{m})})$ is an even function with respect to $r^{(\mathrm{m})}_x$ and $r^{(\mathrm{m})}_y$, i.e.,

$$\rho(R,(r^{(\mathrm{m})}_x,r^{(\mathrm{m})}_y,r^{(\mathrm{m})}_z)) = \rho(R,(-r^{(\mathrm{m})}_x,r^{(\mathrm{m})}_y,r^{(\mathrm{m})}_z)) = \rho(R,(r^{(\mathrm{m})}_x,-r^{(\mathrm{m})}_y,r^{(\mathrm{m})}_z)), \tag{2.209}$$

whereas the terms $r^{(\mathrm{m})}_\alpha$ and $r^{(\mathrm{m})}_\beta$ in (2.208) are odd functions and because $\alpha\neq\beta$ implies that at least

one of the indices α or β is x or y, the integral in (2.208) vanishes for $\alpha \neq \beta$. Furthermore, because ρ is invariant under permutation of the x- and y-coordinate, i.e.,

$$\rho(R, (r_x^{(\mathrm{m})}, r_y^{(\mathrm{m})}, r_z^{(\mathrm{m})})) = \rho(R, (r_y^{(\mathrm{m})}, r_x^{(\mathrm{m})}, r_z^{(\mathrm{m})})), \tag{2.210}$$

the first two diagonal components are equal: $Q^{(\mathrm{m})}_{\mathrm{elec},n,xx}(R) = Q^{(\mathrm{m})}_{\mathrm{elec},n,yy}(R)$.

As the same properties have already been shown for the nuclear part, we may conclude that the *total* quadrupole moment of the molecule shows these properties. The molecule-fixed coordinate system corresponds thus to the system of eigenvectors of the electric-quadrupole moment tensor mentioned in Sec. 2.2.6. Because the quadrupole moment tensor is also traceless, only one independent parameter appears in the quadrupole moment of a diatomic molecule in molecule-fixed coordinates. This is usually chosen to be $Q^{(\mathrm{m})}_{n,zz}$, which is then called *the* quadrupole moment of a certain molecule (in the electronic state n, which is often implicitly assumed as the ground state) [52]. Examples for electric-quadrupole moments of some diatomic molecules can be found in [80] and [75]. The particular values for N_2^+ are given in [45] based on a computational study.

Summarizing, we have,

$$Q^{(\mathrm{m})}_{n,\alpha\beta}(R) = 0 \quad \text{for} \quad \alpha \neq \beta, \tag{2.211}$$

and,

$$Q^{(\mathrm{m})}_{n,xx}(R) = Q^{(\mathrm{m})}_{n,yy}(R) = -\frac{1}{2} Q^{(\mathrm{m})}_{,n,zz}(R), \tag{2.212}$$

or written as a matrix,

$$\mathsf{Q}^{(\mathrm{m})}_n(R) = \begin{bmatrix} -\frac{1}{2}Q^{(\mathrm{m})}_{n,zz}(R) & 0 & 0 \\ 0 & -\frac{1}{2}Q^{(\mathrm{m})}_{n,zz}(R) & 0 \\ 0 & 0 & Q^{(\mathrm{m})}_{n,zz}(R) \end{bmatrix}. \tag{2.213}$$

In spherical tensor notation, these symmetries cause all but the zeroth component of the quadrupole moment to vanish in molecule-fixed coordinates, i.e.,

$$\mathrm{T}^2_q \left[\mathsf{Q}^{(\mathrm{m})}_n\right] = 0 \quad \text{for} \quad q = \pm 1, \pm 2, \tag{2.214a}$$

$$\mathrm{T}^2_0 \left[\mathsf{Q}^{(\mathrm{m})}_n\right] = \sqrt{\frac{3}{2}} Q^{(\mathrm{m})}_{n,zz}. \tag{2.214b}$$

The quadrupole moment in space-fixed coordinates is obtained, likewise as for the dipole moment, by a Wigner rotation matrix with the Euler angles ϕ and θ, which again is expressed as a spherical harmonic:

$$\mathrm{T}^2_p \left[\mathsf{Q}^{(\mathrm{s})}_n(R)\right] = \sum_{q=-2}^{2} \left[\mathscr{D}^{(2)}_{pq}(\phi, \theta, 0)\right]^* \mathrm{T}^2_q \left[\mathsf{Q}^{(\mathrm{m})}_n(R)\right] \tag{2.215}$$

$$= \left[\mathscr{D}^{(2)}_{p0}(\phi, \theta, 0)\right]^* \mathrm{T}^2_0 \left[\mathsf{Q}^{(\mathrm{m})}_n(R)\right] \tag{2.216}$$

$$= \sqrt{\frac{4\pi}{5}} Y_{2p}(\theta, \phi) \sqrt{\frac{3}{2}} Q^{(\mathrm{m})}_{n,zz}(R). \tag{2.217}$$

Upon substituting this result into (2.198), adopting spherical tensor notation and switching to spherical coordinates for the integration over $\mathbf{R}$, we obtain the following expression for the transition matrix

element:

$$\left\langle \psi_\mathrm{b} \left| \, \mathrm{T}_p^2 \left[\hat{\mathsf{Q}}_n^{(\mathrm{s})} \right] \right| \psi_\mathrm{a} \right\rangle = \sqrt{\frac{4\pi}{5}} \sqrt{\frac{3}{2}} \int_0^\infty \int_0^{2\pi} \int_0^\pi R^{-2} \, \psi^*_{\mathrm{vib},v'} \, Q^{(\mathrm{m})}_{n,zz}(R) \, \psi_{\mathrm{vib},v''}(R) \\ Y^*_{J'M'}(\theta,\phi) Y_{2p}(\theta,\phi) Y_{J''M''}(\theta,\phi) \, R^2 \sin\theta \, \mathrm{d}\theta \, \mathrm{d}\phi \, \mathrm{d}R \tag{2.218}$$

$$= \sqrt{\frac{3}{2}} \mathscr{A}(J', M', J'', M'', p) \, \mathscr{R}(v', v''). \tag{2.219}$$

Here, again a separation into an angular (rotational) part,

$$\mathscr{A}(J', M', J'', M'', p) = \sqrt{\frac{4\pi}{5}} \int_0^{2\pi} \int_0^\pi Y^*_{J'M'}(\theta,\phi) Y_{2p}(\theta,\phi) Y_{J''M''}(\theta,\phi) \sin\theta \, \mathrm{d}\theta \, \mathrm{d}\phi, \tag{2.220}$$

and radial (or vibrational) part,

$$\mathscr{R}(v', v'') = \int_0^\infty \psi^*_{\mathrm{vib},v'}(R) \, Q^{(\mathrm{m})}_{n,zz}(R) \, \psi_{\mathrm{vib},v''}(R) \, \mathrm{d}R, \tag{2.221}$$

has been achieved.

The angular part is again readily calculated using the Wigner-Eckart theorem with the reduced matrix element obtained from the particular value for vanishing projection quantum numbers. The result is

$$\mathscr{A}(J', M', J'', M'', p) = (-1)^{M'} \sqrt{2J'+1} \sqrt{2J''+1} \begin{pmatrix} J' & 2 & J'' \\ -M' & p & M'' \end{pmatrix} \begin{pmatrix} J' & 2 & J'' \\ 0 & 0 & 0 \end{pmatrix}. \tag{2.222}$$

From the properties of the 3j-symbols appearing in the above expression, the angular selection rules for an electric-quadrupole rotation-vibration transition within an electronic $^1\Sigma$ state are obtained, namely:

$$\Delta J = 0, \pm 2 \text{ (but not } J' = J'' = 0), \tag{2.223}$$

$$\Delta M = 0, \pm 1, \pm 2. \tag{2.224}$$

So, in contrast to electric-dipole transitions, the angular momentum quantum number may change by two in an electric-quadrupole transition. Formally, this reflects the character of the quadrupole tensor as a second-rank spherical tensor. Physically, the transfer of two units of angular momentum to (or from) the molecule is possible, because the molecule interacts with the "gradient" of the electric field over an extended region. If the interaction of the molecule with the electric field is pictured as an absorption (or emission) of a photon, this photon carries orbital angular momentum additional to its spin (with magnitude one) and the total angular momentum transferred to or from the molecule may thus be higher than one angular momentum unit [30].[20]

The radial term in (2.219) is calculated along the same lines as for an electric-dipole transition: in absence of precise information about the molecular electric-quadrupole moment as a function of the internuclear separation R, the quadrupole moment is expanded into a Taylor series up to the linear

[20] However, as mentioned at the beginning of this chapter, the electric field is treated here as a classical field. The concept of a photon does not fit in this description. Therefore, this pictures goes beyond the theory described here.

term around $R = R_\mathrm{e}$:

$$Q^{(\mathrm{m})}_{n,zz}(R) \approx Q^{(\mathrm{m})}_{n,zz}(R_\mathrm{e}) + (R - R_\mathrm{e}) \left.\frac{\mathrm{d}Q^{(\mathrm{m})}_{n,zz}}{\mathrm{d}R}\right|_{R=R_\mathrm{e}} . \tag{2.225}$$

This treatment is justified by calculations of the quadrupole moment of diatomic molecules showing a smooth variation with the internuclear separation (see e.g. [45] or [81]).

If, moreover, we approximate the vibrational states by the states of a shifted harmonic oscillator and extend the lower bound of the radial integral to $-\infty$, we get,

$$\mathscr{R}(v', v'') \approx \left.\frac{\mathrm{d}Q^{(\mathrm{m})}_{n,zz}}{\mathrm{d}R}\right|_{R=R_\mathrm{e}} \left\langle \widetilde{\psi}_{\mathrm{vib},v'} \middle| \hat{\zeta} \middle| \widetilde{\psi}_{\mathrm{vib},v''} \right\rangle . \tag{2.226}$$

In the double-harmonic approximation, we therefore obtain the same vibrational selection rule as for an electric-dipole rotation-vibration transition, i.e.,

$$\Delta v = \pm 1. \tag{2.227}$$

Within this approximation, we thus have $v' = v''+1$ and the matrix element in (2.226) can be calculated explicitly by expressing the position operator $\hat{\zeta}$ in terms of the raising and lowering operator:

$$\left\langle \widetilde{\psi}_{\mathrm{vib},v''+1} \middle| \hat{\zeta} \middle| \widetilde{\psi}_{\mathrm{vib},v''} \right\rangle = \frac{1}{\sqrt{2}\xi} \left\langle \widetilde{\psi}_{\mathrm{vib},v''+1} \middle| \left(\hat{a}^\dagger + \hat{a}\right) \middle| \widetilde{\psi}_{\mathrm{vib},v''} \right\rangle \tag{2.228}$$

$$= \frac{1}{\sqrt{2}\xi} \left(\sqrt{v''+1} \left\langle \widetilde{\psi}_{\mathrm{vib},v''+1} \middle| \widetilde{\psi}_{\mathrm{vib},v''+1} \right\rangle + \sqrt{v''} \left\langle \widetilde{\psi}_{\mathrm{vib},v''+1} \middle| \widetilde{\psi}_{\mathrm{vib},v''-1} \right\rangle \right) \tag{2.229}$$

$$= \frac{1}{\sqrt{2}\xi} \sqrt{v''+1}. \tag{2.230}$$

Here, as before, ξ denotes the characteristic constant of the harmonic oscillator wavefunctions given in (2.153). As ξ is not a quantity usually found in the spectroscopic literature, it is worth expressing it in terms of quantities usually given in the literature, such as the rotational constant B_e, the harmonic vibrational frequency ω_e and the equilibrium internuclear distance R_e of a molecule. Substituting the relation between the rotational constant B_e (in units of energy) and the effective mass M_eff [57],

$$B_\mathrm{e} = \frac{\hbar^2}{2 M_\mathrm{eff} R_\mathrm{e}^2}, \tag{2.231}$$

into equation (2.153), we get,

$$\xi = \sqrt{\frac{\hbar\omega_\mathrm{e}}{2 B_\mathrm{e} R_\mathrm{e}^2}}, \tag{2.232}$$

and thus:

$$\left\langle \widetilde{\psi}_{\mathrm{vib},v''+1} \middle| \hat{\zeta} \middle| \widetilde{\psi}_{\mathrm{vib},v''} \right\rangle = R_\mathrm{e} \sqrt{\frac{B_\mathrm{e}}{\hbar\omega_\mathrm{e}}} \sqrt{v''+1}. \tag{2.233}$$

In molecular spectroscopy, spectroscopic constants are often expressed in units of inverse length by referring to the inverse of the wavelength ("wave number") of electromagnetic radiation with a corresponding photon energy. The constants $\widetilde{B}_\mathrm{e}$ and $\widetilde{\omega}_\mathrm{e}$ in these units are related to those defined above

by,

$$\widetilde{B}_\mathrm{e} = \frac{B_\mathrm{e}}{2\pi\hbar c}, \tag{2.234}$$

$$\widetilde{\omega}_\mathrm{e} = \frac{\omega_\mathrm{e}}{2\pi c}, \tag{2.235}$$

such that we get:

$$\left\langle \widetilde{\psi}_{\mathrm{vib},v''+1} \,\middle|\, \hat{\zeta} \,\middle|\, \widetilde{\psi}_{\mathrm{vib},v''} \right\rangle = R_\mathrm{e}\sqrt{\frac{\widetilde{B}_\mathrm{e}}{\widetilde{\omega}_\mathrm{e}}}\sqrt{v''+1}. \tag{2.236}$$

The radial part of the transition matrix element of an electric-quadrupole rotation-vibration transition is thus given in the double-harmonic approximation as:

$$\mathscr{R}(v',v'') = \left.\frac{\mathrm{d}Q^{(\mathrm{m})}_{n,zz}}{\mathrm{d}R}\right|_{R=R_\mathrm{e}} R_\mathrm{e}\sqrt{\frac{\widetilde{B}_\mathrm{e}}{\widetilde{\omega}_\mathrm{e}}}\sqrt{v''+1}. \tag{2.237}$$

This result is given in equation (18) of [82].[21] It is usually used to estimate the intensity of an electric-quadrupole rotation-vibration transition, such as in [83, 33, 84].

The line strength of an electric-quadrupole rotation vibration-transition is, likewise as for a dipole transition, obtained by summing the squared absolute magnitude of the transition matrix element over all spherical tensor components of the quadrupole operator and all degenerate states in the upper and lower level, i.e.,

$$S^{(\mathrm{E2})}_\mathrm{ba} = \sum_{M'=-J'}^{J'}\sum_{M''=-J''}^{J''}\sum_{p=-2}^{2}\left|\left\langle \psi_\mathrm{b} \,\middle|\, \mathrm{T}^2_p\left[\hat{\mathrm{Q}}^{(\mathrm{s})}_n\right] \,\middle|\, \psi_\mathrm{a}\right\rangle\right|^2 \tag{2.238}$$

$$= \sum_{M'=-J'}^{J'}\sum_{M''=-J''}^{J''}\sum_{p=-2}^{2}\frac{3}{2}\left|\mathscr{A}(J',M',J'',M'',p)\right|^2\left|\mathscr{R}(v',v'')\right|^2 \tag{2.239}$$

$$= \frac{3}{2}(2J'+1)(2J''+1)\begin{pmatrix} J' & 2 & J'' \\ 0 & 0 & 0 \end{pmatrix}^2\left|\mathscr{R}(v',v'')\right|^2, \tag{2.240}$$

where we have once more made use of the orthogonality properties of the 3j-symbols.

The most remarkable difference between the electric-dipole and the electric-quadrupole operator from the point of view of molecular rotation-vibration spectroscopy is that the latter may induce rotation-vibration transitions even in homonuclear diatomic molecules. As mentioned in the last section, the electron density of a homonuclear diatomic molecule is an even function with respect to the inversion of the z-coordinate (as well as with respect to the x- and y-coordinates). However, as the prefactor $r_\alpha r_\alpha = r_\alpha^2$ for the diagonal terms of the quadrupole matrix element in (2.208) is an even function too, this does not imply the diagonal terms to vanish. Furthermore, the nuclear part of the quadrupole moment also contributes to the transition matrix element: since the two terms in (2.204) related to nucleus 1 and 2 are summed—instead of subtracted from each other, as in the corresponding expression for an electric-dipole transition—this term, too, yields a non-vanishing contribution. If the total molecular quadrupole moment does also change as a function of the internuclear distance (which

[21] Note that there is a slight inconsistency with the units in the article of Karl and Poll [82]. The rotational constant B used there is defined exactly as our B_e, i.e., in units of energy. Furthermore, their ω "denotes the harmonic-oscillator frequency", which implies the dimension of inverse time. However, the ratio B/ω is then not dimensionless as it is supposed to be. So strictly speaking, an additional factor $\hbar$ should appear in their expression, as it does here in (2.233).

it does in general), the quadrupole operator may induce rotation-vibration transitions. However, as discussed in the preceding chapter in the context of the general interaction between matter and radiation, the intensity of rotation-vibration transitions driven by the electric-quadrupole operator is very low, since the extent of the molecular wavefunction is small compared to the wavelength of electromagnetic radiation at resonance. Hence, the "gradient" of the electric field—the quantity relevant for electric-quadrupole transitions—is small over the extension of the molecule.

2.4 An intuitive picture

In this chapter, the physics of electric-dipole and electric-quadrupole rotation-vibration transitions in hetero- and homonuclear diatomic molecules has been described quantum mechanically. These transitions may also be described in an intuitive, less mathematical way: as the electronic state does not change in these transitions, they are governed by the diagonal matrix elements of the electric-dipole or quadrupole operator with respect to electronic states. These diagonal elements describe the expectation value of the respective electric multipole moments in a particular electronic state. We may thus think of the vibrational excitation of a molecule in an electric field in a similar way as of a classical electric charge distribution and we may equally well speak of different multipole moments of the charge distribution as of the multipole moments of the interaction operator of matter and radiation. In contrast, spectroscopic transitions in atoms are driven by the off-diagonal elements of the transition operator that lack an obvious intuitive meaning.

In a heteronuclear diatomic molecule, the charge distribution may in general be divided into a more positively and a more negatively charged part, an electric dipole. In an electric field these two parts experience a force parallel and antiparallel to the field, respectively. In an oscillating field, the molecule vibrates. For a homonuclear molecule such a partition into a region with a positive and a negative (relative) charge cannot be achieved. However, a partition into four regions, two of them more positively and two of them more negatively charged, i.e., an electric quadrupole, is usually possible. This electric quadrupole may be considered as two spatially separated electric dipoles (such as an electric dipole may be regarded as two separated electric monopoles, i.e., charges). If the electric field were uniform, these two dipoles would oscillate in phase and the relative motion of the two nuclei in the molecule, the vibration, would not be excited. However, because the field of an electromagnetic wave is not uniform but rather exhibits a phase shift over the extent of the molecule, these two dipoles oscillate slightly out of phase and thus the vibration is excited. As the molecule is considerably smaller than the wavelength of the wave, this phase shift is rather small and hence electric-quadrupole vibrational transitions are weak.

Chapter 3

Theory of electric-quadrupole rotation-vibration transitions in the molecular nitrogen cation

3.1 Introduction

In this chapter, the particular system used in this work to probe electric-quadrupole rotation-vibration transitions in a molecular ion is introduced, namely the infrared fundamental transition within the electronic ground state of the molecular nitrogen cation N_2^+. First, the general properties of the nitrogen cation and particularly, the energy level structure in the electronic ground state are presented. Emphasis is placed on the fine and hyperfine structure of $^{14}N_2^+$ because this structure allowed us to assign the observed spectrum unambiguously as due to electric-quadrupole vibration transitions in the nitrogen cation. Subsequently, the theory of electric-quadrupole transitions presented in the previous chapter is extended to include fine- and hyperfine-structure effects. As we are not aware of any treatment covering hyperfine-structure effects in electric-quadrupole rotation-vibration spectra, this theory has been newly developed as part of this work and represents a major result of this thesis. The theory is not limited to the N_2^+ ion, but may be applied to other molecular ions or neutral molecules showing a similar angular momentum coupling structure as well. A shortened version of this chapter has been published in Molecular Physics [85].

3.2 Spectroscopic investigation of the molecular nitrogen cation

The molecular nitrogen cation is one of the most extensively studied molecular ions in spectroscopy. The investigation may be traced back to the first half of the twentieth century with the observations of Fassbender [86], Coster and Brons [87] and Childs [88], among others (see [89]), and has continued until today. The interest in the N_2^+ ion was driven by natural phenomena such as aurorae or comet tails [90, 91] which show the spectroscopic signature of this molecule as well as technical applications such as the atmospheric reentry of space probes [92, 93]. Compilations of the spectroscopic data on the N_2^+ ion may be found in the review articles by Lofthus and Krupenie [94] and Gilmore, Laher and Espy [95].

The electronic ground state $X^2\Sigma_g^+$ of N_2^+ shows the dominant molecular orbital configuration [96] $1\sigma_g^2 1\sigma_u^2 2\sigma_g^2 2\sigma_u^2 3\sigma_g^1 1\pi_u^4$ and is thus obtained from the ground state of the neutral N_2 molecule $X^1\Sigma_g^+$ with the dominant configuration [94] $1\sigma_g^2 1\sigma_u^2 2\sigma_g^2 2\sigma_u^2 3\sigma_g^2 1\pi_u^4$ upon removal of an electron from the $3\sigma_g$ orbital. For the spectroscopic investigation, two excited electronic states are of particular importance, the $A^2\Pi_u$ state and the $B^2\Sigma_u^+$ state. Rovibronic transitions between the X and the A state lie mostly in the visible and near infrared part of the electromagnetic spectrum and form the "Meinel system", those of the X-B or "first negative" system also reach into the ultraviolet. Both of these systems have been extensively studied with ever increasing precision. Relatively recent studies include the ones from Miller, Suzuki and Hirota [97], Ferguson et al. [98] and Harada, Wada and Tanaka [90] for the Meinel system, as well as the ones by Dick et al. [99], Gottscho et al. [100] and Michaud et al. [92, 93] for the first negative system. From these measurements, a set of spectroscopic constants for the rotational and vibrational terms in the Hamiltonian of the electronic ground state of N_2^+ is available (see Tab. 3.1).

Beginning in the 1980s, the hyperfine structure of the N_2^+ ion has also been extensively investigated using Doppler-tuned laser fluorescence spectroscopy, e.g., in the studies by Rosner, Gaily and Holt [91, 101] and the one by Scholl, Holt and Rosner [102]. These investigations culminated in a laser-rf-laser double-resonance study by Berrah Mansour et al. [96] that yielded a set of molecular hyperfine-structure parameters with precisions in the kHz range or even better (Tab. 3.2).

The ion sources used in these experiments, such as electrical discharge sources, hollow cathode lamps, etc., produce N_2^+ ions with thermally populated internal quantum states. However, N_2^+ ions may also be produced by the method of resonance-enhanced multiphoton ionization (REMPI) as in the experiments by Vrakking, Bracker and Lee [103], Lykke and Kay [104] and Hanisco and Kummel [105]. This technique was refined by Mackenzie et al. into a two-colour REMPI scheme and combined with the method of delayed pulsed-field ionization to produce N_2^+ ions in selected rotational-vibrational quantum states [106]. A similar technique known as "pulsed-field-ionization zero-kinetic-energy photoelectron spectroscopy" (PFI-ZEKE) was later utilized by Seiler et al. [107] to precisely determine the ionization potential of the N_2 molecule. Finally, the method of threshold REMPI was employed by Tong, Winney and Willitsch [108] and Tong, Wild and Willitsch [109] and combined with ion trapping and sympathetic cooling to produce rotational-vibrational state-selected, translationally cold and spatially confined N_2^+ ions. This state preparation was achieved in the same laboratory as the experimental data for this thesis were taken. The N_2^+ ion also is particularly suited for such experiments, because a well-studied charge transfer reaction of N_2^+ with Ar atoms [110] may be used for state detection (see Ch. 4). For these reasons, the N_2^+ ion was chosen as a test system to demonstrate the addressability of electric-quadrupole rotation-vibration transitions in a molecular ion.

3.3 Energy level structure of the molecular nitrogen cation

The Hamiltonian of the $^{14}N_2^+$ ion in the electronic ground $X^2\Sigma_g^+$ state consists of several terms describing the vibration, the rotation, the fine and the hyperfine structure:

$$\hat{H}_{\mathrm{int}}(N_2^+, X^2\Sigma_g^+) = \hat{H}_{\mathrm{vib}} + \hat{H}_{\mathrm{rot}} + \hat{H}_{\mathrm{fs}} + \hat{H}_{\mathrm{hfs}}. \tag{3.1}$$

The vibrational and rotational Hamiltonians are treated by common models for diatomic molecules [60, 79] and are thus only briefly discussed here. The contributions due to the electronic spin (fine structure) and the nuclear spin (hyperfine structure) are more involved and the relevant expressions are given below.

For the vibrational Hamiltonian, the anharmonic oscillator model may be used (as in [97, 98]) with the corresponding term values $G(v)$ (in units of cm^{-1}) given as [79],

$$G(v) = \omega_\mathrm{e}(v+1/2) - \omega_\mathrm{e}x_\mathrm{e}(v+1/2)^2 + \omega_\mathrm{e}y_\mathrm{e}(v+1/2)^3. \tag{3.2}$$

Some of the most accurate measurements of relative vibrational term values $\Delta G(v) = G(v) - G(0)$ of N_2^+ are reported in [93]. These values are shown in Tab. 3.1.

The angular part of the N_2^+ Hamiltonian involves several angular momenta, which are due to the rotation of the nuclear frame of the molecule, the electronic and the nuclear spin. As a doublet state, the $\mathrm{X}^2\Sigma_\mathrm{g}^+$ state exhibits a total electronic spin of $S = 1/2$. Furthermore, each of the two $^{14}\mathrm{N}$ nuclei in $^{14}\mathrm{N}_2^+$ exhibits a nuclear spin of $I_{^{14}\mathrm{N}} = 1$ giving rise to a total nuclear spin of $I = 0$ or 2 (ortho-N_2^+) and $I = 1$ (para-N_2^+). The spin-rotational part of the Hamiltonian may be well described with a Hund's case (b_{β_J}) coupling scheme [111, 112, 60] meaning that the rotational angular momentum of the molecular frame[1] $\hat{\mathbf{N}}$ is first coupled with the electronic spin $\hat{\mathbf{S}}$ to form $\hat{\mathbf{J}} = \hat{\mathbf{N}} + \hat{\mathbf{S}}$, the total angular momentum excluding nuclear spin.[2] The resultant angular momentum $\hat{\mathbf{J}}$ is then coupled to the total nuclear spin $\hat{\mathbf{I}}$ to form the total angular momentum $\hat{\mathbf{F}}$ according to $\hat{\mathbf{F}} = \hat{\mathbf{J}} + \hat{\mathbf{I}}$. The basis states related to this coupling scheme are the states $|NSJIFM_F\rangle$ with N, S, J, I and F the eigenvalues of the above-mentioned angular momentum operators and M_F the eigenvalue of $\hat{F}_z$, the projection of the total angular momentum on the space-fixed z-axis.[3]

These quantum numbers are associated with energy levels of the molecular Hamiltonian on different levels of precision. The rotational levels labelled by N are spaced by more than hundred GHz between each other for low values of N. J labels the fine-structure (fs) levels with spacings of a few hundreds of MHz and F the hyperfine-structure (hfs) levels, lying only a few tens to about one hundred MHz next to each other. This hierarchy is depicted in Fig. 3.1.

The rotational Hamiltonian up to the fourth order in $\hat{\mathbf{N}}$ reads [97, 42]

$$\hat{H}_\mathrm{rot} = B_v\hat{\mathbf{N}}^2 - D_v\hat{\mathbf{N}}^4. \tag{3.3}$$

Here, B_v denotes the rotational constant and D_v the centrifugal distortion constant for a particular vibrational quantum state v (both in units of cm^{-1}). This Hamiltonian is diagonal in the Hund's case

[1] The projection of the electronic angular momentum on the internuclear axis Λ vanishes, as we are considering a Σ state.

[2] The symbols used here for the different angular momenta, follow the usual conventions for the Hund's case (b) angular momentum coupling scheme. In the previous chapter, J was used for the angular momentum quantum number of the nuclear frame of the molecule following the usual terminology in angular momentum theory of closed-shell molecules. Here, N is the analogue to J from Ch. 2.

[3] Other nuclear spin coupling cases include the (a_{β_J}) scheme, where $\hat{\mathbf{F}}$ is also the resultant of $\hat{\mathbf{J}}$ and $\hat{\mathbf{I}}$ but with $\hat{\mathbf{J}}$ obtained according to the Hund's case (a) coupling hierarchy, and the (b_{β_S}) scheme, where the nuclear spin is first coupled to the electron spin and subsequently their resultant to $\hat{\mathbf{N}}$. In principle, quantizing the nuclear spin in the molecule-fixed frame is also possible. Such schemes are known as case (a_α) and (b_α), for Hund's case (a) and (b), respectively. In practice, these cases are unlikely to occur because of the low coupling energies of nuclear magnetic moments as compared to electron moments. A systematic treatment of nuclear spin coupling cases is given in [112].

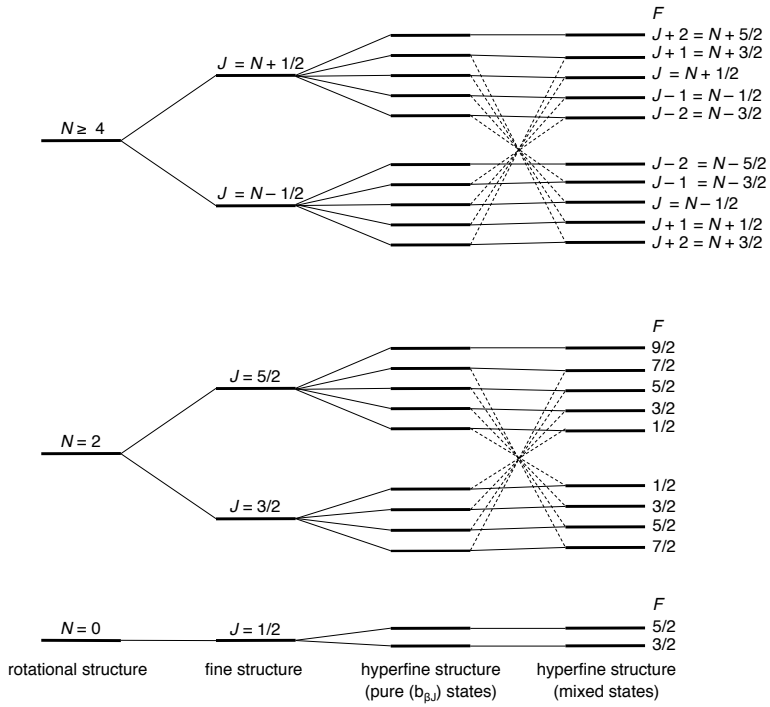

Figure 3.1. Energy level scheme of the angular quantum states of ortho-$^{14}N_2^+$ in the electronic ground state. The rotational levels are denoted by the rotational quantum number N. The level scheme is shown here for the rotational ground state ($N = 0$), the first rotational excited state allowed by the Pauli principle for ortho-$^{14}N_2^+$ ($N = 2$) and for a general state with $N \geq 4$. For $N > 0$, the rotational levels are split into two spin-rotation components, observable in a spectrum as the fine structure (fs), corresponding to the two possible values of J: $J = N-1/2$ and $J = N+1/2$. For $N = 0$, only one spin-rotation component exists and no fs splitting occurs. The spin-rotation components are further split by the interaction with the nuclear spin giving rise to hyperfine-structure (hfs) levels which are labelled by the quantum number F. Because the hfs Hamiltonian is not diagonal in the Hund's case (b_{β_J}) basis, each hfs state exhibits a small admixture of the state belonging to the other of the two spin-rotation components with the same value for F. This effect is indicated by the dashed lines connecting these levels. No mixing occurs for the state $F = 9/2$, $N = 2$ as well as for the states with $F = N - 5/2$ and $F = N + 5/2$ for $N \geq 4$ as they exist only for one of the two spin-rotation components of the respective rotational state.

Table 3.1. Vibrational term values, rotational and centrifugal constants for the $X^2\Sigma_g^+$ state of $^{14}N_2^+$.

v	$\Delta G(v)$	B_v	$D_v \times 10^5$
0	0	1.922316(5)	0.5919(1)
1	2174.746(1)	1.903380(5)	0.5958(1)
2	4316.977(1)	1.884265(5)	0.5996(1)
3	6426.445(2)	1.864985(5)	0.6039(1)

All values in units of cm^{-1} and taken from [93].
Values in parentheses correspond to one-standard-deviation (1σ) uncertainties and apply to the last digits (converted from the 2σ uncertainties given in [93] and rounded to the original number of significant digits).

(b_{β_J})-basis and exhibits the matrix elements (see Appendix B in [42]),

$$\langle N'S'J'I'F'M_F'|H_{\mathrm{rot}}|NSJIFM_F\rangle = \delta_{NN'}\delta_{SS'}\delta_{JJ'}\delta_{II'}\delta_{FF'}\delta_{M_FM_F'}[B_vN(N+1) - D_v[N(N+1)]^2]. \tag{3.4}$$

One of the most recent measurements of the rotational and centrifugal distortion constant for N_2^+ is the one by Michaud et al. [93]. Their results for the $X^2\Sigma_g^+$ state have been compiled in Tab. 3.1.

The fine structure in the spectrum of N_2^+ is described by the coupling of the electronic spin $\hat{\mathbf{S}}$ with the rotation of the molecule $\hat{\mathbf{N}}$,

$$\hat{H}_{\mathrm{fs}} = \gamma_v \hat{\mathbf{N}} \cdot \hat{\mathbf{S}}, \tag{3.5}$$

with γ_v the (effective)[4] spin-rotation coupling constant for a particular vibrational quantum number v which is given in Tab. 3.2 for $v = 0$ and $v = 1$. The fine-structure Hamiltonian is also diagonal in the chosen basis with the matrix elements (see Appendix B in [42]),[5]

$$\langle N'S'J'I'F'M_F'|\hat{H}_{\mathrm{fs}}|NSJIFM_F\rangle = \delta_{NN'}\delta_{SS'}\delta_{JJ'}\delta_{II'}\delta_{FF'}\delta_{M_FM_F'}\frac{\gamma_v}{2}[J(J+1) - N(N+1) - S(S+1)]. \tag{3.6}$$

In molecular spectroscopy, the rotational and fine-structure terms of the Hamiltonian are sometimes merged into a spin-rotational Hamiltonian with the eigenvalues [97],

$$F_1(N) = B_vN(N+1) - D_v[N(N+1)]^2 + 1/2\gamma_vN, \tag{3.7a}$$

$$F_2(N) = B_vN(N+1) - D_v[N(N+1)]^2 - 1/2\gamma_v(N+1), \tag{3.7b}$$

for the two spin-rotation components F_1 corresponding to $J = N + 1/2$ and F_2 for $J = N - 1/2$. (The symbols F_1 and F_2 are not to be confused with the angular momentum quantum number F and are not related to the latter.)

The hyperfine-structure Hamiltonian exhibits several contributions and may be written as [96],

$$\hat{H}_{\mathrm{hfs}} = \hat{H}_{b_F} + \hat{H}_t + \hat{H}_{eqQ} + \hat{H}_{c_I}, \tag{3.8}$$

with H_{b_F} describing the Fermi-contact interaction, H_t the dipolar hyperfine interaction, H_{eqQ} the quadrupolar hyperfine interaction and H_{c_I} the magnetic nuclear spin-rotation interaction. The latter

[4] Physically, the effective spin-rotation constant mainly incorporates second-order spin-orbit and rotation-electronic couplings to nearby $^2\Pi$ states [101, 96].

[5] The spin-rotation constant shows itself a slight dependence on N. In [96], γ_v is thus replaced by a sum consisting of a constant part and a part dependent on N: $\gamma_v \to \gamma_v + \gamma_N N(N+1)$, where γ_N is an additional spectroscopic constant. Because of the low value of $|\gamma_N|$ ($\approx 400\,\mathrm{Hz}$ or $1.4\,\mathrm{ppm}$ of γ_v for $v = 1$), this term may be neglected for the values of N considered and the level of accuracy aimed at here.

Table 3.2. Fine- and hyperfine-structure coupling constants for the $X^2\Sigma_g^+$ state of $^{14}N_2^+$.

Constant	Value for $v = 1$ [MHz][a]	Value for $v = 0$ [MHz][b]
γ_v	276.92253(13)	280.25(45)
$b_{F,v}$	100.6040(15)	102.4(1.1)
t_v	28.1946(13)	23.3(1.0)
eqQ_v	0.7079(60)	–

Values in parentheses represent 1σ-uncertainties and apply to the last digits.
[a] from [96]
[b] from [102]

is neglected here as the corresponding coupling constant of $\approx 11\,\mathrm{kHz}$ is far below our experimental precision (see Ch. 4). The coupling constants $b_{F,v}$, t_v and eqQ_v appearing in $\hat{H}_{b_F}$, $\hat{H}_t$ and $\hat{H}_{eqQ}$, respectively, are given in Tab. 3.2 for the $^{14}N_2^+$ ion in the vibrational ground state and the first vibrational excited state of the electronic $X^2\Sigma_g^+$ state.

In the basis introduced above, the matrix elements of the Fermi-contact Hamiltonian are given by [96]:

$$\begin{aligned}&\langle N'S'J'I'F'M_F'|\hat{H}_{b_F}|NSJIFM_F\rangle\\ &\quad= b_{F,v}\delta_{N'N}\delta_{S'S}\delta_{I'I}\delta_{F'F}\delta_{M_F'M_F}(-1)^{F+I+J'+J+N+S+1}\sqrt{I(I+1)(2I+1)}\\ &\qquad\sqrt{S(S+1)(2S+1)(2J+1)(2J'+1)}\begin{Bmatrix} I & J' & F\\ J & I & 1\end{Bmatrix}\begin{Bmatrix} S & J' & N\\ J & S & 1\end{Bmatrix}.\end{aligned} \tag{3.9}$$

Here, the two-row expressions in curly brackets are Wigner 6j-symbols [61, 76, 77, 62]. The Fermi-contact Hamiltonian is *not* diagonal in this basis but rather mixes states differing in their J quantum numbers but identical in the other quantum numbers.

The matrix elements of the dipolar hyperfine Hamiltonian are [96]:[6]

$$\begin{aligned}&\langle N'S'J'I'F'M_F'|\hat{H}_t|NSJIFM_F\rangle\\ &\quad= t_v\delta_{S'S}\delta_{I'I}\delta_{F'F}\delta_{M_F'M_F}(-1)^{J+I+F+N'+1}\sqrt{30I(I+1)(2I+1)}\\ &\qquad\sqrt{S(S+1)(2S+1)(2J+1)(2J'+1)(2N+1)(2N'+1)}\\ &\qquad\begin{Bmatrix} I & J' & F\\ J & I & 1\end{Bmatrix}\begin{Bmatrix} N' & N & 2\\ S & S & 1\\ J' & J & 1\end{Bmatrix}\begin{pmatrix} N' & 2 & N\\ 0 & 0 & 0\end{pmatrix},\end{aligned} \tag{3.10}$$

where the three-row expressions in curly brackets are Wigner 9j-symbols [61, 76, 77, 62]. This Hamiltonian, too, is not diagonal in the chosen basis and mixes states with different N and J quantum numbers.

Finally, the Hamiltonian describing the electric-quadrupole hyperfine interaction is given by the matrix

[6] Like γ_v, also t_v shows a slight dependence on N. Therefore, an additional N-dependent term is incorporated in t_v in [96], i.e., $t_v \to t_v + t_N N(N+1)$. As the value of t_N, too, is very small ($\approx 74\,\mathrm{Hz}$ or $2.6\,\mathrm{ppm}$ of t_v for $v = 1$), it is neglected here as well.

elements [96]:

$$\begin{aligned}
&\langle N'S'J'I'F'M'_F|\hat{H}_{eqQ}|NSJIFM_F\rangle \\
&\quad= \frac{eqQ_v}{2}\delta_{S'S}\delta_{F'F}\delta_{M'_F M_F}\frac{(-1)^I+(-1)^{I'}}{2}\sqrt{(2I+1)(2I'+1)(2J+1)(2J'+1)} \\
&\quad\sqrt{(2N+1)(2N'+1)}(-1)^{F+2J+I'}(-1)^{2I_1+S+2N'}\begin{Bmatrix} I' & 2 & I \\ J & F & J' \end{Bmatrix}\begin{Bmatrix} I_1 & 2 & I_1 \\ I & I_1 & I' \end{Bmatrix} \\
&\quad\begin{Bmatrix} N' & 2 & N \\ J & S & J' \end{Bmatrix}\begin{pmatrix} N' & 2 & N \\ 0 & 0 & 0 \end{pmatrix}\begin{pmatrix} I_1 & 2 & I_1 \\ -I_1 & 0 & I_1 \end{pmatrix}^{-1},
\end{aligned} \tag{3.11}$$

where $I_1 = I_{^{14}\mathrm{N}} = 1$. This Hamiltonian shows off-diagonal elements with regard to the N, J and I quantum numbers.

Concluding, we see that the rotation and the fine-structure Hamiltonian are diagonal within the $|NSJIFM_F\rangle$ basis, but that the hyperfine-structure Hamiltonian contains off-diagonal elements that mix states with different N, J and I quantum numbers.

Therefore, the Hamiltonian needs to be diagonalized to obtain term values and frequencies of spectroscopic transitions. Mixing of different rotational states (i.e., matrix elements off-diagonal in N) was not considered here, because interactions between them were found to be negligible in [96], as were matrix elements off-diagonal in the nuclear spin I. For the rotational ground state ($N = 0$), the hfs Hamiltonian then only shows the Fermi-contact term that is diagonal in the chosen basis, because only $J = N + 1/2$ is possible for $N = 0$. For rotational excited states ($N > 0$), the Hamiltonian is block diagonal with each value of the total angular momentum F exhibiting contributions of either value of J: $J = N + 1/2$ and $J = N - 1/2$. Diagonalization within the Hilbert subspace of a certain rotational state N may then be achieved analytically with a computer algebra package (Wolfram Mathematica 8.0, Wolfram Research, Inc., Champaign, IL, USA).

In terms of Fig. 3.1, mixing of the two possible values of J for a given N means that each state in the set belonging to $J = N + S$ is mixed with the corresponding state of the set $J = N - S$ with the same value of F, if such a state exists, as indicated by the dashed lines in Fig. 3.1. These mixed states are expressed as linear combinations of Hund's case (b_{β_J}) basis states. The state lying second highest in energy for $N = 2$, e.g., is expressed in Hund's case (b_{β_J}) basis as

$$\begin{aligned}
|\phi_{\text{example}}\rangle = \;& 0.9837\left|N=2, S=\tfrac{1}{2}, J=\tfrac{5}{2}, I=2, F=\tfrac{7}{2}\right\rangle \\
&+0.1800\left|N=2, S=\tfrac{1}{2}, J=\tfrac{3}{2}, I=2, F=\tfrac{7}{2}\right\rangle .
\end{aligned} \tag{3.12}$$

Obviously, when taking this mixing into account, J is no more a good quantum number. However, as seen from the expansion above, one of the two values of J dominates in this linear combination. Therefore, J may still be used as a near "quantum number" [67] and may serve as a label to distinguish the two states. For this near quantum number the symbol $\widetilde{J}$ is used here and the eigenstates of the Hamiltonian are written as $|NS\widetilde{J}IFM_F\rangle$. The above-mentioned state is thus written as

$$|\phi_{\text{example}}\rangle = |N=2, S=\tfrac{1}{2}, \widetilde{J}=\tfrac{5}{2}, I=2, F=\tfrac{7}{2}\rangle . \tag{3.13}$$

In general, the expansion of the eigenstates of the hfs Hamiltonian in the Hund's case (b_{β_J}) basis may

Table 3.3. Expansion coefficients for the eigenstates of the hfs Hamiltonian of $^{14}N_2^+$ ($v = 1, N = 2$) in a Hund's case (b_{β_J}) basis.

State		Coefficients	
$\widetilde{J}$	F	$c_{\widetilde{J},J=N-S,F}$	$c_{\widetilde{J}=N+S,J,F}$
5/2	9/2	0.0000	1.0000
3/2	1/2	-0.9946	0.1033
5/2	1/2	0.1033	0.9946
3/2	7/2	-0.9837	0.1800
5/2	7/2	0.1800	0.9837
3/2	3/2	-0.9846	0.1748
5/2	3/2	0.1748	0.9846
3/2	5/2	-0.9793	0.2024
5/2	5/2	0.2024	0.9793

be written as

$$\left|NS\widetilde{J}IFM_F\right\rangle = \sum_{J=|N-S|}^{N+S} c_{\widetilde{J}JF}\,|NSJIFM_F\rangle\,. \tag{3.14}$$

Here, $c_{\widetilde{J}JF}$ are real expansion coefficients, normalized such that $\sum_{J=|N-S|}^{N+S} c^2_{\widetilde{J}JF} = 1$. They are given for all hyperfine states of $^{14}N_2^+$ with $N = 2$ and $v = 1$ in Tab. 3.3 as obtained by the diagonalization of the Hamiltonian with Wolfram Mathematica using the fine- and hyperfine-structure coupling constants from Tab. 3.2. States with a value for F, which does only appear for one of the two values of J, do not mix. For $N = 2$, this applies only for the $F = 9/2$ state, for higher N, this is true for the states with the maximal (minimal) F for $J = N + S$ ($J = N - S$).

3.4 Fine- and hyperfine-structure effects in electric-quadrupole rotation-vibration transitions

As shown in the preceding section, electronic and nuclear spin play an important role in the $^{14}N_2^+$ ion via the fine- and hyperfine-structure Hamiltonian and need to be considered for high-precision spectroscopic experiments. Therefore, the theory of electric-quadrupole rotation-vibration transitions from the previous chapter is extended here to include effects of electronic and nuclear spin. At the same time, our treatment is extended to cover electronic orbital angular momentum appearing in non-Σ states. We will first consider the approximation of completely separable quantum states and subsequently regard spin-rotation coupling (fine structure) and coupling of the electronic and rotational angular momenta to the nuclear spin (hyperfine structure). Fine- and hyperfine-structure effects will be discussed in a Hund's case (b) and (b_{β_J}) angular momentum coupling scheme, respectively. Finally, the influence of the mixing of the Hund's case (b_{β_J}) states by the hfs Hamiltonian on the line strength is studied.

3.4.1 Electric-quadrupole rotation-vibration transitions in the approximation of completely separable quantum states

In the approximation of completely separable quantum states, a molecular state is regarded as a tensor product of an electronic state $|n\Lambda\rangle$, a vibrational state $|v\rangle$, a rotational state $|N\Lambda M_N\rangle$, as well as an

electronic $|SM_S\rangle$ and nuclear $|IM_I\rangle$ spin state. Here, n is a label for the electronic quantum state of the molecule, v stands for the vibrational quantum number and Λ denotes the quantum number of the projection of the electronic orbital angular momentum on the internuclear axis. The quantum number N describes the magnitude of the total molecular angular momentum $\hat{\mathbf{N}}$ excluding electronic and nuclear spin and M_N the corresponding projection on the space-fixed z-axis. S and I are the quantum numbers for the magnitudes of the electronic and nuclear spin, respectively, and M_S and M_I their projections on the space-fixed z-axis.

Denoting the quantum numbers for the upper and lower state as in the previous chapter by $'$ and $''$, respectively, the upper and lower quantum states are represented by,

$$|n\Lambda\rangle\,|v'\rangle\,|N'\Lambda M_N'\rangle\,|S'M_S'\rangle\,|I'M_I'\rangle = |n\Lambda, v', N'\Lambda M_N', S'M_S', IM_I'\rangle\,, \tag{3.15a}$$

$$|n\Lambda\rangle\,|v''\rangle\,|N''\Lambda M_N''\rangle\,|S''M_S''\rangle\,|I''M_I''\rangle = |n\Lambda, v'', N''\Lambda M_N'', S''M_S'', I''M_I''\rangle\,, \tag{3.15b}$$

where the tensor product states have been written as single kets for brevity. As we are regarding rotation-vibration transitions, the electronic quantum numbers n and Λ are identical in the upper and lower state.

The line strength is calculated as before by the squared absolute value of the electric-quadrupole operator summed over all spherical tensor components and all degenerate states contributing to the upper and lower level, i.e.,[7]

$$S^{(\mathrm{sep.})}_{\substack{n\Lambda\\ v'N'S'I'\\ v''N''S''I''}} = \sum_{M_I', M_I''} \sum_{M_S', M_S''} \sum_{M_N', M_N''} \sum_{p=-2}^{2} \left| \left\langle n\Lambda, v', N'\Lambda M_N', S'M_S', I'M_I' \left| \, \mathrm{T}^2_p \left[\hat{\mathrm{Q}}^{(\mathrm{s})}\right] \right| n\Lambda, v'', N''\Lambda M_N'', S''M_S'', I''M_I'' \right\rangle \right|^2 . \tag{3.16}$$

Here, the sums over the projection quantum numbers include all possible values, i.e. $M_N' = -N', -N'+1, ..., +N'$ and likewise for M_N'', M_S', M_S'', M_I' and M_I''. As indicated in the above equation, we will first calculate the line strength for two particular nuclear spin quantum numbers I' and I'' and later sum over all contributions of the several possible nuclear spin values allowed for particular rotational levels by the Pauli principle.

Since the electric-quadrupole operator does not act on the electronic and nuclear spin states, they may be separated from the transition matrix element, yielding:

$$\begin{aligned} &\left\langle n\Lambda, v', N'\Lambda M_N', S'M_S', IM_I' \left| \, \mathrm{T}^2_p \left[\hat{\mathrm{Q}}^{(\mathrm{s})}\right] \right| n\Lambda, v'', N''\Lambda M_N'', S''M_S'', I''M_I'' \right\rangle \\ &\qquad = \left\langle I'M_I' \,|\, I''M_I'' \right\rangle \left\langle S'M_S' \,|\, S''M_S'' \right\rangle \left\langle n\Lambda, v', N'\Lambda M_N' \left| \, \mathrm{T}^2_p \left[\hat{\mathrm{Q}}^{(\mathrm{s})}\right] \right| n\Lambda, v'', N''\Lambda M_N'' \right\rangle . \end{aligned} \tag{3.17}$$

Assuming orthonormal spin states, we have $\langle I'M_I' \,|\, I''M_I''\rangle = \delta_{I'I''}\delta_{M_I'M_I''}$ and $\langle S'M_S' \,|\, S''M_S''\rangle = \delta_{S'S''}\delta_{M_S'M_S''}$.

In the same way as in the last chapter, the electric-quadrupole operator in the space-fixed frame is

[7] Following usual conventions, a capital letter S is used as a symbol for both, the total electronic spin as well as the line strength. Confusion is avoided by the different sub- and superscripts.

expressed in terms of the molecule-fixed frame by a Wigner rotation matrix:

$$\mathrm{T}^2_p\left[\hat{\mathrm{Q}}^{(\mathrm{s})}\right] = \sum_{q=-2}^{2} \left[\hat{\mathcal{D}}^{(2)}_{pq}\right]^* \mathrm{T}^2_q\left[\hat{\mathrm{Q}}^{(\mathrm{m})}\right]. \tag{3.18}$$

As we are using bra-ket notation and abstract operators here, the Euler angles are not written and rather appear only when evaluating this operator for particular quantum states. The matrix element of the abstract $\hat{\mathcal{D}}^k_{pq}$ operator is then given by the concrete Wigner rotation matrix used in the preceding chapter according to,

$$\langle\phi_1\theta_1\chi_1|\hat{\mathcal{D}}^k_{pq}|\phi_2\theta_2\chi_2\rangle = \delta(\phi_1-\phi_2)\delta(\theta_1-\theta_2)\delta(\chi_1-\chi_2)\mathscr{D}^{(k)}_{pq}(\phi_1,\theta_1,\chi_1), \tag{3.19}$$

where δ is the Dirac delta distribution.

We thus get for the rovibronic transition matrix element:

$$\begin{aligned}\left\langle n\Lambda, v', N'\Lambda M'_N \middle| \mathrm{T}^2_p\left[\hat{\mathrm{Q}}^{(\mathrm{s})}\right] \middle| n\Lambda, v'', N''\Lambda M''_N \right\rangle \\ = \sum_{q=-2}^{2} \left\langle n\Lambda, v', N'\Lambda M'_N \middle| \left[\hat{\mathcal{D}}^{(2)}_{pq}\right]^* \mathrm{T}^2_q\left[\hat{\mathrm{Q}}^{(\mathrm{m})}\right] \middle| n\Lambda, v'', N''\Lambda M''_N \right\rangle.\end{aligned} \tag{3.20}$$

As the Wigner rotation matrix depends only on the Euler angles and since the angular dependence of the molecular state is described by the rotational wavefunction, whereas the molecule-fixed quadrupole operator involves only the vibronic coordinates that appear only in the vibronic function, the transition matrix element may be factorized as follows [67, 60]:

$$\begin{aligned}\left\langle n\Lambda, v', N'\Lambda M'_N \middle| \mathrm{T}^2_p\left[\hat{\mathrm{Q}}^{(\mathrm{s})}\right] \middle| n\Lambda, v'', N''\Lambda M''_N \right\rangle \\ = \sum_{q=-2}^{2} \left\langle n\Lambda, v' \middle| \mathrm{T}^2_q\left[\hat{\mathrm{Q}}^{(\mathrm{m})}\right] \middle| n\Lambda, v'' \right\rangle \left\langle N'\Lambda M'_N \middle| \left[\hat{\mathcal{D}}^{(2)}_{pq}\right]^* \middle| N''\Lambda M''_N \right\rangle.\end{aligned} \tag{3.21}$$

To calculate the angular matrix element, we notice that the angular functions are themselves represented by Wigner rotation matrices, i.e. [60],

$$\langle\phi\,\theta\,\chi|N''\Lambda M''_N\rangle = \sqrt{\frac{2N''+1}{8\pi^2}}\left[\mathscr{D}^{(N'')}_{M''_N\Lambda}(\phi,\theta,\chi)\right]^*, \tag{3.22a}$$

$$\langle N'\Lambda M'_N|\phi\,\theta\,\chi\rangle = \sqrt{\frac{2N'+1}{8\pi^2}}\mathscr{D}^{(N')}_{M'_N\Lambda}(\phi,\theta,\chi). \tag{3.22b}$$

Hence, the angular matrix element is a product of three Wigner rotation matrices integrated over the Euler angles. Integration is readily achieved when exploiting the properties of the Wigner matrices [62]:

$$\begin{aligned}&\left\langle N'\Lambda M'_N \middle| \left[\hat{\mathcal{D}}^{(2)}_{pq}\right]^* \middle| N''\Lambda M''_N \right\rangle \\ &= \frac{\sqrt{2N''+1}\sqrt{2N'+1}}{8\pi^2}\int_0^{2\pi}\int_0^{2\pi}\int_0^{\pi} \mathscr{D}^{(N')}_{M'_N\Lambda}(\phi,\theta,\chi)\left[\mathscr{D}^{(2)}_{pq}(\phi,\theta,\chi)\mathscr{D}^{(N'')}_{M''_N\Lambda}(\phi,\theta,\chi)\right]^* \sin\theta\mathrm{d}\theta\mathrm{d}\phi\mathrm{d}\chi \\ &= \sqrt{2N''+1}\sqrt{2N'+1}(-1)^{M'_N-\Lambda}\begin{pmatrix} N' & 2 & N'' \\ -M'_N & p & M''_N\end{pmatrix}\begin{pmatrix} N' & 2 & N'' \\ -\Lambda & q & \Lambda\end{pmatrix}.\end{aligned} \tag{3.23}$$

Because of the selection rule $-\Lambda + q + \Lambda = 0$ for the second Wigner 3j-symbol, the above expression vanishes for all values of q but $q = 0$. Therefore, only the term with $q = 0$ contributes to the sum in equation (3.20). The transition matrix element appearing in (3.17) is thus:

$$\left\langle n\Lambda, v', N'\Lambda M'_N, S'M'_S, IM'_I \left| \mathrm{T}^2_p \left[\hat{\mathrm{Q}}^{(\mathrm{s})}\right] \right| n\Lambda, v'', N''\Lambda M''_N, S''M''_S, I''M''_I \right\rangle \tag{3.24}$$

$$= \delta_{I'I''}\delta_{M'_IM''_I}\delta_{S'S''}\delta_{M'_SM''_S}\sqrt{2N''+1}\sqrt{2N'+1}(-1)^{M'_N-\Lambda} \begin{pmatrix} N' & 2 & N'' \\ -M'_N & p & M''_N \end{pmatrix} \begin{pmatrix} N' & 2 & N'' \\ -\Lambda & 0 & \Lambda \end{pmatrix} \left\langle n\Lambda, v' \left| \mathrm{T}^2_0 \left[\hat{\mathrm{Q}}^{(\mathrm{m})}\right] \right| n\Lambda, v'' \right\rangle . \tag{3.25}$$

Substituting this result into (3.16), we obtain for the line strength:

$$\begin{aligned} S^{(\mathrm{sep.})}_{\substack{n\Lambda \\ v'N'S'I' \\ v''N''S''I''}} = {} & \delta_{S'S''}\delta_{I'I''} \sum_{M'_I,M''_I} \delta_{M'_IM''_I} \sum_{M'_S,M''_S} \delta_{M'_SM''_S} \\ & (2N'+1)(2N''+1) \begin{pmatrix} N' & 2 & N'' \\ -\Lambda & 0 & \Lambda \end{pmatrix}^2 \left| \left\langle n\Lambda, v' \left| \mathrm{T}^2_0 \left[\hat{\mathrm{Q}}^{(\mathrm{m})}\right] \right| n\Lambda, v'' \right\rangle \right|^2 \\ & \sum_{M'_N,M''_N} \sum_{p=-2}^{2} \begin{pmatrix} N' & 2 & N'' \\ -M'_N & p & M''_N \end{pmatrix}^2 . \end{aligned} \tag{3.26}$$

The sum over M''_N, M'_N and p is calculated using the orthogonality properties of the 3j-symbols (see, e.g., [61]), yielding:

$$\sum_{M'_N,M''_N} \sum_{p=-2}^{2} \begin{pmatrix} N' & 2 & N'' \\ -M'_N & p & M''_N \end{pmatrix}^2 = 1. \tag{3.27}$$

The sum over the total electron spin projection quantum numbers accounts for,

$$\sum_{M'_S,M''_S} \delta_{M'_SM''_S} = 2S''+1, \tag{3.28}$$

and similarly the one over the projections of the nuclear spins is,

$$\sum_{M'_I,M''_I} \delta_{M'_IM''_I} = 2I''+1. \tag{3.29}$$

Thus, the contribution to the line strength of an electric-quadrupole rotation-vibration transition between two states of particular nuclear spin quantum numbers I' and I'' is:

$$\begin{aligned} S^{(\mathrm{sep.})}_{\substack{n\Lambda \\ v'N'S'I' \\ v''N''S''I''}} = {} & \delta_{S'S''}\delta_{I'I''}(2I''+1)(2S''+1)(2N'+1)(2N''+1) \\ & \begin{pmatrix} N' & 2 & N'' \\ -\Lambda & 0 & \Lambda \end{pmatrix}^2 \left| \left\langle n\Lambda, v' \left| \mathrm{T}^2_0 \left[\hat{\mathrm{Q}}^{(\mathrm{m})}\right] \right| n\Lambda, v'' \right\rangle \right|^2 . \end{aligned} \tag{3.30}$$

As expressed by the two Kronecker delta symbols, electronic as well as nuclear spin does not change in such a transition and the two selection rules

$$\Delta S = 0, \tag{3.31}$$

$$\Delta I = 0, \tag{3.32}$$

for $\Delta S = S' - S''$ and $\Delta I = I' - I''$ apply.

The selection rule for the change in the rotational quantum number $\Delta N = N' - N''$ is less restrictive for non-Σ states than the one deduced in Ch. 2 and reads in general,

$$\Delta N = 0, \pm 1, \pm 2, \tag{3.33}$$

with $\Delta N = \pm 1$ forbidden in Σ states as well as $\Delta N = 0$ forbidden for $N'' = 0$.

The vibronic transition matrix element in equation (3.30) may be separated into a vibrational and an electronic part. The integration over the electronic coordinates may be formally carried out. Because the electronic quantum numbers do not change in a rotation-vibration transition, the result of this integration is—as discussed in the preceding chapter—the electric-quadrupole moment of the molecule in the electronic quantum state considered, i.e.,

$$\left\langle n\Lambda, v' \left| \mathrm{T}_0^2 \left[\hat{\mathrm{Q}}^{(\mathrm{m})} \right] \right| n\Lambda, v'' \right\rangle = \left\langle v' \left| \mathrm{T}_0^2 \left[\hat{\mathrm{Q}}_{n\Lambda}^{(\mathrm{m})} \right] \right| v'' \right\rangle = \sqrt{\frac{3}{2}} \left\langle v' \left| \hat{Q}_{n\Lambda,zz}^{(\mathrm{m})} \right| v'' \right\rangle . \tag{3.34}$$

Here, $\hat{\mathrm{Q}}_{n\Lambda}^{(\mathrm{m})}$ stands for the electric-quadrupole moment of the molecule in the electronic state $|n, \Lambda\rangle$ understood as an operator acting on the vibrational state (i.e., the internuclear distance $\mathbf{R}$ appearing in the quadrupole operator is replaced by the corresponding quantum mechanical operator $\hat{\mathbf{R}}$ acting on the vibrational state $|v''\rangle$). Within the double-harmonic approximation, the vibrational transition matrix element may be calculated according to equation (2.237) of the previous chapter.

When the hyperfine structure is not resolved in a spectrum, the line strength is the sum over all hfs components. In other words, transitions differing only in the nuclear spin quantum number, but identical in the others (such as, e.g., $N'' = 0, I'' = 0 \rightarrow N' = 2, I' = 0$ vs. $N'' = 0, I'' = 2 \rightarrow N'' = 2, I' = 2$) are not resolved and observed as a single spectral line. The observed line strength is thus the sum of the contributions of all these transitions:

$$S_{\substack{v'N'S' \\ v''N''S''}}^{(\mathrm{sep.})} = \sum_{I',I''} S_{\substack{v'N'S'I' \\ v''N''S''I''}}^{(\mathrm{sep.})} , \tag{3.35}$$

where the sums over the nuclear spin quantum numbers I' and I'' include all values for I' (I'') that are allowed by the Pauli principle for a given N' (N''), (see [29], pp. 130ff. and [66]). Because of the Kronecker delta $\delta_{I'I''}$ appearing in (3.30), the double sum turns into a single one, which is commonly absorbed together with the factor $(2I'' + 1)$ from (3.29) into a nuclear spin statistical weight factor g_{ns} [67]. For $^{14}\mathrm{N}_2^+$ in the electronic ground state $\mathrm{X}^2\Sigma_\mathrm{g}^+$, we have $I = 0$ or 2 for even values of N and $I = 1$ for odd ones. Therefore, the nuclear statistical weight factor is $g_{\mathrm{ns}}(N) = (2 \times 0 + 1) + (2 \times 2 + 1) = 6$ for even N and $g_{\mathrm{ns}}(N) = (2 \times 1 + 1) = 3$ for odd N.

In conclusion, the line strength of an electric-quadrupole rotation-vibration line in the approximation of completely separable quantum states is:

$$S_{\substack{v'N'S' \\ v''N''S''}}^{(\mathrm{sep.})} = \delta_{S'S''} g_{\mathrm{ns}} (2N' + 1)(2N'' + 1)(2S'' + 1) \begin{pmatrix} N' & 2 & N'' \\ -\Lambda & 0 & \Lambda \end{pmatrix}^2 \left| \left\langle v' \left| \mathrm{T}_0^2 \left[\hat{\mathrm{Q}}_{n,\Lambda}^{(\mathrm{m})} \right] \right| v'' \right\rangle \right|^2 . \tag{3.36}$$

In order to verify this result, the line strength for transitions in the particular case of vanishing

electronic and nuclear spin has been calculated and compared with the values obtained from the expressions derived by Farley and Cattolica [113] for the Hund's case (a) coupling scheme (which corresponds to Hund's case (b) for vanishing electron spin). Using the expressions from Tab. 2 in [113] for $\Delta P = 0$ (corresponding to $\Delta\Lambda = 0$ in our notation), perfect agreement was found for both, Σ and non-Σ states.

3.4.2 Fine-structure effects in electric-quadrupole rotation-vibration transitions

As outlined in Sec. 3.3, the rotation of a molecule may couple to its spin. If so, the tensor product states $|N\Lambda M_N\rangle\,|SM_S\rangle$ used in the preceding section are no more eigenstates of the molecular Hamiltonian. The eigenstates are rather the states $|N\Lambda SJM_J\rangle$ belonging to the coupled angular momentum $\hat{\mathbf{J}} = \hat{\mathbf{N}} + \hat{\mathbf{S}}$. They may be expressed as linear combinations of the previously used tensor product states with Clebsch-Gordan coefficients or 3j-symbols according to,

$$|N\Lambda SJM_J\rangle = \sum_{M_N=-N}^{N} \sum_{M_S=-S}^{S} (-1)^{N-S+M_J} \sqrt{2J+1} \begin{pmatrix} N & S & J \\ M_N & M_S & -M_J \end{pmatrix} |N\Lambda M_N\rangle\,|SM_S\rangle\,. \quad (3.37)$$

Whereas the quantum numbers N and S, describing the magnitude of the rotational angular momentum and the spin, respectively, are still good quantum numbers, the corresponding projection quantum numbers M_N and M_S are not well-defined, because the coupled states are linear combinations of states with different M_N and M_S quantum numbers.

The upper and lower states for a rotation-vibration transition considering spin-rotation interaction are thus,

$$|n\Lambda\rangle\,|v'\rangle\,|N'\Lambda S'J'M'_J\rangle\,|I'M'_I\rangle = |n\Lambda, v', N'\Lambda S'J'M'_J, I'M'_I\rangle\,, \quad (3.38a)$$

$$|n\Lambda\rangle\,|v''\rangle\,|N''\Lambda S''J''M''_J\rangle\,|I''M''_I\rangle = |n\Lambda, v'', N''\Lambda S''J''M''_J, I''M''_I\rangle\,. \quad (3.38b)$$

Accordingly, the line strength for an electric-quadrupole rotation-vibration line is calculated as,

$$S^{(\mathrm{fs})}_{\substack{n\Lambda \\ v'N'S'J'I' \\ v''N''S''J''I''}} = \sum_{M'_I, M''_I} \sum_{M'_J, M''_J} \sum_{p=-2}^{2} \left| \left\langle n\Lambda, v', N'\Lambda S'J'M'_J, I'M'_I \,\middle|\, \mathrm{T}^2_p\left[\hat{\mathbf{Q}}^{(\mathrm{s})}\right] \,\middle|\, n\Lambda, v'', N''\Lambda S''J''M''_J, I''M''_I \right\rangle \right|^2 . \quad (3.39)$$

Like in the previous section, we will first calculate the line strength for specific nuclear spin values I' and I'' and will later include all possible nuclear spin components allowed by the Pauli principle for particular rotational states.

As in the previous section, the electric-quadrupole operator does not act on the nuclear spin states such that the transition matrix element may be factorized:

$$\left\langle n\Lambda, v', N'\Lambda S'J'M'_J, I'M'_I \,\middle|\, \mathrm{T}^2_p\left[\hat{\mathbf{Q}}^{(\mathrm{s})}\right] \,\middle|\, n\Lambda, v'', N''\Lambda S''J''M''_J, I''M''_I \right\rangle = \left\langle I'M'_I \,\middle|\, I''M''_I \right\rangle \left\langle n\Lambda, v', N'\Lambda S'J'M'_J \,\middle|\, \mathrm{T}^2_p\left[\hat{\mathbf{Q}}^{(\mathrm{s})}\right] \,\middle|\, n\Lambda, v'', N''\Lambda S''J''M''_J \right\rangle , \quad (3.40)$$

with $\langle I'M'_I \,|\, I''M''_I\rangle = \delta_{I'I''}\delta_{M'_IM''_I}$.

Expressing the electric-quadrupole operator in the molecule-fixed frame and exploiting that the Wigner rotation matrix involves only the Euler angles, whereas the molecule-fixed quadrupole operator acts only on the vibronic coordinates, the transition matrix element on the right-hand side of the above equation is:

$$\begin{aligned}
&\left\langle n\Lambda, v', N'\Lambda S' J' M'_J \left| \mathrm{T}^2_p \left[\hat{\mathrm{Q}}^{(\mathrm{s})}\right] \right| n\Lambda, v'', N''\Lambda S'' J'' M''_J \right\rangle \\
&= \sum_{q=-2}^{2} \left\langle n\Lambda, v', N'\Lambda S' J' M'_J \left| \left[\hat{\mathcal{D}}^{(2)}_{pq}\right]^* \mathrm{T}^2_q \left[\hat{\mathrm{Q}}^{(\mathrm{m})}\right] \right| n\Lambda, v'', N''\Lambda S'' J'' M''_J \right\rangle \qquad (3.41) \\
&= \sum_{q=-2}^{2} \left\langle n\Lambda, v' \left| \mathrm{T}^2_q \left[\hat{\mathrm{Q}}^{(\mathrm{m})}\right] \right| n\Lambda, v'' \right\rangle \left\langle N'\Lambda S' J' M'_J \left| \left[\hat{\mathcal{D}}^{(2)}_{pq}\right]^* \right| N''\Lambda S'' J'' M''_J \right\rangle . \qquad (3.42)
\end{aligned}$$

The spin-rotational matrix element appearing in the last equation is evaluated with the Wigner-Eckart theorem [61, 62, 76]. The matrix element is thus expressed as a product of a prefactor depending on the three space-fixed projection quantum numbers (M'_J, M''_J, p) and a "reduced" (double-bar) matrix element independent of them:

$$\begin{aligned}
&\left\langle N'\Lambda S' J' M'_J \left| \left[\hat{\mathcal{D}}^{(2)}_{pq}\right]^* \right| N''\Lambda S'' J'' M''_J \right\rangle \\
&\qquad = (-1)^{J'-M'_J} \begin{pmatrix} J' & 2 & J'' \\ -M'_J & p & M''_J \end{pmatrix} \left\langle N'\Lambda S' J' \left\| \left[\hat{\mathcal{D}}^{(2)}_{\cdot q}\right]^* \right\| N''\Lambda S'' J'' \right\rangle . \qquad (3.43)
\end{aligned}$$

Here, we have adopted the notation from [60] with a dot in the subscript of the Wigner rotation matrix indicating that this matrix element is reduced with respect to the space-fixed, but not to the molecule-fixed coordinates.

As shown in (3.37), the spin-rotational states may be expressed in the tensor product basis of spin and rotational states. The Wigner rotation matrix $\hat{\mathcal{D}}^{(2)}_{pq}$ acts only on the rotational part of this tensor product states. We may thus employ the relation for reduced matrix elements of operators acting only on one part of coupled angular momentum states (equation (5.72) in [61]) to factorize the reduced matrix element:

$$\begin{aligned}
&\left\langle N'\Lambda S' J' \left\| \left[\hat{\mathcal{D}}^{(2)}_{\cdot q}\right]^* \right\| N''\Lambda S'' J'' \right\rangle \\
&\qquad = \delta_{S'S''} (-1)^{N'+S'+J''+2} \sqrt{2J'+1}\sqrt{2J''+1} \begin{Bmatrix} N' & J' & S' \\ J'' & N'' & 2 \end{Bmatrix} \left\langle N'\Lambda \left\| \left[\hat{\mathcal{D}}^{(2)}_{\cdot q}\right]^* \right\| N''\Lambda \right\rangle . \qquad (3.44)
\end{aligned}$$

In this way, spin quantum numbers have been eliminated from the reduced matrix element, leaving only the rotational and electronic orbital angular momenta. The resultant reduced matrix element may be calculated by comparing the value obtained from the integration of the three Wigner rotation matrices from the previous section (equation (3.23)) with the corresponding expression given by the Wigner-Eckart theorem. The result is:

$$\left\langle N'\Lambda \left\| \left[\hat{\mathcal{D}}^{(2)}_{\cdot q}\right]^* \right\| N''\Lambda \right\rangle = (-1)^{N'-\Lambda} \sqrt{2N'+1}\sqrt{2N''+1} \begin{pmatrix} N' & 2 & N'' \\ -\Lambda & q & \Lambda \end{pmatrix} . \qquad (3.45)$$

As in the preceding section, the expression above vanishes for all values of q but $q = 0$ and thus only the term with $q = 0$ contributes to the sum in (3.42). Substituting equations (3.42), (3.43), (3.44) and

(3.45) into (3.40), we get for the complete transition matrix element,

$$\begin{aligned}\left\langle n\Lambda, v', N'\Lambda S' J' M'_J, I' M'_I \left| \mathrm{T}^2_p\left[\hat{\mathsf{Q}}^{(\mathrm{s})}\right] \right| n\Lambda, v'', N''\Lambda S'' J'' M''_J, I'' M''_I \right\rangle \\ = \delta_{I'I''}\delta_{M'_I M''_I}\delta_{S'S''}(-1)^{S'+J'+J''-M'_J-\Lambda}\sqrt{2N'+1}\sqrt{2N''+1}\sqrt{2J'+1}\sqrt{2J''+1} \\ \begin{pmatrix} N' & 2 & N'' \\ -\Lambda & 0 & \Lambda \end{pmatrix} \begin{pmatrix} J' & 2 & J'' \\ -M'_J & p & M''_J \end{pmatrix} \begin{Bmatrix} N' & J' & S' \\ J'' & N'' & 2 \end{Bmatrix} \left\langle n\Lambda, v' \left| \mathrm{T}^2_0\left[\hat{\mathsf{Q}}^{(\mathrm{m})}\right] \right| n\Lambda, v'' \right\rangle . \end{aligned} \tag{3.46}$$

Taking the squared absolute value of this expression and evaluating the sums appearing in (3.39), we obtain for the line strength for particular nuclear spin values I' and I'':

$$\begin{aligned} S^{(\mathrm{fs})}_{\substack{n\Lambda \\ v'N'S'J'I' \\ v''N''S''J''I''}} = {} & \delta_{S'S''}\delta_{I'I''}(2N'+1)(2N''+1)(2J'+1)(2J''+1)(2I''+1) \\ & \begin{pmatrix} N' & 2 & N'' \\ -\Lambda & 0 & \Lambda \end{pmatrix}^2 \begin{Bmatrix} N' & J' & S' \\ J'' & N'' & 2 \end{Bmatrix}^2 \left| \left\langle n\Lambda, v' \left| \mathrm{T}^2_0\left[\hat{\mathsf{Q}}^{(\mathrm{m})}\right] \right| n\Lambda, v'' \right\rangle \right|^2 . \end{aligned} \tag{3.47}$$

Here, the orthogonality properties of the 3j-symbols have been used again, i.e.,

$$\sum_{M'_J, M''_J} \sum_{p=-2}^{2} \begin{pmatrix} J' & 2 & J'' \\ -M'_J & p & M''_J \end{pmatrix}^2 = 1. \tag{3.48}$$

As seen from (3.47), the selection rules for ΔN, ΔS and ΔI are exactly as before, namely,

$$\Delta N = 0, \pm 1, \pm 2, \tag{3.49}$$

$$\Delta S = 0, \tag{3.50}$$

$$\Delta I = 0, \tag{3.51}$$

with the aforementioned constraints on ΔN for Σ states and for transitions involving the rotational ground state. The selection rule for the change in the total angular momentum excluding nuclear spin $\Delta J = J' - J''$ is,

$$\Delta J = 0, \pm 1, \pm 2, \tag{3.52}$$

and is thus in the case of Σ states less restrictive than the one for ΔN.

As in the last section, the observed line strength when only resolving the fine and not the hyperfine structure is given as a sum over all possible values for the nuclear spins I' (I'') for certain values of N' (N''). Again, this sum of the terms depending on I'' in (3.47) is usually expressed as a nuclear spin statistical weight factor g_{ns} such that the total line strength is:

$$\begin{aligned} S^{(\mathrm{fs})}_{\substack{n\Lambda \\ v'N'S'J' \\ v''N''S''J''}} = {} & \delta_{S'S''} g_{\mathrm{ns}} (2N'+1)(2N''+1)(2J'+1)(2J''+1) \\ & \begin{pmatrix} N' & 2 & N'' \\ -\Lambda & 0 & \Lambda \end{pmatrix}^2 \begin{Bmatrix} N' & J' & S' \\ J'' & N'' & 2 \end{Bmatrix}^2 \left| \left\langle n\Lambda, v' \left| \mathrm{T}^2_0\left[\hat{\mathsf{Q}}^{(\mathrm{m})}\right] \right| n\Lambda, v'' \right\rangle \right|^2 . \end{aligned} \tag{3.53}$$

The vibronic matrix element appearing above may again be expressed as shown in equation (3.34) of the previous section.

In order to verify this result, the particular case $S' = S'' = 0$ is considered. In this case, we have $J' = N'$ and $J'' = N''$. For quadrupole-allowed transitions, the squared Wigner 6j-symbol is then

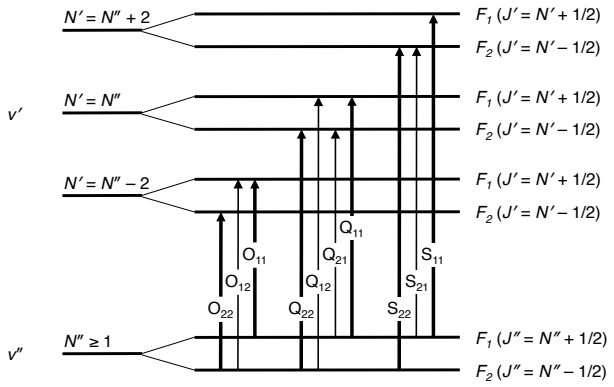

Figure 3.2. Scheme of electric-quadrupole rotation-vibration transitions in a $^2\Sigma$ state with spin-rotation interaction. The lines are labelled by O, Q and S according to $\Delta N = -2, 0, +2$. Two subscripts $_1$ or $_2$ are used to denote the spin-rotation component F_1 and F_2 in the upper (v') and lower (v'') vibrational state.

equal to $1/[(2N''+1)(2N'+1)]$ such that, when multiplied with the prefactor $(2J''+1)(2J'+1) = (2N''+1)(2N'+1)$, the result from the previous section is reproduced. For $S' = S'' > 0$, the same is true, when the total line strength of all fine-structure lines belonging to a certain rotation-vibration line is considered, i.e., when the above expression is summed over all J' and J'' values belonging to certain values for N' and N'': using the orthonormality of the Wigner 6j-symbols (equation (4.11) in [61]), it may be shown that the result from the last section is reproduced again. Hence, upon resolving the fine structure in a spectrum, the line strength is distributed among the several fine-structure transitions belonging to one rotational-vibrational line with the total line strength of that line remaining constant.

To label the fine-structure-resolved lines, we use the notation $S_{11}(4)$, $Q_{12}(2)$, etc. Here, the number given in parentheses is the lower-level rotational quantum number N'', the code letters O, P, Q, R and S stand for $\Delta N = -2, -1, 0, +1$ and $+2$, respectively, and the two subscripts $_1$ or $_2$ refer to the fine-structure component F_1 or F_2 in the upper and lower state (with F_1 corresponding to $J = N + S$ and F_2 to $J = N - S$ as mentioned earlier).

For a $^2\Sigma$ state, there could be in principle twelve fine-structure transitions for a given N'' (with $N'' \geq 3$): with P and R lines being forbidden for $\Lambda = 0$, each of the three possible rotational transitions O, Q and S could in principle be combined with any of the four possible subscripts for the fine-structure components $_{11}$, $_{12}$, $_{21}$ and $_{22}$. From these twelve possibilities, the O_{21} and S_{12} lines are forbidden as they imply $|\Delta J| = 3$. The allowed transitions are illustrated in Fig. 3.2. The spin-rotational factor appearing in the expression for the line strength (known as "Hönl-London factor") of these transitions is given in Tab. 3.4. For Q_{12} and Q_{21} transitions, the line strength is equal due to the symmetry properties of the Wigner 6j-symbol [77].

From dipole-allowed transitions, it is known [60] that the lines fulfilling the relation,

$$\Delta J = \Delta N, \tag{3.54}$$

i.e., transitions between states of the same fine-structure component (such as O_{11}, S_{22}, etc.), show considerable higher intensities than those violating this condition. The former are known as "principal lines", the latter as "satellite lines". Thus, the question arises, if this propensity rule holds for electric-

Table 3.4. Spin-rotational line strength factors for electric-quadrupole rotation-vibration lines in $^2\Sigma$ states.

Spin-rotation component	O Lines	Q Lines	S Lines
$F_1'' \to F_1'$	$\dfrac{3N''(N''-1)(N''+1)}{(2N''-1)(2N''+1)}$	$\dfrac{2N''(N''+1)(N''+2)}{(2N''+1)(2N''+3)}$	$\dfrac{3(N''+1)(N''+2)(N''+3)}{(2N''+3)(2N''+5)}$
$F_1'' \to F_2'$	0	$\dfrac{6N''(N''+1)}{(2N''-1)(2N''+1)(2N''+3)}$	$\dfrac{6(N''+1)(N''+2)}{(2N''+1)(2N''+3)(2N''+5)}$
$F_2'' \to F_1'$	$\dfrac{6N''(N''-1)}{(2N''-3)(2N''-1)(2N''+1)}$	$\dfrac{6N''(N''+1)}{(2N''-1)(2N''+1)(2N''+3)}$	0
$F_2'' \to F_2'$	$\dfrac{3N''(N''-2)(N''-1)}{(2N''-3)(2N''-1)}$	$\dfrac{2N''(N''-1)(N''+1)}{(2N''-1)(2N''+1)}$	$\dfrac{3N''(N''+1)(N''+2)}{(2N''+1)(2N''+3)}$

The actual line strength is given by the table entry multiplied with $g_{\mathrm{ns}} \left| \left\langle n\Lambda, v' \right| \mathrm{T}_0^2 \left[\hat{\mathbf{Q}}^{(\mathrm{m})} \right] \left| n\Lambda, v'' \right\rangle \right|^2$.
O lines are only allowed for $N'' \geq 2$ and Q lines only for $N'' \geq 1$. For the O_{22}, Q_{22} and S_{22} lines the minimal N'' is 3, 2 and 1, respectively. These rules have been assumed to be fulfilled when deriving the values shown.

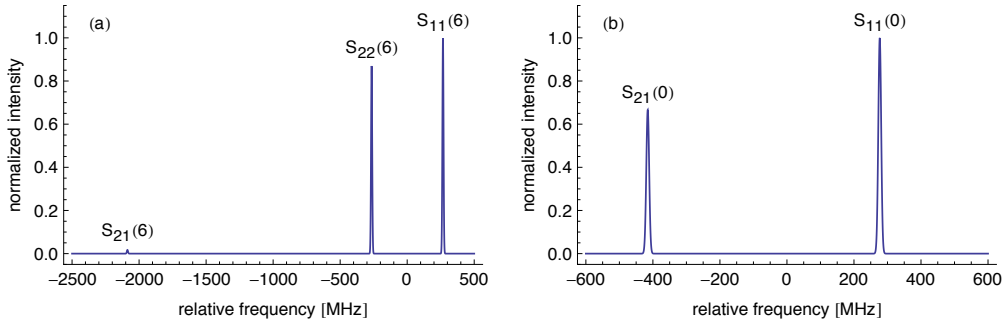

Figure 3.3. Relative line strength of "principal" and "satellite" lines in fine-structure-resolved electric-quadrupole spectra. (a) Infrared fundamental S(6) transitions due to the $I = 0$ nuclear spin isomer in $^{14}N_2^+$: the principal lines $S_{11}(6)$ and $S_{22}(6)$, which fulfill the propensity rule $\Delta N = \Delta J$, are intense, whereas the satellite line $S_{21}(6)$, which violates this rule, shows considerably reduced intensity. **(b)** S(0) transitions in the same system: both, the $S_{11}(0)$ line, which satisfies $\Delta N = \Delta J$, as well as the $S_{21}(0)$ line, which does not, show roughly comparable intensity, i.e., for $N'' = 0$ no clear propensity is observable. (Intensities have been normalized to unity for the most intense peak in each spectrum. Line frequencies are given relative to the pure rotational-vibrational term value and have been calculated as described in Sec. 3.3 using the spin-rotation constants given in Tab. 3.2. Gaussian line shapes have been assumed for the peaks with a full width at half maximum (FWHM) of 10 MHz.)

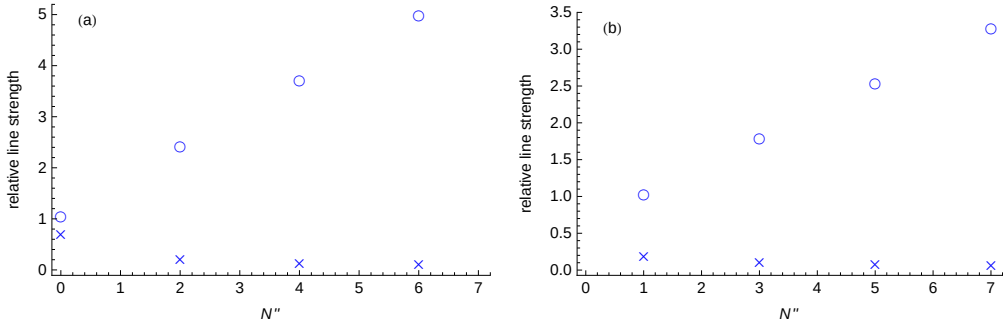

Figure 3.4. Scaling of the line strength of fine-structure-resolved electric-quadrupole rotation-vibration transitions as a function of the rotational quantum number. Relative line strength of S_{11} (circles) vs. S_{21} (crosses) transitions within the $X^2\Sigma_g^+$ state of ortho- **(a)** and para-N_2^+ **(b)** as a function of the lower-level rotational quantum number N''. In accordance with the propensity rule $\Delta N = \Delta J$, the S_{11} transitions ("principal lines") show considerably higher line strength than the S_{21} transitions ("satellite lines") for all but the lowest values of N''. For $N'' = 0$, however, no clear propensity is observed. (Values have been normalized to unity for the lowest possible N''.)

quadrupole lines as well. In general it does, as illustrated in Fig. 3.3 (a) by the example of the fine-structure transitions of the S(6) line due to the $I = 0$ nuclear spin isomer of $^{14}N_2^+$: the principal lines $S_{11}(6)$, $S_{22}(6)$ that fulfill the rule (3.54) are intense, whereas the satellite line $S_{21}(6)$ that violates (3.54) shows considerably reduced intensity. For low N'', however, also lines not fulfilling the propensity rule (3.54) show significant intensity as illustrated with the S(0) line in the same system in Fig. 3.3 (b). The transition between these two regimes is shown in Fig. 3.4.

Physically, the low line strength of transitions connecting the two spin-rotation components reflects the spin flip they involve and are hindered by. With the electric field, which drives rotation-vibration transitions, not coupling directly to the electron spin, this spin flip is only possible via coupling of the electronic spin to the rotational angular momentum. Mathematically, this effect is represented by the Wigner 6j-symbol expressing the recoupling of spin and rotational angular momentum.

For example, in the case of the $S_{11}(N'')$ transitions the squared 6j-symbol is,

$$\begin{Bmatrix} N' & J' & S' \\ J'' & N'' & 2 \end{Bmatrix}^2 = \begin{Bmatrix} N''+2 & N''+5/2 & 1/2 \\ N''+1/2 & N'' & 2 \end{Bmatrix}^2 = \frac{1}{4N''^2+14N''+10}, \tag{3.55}$$

and thus exhibits a factor N''^2 as a leading order in the denominator. The prefactor in (3.53) accounts in that example for,

$$(2N'+1)(2N''+1)(2J'+1)(2J''+1) = N''^4 + 9N''^3 + \tfrac{113}{4}N''^2 + 36N'' + \tfrac{63}{4}, \tag{3.56}$$

and thus contains N''^4 as the highest-order term in N''. Furthermore, the Wigner 3j-symbol appearing in (3.53) is,

$$\begin{pmatrix} N' & 2 & N'' \\ 0 & 0 & 0 \end{pmatrix}^2 = \frac{3(N''+1)(N''+2)}{2(2N''+1)(2N''+3)(2N''+5)}, \tag{3.57}$$

and thus scales asymptotically as $1/N''$. The product of the terms (3.55), (3.56) and (3.57) therefore scales as N'' and hence asymptotically shows the linear increase of the line strength noticeable in Fig. 3.4.

For an $S_{21}(N'')$ transition, on the other hand, the Wigner 6j-symbol is,

$$\begin{Bmatrix} N' & J' & S' \\ J'' & N'' & 2 \end{Bmatrix}^2 = \begin{Bmatrix} N''+2 & N''+3/2 & 1/2 \\ N''+1/2 & N'' & 2 \end{Bmatrix}^2 = \frac{1}{4N''^4+24N''^3+49N''^2+39N''+10}, \tag{3.58}$$

and hence exhibits a factor N''^4 as a leading-order term in the denominator. When multiplied with the other N''-dependent terms in (3.53), this results in a scaling of the line strength according to $1/N''$, which for increasing N'' thus asymptotically approaches zero. As evident from Fig. 3.4, significant deviations from this asymptotic behaviour occur only for $N''=0$, in which case the expressions (3.55) and (3.58) are equal.

In a similar form, this effect is also observed for O and Q lines as can be seen from Tab. 3.4: the line strengths of transitions within the same spin-rotation component (first and last row) scale as N'', whereas the line strengths of those connecting these two components (second and third row) scale as $1/N''$.

3.4.3 Hyperfine-structure effects in electric-quadrupole rotation-vibration transitions

With the techniques developed in the last section, the line strength of an electric-quadrupole rotation-vibration line with resolved hyperfine structure is now readily calculated. As outlined in Sec. 3.3, the angular momentum related to the hyperfine structure is the total angular momentum including nuclear spin $\hat{\mathbf{F}}$, which is formed by coupling the spin-rotational angular momentum $\hat{\mathbf{J}}$ to the total nuclear spin $\hat{\mathbf{I}}$: $\hat{\mathbf{F}} = \hat{\mathbf{I}} + \hat{\mathbf{J}}$. The corresponding eigenstates $|N\Lambda SJIFM_F\rangle$ are related to the previously introduced ones by a Clebsch-Gordan expansion:

$$|N\Lambda SJIFM_F\rangle = \sum_{M_J=-J}^{J} \sum_{M_I=-I}^{I} (-1)^{J-I+M_F}\sqrt{2F+1} \begin{pmatrix} J & I & F \\ M_J & M_I & -M_F \end{pmatrix} |N\Lambda SJM_J\rangle\, |IM_I\rangle\,. \tag{3.59}$$

The upper and lower states for a rotation-vibration transition are thus given by,

$$|n\Lambda\rangle\,|v'\rangle\,|N'\Lambda S'J'I'F'M'_F\rangle = |n\Lambda, v', N'\Lambda S'J'I'F'M'_F\rangle\,, \tag{3.60a}$$

$$|n\Lambda\rangle\,|v''\rangle\,|N''\Lambda S''J''I''F''M''_F\rangle = |n\Lambda, v'', N''\Lambda S''J''I''F''M''_F\rangle\,. \tag{3.60b}$$

The line strength for a hyperfine-structure-resolved electric-quadrupole rotation-vibration line is then calculated as:

$$S^{(\mathrm{hfs})}_{\substack{n\Lambda \\ v'N'S'J'I'F' \\ v''N''S''J''I''F''}} = \sum_{M'_F,M''_F}\sum_{p=-2}^{2}\left|\left\langle n\Lambda, v', N'\Lambda S'J'I'F'M'_F\,\middle|\,\mathrm{T}^2_p\left[\hat{\mathrm{Q}}^{(\mathrm{s})}\right]\,\middle|\,n\Lambda, v'', N''\Lambda S''J''I''F''M''_F\right\rangle\right|^2. \tag{3.61}$$

In contrast to the two previous sections, sums over different I' and I'' values are not needed here, as the transitions belonging to them are all observed as separate lines in a hyperfine-structure-resolved spectrum. Accordingly, a nuclear spin statistical weight factor g_{ns} will not appear either.

Expressing the electric-quadrupole operator in terms of molecule-fixed coordinates and separating spin-rotational from vibronic terms yields:

$$\begin{aligned}&\left\langle n\Lambda, v', N'\Lambda S'J'I'F'M'_F\,\middle|\,\mathrm{T}^2_p\left[\hat{\mathrm{Q}}^{(\mathrm{s})}\right]\,\middle|\,n\Lambda, v'', N''\Lambda S''J''I''F''M''_F\right\rangle\\ &= \sum_{q=-2}^{2}\left\langle n\Lambda, v'\,\middle|\,\mathrm{T}^2_q\left[\hat{\mathrm{Q}}^{(\mathrm{m})}\right]\,\middle|\,n\Lambda, v''\right\rangle\left\langle N'\Lambda S'J'I'F'M'_F\,\middle|\,\left[\hat{\mathcal{D}}^{(2)}_{pq}\right]^*\,\middle|\,N''\Lambda S''J''I''F''M''_F\right\rangle.\end{aligned} \tag{3.62}$$

The spin-rotational matrix element is again calculated by the Wigner-Eckart theorem yielding,

$$\begin{aligned}&\left\langle N'\Lambda S'J'I'F'M'_F\,\middle|\,\left[\hat{\mathcal{D}}^{(2)}_{pq}\right]^*\,\middle|\,N''\Lambda S''J''I''F''M''_F\right\rangle\\ &\qquad= (-1)^{F'-M'_F}\begin{pmatrix}F' & 2 & F''\\ -M'_F & p & M''_F\end{pmatrix}\left\langle N'\Lambda S'J'I'F'\,\middle\|\,\left[\hat{\mathcal{D}}^{(2)}_{\cdot q}\right]^*\,\middle\|\,N''\Lambda S''J''I''F''\right\rangle.\end{aligned} \tag{3.63}$$

As the Wigner rotation matrix elements do not act on the nuclear spin, the same relation (equation (5.72) in [61]) as used before for the electronic spin, may now be applied to eliminate the quantum numbers related to the nuclear spin (I', I'' and F', F'') from the reduced matrix element:

$$\begin{aligned}&\left\langle N'\Lambda S'J'I'F'\,\middle\|\,\left[\hat{\mathcal{D}}^{(2)}_{\cdot q}\right]^*\,\middle\|\,N''\Lambda S''J''I''F''\right\rangle\\ &= \delta_{I'I''}(-1)^{J'+I'+F''+2}\sqrt{2F'+1}\sqrt{2F''+1}\begin{Bmatrix}J' & F' & I'\\ F'' & J'' & 2\end{Bmatrix}\left\langle N'\Lambda S'J'\,\middle\|\,\left[\hat{\mathcal{D}}^{(2)}_{\cdot q}\right]^*\,\middle\|\,N''\Lambda S''J''\right\rangle.\end{aligned} \tag{3.64}$$

The resulting reduced matrix element is calculated exactly as shown in the previous section, i.e., by applying the above mentioned relation once more but with S', S'', J', J'' playing the roles of I', I'', F', F'',

$$\begin{aligned}&\left\langle N'\Lambda S'J'\,\middle\|\,\left[\hat{\mathcal{D}}^{(2)}_{\cdot q}\right]^*\,\middle\|\,N''\Lambda S''J''\right\rangle\\ &\qquad= \delta_{S'S''}(-1)^{N'+S'+J''+2}\sqrt{2J'+1}\sqrt{2J''+1}\begin{Bmatrix}N' & J' & S'\\ J'' & N'' & 2\end{Bmatrix}\left\langle N'\Lambda\,\middle\|\,\left[\hat{\mathcal{D}}^{(2)}_{\cdot q}\right]^*\,\middle\|\,N''\Lambda\right\rangle,\end{aligned} \tag{3.65}$$

and recalling the value of the corresponding rotational reduced matrix element:

$$\left\langle N'\Lambda \left\| \left[\hat{\mathcal{D}}_q^{(2)}\right]^* \right\| N''\Lambda \right\rangle = (-1)^{N'-\Lambda}\,\sqrt{2N'+1}\sqrt{2N''+1}\begin{pmatrix} N' & 2 & N'' \\ -\Lambda & q & \Lambda \end{pmatrix}. \tag{3.66}$$

As before, only the term with $q = 0$ contributes to the sum in (3.62) because of the Wigner 3j-symbol in the above expression.

Substituting equations (3.63) to (3.66) into (3.62), we obtain for the transition matrix element of an electric-quadrupole rotation-vibration transition,

$$\begin{aligned}
&\left\langle n\Lambda, v', N'\Lambda S' J' I' F' M_F' \left| \mathrm{T}_p^2\left[\hat{\mathsf{Q}}^{(\mathrm{s})}\right] \right| n\Lambda, v'', N''\Lambda S'' J'' I'' F'' M_F'' \right\rangle \\
&= \delta_{S'S''}\delta_{I'I''}(-1)^{S'+I'+J'+J''+F'+F''-M_F'-\Lambda}\sqrt{2N'+1}\sqrt{2N''+1}\sqrt{2J'+1}\sqrt{2J''+1} \\
&\quad \sqrt{2F'+1}\sqrt{2F''+1}\begin{pmatrix} N' & 2 & N'' \\ -\Lambda & 0 & \Lambda \end{pmatrix}\begin{pmatrix} F' & 2 & F'' \\ -M_F' & p & M_F'' \end{pmatrix} \\
&\quad \begin{Bmatrix} N' & J' & S' \\ J'' & N'' & 2 \end{Bmatrix}\begin{Bmatrix} J' & F' & I' \\ F'' & J'' & 2 \end{Bmatrix}\left\langle n\Lambda, v' \left| \mathrm{T}_0^2\left[\hat{\mathsf{Q}}^{(\mathrm{m})}\right] \right| n\Lambda, v'' \right\rangle.
\end{aligned} \tag{3.67}$$

The line strength for a hyperfine-structure-resolved electric-quadrupole rotation-vibration line is thus:

$$\begin{aligned}
S^{(\mathrm{hfs})}_{\substack{n\Lambda \\ v'N'S'J'I'F' \\ v''N''S''J''I''F''}} &= \delta_{S'S''}\delta_{I'I''}(2N'+1)(2N''+1)(2J'+1)(2J''+1)(2F'+1)(2F''+1) \\
&\quad \begin{pmatrix} N' & 2 & N'' \\ -\Lambda & 0 & \Lambda \end{pmatrix}^2 \begin{Bmatrix} N' & J' & S' \\ J'' & N'' & 2 \end{Bmatrix}^2 \begin{Bmatrix} J' & F' & I' \\ F'' & J'' & 2 \end{Bmatrix}^2 \\
&\quad \left|\left\langle n\Lambda, v' \left| \mathrm{T}_0^2\left[\hat{\mathsf{Q}}^{(\mathrm{m})}\right] \right| n\Lambda, v'' \right\rangle\right|^2,
\end{aligned} \tag{3.68}$$

where the orthogonality properties of the 3j-symbols,

$$\sum_{M_F', M_F''}\sum_{p=-2}^{2}\begin{pmatrix} F' & 2 & F'' \\ -M_F' & p & M_F'' \end{pmatrix}^2 = 1, \tag{3.69}$$

have been used once more. Equally as in the two preceding sections, the vibronic matrix element appearing in the expression for the line strength may be calculated with equation (3.34) and estimated within the double-harmonic approximation by equation (2.237) from Ch. 2.

The selection rules for ΔN, ΔS, ΔJ and ΔI are exactly as in the previous section. For $\Delta F = F' - F''$ the same selection rule as for ΔJ applies, i.e.,

$$\Delta F = 0, \pm 1, \pm 2. \tag{3.70}$$

For molecules with non-vanishing electronic and nuclear spin, quite a few different combinations of J', J'' and F', F'' quantum numbers are obtained for a transition with particular N' and N'' quantum numbers. For ortho-$^{14}\mathrm{N}_2^+$ in the electronic ground state $\mathrm{X}^2\Sigma_\mathrm{g}^+$, e.g., we have $S = 1/2$ and $I = 0$ or 2. Thus, as discussed in Sec. 3.3, all rotational excited states ($N > 0$) are split into two spin-rotation components, one with $J = N + 1/2$ and one with $J = N - 1/2$. For $I = 2$ and $J \geq 5/2$, each of them is further split into 5 hyperfine-structure states with values for F reaching from $F_\mathrm{min} = J - 2$ in unit steps upto $F_\mathrm{max} = J + 2$ (see Fig. 3.1). In total, there are therefore $2 \times 5 = 10$ hfs levels in the

upper and equally many in the lower rotational-vibrational state, resulting in $10 \times 10 = 100$ potentially possible transitions. For a Q transition, 74 thereof are allowed by the selection rule $|\Delta F| \leq 2$. For O and S transitions, 48 out of the total of 100 transitions fulfill the ΔJ and ΔF selection rules, the others exhibit $|\Delta J| > 2$ or $|\Delta F| > 2$ and are thus forbidden. So, even with the restrictions imposed by the selection rules, the number of possible hyperfine-structure lines is rather substantial and some kind of ordering principle seems desirable.

For electric-dipole allowed transitions, the propensity rule,

$$\Delta N = \Delta J = \Delta F, \tag{3.71}$$

is well established ([60], p. 21). Likewise as in the case of fine-structure-resolved spectra, lines satisfying this rule are called "principal lines" and show significantly higher line strength than those violating it, which are known as "satellite lines" [91, 101, 96, 102]. The question arises, if such a propensity rule is also applicable for electric-quadrupole rotation-vibration lines. If so, it could substantially simplify the interpretation of a hfs-resolved spectrum, as only 10 out of the 74 (48) lines allowed in a certain Q (O, S) transition fulfill this rule.

Calculations of the line strengths given by equation (3.68) for particular values of N' and N'' show that the propensity rule (3.71) is indeed applicable to electric-quadrupole transitions. In Fig. 3.5, the line strength for different hyperfine-structure transitions of the infrared fundamental S(6) line in ortho-$^{14}N_2^+$ is shown: Fig. 3.5 (a) shows an ordered chart of the line strength of the 28 most intense lines belonging to the $I = 2$ nuclear spin isomer. The propensity towards lines obeying the rule (3.71) is clearly visible. Furthermore, the lines group in categories with decreasing intensity, fulfilling at least one of the equalities in (3.71). Fig. 3.5 (b) and (c) show simulated spectra of the S(6) line in the same system. Here, too, the propensity is clearly visible. For low N'', however, no clear propensity is observable as illustrated in Fig. 3.6 by the example of the S(0) infrared fundamental transition in $^{14}N_2^+$.

Physically, the propensity rule (3.71) may be understood on the same grounds as the fine-structure propensity rule presented in the previous section: transitions not fulfilling (3.71) involve a flip of the electronic and/or nuclear spin. With the electric field not directly coupling to these spins, spin flips may only occur via the recoupling of the several angular momenta expressed by the Wigner 6j-symbols. As a consequence, the relative intensities of transitions violating (3.71) are small.

3.4.4 Intensity alteration due to mixing of Hund's case (b_{β_J}) states

In the preceding section, the line strength of electric-quadrupole rotation-vibration transitions for pure Hund's case (b_{β_J}) angular momentum states has been calculated. For this result to be applicable, the molecular Hamiltonian must commute with the angular momentum operators $\hat{\mathbf{N}}$, $\hat{\mathbf{S}}$, $\hat{\mathbf{J}}$, $\hat{\mathbf{I}}$, $\hat{\mathbf{F}}$ and $\hat{F}_z$, i.e., the Hamiltonian must be diagonal in the Hund's case (b_{β_J}) basis. As shown in Sec. 3.3, this is not true for the hyperfine-structure Hamiltonian of $^{14}N_2^+$. This Hamiltonian exhibits off-diagonal matrix elements with respect to the N, J and I quantum numbers. Whereas the matrix elements off-diagonal in the N and I quantum numbers may have been neglected at the level of accuracy appropriate for the interpretation of our experiments (see Ch. 4), mixing of states with different J quantum numbers needs to be considered. Each eigenstate of the hfs Hamiltonian in $^{14}N_2^+$ is thus given according to

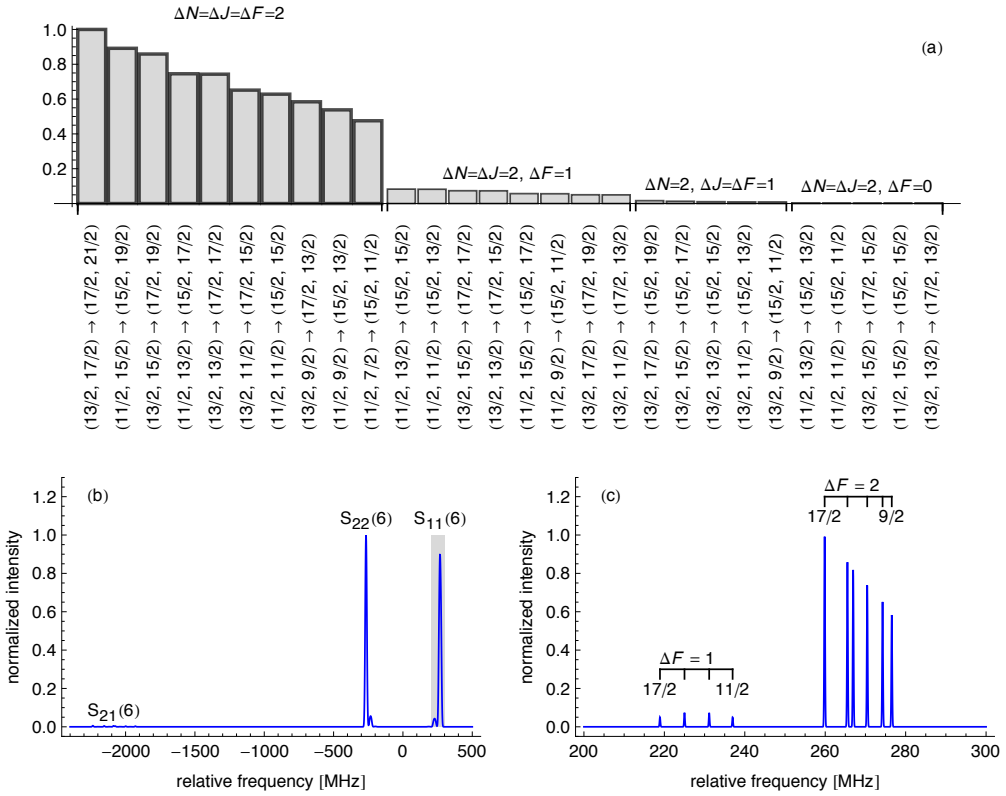

Figure 3.5. Line strengths of hyperfine-structure-resolved electric-quadrupole rotation-vibration transitions of the infrared fundamental S(6) line in ortho-$^{14}N_2^+$. (a) Bar chart of the normalized line strengths of the 28 most intense transitions belonging to the $I = 2$ nuclear spin isomer in decreasing order (labelled as $(J'', F'') \rightarrow (J', F')$ below the chart). The 10 transitions in accordance with the propensity rule $\Delta N = \Delta J = \Delta F$ (bars with bold edges) are most intense. They are followed by transitions fulfilling at least one of the equalities in this propensity rule. The remaining 20 lines (not shown) out of the total of 48 electric-quadrupole-allowed lines exhibit almost negligible line strength. **(b)** Simulated spectrum of the S(6) line in ortho-$^{14}N_2^+$ as seen at lower resolution (FWHM: 10 MHz). The labels indicate the positions of the lines belonging to the $I = 0$ nuclear spin isomer. The principal hfs lines belonging to the $I = 2$ nuclear spin isomer lie close to the $I = 0$ lines. They are accompanied by satellite lines visible as small humps next to them. **(c)** Detailed view showing the gray-marked area in (b) at higher resolution (FWHM: 0.25 MHz). The different hyperfine-structure lines are resolved. The principal lines ($\Delta F = 2$) show again considerably higher line strength than the satellite lines ($\Delta F = 1$). The peaks due to the $I = 2$ nuclear spin isomer are labelled by the corresponding F'' quantum numbers below the assignment bars. The peak next to the one of the $\Delta F = 2$, $F'' = 15/2$ transition is due to the $J'' = 13/2 \rightarrow J' = 17/2$, $I = 0$ transition. (The frequencies in (b) and (c) are given relative to the pure rotational-vibrational term value and have been calculated as described in Sec. 3.3 using the molecular constants given in Tab. 3.2. The intensities are normalized to unity for the most intense peaks. Gaussian line shapes are assumed.)

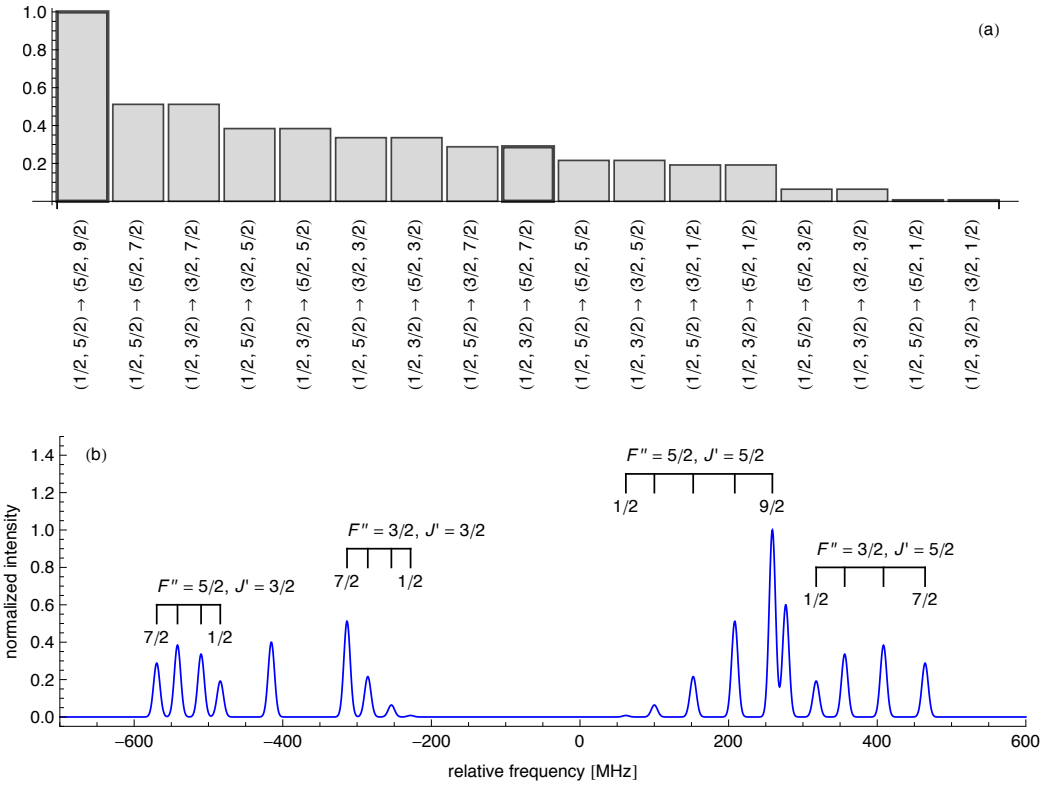

Figure 3.6. Line strengths of hyperfine-structure-resolved electric-quadrupole rotation-vibration transitions of the infrared fundamental S(0) line in ortho-$^{14}N_2^+$. (a) Bar chart of the normalized line strengths of all electric-quadrupole-allowed S(0) transitions (labelled as $(J'', F'') \to (J', F')$ below the chart). The two transitions fulfilling the propensity rule $\Delta N = \Delta J = \Delta F$ are marked with bold edges. Despite one of these two transitions ($J'' = 1/2, F'' = 5/2 \to J' = 5/2, F' = 9/2$) showing the highest line strength among all of them, the other one ($J'' = 1/2, F'' = 3/2 \to J' = 5/2, F' = 7/2$) does not exhibit particularly high line strength and seven other transitions not satisfying this propensity rule show higher or equal line strength. **(b)** Simulated spectrum of the S(0) line in ortho-$^{14}N_2^+$: in contrast to the spectrum of the S(6) line shown in Fig. 3.5, no clear propensity is recognizable and both, lines satisfying the propensity rule (3.71) as well as those that do not, show considerable line strength. Peaks due to the $I = 2$ nuclear spin isomer are labelled with the F'' and J' quantum numbers of the respective transitions above and the F' quantum numbers below the assignment bars. The peaks near −400 MHz and +300 MHz are due to the $J'' = 1/2 \to J' = 3/2$ and the $J'' = 1/2 \to J' = 5/2$ transitions of the $I = 0$ nuclear spin isomer, respectively. (Line frequencies have been calculated as described in Sec. 3.3 using the molecular constants given in Tab. 3.2 and are given relative to the pure rotational-vibrational term value. Intensities are normalized to unity for the most intense peak. Gaussian line shapes are assumed for the peaks with a FWHM of 10 MHz.)

equation (3.14) as a linear combination of the two Hund's case (b_{β_J}) basis states that correspond to the two possible values of J for a given rotational quantum number N. The upper and lower states for a rotation-vibration transition when taking into account the mixing of the Hund's case (b_{β_J}) basis states due to the hfs Hamiltonian are thus given as,

$$|n\Lambda, v', N'\Lambda S'\widetilde{J}'I'F'M_F'\rangle = \sum_{J'=|N'-S'|}^{N'+S'} c'_{\widetilde{J}'J'F'} \, |n\Lambda, v', N'\Lambda S'J'I'F'M_F'\rangle \,, \tag{3.72a}$$

$$|n\Lambda, v'', N''\Lambda S''\widetilde{J}''I''F''M_F''\rangle = \sum_{J''=|N''-S''|}^{N''+S''} c''_{\widetilde{J}''J''F''} \, |n\Lambda, v'', N''\Lambda S''J''I''F''M_F''\rangle \,, \tag{3.72b}$$

with normalized expansion coefficients $c'_{\widetilde{J}'J'F'}, c''_{\widetilde{J}''J''F''} \in \mathbb{R}$. The near quantum numbers $\widetilde{J}'$ and $\widetilde{J}''$ are used to label such transitions.

The line strength of an electric-quadrupole transition between these states is calculated in a similar way as in the preceding section. The upper and lower quantum states used so far in the transition matrix element with well-defined J' and J'' quantum numbers are replaced by the expansions (3.72a) and (3.72b). The terms depending on J' and J'' are thus weighted by the coefficients $c'_{\widetilde{J}'J'F'}$ and $c''_{\widetilde{J}''J''F''}$. The line strength obtained in this way is:

$$\begin{aligned} S^{(\mathrm{mixed})}_{\substack{n\Lambda \\ v'N'S'\widetilde{J}'I'F' \\ v''N''S''\widetilde{J}''I''F''}} &= \delta_{S'S''}\delta_{I'I''}(2N'+1)(2N''+1)(2F'+1)(2F''+1) \\ &\quad \begin{pmatrix} N' & 2 & N'' \\ -\Lambda & 0 & \Lambda \end{pmatrix}^2 \left| \left\langle n\Lambda, v' \middle| \, \mathrm{T}^2_0\left[\hat{\mathrm{Q}}^{(\mathrm{m})}\right] \middle| \, n\Lambda, v'' \right\rangle \right|^2 \\ &\quad \left| \sum_{J'=|N'-S'|}^{N'+S'} \sum_{J''=|N''-S''|}^{N''+S''} c'_{\widetilde{J}'J'F'} c''_{\widetilde{J}''J''F''} (-1)^{J'+J''} \right. \\ &\quad \left. \sqrt{2J'+1}\sqrt{2J''+1} \begin{Bmatrix} N' & J' & S' \\ J'' & N'' & 2 \end{Bmatrix} \begin{Bmatrix} J' & F' & I' \\ F'' & J'' & 2 \end{Bmatrix} \right|^2 . \end{aligned} \tag{3.73}$$

For the particular case of S(0) transitions, only one value for J'' (namely $J'' = S''$) is possible and no mixing in the lower state occurs. Equation (3.73) may thus be simplified (for a Σ state) to:

$$\begin{aligned} S^{(\mathrm{mixed})}_{\substack{n\Lambda=0 \\ v'N'S'\widetilde{J}'I'F' \\ v''N''=0\,S''J''=S''I''F''}} &= \delta_{S'S''}\delta_{I'I''}(2N'+1)(2J''+1)(2F'+1)(2F''+1) \\ &\quad \begin{pmatrix} N' & 2 & 0 \\ 0 & 0 & 0 \end{pmatrix}^2 \left| \left\langle n\,0, v' \middle| \, \mathrm{T}^2_0\left[\hat{\mathrm{Q}}^{(\mathrm{m})}\right] \middle| \, n\,0, v'' \right\rangle \right|^2 \\ &\quad \left| \sum_{J'=|N'-S'|}^{N'+S'} c'_{\widetilde{J}'J'F'} (-1)^{J'} \sqrt{2J'+1} \begin{Bmatrix} N' & J' & S' \\ J'' & 0 & 2 \end{Bmatrix} \begin{Bmatrix} J' & F' & I' \\ F'' & J'' & 2 \end{Bmatrix} \right|^2 . \end{aligned} \tag{3.74}$$

In order to verify this result, we derived the analogue of equation (3.74) for the electric-dipole, rotation-vibration-electronic R(0) line ($N''=0, J''=1/2 \rightarrow N'=1, \widetilde{J}'=1\pm1/2$) of the $X^2\Sigma^+_g, v''=0 \rightarrow$

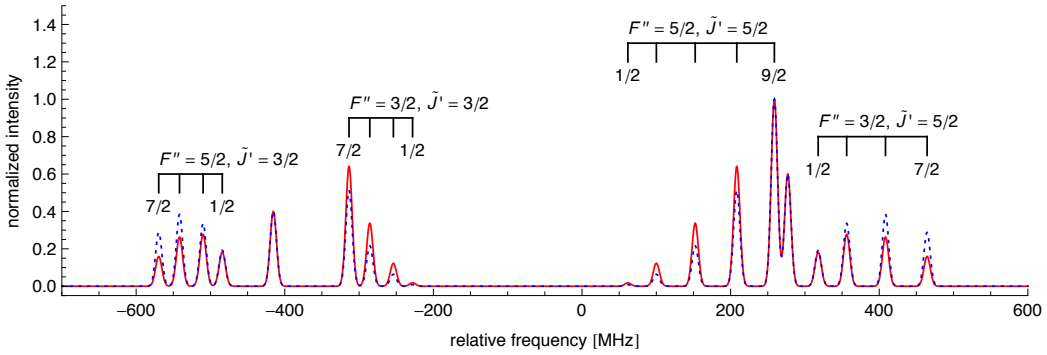

Figure 3.7. Effect of the mixing of the Hund's case (b_{β_J}) basis states by the hfs Hamiltonian on the line strength in an electric-quadrupole rotation-vibration spectrum. Simulated spectrum of the electric-quadrupole infrared fundamental S(0) line in ortho-$^{14}N_2^+$. The red, solid curve shows the spectrum with intensities calculated from (3.74), i.e. with mixing of the Hund's case (b_{β_J}) basis states taken into account. For the blue, dashed curve, intensities have been calculated using equation (3.68) from the previous section, i.e., mixing of basis states has been neglected. The mixing of the basis states results in a significant redistribution of intensity among the lines. Peaks due to the $I = 2$ nuclear spin isomer are labelled with the F'' and $\widetilde{J}'$ quantum numbers of the respective transitions above and the F' quantum numbers below the assignment bars. The peaks near −400 MHz and +300 MHz are due to the $J'' = 1/2 \to J' = 3/2$ and the $J'' = 1/2 \to J' = 5/2$ transitions of the $I = 0$ nuclear spin isomer, respectively. (Line frequencies are given relative to the pure rotational-vibrational term value and have been calculated as described in Sec. 3.3 using the molecular constants given in Tab. 3.2. Intensities are normalized to unity for the most intense peak. Gaussian line shapes are assumed for the peaks with a FWHM of 10 MHz).

$B^2\Sigma_u^+, v' = 1$ band in $^{14}N_2^+$:

$$S^{(\mathrm{E1,\ mixed})}_{\substack{\mathrm{X}\to\mathrm{B,\,R(0)} \\ \widetilde{J}'I'F' \\ I''F''}} = 6\delta_{I'I''}(2F'+1)(2F''+1)\begin{pmatrix} 1 & 1 & 0 \\ 0 & 0 & 0 \end{pmatrix}^2 \left|\left\langle \mathrm{B}^2\Sigma_u^+, v'=1 \left| \mathrm{T}^1_0\left[\hat{\boldsymbol{\mu}}^{(\mathrm{m})}\right] \right| \mathrm{X}^2\Sigma_g^+, v''=0 \right\rangle\right|^2 \left| \sum_{J'=1/2}^{3/2} c'_{\widetilde{J}'J'F'}(-1)^{J'}\sqrt{2J'+1} \begin{Bmatrix} 1 & J' & 1/2 \\ 1/2 & 0 & 1 \end{Bmatrix} \begin{Bmatrix} J' & F' & I' \\ F'' & 1/2 & 1 \end{Bmatrix} \right|^2 . \tag{3.75}$$

Comparison of the relative line strength of different R(0) hfs transitions calculated using this formula with the simulated spectrum in Fig. 4 from Rosner, Gaily and Holt [101] shows good agreement within the precision of their data.

The effect of the mixing of the Hund's case (b_{β_J}) states by the hfs Hamiltonian is illustrated in Fig. 3.7, showing a simulated spectrum of the S(0) line in $^{14}N_2^+$ with and without taking into account the admixture of the non-dominant term in the expansion (3.72a). Considerable redistribution of intensity among the several hfs transitions due to mixing is observed. For higher rotational states, mixing of Hund's case (b_{β_J}) states becomes negligible because of the increasing energetic separation of the two spin-rotation components, which scales linearly with N: $F_1(N) - F_2(N) = \gamma_v(N + 1/2)$.

Concluding, we see that with the material presented in this chapter, the whole theory of electric-quadrupole rotation-vibration transitions in the N_2^+ molecular cation, including fine- and hyperfine-structure effects, has been developed. The fs and hfs Hamiltonian—determining the line frequencies—has been given, line strengths have been calculated and selection, as well as propensity rules have been derived and their applicability has been discussed. In the following chapter, we will show how such transitions were observed experimentally.

Chapter 4

Observation of electric-quadrupole rotation-vibration transitions in the molecular nitrogen cation

4.1 Introduction

As mentioned in the preceding chapters, a major result of this thesis is the observation of electric-quadrupole rotation-vibration transitions in a molecular ion. To our knowledge, this is the first such observation reported so far. In this chapter our observations of electric-quadrupole rotation-vibration transitions in the N_2^+ molecular cation are presented. First, our experimental setup is portrayed. The physical backgrounds of the experimental techniques employed are explained qualitatively and the technical details of their implementation are shortly discussed. For more detailed explanations, references to the relevant literature are given. Thereafter, the measurement of infrared fundamental S(0) transitions in N_2^+ with this setup is described. The measured spectrum is presented and discussed within the frame of the theory of electric-quadrupole rotation-vibration transitions presented in the two preceding chapters. The results presented in this chapter have been published originally in a "letter" having appeared in Nature Physics [114] as well as in a subsequent invited article in CHIMIA [115]. Therefore, this chapter is partly based on these two publications written jointly by Stefan Willitsch, Xin Tong and the author of this thesis.

4.2 Experimental setup and experimental techniques

4.2.1 Overview

An overview of the experimental setup is shown in Fig. 4.1. In contrast to the experiments addressing electric-dipole-forbidden transitions in neutral molecules discussed in Ch. 1, our experiment is not based on high particle densities or a long absorption path. We rather made use of long interrogation times combined with a highly sensitive detection technique to observe even single absorption events. The N_2^+ ions were trapped in a radio frequency (rf) ion trap, which forms the centre of our experimental setup. N_2^+ ions were produced by photoionization of neutral N_2 molecules from a molecular beam

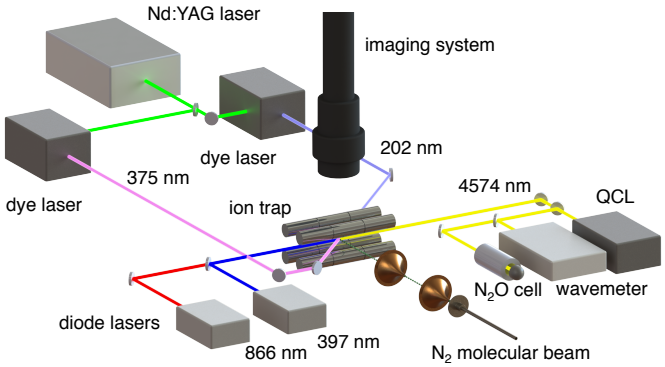

Figure 4.1. Experimental setup for the observation of electric-quadrupole rotation-vibration transitions in N_2^+ ions. Transitions were observed with N_2^+ ions trapped in a linear radio frequency ion trap. N_2^+ ions were loaded into this trap by state-selective photoionization of neutral N_2 from a molecular beam and sympathetically cooled by simultaneously trapped laser-cooled Ca^+ ions to form bicomponent Coulomb crystals. The electric-quadrupole S(0) rotational-vibrational transition was excited with mid-IR radiation produced by a quantum cascade laser (QCL). The fluorescence light of the Ca^+ ions was collected by a CCD camera to image the crystals. The frequency of the mid-IR radiation is monitored and stabilized with an IR wavemeter calibrated to N_2O absorption lines (see text for details).

with ultraviolet (UV) radiation from two pulsed dye lasers (202 nm and 375 nm). Within the ion trap, the N_2^+ ions thermalized with cotrapped, laser cooled Ca^+ ions by the Coulomb interaction and were cooled to millikelvin temperatures. For laser cooling, diode lasers at 397 nm and 866 nm were used. The fluorescence light due to laser cooling was captured by an imaging system consisting of a microscope and an electron multiplying CCD camera (Andor Luca R, Andor Technology Ltd., Belfast, UK). Electric-quadrupole rotation-vibration transitions in N_2^+ were excited by mid-infrared (mid-IR) radiation produced by a quantum cascade laser (QCL) [116, 58]. Excited ions were detected by a state-selective charge transfer reaction with Ar atoms. Vibrationally excited ions are neutralized in this reaction and were lost from the trap, which was observable as a change in the structure of the Coulomb crystal as seen with the camera. By comparing images of the crystal taken before and after the IR-excitation-CT-reaction sequence, the quadrupole transition was probed at the frequency addressed with the QCL. Repeated application of this scheme while scanning the QCL frequency enabled us to take a spectrum of the electric-quadrupole infrared fundamental transition in N_2^+.

4.2.2 Ion trapping

In our setup, N_2^+ and Ca^+ ions were trapped in a radio frequency quadrupole trap. Charged particles may not be trapped by purely electrostatic fields in charge free space as may be seen from the first of Maxwell's equation. In free space, the charge density vanishes and the first of Maxwell's equation describing the electric field corresponds to the Laplace equation for the electrostatic potential. The sum of the second derivatives of the electrostatic potential thus vanishes. This is contradictory to the properties of a continuous function exhibiting a minimum at this position. The electrostatic potential may thus not exhibit a minimum in free space, as would be needed for trapping—a tenet known as Earnshaw's theorem [117]. One solution to this issue is trapping of charged particles by oscillatory (instead of static), inhomogeneous electric fields. A type of apparatus exploiting this technique was developed by Paul [118] and is known as a "Paul trap". The theory of charged particle trapping by this and similar setups is well-known and described in many monographs and review articles

[119, 120, 121, 118, 122, 123, 124, 125]. In short, for suitable chosen experimental parameters, the motion of a charged particle in an inhomogeneous, oscillatory electric field may be separated into two components: a fast oscillation at the frequency of the field evolving around an equilibrium position, which itself moves considerably slower. The oscillatory motion at the frequency of the electric field is known as "micromotion", the comparatively slow motion of the mean position as "secular motion". For suitably chosen experimental conditions, the time-averaged kinetic energy of the charged particle is conserved (which is in general *not* true for a system with time-varying external forces). Furthermore, the time-averaged micromotion amplitude (observed on time scales $\gg$ rf period) solely depends on the position of the particle and not on other variables such as the time, etc. Hence, the part of the kinetic energy associated with the micromotion may be expressed mathematically in terms of a scalar potential. This potential is known as the"effective potential" or "pseudopotential". In regions of higher electric field strength, the micromotion amplitude and, correspondingly, the pseudopotential energy increases. Accordingly, the kinetic energy associated with the secular motion decreases—and vice versa in regions of lower electric field strength. An inhomogeneous electric rf field thus creates a pseudopotential for the secular motion of the ion pushing it in direction of decreasing rf amplitude in the inhomogeneous electric field.

Unlike electrostatic potentials, for the pseudopotential electrode geometries may be found creating a pseudopotential minimum in free space. Hence, ions may be trapped in free space in such a pseudopotential. In our setup, this was achieved with an apparatus known as a "linear Paul trap". This trap consists of four cylindrical stainless steel rods with a diameter of 8 mm arranged as the four long edges of an elongated cuboid at a distance of 3.5 mm from the symmetry axis of the trap (see [109, 126] for details). On these rods, sinusoidally oscillating voltages with an amplitude of $V_{\text{rf, zero-to-peak}} = 120\,\text{V}$ and a frequency of $\Omega_{\text{rf}} = 2\pi \times 3.2\,\text{MHz}$ with opposite polarity on neighboring rods were applied. Each rod is segmented into three isolated electrodes, with additional dc voltages of $\approx 1.5\,\text{V}$ applied to the end-segment electrodes for axial confinement. For this configuration, the pseudo and the electrostatic end-segment potential form together a nearly harmonic potential well with respect to all three dimensions in vicinity of the trap centre. The equations of motion for a single trapped ion may then be solved analytically [124, 123, 125]. For large ensembles of ions, the equations of motion are integrated numerically (see Sec. 4.3.2).

4.2.3 Laser cooling of Ca^+ ions

As mentioned above, the N_2^+ ions were sympathetically cooled using Doppler laser-cooled Ca^+ ions. Doppler laser cooling is a well-established method of atomic physics and has been described in several textbooks (e.g. [127, 128, 119, 120]). In essence, an atomic ensemble is exposed to a laser beam with a frequency slightly red-detuned from an atomic transition. Due to the Doppler effect, the laser frequency is shifted closer to resonance for atoms moving against the direction of propagation of the laser beam in the moving frame of reference of the atoms and away from resonance for those moving along with the laser light. Atoms exhibiting a velocity component antiparallel to the laser beam—or more precisely, to the wavevector of the optical wave—experience thus an increased probability for absorbing a photon compared to those without such a component or with a component parallel to the wavevector. In an absorption event, the momentum of the photon is transferred to the atom, which thus looses momentum and is decelerated. The subsequent emission is isotropic and therefore the momentum antiparallel to the direction of propagation of the laser is diminished effectively in average

over many absorption-emission cycles. Although a single laser beam in principle only decelerates atoms in one direction, the coupling of the motion along different directions by the Coulomb interaction in an ensemble of trapped ions results in an efficient cooling along all directions. A prerequisite for laser cooling is a closed optical cycling transition being addressable in the particle to be cooled. This restricts laser cooling usually to simple atoms or atomic ions (mostly alkali atoms and alkaline earth ions) and excludes molecules (aside from a few very particular species [129, 130]). Therefore, N_2^+ ions may not be laser-cooled and sympathetical cooling by atomic Ca^+ ions was used for our experiments.

In our setup, the $4s^2S_{1/2} \rightarrow 4p^2P_{1/2}$ transition in Ca^+ at 397 nm was used for Doppler laser cooling. The trap was loaded with Ca^+ ions by photoionization of the skimmed effusion from a Ca oven heated to $300 - 350\,°C$. Ca atoms were non-resonantly photoionized using the same laser (375 nm) as for the third photon in the ionization of N_2^+ (see below). During laser cooling, Ca^+ ions excited to the $4p^2P_{1/2}$ state may decay with a small probability to the metastable $3d^2D_{3/2}$ state. These ions were repumped into the cooling cycle with an additional laser at 866 nm addressing the $3d^2D_{3/2} \rightarrow 4p^2P_{1/2}$ transition. Both, the cooling and the repumper beams were introduced along the trap axis. The cooling beam (397 nm) was reflected with a mirror behind the vacuum chamber and reinserted into the trap in order to balance radiation pressure forces on the Ca^+ ions. Using this setup, the Ca^+ ions were Doppler laser cooled to a secular temperature of $T_{Ca^+} \approx 18\,\mathrm{mK}$ and a secular temperature for the sympathetically cooled N_2^+ ions of $T_{N_2^+} \approx 20\,\mathrm{mK}$ was achieved (as determined by comparison with numerical simulations of the ion dynamics, see Sec. 4.3.2).

4.2.4 State-selective production of N_2^+ ions

In order to observe the extremely weak electric-quadrupole transitions in N_2^+, the N_2^+ ions were produced state-selectively in the rotational-vibrational ground state. This way, the N_2^+ population is confined to the to the lower rovibrational quantum state of the electric-quadrupole transition studied. This state-selective production is achieved with a two-colour resonance-enhanced multiphoton ionization (REMPI) scheme (see Fig. 4.2). In this scheme, neutral N_2 molecules in the rovibronic ground state ($X^1\Sigma_g^+$, $J'' = 0$, $v'' = 0$) are first excited to the $a''\,^1\Sigma_g^+$ $J' = 2$, $v' = 0$ state of neutral N_2 by two photons at $\approx 202\,\mathrm{nm}$. From this intermediate state, N_2 is ionized by a third photon at $\approx 375\,\mathrm{nm}$. The ionization process is governed by the selection rule $\Delta N = N^{+\prime\prime} - J' = \text{even}$ [131, 132] and the strong propensity rule $\Delta N = N^{+\prime\prime} - J' = 0, \pm 2$ ([105, 106], see also Ch. 5). Therefore, only the ionic rotational states $N^{+\prime\prime} = 0$ and $N^{+\prime\prime} = 2$ are accessible from the $J' = 0$ level in the neutral $a''\,^1\Sigma_g^+$ state. Here, J'' (J') and v'' (v') stand for the rotational and vibrational quantum numbers in the $X^1\Sigma_g^+$ ground ($a''\,^1\Sigma_g^+$ excited) state of neutral N_2. $N^{+\prime\prime}$ denotes the rotational quantum number in the vibrational ground state ($v^{+\prime\prime} = 0$) of the N_2^+ ion. The energy for the third photon is chosen to reach just above the ionization threshold for the rotational ground state, but not above the threshold for $N^{+\prime\prime} = 2$, the energetically lowest accessible rotational excited state. Hence, state-selective production is achieved.

UV radiation for photoionization was produced by two pulsed, 532 nm-Nd:YAG-pumped dye lasers: a "Radiant Dyes NarrowScan" (Radiant Dyes Laser & Accessories GmbH, Wermelskirchen, Germany) and a "FindeAdjustment Pulsare" (ERÜ Kunststofftechnik GmbH, Radevormwald, Germany) for 375 nm and 202 nm, respectively. For 375 nm, the frequency-doubled emission from a Styryl 8 dye solution was used, whereas 202 nm radiation was generated by the frequency-tripled emission from a Rhodamine B / Rhodamine 101 dye mixture.

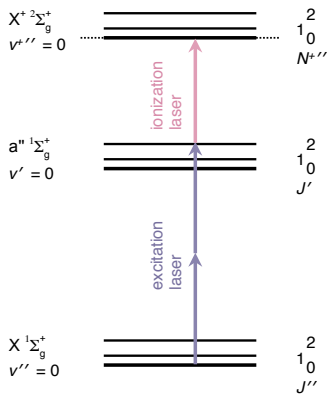

Figure 4.2. REMPI scheme for state-selective production of molecular nitrogen ions. Resonance-enhanced [2+1']-photon threshold ionization scheme used to produce N_2^+ ions state-selectively in the rotational-vibrational ground state ($v^{+\prime\prime} = 0, N^{+\prime\prime} = 0$): neutral N_2 molecules in the rovibronic ground state ($v'' = 0, J'' = 0$) are excited by two photons at 202 nm to the $a''\,^1\Sigma_g^+$ $v' = 0, J' = 2$ state. From this intermediate state, N_2 is ionized by a third photon at 375 nm. State selectivity is ensured by setting the energy of the third photon to reach just slightly above the lowest ionization threshold (dotted line).

The two counterpropagating laser beams were focused to beam diameters of a few hundred micrometers inside the ion trap, where they intersected with each other as well as with a double skimmed N_2 molecular beam. The molecular beam was formed by the supersonic expansion of N_2 gas from a pulsed valve (pulse duration 10 ms, repetition rate 10 Hz, stagnation pressure $\approx$ 1 bar) into a high-vacuum vessel (base pressure $10^{-8}-10^{-7}$mbar). The supersonic expansion internally cooled the N_2 molecules to typical rotational temperatures of ≈ 10 K [133] increasing the population in the rovibrational ground state addressed by our REMPI scheme. The skimmers collimated the beam and separated three differential pumping stages to sustain ultra high vacuum conditions in the trap region (background pressure $\approx 3 \times 10^{-10}$ mbar). In order to avoid state changing collisions of previously loaded N_2^+ ions with neutral N_2 molecules from the molecular beam, the beam passed the trapping region $\approx 250\,\mu$m beside the trap centre.

The intensities of the two REMPI laser beams were chosen such that non-resonant, one-colour ionization of N_2, which depreciates state-selectivity, is suppressed. Typical pulse energies were about 0.15 mJ per pulse and 3 mJ per pulse for 202 nm and 375 nm, respectively. The ratio of the one- to the two-colour ionization rate was periodically checked between measurements of N_2^+ quadrupole transitions. As shown in [108, 109], high state-selectivity in the production of N_2^+ ions may be achieved with this scheme.

4.2.5 Mid-infrared radiation source

Electric-quadrupole vibrational transitions in N_2^+ were excited with mid-IR radiation from an external-cavity continuous-wave QCL (Daylight Solutions 21045-MHF, Daylight Solutions, Inc., San Diego, CA, USA) delivering an effective power of ≈ 170 mW at a wavelength of 4574 nm (2186 cm^{-1}) with a nominal bandwidth < 0.001 cm^{-1} [134]. The mid-IR beam was focused to a spot size of $\approx 140\,\mu$m FWHM at the position of the N_2^+ ions resulting in a IR irradiance of $\approx 7.7 \times 10^6$ W m^{-2}.

The frequency of the QCL was monitored with a mid-IR wavelength meter (Bristol Instruments 621-A IR, Bristol Instruments, Inc., Victor, NY, USA) with a quoted resolution of 9 MHz which was

calibrated with an accuracy of 8 MHz against absorption lines of N_2O with frequencies known from the HITRAN database [135]. Absorption spectra of N_2O were taken using a 15 cm long absorption cell filled with N_2O at a pressure of a roughly 1 mbar. The transmitted intensity was measured with a PbSe photoconductive detector (Hamamatsu P9696-03, Hamamatsu Photonics K. K., Hamamatsu City, Shizuoka, Japan). For suppressing electrical as well as optical noise present on the photodetector signal, the IR beam was mechanically chopped at a frequency of about 250 Hz and the photodetector voltage was capacitively coupled to a digital oscilloscope. The amplitude of this modulated signal was used to detect the relative IR intensity nearly background- and noise-free.

Active stabilization of the QCL frequency was achieved with a PI (proportional integral) feedback loop. The frequency measurements of the wavelength meter were processed on a personal computer and compared to a given set point. Based on the observed deviation, a correction voltage was applied to a piezo element acting on the external cavity grating of the QCL. The piezo voltage was updated about once every second. In order to sweep the QCL frequency, the set point was slowly scanned by the control program with the locked laser frequency following accordingly. For QCL frequency locking and scanning, a control program based on the LabVIEW software package (National Instruments Corporation, Austin, TX, USA) has been developed.

4.3 Measurement of hyperfine-structure-resolved IR fundamental S(0) transitions in N_2^+

Using the experimental setup and the experimental techniques presented above, the spectrum of the IR fundamental S(0) transition, i.e., the transition $(v^{+\prime\prime} = 0,\ N^{+\prime\prime} = 0) \rightarrow (v^{+\prime} = 1,\ N^{+\prime} = 2)$ within the electronic ground state $X^2\Sigma_g^+$ of N_2^+ was measured. More precisely, the principal hfs-resolved transitions, meaning those fulfilling the propensity rule $\Delta N = \Delta J = \Delta F$, were probed. There are in total three transitions fulfilling this rule: two for the $I = 2$ nuclear spin isomer of N_2^+, namely the $F^{+\prime\prime} = 3/2 \rightarrow F^{+\prime} = 7/2$ and the $F^{+\prime\prime} = 5/2 \rightarrow F^{+\prime} = 9/2$ transition, as well as one belonging to the $I = 0$ nuclear spin isomer, namely the $J^{+\prime\prime} = 1/2 \rightarrow J^{+\prime} = 5/2$ transition (see Fig. 4.3 for a level scheme). Here, $N^{+\prime\prime}$ ($N^{+\prime}$), $J^{+\prime\prime}$ ($J^{+\prime}$) and $F^{+\prime\prime}$ ($F^{+\prime}$) denote the rotational angular momentum, the total angular momentum without nuclear spin and the total angular momentum including nuclear spin in the vibrational ground (first excited) state of N_2^+ (see Sec. 3.3 for details on the angular momentum coupling in N_2^+).

Though, in view of the theory of hfs-resolved electric-quadrupole rotation-vibration transitions from Ch. 3, there are in the particular case of the S(0) line other transitions exhibiting similar or even higher line strengths than these "principal" transitions, they were chosen here in lack of any detailed knowledge about the strength of the different hfs-resolved line components—the theory presented in Ch. 3 was only developed after having measured this spectrum in the process of interpreting the experimental data.

4.3.1 Experimental procedure

In a typical experiment, first a pure Ca^+ crystal of ≈ 1000 ions was loaded, followed by the loading of about $20 - 25$ N_2^+ ions. Due to the dependence of the pseudopotential on the ion mass (lighter ions

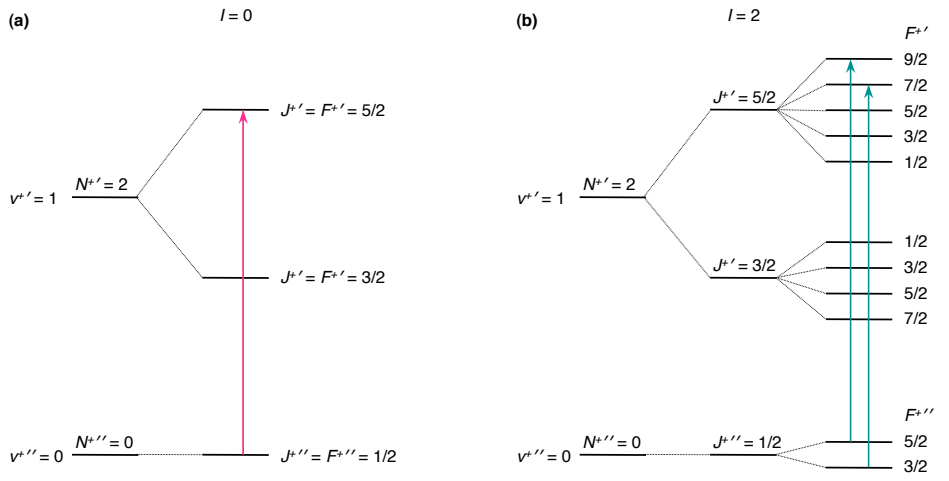

Figure 4.3. Level scheme for S(0) electric-quadrupole rotation-vibration transitions in N_2^+. (a) $I = 0$ nuclear-spin isomer: the excited level is split by the spin-rotation interaction into two fine-structure components associated with different $J^{+\prime}$ quantum numbers. **(b)** $I = 2$ nuclear-spin isomer: the levels are further split by the hyperfine interaction into several hfs levels labelled by $F^{+\prime\prime}$ and $F^{+\prime}$ quantum numbers. The principal electric-quadrupole transitions (those in accordance with $\Delta N = \Delta J = \Delta F$) are indicated by vertical arrows. (See Sec. 3.3 in the preceding Ch. for details about the fine and hyperfine structure in N_2^+.)

show a larger micromotion amplitude and therefore experience a steeper pseudopotential), the N_2^+ ions accumulated at the centre of such a bicomponent Coulomb crystal, observable as a dark, non-fluorescent core (Fig. 4.4 (a)). Immediately after loading N_2^+, mid-IR radiation was irradiated on the crystal to excite electric-quadrupole rotation-vibration transitions in N_2^+. Simultaneously, Ar gas was introduced into the chamber through a leak valve at a partial pressure of about 2 to 4×10^{-8} mbar. Ar atoms react with vibrationally excited N_2^+ ions in a charge transfer (CT) reaction according to (see [110])

$$N_2^+(v^+ \geq 1) + \mathrm{Ar} \rightarrow N_2 + \mathrm{Ar}^+. \tag{4.1}$$

Neutral N_2 molecules formed in this reaction were lost from the trap, whereas the newly produced Ar^+ ions diffused into the Ca^+-Coulomb crystal because of the similar masses of these two species. The CT reaction was thus observable as a shrinking of the dark N_2^+-core in the Coulomb crystal. For ions in the vibrational ground state, the above reaction is endothermic and thus suppressed [110]. The number of lost N_2^+ ions therefore directly resembles the number of vibrationally excited N_2^+ ions. After ≈ 2 min, the Ar leak valve was closed and the pressure in the chamber dropped to ultrahigh vacuum levels again. Loss of ions due to other processes than laser excitation was excluded by "blind" experiments with the QCL beam blocked done regularly in between actual measurements. In the very rare cases (only two out of 136 individual measurements comprising the spectrum shown in Fig. 4.5), in which such background ion loss was observed, a background loss rate was determined and the data were corrected accordingly.

To pin down the frequency of the IR fundamental S(0) line in N_2^+, the QCL frequency was first scanned over adjacent frequency intervals in vicinity of the theoretically predicted transition frequencies (see Sec. 3.3 and 4.3.4). Upon indication of CT, the interval was split and the procedure repeated to subsequently further constraining the transition frequency. Finally, the electric-quadrupole IR fundamental S(0) hyperfine transitions were probed by scanning the QCL frequency in steps of $0.0003\,\mathrm{cm}^{-1}$ (9 MHz).

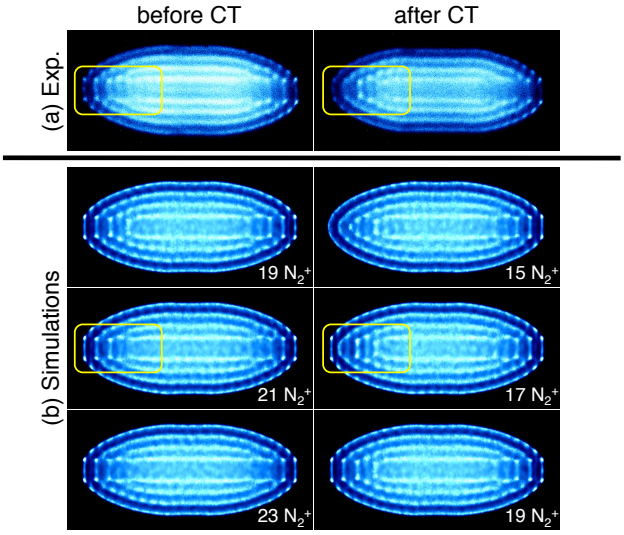

Figure 4.4. Fluorescence images of bicomponent Ca^+/N_2^+ Coulomb crystals. (a) Images taken during one experimental cycle before and after IR irradiation and charge-transfer (CT) detection of N_2^+ ions. The N_2^+ ions appear as a non-fluorescent core in the centre of the crystals. Slight changes in the structure of the core indicate the removal of N_2^+ ions by CT reactions following their excitation (see highlighted regions). **(b)** Synthetic images obtained from numerical simulations of the ion dynamics containing different numbers of N_2^+ ions. The simulated images with 21 and 17 N_2^+ ions best fit the experimental images taken before and after CT, respectively.

4.3.2 Data analysis

In order to accurately determine the number of CT events, i.e., of vibrationally excited N_2^+ ions, the experimental images of the Coulomb crystals were compared to synthetic images generated from numerical simulations of the ion dynamics (see, e.g., [136] for details on these methods) with known numbers of N_2^+ ions. Trajectories of the ions were calculated by numerical integration of the classical equations of motion incorporating the relevant forces for ion trapping and cooling as well as the Coulomb interaction between ions. These simulations were done with the ProtoMol software package [137] combined with custom-written extensions. From the simulated ion trajectories, three-dimensional histograms were generated, which, when projected onto an imaging plane, reproduce the experimental fluorescence images of the Coulomb crystals. The blurring of the experimental images, caused by the finite depth of focus of the imaging system, was emulated by Gaussian smoothing of the synthetic images implemented as a post-processing code based on MATLAB (The MathWorks, Inc., Natick, MA, USA) and MathWorks' Image Processing Toolbox. By careful tuning of simulation parameters, synthetic images were obtained, which reproduce even subtle details in the experimental ones. Comparing experimental with synthetic images allowed the determination of the number of vibrationally excited N_2^+ ions with an accuracy of ± 1 (see Fig. 4.4) [108, 109].

4.3.3 Measured spectrum

The spectrum of electric-quadrupole IR fundamental S(0) hfs-resolved transitions in N_2^+ obtained by this method is shown in Fig. 4.5. Each data point represents the mean number of CT events averaged over 8 or 16 individual measurements shown as a function of the excitation frequency. The spectrum shows two well-separated peaks: a broader one around 2186.173 cm^{-1} (65 539.82 GHz) and

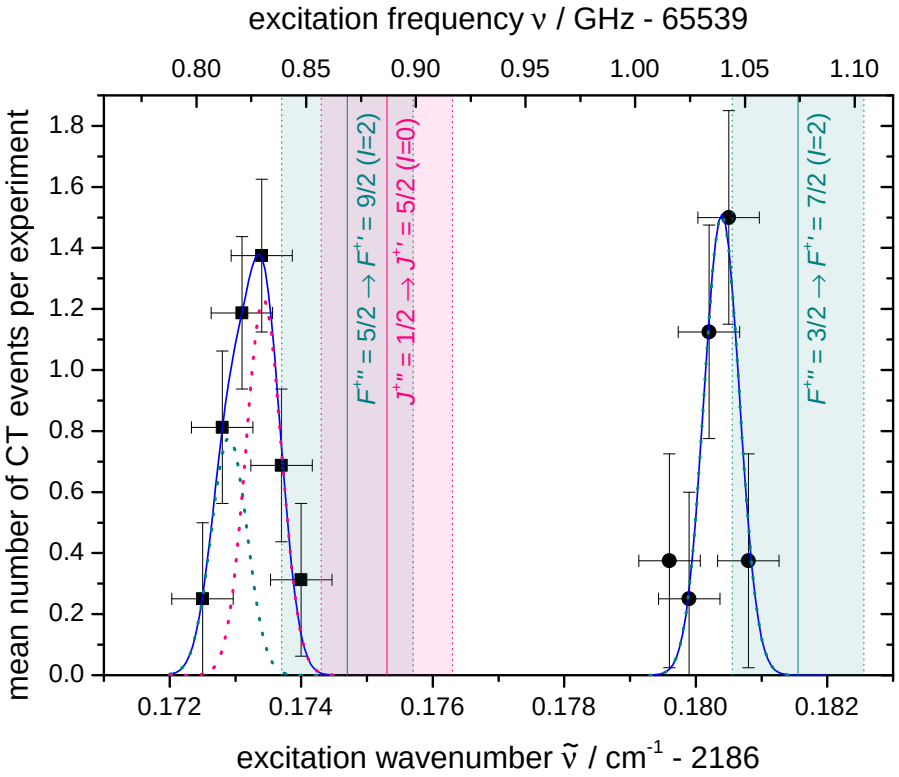

Figure 4.5. Spectrum of hyperfine components of the S(0) electric-quadrupole rotation-vibration IR fundamental transition in ortho-N_2^+ represented as the mean number of CT events per experimental cycle as a function of the excitation frequency. Data points marked with squares (circles) were averaged over 16 (8) experiments. The horizontal and vertical error bars correspond to the relevant 1σ uncertainties. The dotted lines represent Gaussian fits of the three spectral transitions to the data points, the solid blue line shows their sum. The theoretically predicted positions of the hyperfine transitions belonging to the $I = 2$ ($I = 0$) nuclear spin isomer indicated in Fig. 4.3 are shown by solid green (pink) vertical lines. These values were calculated as outlined in Sec. 3.3 and 4.3.4 based on the spectroscopic constants taken from [96, 102, 93]. The shaded areas represent their 1σ uncertainties.

a narrower one at 2186.1804(4) cm^{-1} (65 540.039(12) GHz). The higher-frequency peak is assigned to the $F^{+\prime\prime} = 3/2 \rightarrow F^{+\prime} = 7/2$ ($I = 2$) transition based on theoretically predicted transition frequencies (see Sec. 4.3.4) that are shown as solid vertical lines in Fig. 4.5. The width of this peak (≈ 19 MHz FWHM) is attributed to the bandwidth of the IR laser radiation (specified to be < 30 MHz [134] as mentioned above). Collisional broadening is widely suppressed for trapped ions in an ultra high vacuum environment and the Doppler width of ≈ 1.3 MHz at the secular ion temperature of $T_{N_2^+} \approx 20$ mK as well as the natural linewidth (nanohertz range, see Appendix B) are considerably smaller. The lower-frequency peak is assigned to the two overlapping transitions $F^{+\prime\prime} = 5/2 \rightarrow F^{+\prime} = 9/2$ ($I = 2$) and $J^{+\prime\prime} = 1/2 \rightarrow J^{+\prime} = 5/2$ ($I = 0$), which are not resolved at the present laser bandwidth. This overlap is reflected in the higher width of this peak of ≈ 30 MHz FWHM.

The frequencies of these transitions were determined by fitting a model consisting of three Gaussian peaks to the measured spectrum. The individual peaks of this model are shown as dotted lines in Fig. 4.5 and their sum as a blue, solid line. The line intensities are constrained by the theory of hyperfine-structure-resolved electric-quadrupole rotation-vibration transitions presented in Ch. 3. For fitting this model to the experimental spectrum, the frequency of each transition was treated as an

individual free parameter. The integrated intensity, the linewidth and the ratio of the populations in the two hfs levels of the $I = 2$ nuclear spin manifold, which are not thermal but rather reflect the photoionization dynamics of the REMPI process the ions are produced with (see Ch. 5), were treated as common free parameters for all peaks. The ratio of the total population in the $I = 2$ to the $I = 0$ nuclear spin manifold was fixed at 5:1 according to nuclear spin statistics. From this fit, the transition frequencies of the $F^{+\prime\prime} = 5/2 \rightarrow F^{+\prime} = 9/2$ ($I = 2$) and the $J^{+\prime\prime} = 1/2 \rightarrow J^{+\prime} = 5/2$ ($I = 0$) transitions were determined as 2186.1729(4) cm^{-1} [65539.815(12) GHz] and 2186.1734(4) cm^{-1} [65539.831(12) GHz], respectively. The relative positions of the peaks, i.e., the hyperfine splittings of the rovibrational line, have been obtained as 16(1) MHz, 209(17) MHz and 225(17) MHz.

4.3.4 Comparison with theoretical predictions

Line positions (transition frequencies)

The fine and hyperfine splittings of the S(0) IR fundamental line may be calculated using the Hamiltonian from [96] and the molecular constants compiled in Tab. 3.2 as explained in Sec. 3.3. The absolute transition frequencies are obtained when adding the rovibrational term value using the spectroscopic constants from Tab. 3.1. The frequencies obtained from this calculation are given in Tab. 4.1 and shown as vertical lines in Fig. 4.5. Their 1σ-uncertainties are indicated by shaded areas in Fig. 4.5 as obtained by propagating the uncertainties in the spectroscopic constants from the respective sources [96, 102, 93].

As evident from Fig. 4.5, all transitions appear at slightly (≈ 1 standard uncertainty) lower absolute frequencies than predicted. This deviation might indicate the vibrational frequency and/or the rotational constant of N_2^+ in the excited state being slightly lower than the values used in our calculations. Vibrational frequencies of N_2^+ have so far only been determined indirectly from the analysis of electronic spectra. The values from such studies reported in the literature [97, 98, 90, 93] differ by a few hundreds of MHz. Though, one of the most accurate and latest studies [93] was used for our calculations, deviations from the calculated values are to be expected at the level of precision of our measurements. Put into that perspective, the observed deviations between measured and predicted absolute transition frequencies thus seem acceptable.

For the relative line positions, i.e., hyperfine splittings, the values of 18(1) MHz, 187(2) MHz and 206(3) MHz were predicted. The observed splittings are thus in reasonable agreement with these predictions and allowed the aforementioned assignment of the observed features in the spectrum. Together with the control experiments described above, we may thus conclude that we indeed did observe electric-quadrupole rotation-vibration transitions of N_2^+ and that we were able to assign the features in the measured spectrum to the different fs and hfs components as mentioned above.

Line intensities (excitation rates)

The observed excitation rates (CT events per unit time interval) are considerably lower than expected from the theory developed in Ch. 2 and 3. When using for the derivative of the electric-quadrupole moment the result from the computational study by Bruna and Grein [45], we obtain an excitation rate of $\approx 9.1 \times 10^{-2}\,\mathrm{s}^{-1}$ per ion for the $F^{+\prime\prime} = 3/2 \rightarrow F^{+\prime} = 7/2$ ($I = 2$) transition at our experimental

Table 4.1. Transition frequencies for principle S(0) IR fundamental hfs line components in N_2^+.

Rovibrational transition frequencies (absolute line positions)

Transition	Measured [cm^{-1}][a]	Predicted [cm^{-1}][a,b]
$F^{+\prime\prime} = 5/2 \rightarrow F^{+\prime} = 9/2$ $(I = 2)$ [Peak 1]	2186.1729(4)	2186.1747(10)
$J^{+\prime\prime} = 1/2 \rightarrow J^{+\prime} = 5/2$ $(I = 0)$ [Peak 2]	2186.1734(4)	2186.1753(10)
$F^{+\prime\prime} = 3/2 \rightarrow F^{+\prime} = 7/2$ $(I = 2)$ [Peak 3]	2186.1804(4)	2186.1816(10)

Hyperfine splittings (relative line positions)

Splitting	Measured [MHz][a]	Predicted [MHz][a,b]
Peak 1 to Peak 2 [c]	16(1)	18(1)
Peak 1 to Peak 3	225(17)	206(3)
Peak 2 to Peak 3	209(17)	187(2)

[a] Values in parentheses correspond to one standard uncertainty and apply to the last digits.
[b] Based on spectroscopic constants from [96, 102, 93] compiled in Tab. 3.1 and 3.2.
[c] The higher precision in this splitting was achieved because the data this value is based on were taken in close succession (for the most part within a few days). The other splittings involve measurements over a more extended period of time (a few weeks). As a result, their uncertainties include estimates for additional long-term drifts in the IR frequency.

conditions (see Appendix B). This translates into a total excitation rate of $\approx 0.76\,s^{-1}$ for 25 ions when a fraction of 1/3 of them is supposed to be in the $F^{+\prime\prime} = 3/2$ $(I = 2)$ state (according to the degeneracy of the three $N^{+\prime\prime} = 0$ levels). Therefore, almost all N_2^+ ions addressed are expected to undergone CT reactions during the experimental period of $\approx 2\,min$. Observed were, however, only about 1.5 excitation events during that period, corresponding to an excitation rate of $\approx 1.5/120\,s \approx 1.3 \times 10^{-2}\,s^{-1}$. This experimental excitation rate accounts for only roughly 1/60 of the theoretically expected value. In addition to the absolute excitation rate being lower than expected, also the relative excitation rates for the different hfs transitions, i.e., the ratio of the peak heights in the spectrum of Fig. 4.5, deviates from the theoretical calculations presented in Ch. 3 (cf. Fig. 3.7).

The reason for this discrepancy has been investigated quite extensively but no definite answer has been found so far. The deviation might be either due to an erroneous or inadequate theoretical calculation or unconsidered or wrongly determined experimental factors. In general, determination of line intensities from "action spectroscopy" experiments, such as the laser-induced charge-transfer spectroscopy used here, is difficult because the measured signal (here the number of neutralized N_2^+ ions) is only indirectly linked to the actual spectroscopic excitation (see Fig. 4.6). The processes linking the initial spectroscopic excitation to the measured signal compete with other processes diminishing this signal. Deviations of the observed from the theoretically expected excitation rate may thus result from the interplay of these processes.

In detail, the following factors have been considered as possible reasons for the observed discrepancy:

Electric-quadrupole transition matrix element. The dominating uncertainty in the theoretically calculated excitation rate lies in the value of the derivative of the molecular electric-quadrupole moment with respect to the internuclear separation. In lack of any experimental data, we used the above-mentioned value obtained by Bruna and Grein [45] from an ab-initio calculation. Generally, ab-initio calculations of accurate values for molecular multipole moments and their derivatives are

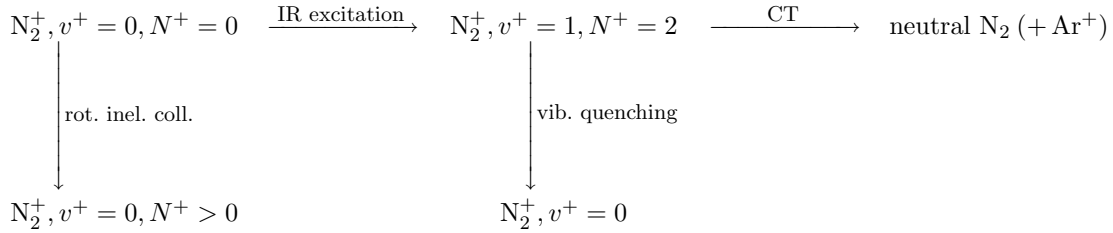

Figure 4.6. Processes involved in N_2^+ CT spectroscopy. The actual spectroscopic excitation (labelled "IR excitation") is not observed directly, but is indirectly linked to the observed signal (number of neutralized N_2^+ ions). The processes forming this link (horizontal arrows) compete with other processes (vertical arrows), such as rotationally inelastic collisions or vibrational quenching (see text for other potentially possible processes), diminishing the number of neutralized N_2^+ ions and thus reducing the apparent excitation rate. Hence, this apparent rate does not only depend on the actual spectroscopic excitation rate, but also on the rate constants (and associated particle densities) of these competing processes.

challenging and assessing the accuracy of the result in [45] is difficult in absence of other theoretical studies or experimental measurements. Indeed, even the authors of this study admit that their "N_2^+ value is probably about 10% too high" ([45], p. 73).

On the other hand, many diatomic molecules (see [80]) exhibit electric quadrupole moment derivatives on the order of roughly $ea_0 = 8.5 \times 10^{-30}\,\mathrm{C\,m}$ (e: elementary charge, a_0: Bohr radius) such that at least the order of magnitude of the value used might be assumed correct. Nevertheless, as the excitation rate depends quadratically on this quantity, still, a too high value for the quadrupole moment derivative could at least partially explain the observed discrepancy.

Besides on the derivative of the molecular quadrupole moment, the predicted excitation rate also depends on how the rovibrational transition matrix element is derived from this quantity and particularly, if the double-harmonic approximation (equation (2.237)) is applicable. In general, this approximation is reasonable for calculations of electric-quadrupole rovibrational line strengths between low-lying vibrational states in the electronic ground state of stable molecules (see, e.g., [83, 33, 84]). On the contrary, deviations from this approximation are known for electric-dipole vibrational transitions in certain heteronuclear molecules ([70], p. 165). Nonetheless, it seems unlikely that higher-order terms in the expansions (2.225) and (2.148) shall substantially diminish the harmonic contributions.

Over estimation of the IR intensity at the position of the N_2^+ ions. The intensity of the IR radiation to which the N_2^+ ions were exposed depends on the diameter of the IR beam as well as on the position of the ions within the beam. As the mid-IR radiation is neither visible by the naked eye, nor with the CCD camera and because the centre of the ion trap is not directly accessible, these quantities are not easily determined. The beam diameter was determined from a beam profile recorded by measuring the transmitted power when introducing an absorbing mechanical target in the beam path. Despite some uncertainty in the beam diameter inherent to this method, a deviation in the diameter large enough to fully explain the discrepancy in the excitation rate seems unlikely. Alignment of the IR beam was verified on a daily basis using the same target. The accuracy of this alignment method was found to be better than $\approx 50\,\mu\mathrm{m}$ (at a beam diameter of $140\,\mu\mathrm{m}$ FWHM). Concluding, misalignment of the IR laser beam and underestimation of the beam diameter may possibly partially, but not fully account for the observed discrepancy in the excitation rate.

Accidental excitation of electronic transitions in N_2^+. N_2^+ exhibits a dipole-allowed electronic transition at 391 nm due to the $X^2\Sigma_g^+$, $v^{+\prime\prime} = 0 \rightarrow B^2\Sigma_u^+$, $v^{+\prime} = 0$ band (see Ch. 3 and 6). Possibly, this transition could have been excited by the weak, broadband background emission of the 397 nm laser used for Ca^+ cooling. Decay of ions from the excited $B^2\Sigma_u^+$ state then resulted in rovibrational redistribution of the population from the in initially prepared rovibrational quantum state to other rovibrational levels of the electronic ground state, i.e., in a diminished population in the level addressed by the QCL. This process, however, was ruled out, because the decay of the excited electronic state had resulted in populating vibrationally excited states of the electronic ground state (according to known Franck-Condon factors [94, 95]). Therefore, CT reactions would have been observed even without IR excitation. Such reactions were not observed in several dozens of "background" measurements with the QCL beam blocked done regularly in between actual measurements.

Effective Ar particle density. The CT reaction rate depends directly on the Ar particle density at the position of the N_2^+ ions. The pressure in the vacuum chamber while leaking in Ar gas was monitored with a cold cathode vacuum gauge (IKR 270, Pfeiffer Vacuum Technology AG, Aßlar, Germany) mounted at the side of the chamber. As the distribution of the gas is subject to the so-called "molecular flow", meaning that gas molecules fly in straight lines in between collisions with surfaces (mean free path length $\gg$ chamber dimensions), a deviation between the particle density inferred from the pressure reading and the actual Ar particle density within the trapping volume, which is partially screened by the trap electrodes, might be suspected. However, a rough model of the gas flow with the ion trap approximated as a one-side-open cuboid showed in and outside pressure to equilibrate within milliseconds. Hence, these effects are negligible on the time scale of our experiments.

Vibrational quenching of N_2^+ by Ar. Quenching of vibrationally excited N_2^+ competes with CT and hence could result in a lower apparent excitation rate (see Fig. 4.6). With the CT rate constant accounting for about half of the Langevin collision rate, a decrease by a factor of two in the apparent excitation rate could be reached when assuming all non-CT-reactive collisions being vibrationally inelastic. However, previous measurements of the vibrational quenching rate constant of N_2^+ in Ar by Kato et al. [138] yielded an upper bound of $k_{\text{vib. quench.}} \leq 1.2 \times 10^{-11}\,\text{cm}^3\,\text{s}^{-1}$ or less than 1.7 % of the Langevin rate constant. Therefore, this effect seems not to be an issue.

Rotationally inelastic collisions of N_2^+ with Ar. Collisions of N_2^+ ions with Ar atoms prior to IR excitation would result in a redistribution of the population from the initially prepared rotational-vibrational quantum state (see Fig. 4.6). Similar as for accidental electronic excitation, part of the population would then no more be addressed by the QCL resulting in a diminished apparent excitation rate.

The rotationally-inelastic N_2^+-Ar collision rate constant was measured by Schlemmer et al. [110] to account for $\approx 1/50$ of the Langevin rate constant. Using their value, we found rotationally inelastic collisions to play a minor role in our experiment, based on a simple kinetic rate model (see Fig. 4.7 (a)). To asses the sensitivity of the apparent excitation rate on the rotationally-inelastic collision rate, we repeated this calculation for a rotationally-inelastic collision rate constant higher by about one order of magnitude. For that value, a considerable decrease in the vibrationally excited population is observed in our model (Fig. 4.7 (b)).

The low rotationally-inelastic rate constant found in [110] has already by the authors of this publication been considered a "surprising result", because N_2^+ and Ar may form a strongly bound intermediate complex [110] and reaction mechanisms based on such an intermediate complex usually result in a mixing of all accessible product channels (see, e.g., [133]). Hence, a rotationally-inelastic collision rate close to the Langevin rate would be expected and no explanation for the considerably lower value reported in [110] has been found. Indeed, simulations of N_2^+ + Ar collisions motivated by our observations that were done in the Computational Chemistry Group of Prof. Markus Meuwly at the University of Basel showed rotationally inelastic collisions to occur considerably more frequently at our experimental conditions [139].

Moreover, rotationally inelastic collisions may already partially explain the observed discrepancy between the measured and the expected excitation rate—even when as infrequent as found in [110]—if also a reduced vibrational excitation rate is assumed. A reduction of the electric-quadrupole excitation rate constant (e.g., due to an overestimated IR intensity or transition matrix element) by just a factor of 1/30 (instead of the above mentioned 1/60) yields the experimentally observed result of about 1.5 excitation events during a period of $\approx 2\,\mathrm{min}$, if rotationally inelastic collisions with the rate constant given in [110] are taken into account (Fig. 4.7 (c)).

Therefore, we may speculate that rotationally inelastic collisions may—at least partially—account for the low apparent excitation rate measured. This effect could possibly explain both, the discrepancy in the absolute excitation rate as well as the deviation of the relative intensities of the several hfs transitions probed from the theoretical expectations. Measurements to investigate this issue and eventually support this hypothesis are in preparation at the time of this writing.

4.4 Conclusion

The observations reported in this chapter show that very weak electric-quadrupole rotation vibration transitions in N_2^+ may be addressed with our experimental approach. This is—as mentioned earlier—to our knowledge the first such observation in a molecular ion. It was achieved by a combination of advanced and partly just recently developed techniques of atomic and molecular physics, namely state-selective production, trapping and sympathetic cooling of molecular ions as well as detection of excited ions by a state-selective charge transfer reaction and the use of a frequency-stabilized QCL as an IR radiation source.

The features observed in our spectrum were successfully assigned to hyperfine-structure components of the S(0) IR fundamental transition of N_2^+. The reasonable agreement of the observed hfs splittings with theoretical predictions as well as the exclusion of other loss-mechanisms than laser induced CT by numerous background experiments prove that indeed electric-quadrupole rotation vibration transitions were addressed in our experiments. The mentioned discrepancies in the vibrational excitation rate are not yet fully understood but a thorough analysis of this issue yielded strong hints to possible reasons causing this discrepancy.

The observation of electric-dipole-forbidden rotation-vibration transitions in a molecular ion opens up numerous new applications such as those discussed in Ch. 1 due to the ultra small natural linewidth of these transitions and—correspondingly—the extremely high lifetime of their excited states.

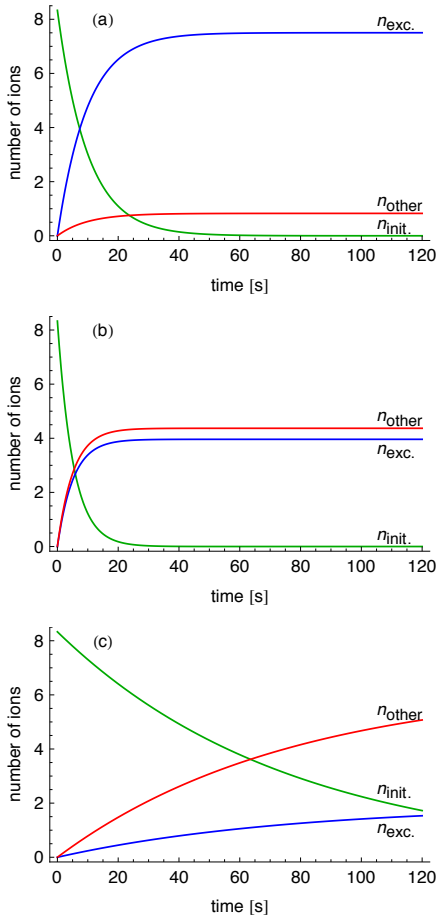

Figure 4.7. Evolution of the N_2^+ population during an electric-quadrupole-excitation/CT-reaction experiment. The evolution was studied by means of a kinetic model based on the reaction pathways shown in Fig. 4.6 (with neglected vibrational quenching). The initial population in the $F^{+\prime\prime} = 3/2$ level is depleted by two competing processes: rovibrational excitation with subsequent CT and inelastic collisions with Ar atoms. The evolution of the populations in the initial level $n_{\mathrm{init.}}(t)$, in other rovibrational states $n_{\mathrm{other}}(t)$ and in the vibrationally excited (and hence CT-reacting) state $n_{\mathrm{exc.}}(t)$ are given as a function of time t by the equations,

$$\begin{aligned}
\mathrm{d}n_{\mathrm{init.}}(t)/\mathrm{d}t &= -(k_{\mathrm{vib.\ exc.}} + k_{\mathrm{inel.\ coll.}})n_{\mathrm{init}}(t),\\
\mathrm{d}n_{\mathrm{exc.}}(t)/\mathrm{d}t &= k_{\mathrm{vib.\ exc.}}n_{\mathrm{init}}(t),\\
n_{\mathrm{other}}(t) &= n_{\mathrm{tot}} - n_{\mathrm{init.}}(t) - n_{\mathrm{exc.}}(t),
\end{aligned}$$

with n_{tot} the total number of N_2^+. **(a)** When using the excitation rate constant $k_{\mathrm{vib.\ exc.}} = 9.1 \times 10^{-2}\,\mathrm{s}^{-1}$ as calculated in Appendix B and the rotationally-inelastic collision rate constant $k_{\mathrm{inel.\ coll.}} = 1.0 \times 10^{-2}\,\mathrm{s}^{-1}$ (based on the value of $1.4 \times 10^{-11}\,\mathrm{cm}^3\,\mathrm{s}^{-1}$ from [110] and an Ar particle density of $7.2 \times 10^{8}\,\mathrm{cm}^{-3}$), nearly the whole population addressed by the QCL is expected to become vibrationally excited and undergo CT reactions. **(b)** Assumption of an inelastic collision rate constant higher by one order of magnitude considerably diminishes the number of vibrationally excited ions, even with the same vibrational excitation rate constant as in (a) because of the noticeable competition between these two processes. **(c)** If, on the other hand, the inelastic collision rate constant from [110] is used, a reduction of the vibrational excitation rate by a just a factor of 1/30 (instead of the ratio between measured and calculated excitation rates of 1/60) reproduces our experimental finding of ≈ 1.5 ions being excited during a period of 2 min. Hence, rotationally inelastic collisions may partially explain the observed discrepancy in the excitation rate, even at this low value for the inelastic collision rate constant, if at the same time a reduced vibrational excitation rate is assumed.

A prerequisite for such applications are stable, spectrally narrow mid-IR radiation sources. In view of recent developments in this area, such as mid-IR frequency combs [140] or novel frequency stabilization techniques that provide spectrally exceptionally narrow emission, high frequency stability and frequency accuracy by linking a quantum cascade laser to a near-infrared frequency comb [141] or even directly to primary frequency standards [142], such applications may soon come into reach.

The full potential of electric-dipole-forbidden transitions in molecular ions will be exploited when these narrow radiation sources are combined with non-destructive, coherent quantum-state-detection techniques based on the long-range Coulomb interaction—unique to ions and not present in neutrals—such as the one described in Ch. 6.

Chapter 5

Fine- and hyperfine-structure effects in molecular photoionization

5.1 Introduction

Molecular photoionization, as a major method to produce molecular ions for trapped-particle experiments, represents a crucial technique for high-precision studies of molecular ions. Particularly, the ability to produce molecular ions state-selectively and hence to initialize them for subsequent experiments renders molecular photoionization a valuable technique for high-precision studies. A detailed understanding of the photoionization process is thus essential for precision experiments with molecular ions.

With the electronic, vibrational and rotational structure being investigated for several decades in molecular photoionization and photoelectron spectra, models describing the rovibronic effects in photoionization are nowadays well established. These models, i.e., their selection and propensity rules, laid the basis for the production of rovibronic state-selected molecular ions by photoionization [106, 143, 108, 109].

In contrast to the rovibronic effects, the roles of the electron and the nuclear spin, associated with the spin-rotational fine structure and the hyperfine structure, respectively, are not covered by common photoionization models, as these features are usually—we will encounter exceptions below—not resolved in (traditional) photoionization or photoelectron spectra. The limited knowledge about these effects is reflected in the electric-quadrupole rotation-vibration spectrum of the N_2^+ ion presented in the preceding chapter: with the relative populations in the hfs levels of the N_2^+ ions produced in our REMPI scheme being unknown, they had to be described by a free parameter.

Motivated by this issue and in view of the importance of photoionization for future high-precision experiments, we have developed a model for fine- and hyperfine-structure effects in molecular photoionization which is presented in this chapter.

Besides the application in high-precision experiments, our model is also of interest from a general point of view in molecular physics. Photoionization and photoelectron spectroscopy provided valuable information on central aspects of molecular structure theory, supporting the development of such essential concepts as, e.g., molecular orbital theory (see, e.g., [144], p. 415 or [145]). Since the first photoelectron

spectroscopic studies of molecules in the 1960s, their resolution has steadily been improved, such that vibrational and thereon rotational structure were resolved during the following decades [146]. Along with experimental progress, the theoretical models have been refined. Vibrational structure has been understood in terms of the Franck-Condon principle (see, e.g., [147]). Concerning rotational structure, Buckingham, Orr and Sichel presented in 1970 in a seminal paper [148] a model to describe rotational line intensities in photoelectron spectra, now known as the "BOS model". During the 1980s and 1990s, extended models, such as to describe resonance-enhanced multiphoton ionization (e.g., [149]) or to interpret not only the total ionization intensity but also the angular distribution of the photoelectrons (e.g., [150, 151]) have been developed. Also, the BOS model has been rephrased in terms of spherical tensor algebra [132], the form it is used here, and extended to asymmetric rotors [143].

However, spin-rotational fine structure has been resolved only in a few photoionization experiments, e.g., in the ionization spectra of O_2 from Palm and Merkt [152] and of H_2O from Merkt et al. [153], and we are not aware of any hyperfine-structure-resolved direct photoelectron spectrum of a molecule. As a consequence, models for direct photoionization so far do not cover these effects.

Studying fine and hyperfine structure in molecular photoionization is the domain of PFI-ZEKE (pulsed-field-ionization zero-kinetic-energy) and Rydberg spectroscopy [152, 153, 154, 155, 156, 157]. In these techniques, data obtained from electronic transitions to highly excited neutral states are interpreted as series converging to certain ionic states. Results from these experiments are well understood within the framework of multichannel quantum-defect theory (MQDT) and provide detailed information on the fine and hyperfine structure of molecular ions [154, 155, 156, 158, 157]. For the direct ionization process utilized in trapped-ion experiments, a less involved treatment is possible by including fine- and hyperfine-structure effects into the BOS model. This is the approach pursued in this chapter.

The chapter is structured as follows: first, a model for the spin-rotational fine structure in direct, i.e. one-photon, photoionization is developed. Then this model is extended to cover transitions between individual hfs levels in photoionization. To validate our model, we apply it to the fine-structure-resolved photoelectron spectrum of O_2 recorded by Palm and Merkt [152]. The implications of our model for hfs-resolved ionization transitions are illustrated with the example of the photoionization of molecular nitrogen.

Thereafter, we consider the three-photon, two-colour REMPI process used in the experiment of the previous chapter to produce N_2^+ ions. This [2+1'] REMPI scheme is regarded as two subsequent processes: a two-photon excitation step, followed by a one-photon ionization step. For both of these steps, a hfs-resolved description is developed. The REMPI model obtained from these descriptions is first applied to the non-hfs-state-selective ionization technique described in the previous chapter. After that, implications of our model for possible future hfs-state-selective ionization schemes are discussed. The chapter finishes by concluding the findings obtained and discussing the suitability of the approximations employed in our model.

5.2 Direct photoionization

We consider the ionization of a diatomic molecule AB yielding the molecular ion AB^+ by ejection of a photoelectron e^- through interaction with electromagnetic radiation via the electric-dipole opera-

tor $\hat{\boldsymbol{\mu}}$:

$$\mathrm{AB} \xrightarrow{\hat{\boldsymbol{\mu}}} \mathrm{AB}^+ + \mathrm{e}^-. \tag{5.1}$$

In the language of quantum mechanics, this process is described by the transition matrix element

$$(\langle\psi_{\mathrm{AB}^+}| \langle\psi_{\mathrm{e}^-}|)\hat{\boldsymbol{\mu}} |\psi_{\mathrm{AB}}\rangle , \tag{5.2}$$

with the symbols $|\psi_{\mathrm{AB}}\rangle$ and $|\psi_{\mathrm{AB}^+}\rangle$ standing for the internal quantum states of the neutral molecule AB and the molecular ion AB^+, respectively, and $|\psi_{\mathrm{e}^-}\rangle$ for the quantum state of the photoelectron.

In analogy to the spectroscopic line strength for transitions between bound states, we define the quantity $P(\mathrm{AB} \rightarrow \mathrm{AB}^+)$, proportional to the ionization probability per unit time, as the squared absolute value of the transition matrix element summed over all the quantum states contributing to the observed ionization rate, i.e.,

$$P(\mathrm{AB} \rightarrow \mathrm{AB}^+) = \sum_{\psi_{\mathrm{AB}}} \sum_{\psi_{\mathrm{AB}^+}} \sum_{\psi_{\mathrm{e}^-}} |(\langle\psi_{\mathrm{AB}^+}| \langle\psi_{\mathrm{e}^-}|)\hat{\boldsymbol{\mu}} |\psi_{\mathrm{AB}}\rangle|^2 . \tag{5.3}$$

Here, the sums over ψ_{AB} and ψ_{AB^+} include all degenerate (or unresolved) states of the neutral molecule and the molecular ion, respectively, belonging to the neutral and the ionic energy level of the transition studied. The sum over ψ_{e^-} includes the orbital angular momentum and the spin state of the emitted photoelectron. We suppose that neither the energy, nor the angular distribution or the spin state of the photoelectron is detected in the photoionization experiment.

The quantity of interest here is the ionization rate. This rate $R(\mathrm{AB} \rightarrow \mathrm{AB}^+)$ is proportional[1] to the above-defined transition probability multiplied by the population $\rho(E_{\mathrm{AB}})$ in the addressed neutral level and divided by the degeneracy $g(E_{\mathrm{AB}})$ of that level,

$$R(\mathrm{AB} \rightarrow \mathrm{AB}^+) \propto \frac{1}{g(E_{\mathrm{AB}})} P(\mathrm{AB} \rightarrow \mathrm{AB}^+)\rho(E_{\mathrm{AB}}), \tag{5.4}$$

with E_{AB} the energy of the neutral level.

For a neutral-state population following a Boltzmann distribution (with the temperature T and the Boltzmann constant k_{B}),

$$\rho(E_{\mathrm{AB}}) \propto g(E_{\mathrm{AB}}) \exp(-E_{\mathrm{AB}}/k_{\mathrm{B}}T), \tag{5.5}$$

the ionization rate thus accounts for,

$$R(\mathrm{AB} \rightarrow \mathrm{AB}^+) \propto P(\mathrm{AB} \rightarrow \mathrm{AB}^+) \exp(-E_{\mathrm{AB}}/k_{\mathrm{B}}T). \tag{5.6}$$

In the following, explicit expressions for the ionization probability $P(\mathrm{AB} \rightarrow \mathrm{AB}^+)$ for particular neutral and ionic fs and hfs levels will be derived. That way, the roles of the electron and the nuclear spin in molecular photoionization are studied.

[1] See the relation between the line strength and Einstein B-coefficient of excitation discussed in Ch. 2 as well as equation (1) in [148].

Table 5.1. Angular momentum quantum numbers relevant to the photoionization of diatomic molecules.

Magnitude quant. num.	Mol.-fixed projection	Space-fixed projection	Description
N	Λ	M_N	Orbital-rotational angular momentum of the neutral molecule (AB)
S	–	M_S	Total electron spin of the neutral molecule
J	–	M_J	Total angular momentum of the neutral molecule excluding nuclear spin
I	–	M_I	Nuclear spin of the neutral molecule[†]
F	–	M_F	Total angular momentum of the neutral molecule[†]
N^+	Λ^+	M_N^+	Orbital-rotational angular momentum of the molecular ion (AB^+)
S^+	–	M_S^+	Total electron spin of the molecular ion
J^+	–	M_J^+	Total angular momentum of the molecular ion excluding nuclear spin
I^+	–	M_I^+	Nuclear spin of the molecular ion[†]
F^+	–	M_F^+	Total angular momentum of the molecular ion[†]
l	–	m_l	Orbital angular momentum (partial wave) of the photoelectron
s	–	m_s	Spin of the photoelectron ($s = 1/2$)
1	–	μ_0	Angular momentum due to the electric-dipole interaction with the electromagnetic field
k	q	p	Total orbital angular momentum transferred to/from the molecule in the ionization process ($p = -m_l + \mu_0$)
u	–	w	Total angular momentum transferred to/from the molecule in the ionization process ($w = -m_s + p$)

[†]Only used in the hfs-resolved photoionization model (Sec. 5.2.2).

5.2.1 Fine-structure effects in molecular photoionization

In order to study spin-rotational, i.e. fine-structure effects, in molecular photoionization, we express the quantum states of the neutral molecule $|\psi_{\mathrm{AB}}\rangle$ and the molecular ion $|\psi_{\mathrm{AB}^+}\rangle$ in Hund's case (b) bases as $|n\Lambda, v, N\Lambda SJM_J\rangle$ and $\left|n^+\Lambda^+, v^+, N^+\Lambda^+S^+J^+M_J^+\right\rangle$, respectively. Here, n (n^+) and v (v^+) denote electronic and the vibrational quantum number in the neutral molecule (molecular ion). The angular momentum quantum numbers have their usual meanings summarized in Tab. 5.1. The state of the photoelectron $|\psi_{\mathrm{e}^-}\rangle$ is expressed as $|s, m_s\rangle\,|l, m_l\rangle$, a tensor product of its spin state and its orbital angular momentum state. The former is characterized by the single-electron spin $s = 1/2$ with associated space-fixed projection m_s. The latter, which is also referred to as the electron "partial wave" in the terminology of scattering processes, is given by the quantum number l for the magnitude of the electron orbital angular momentum and the corresponding projection m_l on the space-fixed z-axis.

The quantity $P(J, J^+)$ may then be written as[2]

$$P(J,J^+) = \sum_{l=0}^{\infty}\sum_{m_l=-l}^{l}\sum_{m_s=-s}^{s}\sum_{M_J=-J}^{J}\sum_{M_J^+=-J^+}^{J^+}\Big|\left\langle n^+\Lambda^+, v^+, N^+\Lambda^+S^+J^+M_J^+\right|\langle s, m_s|\,\langle l, m_l|\,\hat{\boldsymbol{\mu}}\,|n\Lambda, v, N\Lambda SJM_J\rangle\Big|^2. \tag{5.7}$$

We follow the approach of Xie and Zare [132] and identify the electric-dipole operator $\hat{\boldsymbol{\mu}}$ with a spherical tensor $\mathrm{T}^1_{\mu_0}$ as well as the photoelectron state $\langle l, m_l|$ with a spherical tensor $\mathrm{T}^l_{-m_l}$. We then contract

[2]From here on, the parentheses around the bras to the left of the transition operator are omitted, as it is clear from their physical meaning that they are to be regarded as a single entity.

the product of these two spherical tensors according to spherical tensor algebra [61, 77, 60],

$$\mathrm{T}^{l}_{-m_l} \otimes \mathrm{T}^{1}_{\mu_0} = \sum_{k=|l-1|}^{l+1} C^{kp}_{l-m_l 1\mu_0} \mathrm{T}^{k}_{p}, \tag{5.8}$$

where $p = -m_l + \mu_0$. Here and in the following, symbols as $C^{jm}_{j_1 m_1 j_2 m_2}$ stand for the Clebsch-Gordan coefficient $\langle j_1 m_1, j_2 m_2 | j_1 j_2 j m \rangle$, which is expressed in terms of a Wigner 3j-symbol as

$$C^{jm}_{j_1 m_1 j_2 m_2} = \langle j_1 m_1, j_2 m_2 | j_1 j_2 j m \rangle = (-1)^{j_1 - j_2 + m} \sqrt{2j+1} \begin{pmatrix} j_1 & j_2 & j \\ m_1 & m_2 & -m \end{pmatrix}. \tag{5.9}$$

The spherical tensor operator T^{k}_{p} newly introduced in (5.8) describes the combined effect of absorbing electromagnetic radiation via the electric-dipole operator and ejecting a photoelectron in the state $|l, m_l\rangle$.

The term with $k = l$ does not contribute to the sum in (5.7) because of parity selection rules and may be omitted [132, 131]. The matrix element in (5.7) is thus expressed as,

$$\begin{aligned} &\left\langle n^+\Lambda^+, v^+, N^+\Lambda^+ S^+ J^+ M_J^+ \right| \langle s, m_s | \langle l, m_l | \, \hat{\boldsymbol{\mu}} \, | n\Lambda, v, N\Lambda S J M_J \rangle \\ &\qquad = \sum_{k=l\pm 1} C^{kp}_{l-m_l 1\mu_0} \left\langle n^+\Lambda^+, v^+, N^+\Lambda^+ S^+ J^+ M_J^+ \right| \langle s, m_s | \, \mathrm{T}^{k}_{p} \, | n\Lambda, v, N\Lambda S J M_J \rangle \,, \end{aligned} \tag{5.10}$$

where negative values for k are to be excluded.

Since the tensor T^{k}_{p} does not operate on the spin state, we decouple spin and orbital-rotational angular momenta in the molecular quantum states, i.e., we express the spin-rotational state of the molecular ion and its neutral precursor in the tensor product basis of pure spin and rotational-vibronic states according to

$$|n\Lambda, v, N\Lambda S J M_J\rangle = \sum_{M_N, M_S} C^{JM_J}_{NM_N SM_S} \, |n\Lambda, v, N\Lambda M_N, S M_S\rangle \,, \tag{5.11a}$$

$$\left\langle n^+\Lambda^+, v^+, N^+\Lambda^+ S^+ J^+ M_J^+ \right| = \sum_{M_N^+, M_S^+} C^{J^+ M_J^+}_{N^+ M_N^+ S^+ M_S^+} \left\langle n^+\Lambda^+, v^+, N^+\Lambda^+ M_N^+, S^+ M_S^+ \right| . \tag{5.11b}$$

The transition matrix element in (5.10) then reads,

$$\begin{aligned} &\left\langle n^+\Lambda^+, v^+, N^+\Lambda^+ S^+ J^+ M_J^+ \right| \langle s, m_s | \, \mathrm{T}^{k}_{p} \, | n\Lambda, v, N\Lambda S J M_J \rangle \\ &\qquad = \sum_{M_N, M_S} \sum_{M_N^+, M_S^+} C^{JM_J}_{NM_N SM_S} C^{J^+ M_J^+}_{N^+ M_N^+ S^+ M_S^+} \\ &\qquad\quad \left\langle n^+\Lambda^+, v^+, N^+\Lambda^+ M_N^+, S^+ M_S^+ \right| \langle s, m_s | \, \mathrm{T}^{k}_{p} \, | n\Lambda, v, N\Lambda M_N, S M_S \rangle \,. \end{aligned} \tag{5.12}$$

Exploiting that T^{k}_{p} does not operate on the spin states, we separate the matrix element on the last line of the above expression into a rotational-vibronic and a pure spin factor:

$$\begin{aligned} &\left\langle n^+\Lambda^+, v^+, N^+\Lambda^+ M_N^+, S^+ M_S^+ \right| \langle s, m_s | \, \mathrm{T}^{k}_{p} \, | n\Lambda, v, N\Lambda M_N, S M_S \rangle \\ &\qquad = \left\langle n^+\Lambda^+, v^+, N^+\Lambda^+ M_N^+ \right| \mathrm{T}^{k}_{p} \left| n\Lambda, v, N\Lambda M_N \right\rangle \left(\left\langle S^+ M_S^+ \right| \langle s, m_s | \right) | S M_S \rangle \,. \end{aligned} \tag{5.13}$$

In order to calculate the rotational-vibronic factor, we transform the spherical tensor operator T^k_p from space-fixed to molecule-fixed coordinates using a Wigner rotation matrix,

$$\mathrm{T}^k_p = \sum_{q=-k}^{k} [\hat{\mathcal{D}}^k_{pq}]^* \mathrm{T}'^k_q, \tag{5.14}$$

where the superscript $'$ has been added to indicate that this tensor refers to molecule-fixed coordinates.

The Wigner rotation matrix involves only the angular coordinates, whereas the tensor T'^k_q operates only on the vibronic state. Therefore, we have:

$$\begin{aligned}
&\left\langle n^+\Lambda^+, v^+, N^+\Lambda^+ M_N^+ \,\middle|\, \mathrm{T}^k_p \,\middle|\, n\Lambda, v, N\Lambda M_N \right\rangle \\
&\quad = \sum_{q=-k}^{k} \left\langle n^+\Lambda^+, v^+, N^+\Lambda^+ M_N^+ \,\middle|\, [\hat{\mathcal{D}}^k_{pq}]^* \mathrm{T}'^k_q \,\middle|\, n\Lambda, v, N\Lambda M_N \right\rangle &(5.15)\\
&\quad = \sum_{q=-k}^{k} \left\langle n^+\Lambda^+, v^+ \,\middle|\, \mathrm{T}'^k_q \,\middle|\, n\Lambda, v \right\rangle \left\langle N^+\Lambda^+ M_N^+ \,\middle|\, [\hat{\mathcal{D}}^k_{pq}]^* \,\middle|\, N\Lambda M_N \right\rangle . &(5.16)
\end{aligned}$$

Upon substituting the angular states of the neutral molecule and the ion, which are themselves given by Wigner rotation matrices,

$$\langle \phi\, \theta\, \chi \,|\, N\Lambda M_N \rangle = \sqrt{\frac{2N+1}{8\pi^2}} \left[\mathscr{D}^{(N)}_{M_N\Lambda}(\phi,\theta,\chi) \right]^*, \tag{5.17a}$$

$$\left\langle N^+\Lambda^+ M_N^+ \,\middle|\, \phi\, \theta\, \chi \right\rangle = \sqrt{\frac{2N^++1}{8\pi^2}} \mathscr{D}^{(N^+)}_{M_N^+\Lambda^+}(\phi,\theta,\chi), \tag{5.17b}$$

we obtain for the angular part in (5.16) an integral over a product of three Wigner rotation matrices, which accounts for [62, 60]:

$$\begin{aligned}
&\left\langle N^+\Lambda^+ M_N^+ \,\middle|\, [\hat{\mathcal{D}}^k_{pq}]^* \,\middle|\, N\Lambda M_N \right\rangle \\
&\qquad = \sqrt{2N^++1}\sqrt{2N+1}(-1)^{M_N^+-\Lambda^+} \begin{pmatrix} N^+ & k & N \\ -M_N^+ & p & M_N \end{pmatrix} \begin{pmatrix} N^+ & k & N \\ -\Lambda^+ & q & \Lambda \end{pmatrix}. &(5.18)
\end{aligned}$$

Because of the second Wigner 3j-symbol, this expression vanishes for all values of q but $q = \Lambda^+ - \Lambda =: \Delta\Lambda$. Hence, only this value contributes to the sum in (5.16) and we may write

$$\begin{aligned}
&\left\langle n^+\Lambda^+, v^+, N^+\Lambda^+ M_N^+ \,\middle|\, \mathrm{T}^k_p \,\middle|\, n\Lambda, v, N\Lambda M_N \right\rangle \\
&= \left\langle n^+\Lambda^+, v^+ \,\middle|\, \mathrm{T}'^k_{\Delta\Lambda} \,\middle|\, n\Lambda, v \right\rangle \sqrt{2N^++1}\sqrt{2N+1}(-1)^{M_N^+-\Lambda^+} \begin{pmatrix} N^+ & k & N \\ -M_N^+ & p & M_N \end{pmatrix} \begin{pmatrix} N^+ & k & N \\ -\Lambda^+ & \Delta\Lambda & \Lambda \end{pmatrix}.
\end{aligned} \tag{5.19}$$

Having calculated the rotational-vibronic part of (5.13), we now turn to the spin part. To this end, we

couple the spin of the ion and the photoelectron to get the total electronic spin after ionization,

$$\left\langle S^+ M_S^+, s m_s \right| = \sum_{S_{\mathrm{tot}}=|S^+-s|}^{S^++s} \sum_{M_{S_{\mathrm{tot}}}=-S_{\mathrm{tot}}}^{S_{\mathrm{tot}}} C^{S_{\mathrm{tot}} M_{S_{\mathrm{tot}}}}_{S^+ M_S^+ s m_s} \left\langle S_{\mathrm{tot}} M_{S_{\mathrm{tot}}} \right|, \tag{5.20}$$

Assuming orthonormal spin states, we thus obtain for the spin factor in (5.13):

$$\begin{aligned}
\left\langle S^+ M_S^+, s m_s \,\middle|\, S M_S \right\rangle &= \sum_{S_{\mathrm{tot}}=|S^+-s|}^{S^++s} \sum_{M_{S_{\mathrm{tot}}}=-S_{\mathrm{tot}}}^{S_{\mathrm{tot}}} C^{S_{\mathrm{tot}} M_{S_{\mathrm{tot}}}}_{S^+ M_S^+ s m_s} \left\langle S_{\mathrm{tot}} M_{S_{\mathrm{tot}}} \,\middle|\, S M_S \right\rangle && (5.21)\\
&= \sum_{S_{\mathrm{tot}}=|S^+-s|}^{S^++s} \sum_{M_{S_{\mathrm{tot}}}=-S_{\mathrm{tot}}}^{S_{\mathrm{tot}}} C^{S_{\mathrm{tot}} M_{S_{\mathrm{tot}}}}_{S^+ M_S^+ s m_s} \delta_{S_{\mathrm{tot}} S} \delta_{M_{S_{\mathrm{tot}}} M_S} && (5.22)\\
&= C^{S M_S}_{S^+ M_S^+ s m_s}. && (5.23)
\end{aligned}$$

Collecting these results and substituting them into (5.10), the complete matrix element for spin-rotation-resolved photoionization transitions is:

$$\begin{aligned}
&\left\langle n^+\Lambda^+, v^+, N^+\Lambda^+ S^+ J^+ M_J^+ \right| \left\langle s, m_s \right| \left\langle l, m_l \right| \hat{\boldsymbol{\mu}} \left| n\Lambda, v, N\Lambda S J M_J \right\rangle \\
&\quad = \sqrt{2N^+ + 1}\sqrt{2N+1}\sqrt{2S+1}\sqrt{2J^+ + 1}\sqrt{2J+1}(-1)^{l-1+p+N+N^+-\Lambda^+-S-s+M_J^+ + M_J} \\
&\qquad \sum_{k=l\pm 1} \sqrt{2k+1} \begin{pmatrix} l & 1 & k \\ -m_l & \mu_0 & -p \end{pmatrix} \left\langle n^+\Lambda^+, v^+ \,\middle|\, \mathrm{T}'^k_{\Delta\Lambda} \,\middle|\, n\Lambda, v \right\rangle \begin{pmatrix} N^+ & k & N \\ -\Lambda^+ & \Delta\Lambda & \Lambda \end{pmatrix} \\
&\qquad \sum_{M_S^+, M_S} \sum_{M_N^+, M_N} (-1)^{M_N^+ + M_S} \begin{pmatrix} N^+ & S^+ & J^+ \\ M_N^+ & M_S^+ & -M_J^+ \end{pmatrix} \begin{pmatrix} N & S & J \\ M_N & M_S & -M_J \end{pmatrix} \\
&\qquad \begin{pmatrix} N^+ & k & N \\ -M_N^+ & p & M_N \end{pmatrix} \begin{pmatrix} S^+ & s & S \\ M_S^+ & m_s & -M_S \end{pmatrix},
\end{aligned} \tag{5.24}$$

where the Clebsch-Gordan coefficients have been replaced by Wigner 3j-symbols.

In principle, this matrix element completely describes the fine-structure-resolved photoionization process and could (when substituted in (5.7)) be used for analyzing measured photoionization and photoelectron spectra and predicting fine-structure-resolved photoionization line intensities.

However, the complexity of the above expression hinders a deeper insight into the physics of the photoionization process and the multiple sums render the evaluation of this expression time consuming even when working with a computer algebra system.

Fortunately, the matrix element may be simplified considerably when exploiting the properties of the Wigner 3j-symbols. Moreover, the expression obtained in this way may be further simplified when calculating its absolute value summed over the projection quantum numbers appearing in (5.7). In that way, an expression more convenient for numerical evaluation as well as better comprehensible regarding its physical insight is obtained.

We first consider the sums over M_S^+, M_S, M_N^+, M_N on the last and next-to-last line in (5.24). Using the symmetries (equation (2.29) and (2.30) in [61]) and the selection rules of the Wigner 3j-symbols,

the phase factor appearing in this term may be separated from the sums:

$$\begin{aligned}
&\sum_{M_S^+,M_S}\sum_{M_N^+,M_N}(-1)^{M_N^+ + M_S}\begin{pmatrix} N^+ & S^+ & J^+ \\ M_N^+ & M_S^+ & -M_J^+\end{pmatrix}\begin{pmatrix} N & S & J \\ M_N & M_S & -M_J\end{pmatrix}\\
&\begin{pmatrix} N^+ & k & N \\ -M_N^+ & p & M_N\end{pmatrix}\begin{pmatrix} S^+ & s & S \\ M_S^+ & m_s & -M_S\end{pmatrix}\\
&= (-1)^{p+N^+ +k+S+J+M_J}\sum_{M_S^+,M_S}\sum_{M_N^+,M_N}\begin{pmatrix} J^+ & N^+ & S^+ \\ -M_J^+ & M_N^+ & M_S^+\end{pmatrix}\begin{pmatrix} J & N & S \\ M_J & -M_N & -M_S\end{pmatrix}\\
&\quad\begin{pmatrix} N^+ & k & N \\ M_N^+ & -p & -M_N\end{pmatrix}\begin{pmatrix} S^+ & s & S \\ M_S^+ & m_s & -M_S\end{pmatrix}
\end{aligned} \tag{5.25}$$

Applying now the relation between Wigner 9j- and 3j-symbols given in Appendix C.2, the quadruple sum in (5.25) is expressed in form of a 9j-symbol as

$$\begin{aligned}
&\sum_{M_S^+,M_S}\sum_{M_N^+,M_N}\begin{pmatrix} J^+ & N^+ & S^+ \\ -M_J^+ & M_N^+ & M_S^+\end{pmatrix}\begin{pmatrix} J & N & S \\ M_J & -M_N & -M_S\end{pmatrix}\begin{pmatrix} N^+ & k & N \\ M_N^+ & -p & -M_N\end{pmatrix}\begin{pmatrix} S^+ & s & S \\ M_S^+ & m_s & -M_S\end{pmatrix}\\
&= \sum_{u=|k-s|}^{k+s}(2u+1)\begin{pmatrix} J^+ & u & J \\ -M_J^+ & w & M_J\end{pmatrix}\begin{pmatrix} u & k & s \\ w & -p & m_s\end{pmatrix}\begin{Bmatrix} J^+ & u & J \\ N^+ & k & N \\ S^+ & s & S\end{Bmatrix}.
\end{aligned} \tag{5.26}$$

Here, the angular momentum quantum number u with the associated space-fixed projection w (given by $w = -m_s + p$) has been introduced. u represents the resultant of the coupling of k and s. Its physical meaning is described further below.

Substituting these results into (5.24), we obtain for the transition matrix element

$$\begin{aligned}
&\left\langle n^+\Lambda^+, v^+, N^+\Lambda^+S^+J^+M_J^+\right| \left\langle s, m_s\right| \left\langle l, m_l\right| \hat{\boldsymbol{\mu}} \left| n\Lambda, v, N\Lambda SJM_J\right\rangle\\
&\quad= \sqrt{2N^+ +1}\sqrt{2N+1}\sqrt{2S+1}\sqrt{2J^+ +1}\sqrt{2J+1}(-1)^{l-1-\Lambda^+ +N+J-s+2M_J+M_J^+}\\
&\qquad\sum_{k=l\pm 1}(-1)^k\sqrt{2k+1}\begin{pmatrix} l & 1 & k \\ -m_l & \mu_0 & -p\end{pmatrix}\left\langle n^+\Lambda^+, v^+\right| \mathrm{T}'^k_{\Delta\Lambda}\left| n\Lambda, v\right\rangle\begin{pmatrix} N^+ & k & N \\ -\Lambda^+ & \Delta\Lambda & \Lambda\end{pmatrix}\\
&\qquad\sum_{u=|k-s|}^{k+s}(2u+1)\begin{pmatrix} J^+ & u & J \\ -M_J^+ & w & M_J\end{pmatrix}\begin{pmatrix} u & k & s \\ w & -p & m_s\end{pmatrix}\begin{Bmatrix} J^+ & u & J \\ N^+ & k & N \\ S^+ & s & S\end{Bmatrix}.
\end{aligned} \tag{5.27}$$

According to (5.7), the transition probability is thus:

$$P(J,J^+) = (2N^+ + 1)(2N+1)(2S+1)(2J^+ + 1)(2J+1) \sum_l \sum_{m_l} \sum_{m_s} \sum_{M_J, M_J^+}$$
$$\left| \sum_{k=l\pm 1} (-1)^k \sqrt{2k+1} \begin{pmatrix} l & 1 & k \\ -m_l & \mu_0 & -p \end{pmatrix} \left\langle n^+\Lambda^+, v^+ \middle| \mathrm{T}'^k_{\Delta\Lambda} \middle| n\Lambda, v \right\rangle \begin{pmatrix} N^+ & k & N \\ -\Lambda^+ & \Delta\Lambda & \Lambda \end{pmatrix} \right.$$
$$\left. \sum_{u=|k-s|}^{k+s} (2u+1) \begin{pmatrix} J^+ & u & J \\ -M_J^+ & w & M_J \end{pmatrix} \begin{pmatrix} u & k & s \\ w & -p & m_s \end{pmatrix} \begin{Bmatrix} J^+ & u & J \\ N^+ & k & N \\ S^+ & s & S \end{Bmatrix} \right|^2 . \tag{5.28}$$

When calculating the square of the absolute magnitude in the expression above, several cross terms due to the sums over k and u appear. However, since we are summing over all possible values of M_J and M_J^+, these cross terms vanish because of the orthogonality of the 3j-symbols (equation (2.32) in [61]). Equation (5.28) hence may be simplified[3] to:

$$P(J,J^+) = (2N^+ + 1)(2N+1)(2S+1)(2J^+ + 1)(2J+1)$$
$$\sum_l \sum_{k=l\pm 1} (2k+1) \begin{pmatrix} N^+ & k & N \\ -\Lambda^+ & \Delta\Lambda & \Lambda \end{pmatrix}^2 \left| \left\langle n^+\Lambda^+, v^+ \middle| \mathrm{T}'^k_{\Delta\Lambda} \middle| n\Lambda, v \right\rangle \right|^2$$
$$\sum_{u=|k-s|}^{k+s} (2u+1) \begin{Bmatrix} J^+ & u & J \\ N^+ & k & N \\ S^+ & s & S \end{Bmatrix}^2 \sum_{m_l} \begin{pmatrix} l & 1 & k \\ -m_l & \mu_0 & -p \end{pmatrix}^2 \sum_{m_s} \begin{pmatrix} u & k & s \\ w & -p & m_s \end{pmatrix}^2 . \tag{5.29}$$

For linearly polarized radiation (as in our experiment), we have $\mu_0 = 0$ in a suitably chosen coordinate system. The sums over m_l and m_s then account for $1/(3(2k+1))$ and we get:

$$P(J,J^+) = \frac{1}{3}(2N^+ + 1)(2N+1)(2S+1)(2J^+ + 1)(2J+1) \sum_l \sum_{k=l\pm 1} \begin{pmatrix} N^+ & k & N \\ -\Lambda^+ & \Delta\Lambda & \Lambda \end{pmatrix}^2$$
$$\left| \left\langle n^+\Lambda^+, v^+ \middle| \mathrm{T}'^k_{\Delta\Lambda} \middle| n\Lambda, v \right\rangle \right|^2 \sum_{u=|k-s|}^{k+s} (2u+1) \begin{Bmatrix} J^+ & u & J \\ N^+ & k & N \\ S^+ & s & S \end{Bmatrix}^2 . \tag{5.30}$$

The physics described by equation (5.30) may be understood as follows: the photoelectron ejected in the ionization process is described as a partial wave l. The probability of a transition from a certain neutral to a certain ionic state is given by a sum over all partial waves. The partial waves possible for a particular electronic state of the ion and the neutral precursor are constrained by the parity of these states. If neutral and ionic states have the same parity ($\pm \leftrightarrow \pm$ transitions), only odd values of l occur, i.e., terms with $l = 1, 3, 5, \ldots$ appear in the sum in (5.30). In case of unequal parities of neutral and ionic state ($\pm \leftrightarrow \mp$), only even values are allowed for l, i.e., the sum over l includes the values $l = 0, 2, 4, \ldots$ [132].

[3] The complete derivation of this simplification is rather lengthy and thus not reproduced here. In essence, the sums over u and k are expanded and the relation $|x_1 z_1 + x_2 z_2|^2 = x_1^2|z_1|^2 + x_2^2|z_2|^2 + x_1 x_2 |z_1 z_2^* - z_1^* z_2|$ for $x_1, x_2 \in \mathbb{R}$ and $z_1, z_2 \in \mathbb{C}$ is applied. Then, the sums over M_J, M_J^+ are evaluated and the orthogonality of the 3j-symbols is used to show that the cross terms vanish.

Additional to the angular momentum carried by the departing photoelectron, the molecule also exchanges angular momentum with the electric field as described by the electric-dipole operator. The angular momenta associated with the photoelectron partial wave and the electric-dipole excitation are thus coupled to form k. Since the dipole operator is a first-rank spherical tensor, k exhibits the values $k = l - 1$ or $k = l + 1$ with $k = l$ forbidden because of parity selection rules [132, 131]. We thus have $k = 0, 2, 4, \ldots$ for $\pm \leftrightarrow \pm$ transitions and $k = 1, 3, 5, \ldots$ for $\pm \leftrightarrow \mp$ transitions [132].

The value of k determines the maximal change of the orbital-rotational angular momentum in the photoionization process, i.e., $|\Delta N| = |N^+ - N| \leq k$, as may be seen from the 3j-symbol or the middle row of the 9j-symbol in (5.30). Transitions with $k = 0$, e.g., do not allow any change in the orbital-rotational angular momentum, i.e., $N^+ = N$. For transitions with $k = 2$, the values $\Delta N = 0, \pm 1$ and ± 2 are possible (with $\Delta N = \pm 1$ forbidden for Σ-Σ transitions). Which transitions occur, as well as their relative abundance is determined by the absolute value of the vibronic transition matrix elements $\left\langle n^+ v^+ \middle| \mathrm{T}'^{k}_{\Delta\Lambda} \middle| n, v \right\rangle$. To calculate these matrix elements, the electronic structure of the molecular ion and its precursor must be known. Thus, they either may be obtained from an ab-initio calculation or treated as free parameters when describing a measured photoelectron spectrum. Usually, only the vibronic transition matrix elements with the few lowest values of k (such as $k = 0$ and $k = 2$) contribute substantially to the total transition probability and for higher k-values they essentially vanish. Hence, only a few free parameters are needed to describe the intensities in a rotationally resolved photoelectron spectrum of a diatomic molecule.

As the (squared) absolute values of the vibronic transition matrix elements have first appeared as free parameters in the photoionization model by Buckingham, Orr and Sichel ("BOS model", [148]) they are known as the "BOS coefficients" C_k, i.e.,

$$C_k = \left| \left\langle n^+ v^+ \middle| \mathrm{T}'^{k}_{\Delta\Lambda} \middle| n, v \right\rangle \right|^2 . \tag{5.31}$$

For our purposes, the vibronic transition matrix elements are just treated as free parameters. If the electronic structure of the system considered is known, they may be calculated by expressing the electronic state of the molecular ion and its neutral precursor as well as the photoelectron partial wave and the electric-dipole operator in the molecule-fixed frame [148]. An intuitive understanding of the vibronic transition matrix elements is achieved when approximately describing the electronic state of the molecule by a single Slater determinant in the Hartree-Fock formalism and assuming that the photoelectron is ejected from one particular molecular orbital, while the others are not affected by the ionization process (Koopman's theorem). We may then picture the removal of an electron within a set of occupied electron states as creating a "hole" among these states. The quantum number k may then be associated with the angular momentum of this hole [143].

As well as the orbital angular momentum l, the photoelectron also carries its spin $s = 1/2$. This spin is coupled to k to form u. The possible values for u are thus $u = |k - 1/2|$ and $u = k + 1/2$. Similar to k determining the change in the orbital-rotational angular momentum, u determines the change in the total angular momentum (excluding nuclear spin) according to the selection rule $|\Delta J| = |J^+ - J| \leq u$, as inferred from the first row of the 9j-symbol in (5.30). For $k = 0$, e.g., only $u = 1/2$ is possible and thus only transitions with $|\Delta J| = 1/2$ are allowed. For $k = 2$, on the other hand, $u = 3/2$ and $u = 5/2$ are possible, allowing values of $|\Delta J|$ up to $5/2$.

Since the values of u are determined by the values of k, the vibronic transition matrix elements $\left\langle n^+v^+ \middle| \mathrm{T}'^{k}_{\Delta\Lambda} \middle| n, v \right\rangle$ describing the relative intensities of different rotational lines in a photoelectron spectrum also determine the relative intensities of transitions of different fine-structure components. Hence, our model describes the spin-rotational effects in photoionization without additional free parameters.

Summarizing, we see that the whole interplay between the different angular momenta is expressed by the 9j-symbol in (5.30) in a compact way: the couplings in the ionic and the neutral state are expressed by the first and the last column, respectively. The coupling of the angular momenta transferred to or from the molecule is described by the middle column: the spin of the photoelectron s is coupled to k (the angular momentum associated with the photoelectron and the interaction with the electromagnetic field) to form u. The rows of the 9j-symbol represent the angular momentum transfer during photoionization: according to the first row, u determines the change in the total angular momentum (excluding nuclear spin), whereas k decides on the change in the orbital-rotational angular momentum (second row). Finally, s describes the spin removed from the molecule in the ionization process, as seen from the last row in the 9j-symbol.

Besides elucidating the role of the electron spin in molecular photoionization and its effect on the probability of transitions between particular fine-structure levels in photoionization, equation (5.30) also provides an efficient way for numerical calculation of these transition probabilities as compared to direct evaluation of the transition matrix element in (5.24) and summation over projection angular momentum quantum numbers (as in (5.7)), since the computationally demanding multiple sums are largely avoided.

Our result may be compared with the findings of Dixit et al. [159]. Indeed, when taking the squared absolute value of their matrix element (equation (6) in [159]), integrating over the entire unit sphere and making use of orthogonality properties of Wigner symbols and spherical harmonics, the result in our equation (5.30) may be reproduced in essence.

Often, the neutral molecule AB is in a singlet state, i.e, $S = 0$. If so, we have $J = N$ and $S^+ = s = 1/2$ and our result may be simplified even further. The 9j-symbol then equals a 6j-symbol (see equation (4.25) in [61]),

$$\begin{Bmatrix} J^+ & u & N \\ N^+ & k & N \\ S^+ & s & 0 \end{Bmatrix}^2 = \frac{1}{2(2N+1)} \begin{Bmatrix} J^+ & u & N \\ k & N^+ & s \end{Bmatrix}^2, \tag{5.32}$$

and equation (5.30) becomes,

$$P_{S=0}(N, J^+) = \frac{1}{6}(2N+1)(2N^+ + 1)(2J^+ + 1) \sum_l \sum_{k=l\pm1} \begin{pmatrix} N^+ & k & N \\ -\Lambda^+ & \Delta\Lambda & \Lambda \end{pmatrix}^2 \left| \left\langle n^+\Lambda^+, v^+ \middle| \mathrm{T}'^{k}_{\Delta\Lambda} \middle| n\Lambda, v \right\rangle \right|^2 \sum_{u=|k-s|}^{k+s} (2u+1) \begin{Bmatrix} J^+ & u & N \\ k & N^+ & s \end{Bmatrix}^2. \tag{5.33}$$

5.2.2 Hyperfine-structure effects in molecular photoionization

Having developed a photoionization model describing the relative intensity of transitions between fine-structure levels in Hund's case (b), i.e., spin-rotation components, we now extend this model to cover transitions between different hyperfine levels in the photoionization process. To that end, we need to consider the role of the nuclear spin in the neutral and ionic levels. We assume that both of these levels may be described with the Hund's case (b_{β_J}) angular momentum coupling scheme as discussed in Ch. 3. The transition probability is then proportional to the quantity

$$P(F,F^+) = \sum_{l=0}^{\infty}\sum_{m_l=-l}^{l}\sum_{m_s=-s}^{s}\sum_{M_F=-F}^{F}\sum_{M_F^+=-F^+}^{F^+} \left| \left\langle n^+\Lambda^+, v^+, N^+\Lambda^+S^+J^+I^+F^+M_F^+ \right| \langle s,m_s| \langle l,m_l| \hat{\boldsymbol{\mu}} \left| n\Lambda, v, N\Lambda SJIFM_F \right\rangle \right|^2. \tag{5.34}$$

Here, I and F (I^+ and F^+) denote the nuclear spin and the total angular momentum quantum number, respectively, in the neutral (ionic) state. M_F and M_F^+ denote the projection angular momentum quantum numbers with respect to the space-fixed z-axis associated with F and F^+ .

As outlined in Ch. 3, the coupled angular momentum states are expressed in the (decoupled) tensor product basis of the spin-rotational-vibronic and the nuclear spin states as

$$\left| n\Lambda, v, N\Lambda SJIFM_F \right\rangle = \sum_{M_I}\sum_{M_J} C^{FM_F}_{JM_JIM_I} \left| n\Lambda, v, N\Lambda SJM_J, IM_I \right\rangle, \tag{5.35a}$$

$$\begin{aligned}\left\langle n^+\Lambda^+, v^+, N^+\Lambda^+S^+J^+I^+F^+M_F^+ \right| = &\sum_{M_I^+}\sum_{M_J^+} C^{F^+M_F^+}_{J^+M_J^+I^+M_I^+} \\ &\left\langle n^+\Lambda^+, v^+, N^+\Lambda^+S^+J^+M_J^+, I^+M_I^+ \right|.\end{aligned} \tag{5.35b}$$

In this basis, the transition matrix element appearing in (5.34) accounts for

$$\begin{aligned}&\left\langle n^+\Lambda^+, v^+, N^+\Lambda^+S^+J^+I^+F^+M_F^+ \right| \langle s,m_s| \langle l,m_l| \hat{\boldsymbol{\mu}} \left| n\Lambda, v, N\Lambda SJIFM_F \right\rangle \\ &\quad= \sum_{M_I^+,M_I}\sum_{M_J^+,M_J} C^{F^+M_F^+}_{J^+M_J^+I^+M_I^+} C^{FM_F}_{JM_JIM_I} \left\langle n^+\Lambda^+, v^+, N^+\Lambda^+S^+J^+M_J^+, I^+M_I^+ \right| \langle s,m_s| \langle l,m_l| \\ &\quad\quad \hat{\boldsymbol{\mu}} \left| n\Lambda, v, N\Lambda SJM_J, IM_I \right\rangle.\end{aligned} \tag{5.36}$$

Since the nuclear spin is neither affected by the absorption of electromagnetic radiation, nor by the ejection of the photoelectron, we may separate the nuclear spin states from the remaining transition matrix element, obtaining

$$\begin{aligned}&\left\langle n^+\Lambda^+, v^+, N^+\Lambda^+S^+J^+M_J^+, I^+M_I^+ \right| \langle s,m_s| \langle l,m_l| \hat{\boldsymbol{\mu}} \left| n\Lambda, v, N\Lambda SJM_J, IM_I \right\rangle \\ &= \left\langle I^+M_I^+ \,\middle|\, IM_I \right\rangle \left\langle n^+\Lambda^+, v^+, N^+\Lambda^+S^+J^+M_J^+ \right| \langle s,m_s| \langle l,m_l| \hat{\boldsymbol{\mu}} \left| n\Lambda, v, N\Lambda SJM_J \right\rangle \qquad (5.37) \\ &= \delta_{I^+I}\delta_{M_I^+M_I} \left\langle n^+\Lambda^+, v^+, N^+\Lambda^+S^+J^+M_J^+ \right| \langle s,m_s| \langle l,m_l| \hat{\boldsymbol{\mu}} \left| n\Lambda, v, N\Lambda SJM_J \right\rangle. \qquad (5.38)\end{aligned}$$

For orthonormal nuclear spin states, the first factor, as indicated above, simply results in two Kronecker deltas, expressing the conservation of the nuclear spin. The remaining transition matrix element is known from equation (5.27) in the previous section. Substituting this result into (5.38), replacing the

Clebsch-Gordan coefficients by 3j-symbols and evaluating the sum over M_I^+ yields:

$$\begin{aligned}
&\left\langle n^+\Lambda^+, v^+, N^+\Lambda^+S^+J^+I^+F^+M_F^+\right| \left\langle s, m_s\right| \left\langle l, m_l\right| \hat{\boldsymbol{\mu}} \left| n\Lambda, v, N\Lambda SJIFM_F\right\rangle \\
&\quad = \sqrt{2N^+ + 1}\sqrt{2N + 1}\sqrt{2S + 1}\sqrt{2J^+ + 1}\sqrt{2J + 1}\sqrt{2F^+ + 1}\sqrt{2F + 1}\delta_{II^+} \\
&\qquad (-1)^{l-1-\Lambda^+-s+N+2J+J^+-2I+M_F+M_F^+} \sum_{k=l\pm1} (-1)^k \sqrt{2k+1} \begin{pmatrix} l & 1 & k \\ -m_l & \mu_0 & -p \end{pmatrix} \\
&\qquad \left\langle n^+\Lambda^+, v^+ \right| \mathrm{T}'^k_{\Delta\Lambda} \left| n\Lambda, v \right\rangle \begin{pmatrix} N^+ & k & N \\ -\Lambda^+ & \Delta\Lambda & \Lambda \end{pmatrix} \sum_{u=|k-s|}^{k+s} (2u+1) \begin{pmatrix} u & k & s \\ w & -p & m_s \end{pmatrix} \begin{Bmatrix} J^+ & u & J \\ N^+ & k & N \\ S^+ & s & S \end{Bmatrix} \\
&\qquad \sum_{M_J^+, M_J, M_I} (-1)^{2M_J+M_J^+} \begin{pmatrix} J^+ & u & J \\ -M_J^+ & w & M_J \end{pmatrix} \begin{pmatrix} J^+ & I & F^+ \\ M_J^+ & M_I & -M_F^+ \end{pmatrix} \begin{pmatrix} J & I & F \\ M_J & M_I & -M_F \end{pmatrix}.
\end{aligned} \tag{5.39}$$

As in the previous section, we aim at a simpler expression for the product of 3j-symbols summed over projection quantum numbers. The selection rules for the 3j-symbols imply the relations $M_J = M_F - M_I$ and $M_J^+ = M_F^+ - M_I$. Therefore, the phase factor in the last line above is

$$(-1)^{2M_J+M_J^+} = (-1)^{2M_F+M_F^+-3M_I} = (-1)^{2M_F+M_F^+}(-1)^{-2M_I}(-1)^{-M_I}. \tag{5.40}$$

The nuclear-spin quantum number I may either be integer or half-integer. If I is integer, so are all possible values for M_I ($M_I = -I, -I+1, ..., I$), and vice versa if I is half-integer. For integer I (and thus integer M_I), we have $(-1)^{-2M_I} = 1$ for all possible M_I. For half-integer I, we have $(-1)^{-2M_I} = -1$ for all possible M_I.[4] In either case, the value of $(-1)^{-2M_I}$ does not depend on M_I but only on I. We may thus define a function $\eta(I)$ according to,

$$\eta(I) \coloneqq \begin{cases} 1 & \text{for integer } I \\ -1 & \text{for half-integer } I \end{cases} \tag{5.41}$$

and write the phase factor in (5.40) as $(-1)^{2M_J+M_J^+} = (-1)^{2M_F+M_F^+}\eta(I)(-1)^{-M_I}$.

With these manipulations, the last line of equation (5.39) equals

$$\begin{aligned}
&\sum_{M_J^+, M_J, M_I} (-1)^{2M_J+M_J^+} \begin{pmatrix} J^+ & u & J \\ -M_J^+ & w & M_J \end{pmatrix} \begin{pmatrix} J^+ & I & F^+ \\ M_J^+ & M_I & -M_F^+ \end{pmatrix} \begin{pmatrix} J & I & F \\ M_J & M_I & -M_F \end{pmatrix} \\
&= (-1)^{2M_F+M_F^+}\eta(I) \sum_{M_J^+, M_J, M_I} (-1)^{-M_I} \begin{pmatrix} J^+ & u & J \\ -M_J^+ & w & M_J \end{pmatrix} \begin{pmatrix} J^+ & I & F^+ \\ M_J^+ & M_I & -M_F^+ \end{pmatrix} \begin{pmatrix} J & I & F \\ M_J & M_I & -M_F \end{pmatrix},
\end{aligned} \tag{5.42}$$

where we made use of $\eta(I)$ being independent of M_I such that it may be put in front of the sums.

The term within the sums on the right-hand side of the above equation has the form of the general relation between Wigner 3j- and 6j-symbols shown in Appendix C.1. Applying equation (C.2) from

[4] Proof: let $I = k/2$ be half-integer with some *odd* integer number k. The possible values for M_I are then $M_I = -k/2, -k/2+1, -k/2+2, ..., k/2$ or generally $M_I = -k/2 + n$ with $n \in \mathbb{N}$. Therefore, $(-1)^{-2M_I} = (-1)^{k-2n} = (-1)^k(-1)^{-2n} = -1 \times 1 = -1$, since n is integer and k is integer and odd.

this appendix, we obtain for the transition matrix element in (5.39)

$$\begin{aligned}
&\left\langle n^+\Lambda^+, v^+, N^+\Lambda^+S^+J^+I^+F^+M_F^+\right| \left\langle s, m_s\right| \left\langle l, m_l\right| \hat{\boldsymbol{\mu}} \left| n\Lambda, v, N\Lambda SJIFM_F\right\rangle \\
&\quad = \sqrt{2N^+ + 1}\sqrt{2N+1}\sqrt{2S+1}\sqrt{2J^+ + 1}\sqrt{2J+1}\sqrt{2F^+ + 1}\sqrt{2F+1}\delta_{II^+} \\
&\qquad (-1)^{l-1-\Lambda^+-s+N+J+2J^+-3I-F^+-F+3M_F+2M_F^+}\eta(I) \\
&\qquad \sum_{k=l\pm1} (-1)^k\sqrt{2k+1} \begin{pmatrix} l & 1 & k \\ -m_l & \mu_0 & -p \end{pmatrix} \left\langle n^+\Lambda^+, v^+ \right| \mathrm{T}'^k_{\Delta\Lambda} \left| n\Lambda, v \right\rangle \begin{pmatrix} N^+ & k & N \\ -\Lambda^+ & \Delta\Lambda & \Lambda \end{pmatrix} \\
&\qquad \sum_{u=|k-s|}^{k+s} (-1)^{-u+w}(2u+1) \begin{pmatrix} u & k & s \\ w & -p & m_s \end{pmatrix} \begin{Bmatrix} J^+ & u & J \\ N^+ & k & N \\ S^+ & s & S \end{Bmatrix} \begin{Bmatrix} u & J & J^+ \\ I & F^+ & F \end{Bmatrix} \begin{pmatrix} F^+ & u & F \\ -M_F^+ & w & M_F \end{pmatrix}.
\end{aligned} \tag{5.43}$$

Substituting this result into (5.34) and employing $|\eta(I)| = 1$ yields

$$\begin{aligned}
P(F, F^+) = (2N^+ + 1)(2N+1)(2S+1)(2J^+ + 1)(2J+1)(2F^+ + 1)(2F+1)\delta_{II^+} \sum_l \sum_{m_l} \sum_{m_s} \sum_{M_F, M_F^+} \\
\left| \sum_{k=l\pm1} (-1)^k\sqrt{2k+1} \begin{pmatrix} l & 1 & k \\ -m_l & \mu_0 & -p \end{pmatrix} \left\langle n^+\Lambda^+, v^+ \right| \mathrm{T}'^k_{\Delta\Lambda} \left| n\Lambda, v \right\rangle \begin{pmatrix} N^+ & k & N \\ -\Lambda^+ & \Delta\Lambda & \Lambda \end{pmatrix} \right. \\
\sum_{u=|k-s|}^{k+s} (-1)^{-u+w}(2u+1) \begin{pmatrix} u & k & s \\ w & -p & m_s \end{pmatrix} \begin{Bmatrix} J^+ & u & J \\ N^+ & k & N \\ S^+ & s & S \end{Bmatrix} \\
\left. \begin{Bmatrix} u & J & J^+ \\ I & F^+ & F \end{Bmatrix} \begin{pmatrix} F^+ & u & F \\ -M_F^+ & w & M_F \end{pmatrix} \right|^2.
\end{aligned} \tag{5.44}$$

Like in the previous section, the cross terms in the above equation vanish when summed over all possible values for M_F and M_F^+ due to the orthogonality of the Wigner 3j-symbols.[5] Hence, we obtain

$$\begin{aligned}
P(F, F^+) = (2N^+ + 1)(2N+1)(2S+1)(2J^+ + 1)(2J+1)(2F^+ + 1)(2F+1)\delta_{II^+} \\
\sum_l \sum_{k=l\pm1} (2k+1) \left| \left\langle n^+\Lambda^+, v^+ \right| \mathrm{T}'^k_{\Delta\Lambda} \left| n\Lambda, v \right\rangle \right|^2 \begin{pmatrix} N^+ & k & N \\ -\Lambda^+ & \Delta\Lambda & \Lambda \end{pmatrix}^2 \\
\sum_{u=|k-s|}^{k+s} (2u+1) \begin{Bmatrix} J^+ & u & J \\ N^+ & k & N \\ S^+ & s & S \end{Bmatrix}^2 \begin{Bmatrix} u & J & J^+ \\ I & F^+ & F \end{Bmatrix}^2 \\
\sum_{m_l} \begin{pmatrix} l & 1 & k \\ -m_l & \mu_0 & -p \end{pmatrix}^2 \sum_{m_s} \begin{pmatrix} u & k & s \\ w & -p & m_s \end{pmatrix}^2.
\end{aligned} \tag{5.45}$$

The terms on the last line above account for $1/(3(2k+1))$ for linearly polarized radiation ($\mu_0 = 0$),

[5] Similarly as in the previous section, this can be shown in a rather lengthy calculation, where the sums inside the absolute value function in (5.44) are written explicitly. Then the terms are summed over M_F and M_F^+ while applying the orthogonality properties of the Wigner 3j-symbols (equation (2.32) in [61]).

i.e.,

$$P(F,F^+) = \frac{1}{3}(2N^+ + 1)(2N+1)(2S+1)(2J^+ + 1)(2J+1)(2F^+ + 1)(2F+1)\delta_{II^+}$$
$$\sum_l \sum_{k=l\pm 1} \left| \left\langle n^+\Lambda^+, v^+ \left| \, \mathrm{T'}^k_{\Delta\Lambda} \, \right| n\Lambda, v \right\rangle \right|^2 \begin{pmatrix} N^+ & k & N \\ -\Lambda^+ & \Delta\Lambda & \Lambda \end{pmatrix}^2$$
$$\sum_{u=|k-s|}^{k+s} (2u+1) \begin{Bmatrix} J^+ & u & J \\ N^+ & k & N \\ S^+ & s & S \end{Bmatrix}^2 \begin{Bmatrix} u & J & J^+ \\ I & F^+ & F \end{Bmatrix}^2 . \tag{5.46}$$

In essence, we have reproduced in (5.46) the result from (5.30) with an additional Wigner 6j-symbol describing the influence of the nuclear spin, i.e., the hyperfine-structure effects. Since the photoelectron does not carry nuclear spin, the same selection rule as for ΔJ applies also for ΔF, namely $|\Delta F| = |F^+ - F| \leq u$. Once more, due to the separability of the transition matrix element, the relative intensities of transitions between particular hyperfine levels in the neutral molecule and the molecular ion are determined by the magnitude of the vibronic transition matrix elements, which also determine the intensity of different rotational lines in a photoelectron spectrum. Thus, no additional free parameters need to be introduced when extending the BOS model for the rotational structure in photoelectron spectra to hyperfine-structure effects.

Expressions related to those derived above have been found for high-resolution Rydberg spectra of rare gas atoms and hydrogen molecules within the frame work of MQDT (see, e.g., [154, 155]).

5.2.3 Example 1: Fine-structure effects in the photoionization of oxygen

In order to validate our model and to illustrate its physical content, we applied it to a measured photoelectron spectrum. One of the few spin-rotation-resolved photoelectron spectra reported in the literature is the PFI-ZEKE spectrum of oxygen recorded by Palm and Merkt [152]. They presented a spectrum of the O_2 $X^3\Sigma_g^-$ $\rightarrow$ O_2^+ $b^4\Sigma_g^-$ band with several spin-rotation-resolved lines. Since both, the neutral as well as the ionic state of the oxygen molecule exhibit a non-vanishing electron spin, this species is well-suited for testing our model.

Often, PFI-ZEKE spectra are affected by channel interactions and models for direct photoionization are not necessarily applicable to them [160]. For the transitions studied in [152], however, the authors state that "the observed line intensities are not dominated by channel interactions" and we may thus attempt to interpret this spectrum with our model.

The energy level structure of neutral O_2 in the electronic ground state $X^3\Sigma_g^-$ and of the O_2^+ molecular ion in the $b^4\Sigma_g^-$ state is shown in Fig. 5.1. We are interested in the Q(1) line of the $v = 0 \rightarrow v^+ = 0$ band, i.e., in the transition $v = 0, N = 1 \rightarrow v^+ = 0, N^+ = 1$, as this transition has been measured with the highest resolution. Neutral O_2 exhibits an electron spin $S = 1$ in the $X^3\Sigma_g^-$ state, such that there are three spin-rotation components for $N = 1$: $J = 0$, 1 and 2. For O_2^+ in the $b^4\Sigma_g^-$ state, the total electron spin is $S^+ = 3/2$ giving rise to three spin-rotation components with $J^+ = 1/2$, 3/2 and 5/2. Hence, there are in total nine different transitions between the fine-structure components of the neutral and ionic state making up the Q(1) line.

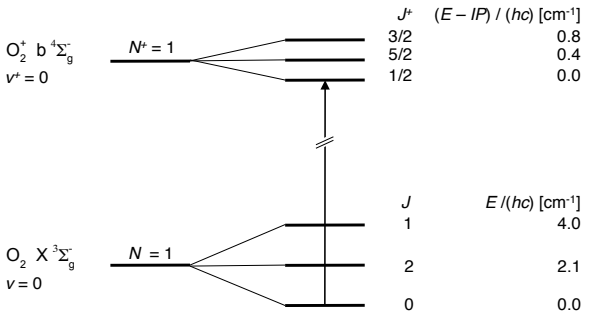

Figure 5.1. Energy level structure of the oxygen molecular ion and the neutral oxygen molecule. The electron spin gives rise to spin-rotational fine structure in both, the ionic $b^4\Sigma_g^-$ as well as the neutral $X^3\Sigma_g^-$ state. Levels are labelled by their total angular momentum quantum number, J and J^+, for the neutral and ionic state, respectively, as well as their relative term value (adapted from [152]).

The photoelectron spectrum of the fine-structure-resolved Q(1) line measured by Palm and Merkt [152] is reproduced in Fig. 5.2 (a). This spectrum shows three well-separated peaks spaced by about $2\,\mathrm{cm}^{-1}$. These peaks reflect the spin-rotation splitting in the $X^3\Sigma_g^-$ state of neutral O_2 with a spacing of about $2\,\mathrm{cm}^{-1}$ between adjacent spin-rotation components. The peaks are themselves composed of three partially overlapping lines, which stem from the spin-rotation components of the ionic $b^4\Sigma_g^-$ state that are spaced by about $0.4\,\mathrm{cm}^{-1}$, totaling to the nine spin-rotation transitions of the Q(1) line.

To compare the measured spectrum with our model, the experimental line intensities have been extracted from the spectrum by fitting it with a set of Gaussian peaks. The empirical intensities found this way are shown as blue circles in the stick spectrum of Fig. 5.2 (b).

Even without any further calculations, we may rationalize this spectrum with our model. From the analysis of rotationally, but not fine-structure-resolved spectra [161], it is known that the photoionization of oxygen mainly occurs via the vibronic transition matrix element $\left\langle n^+\Lambda^+, v^+ \middle| \mathrm{T}'^k_{\Delta\Lambda} \middle| n\Lambda, v \right\rangle$ with $k = 0$ and to a smaller extent via the one with $k = 2$ indicating that ionization occurs out of a molecular orbital with a predominant s character. The absolute value of the vibronic transition matrix elements in equation (5.30) is thus large for $k = 0$ and substantially smaller for $k = 2$. For $k > 2$, the matrix element essentially vanishes.

According to our model, we have for $k = 0$, the value $u = 1/2$, allowing lines with $\Delta J = \pm 1/2$ and we may thus infer that such lines might show high intensities. Indeed the lines with the highest intensity within each of three peaks for $J = 0$, 1 and 2 obey this criterion. On the contrary, transitions with $|\Delta J| > 1/2$ are only possible via the $k = 2$ vibronic matrix element with a considerably reduced magnitude. Indeed, such lines show only low to medium intensities.

For a more in-depth analysis and in order to validate our model, we fitted the normalized intensities shown as blue circles in the stick spectrum of Fig. 5.2 (b) to the relative ionization rates as given by the transition probabilities from equation (5.30) substituted into equation (5.6). For the Boltzmann factor in (5.6), we used the relative term values shown in Fig. 5.1 together with the rotational temperature of 7 K reported in [152]. The two squared absolute values of the vibronic transition matrix elements $\left|\left\langle n^+\Lambda^+, v^+ \middle| \mathrm{T}'^k_{\Delta\Lambda} \middle| n\Lambda, v \right\rangle\right|^2$ for $k = 0, 2$, i.e., the two BOS coefficients C_0 and C_2 were treated as free parameters. The intensities obtained from our model with this fit are shown as green diamonds in Fig. 5.2 (b). As seen from this figure, our model reproduces the measured photoionization intensities

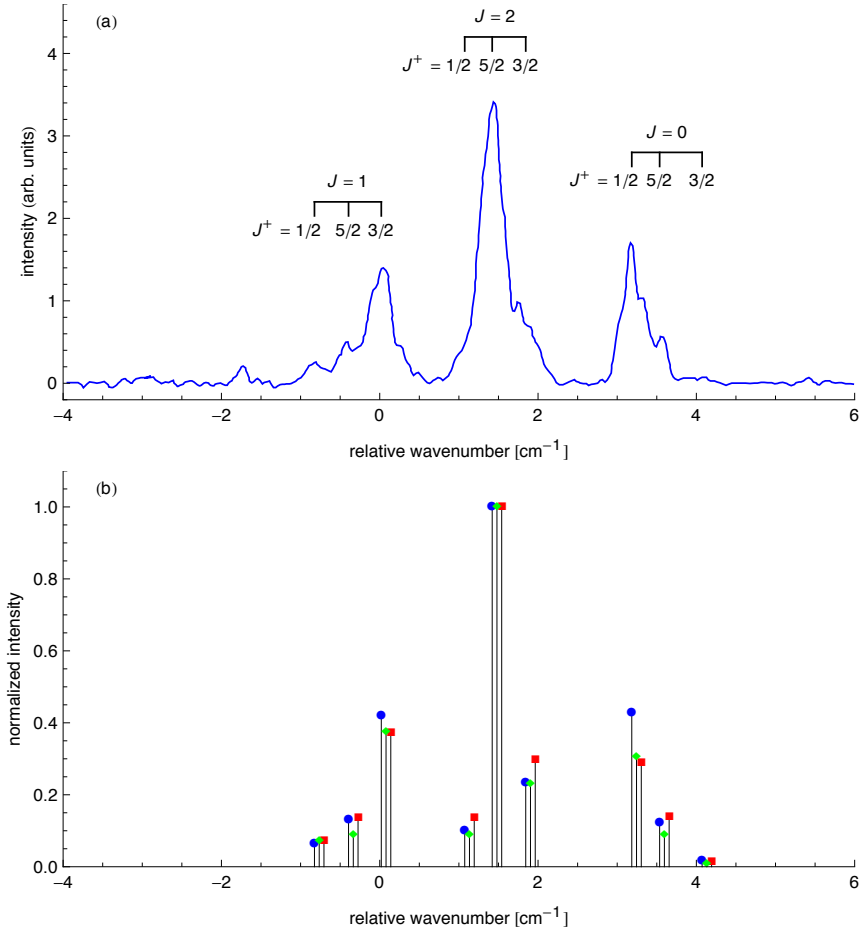

Figure 5.2. Fine-structure effects in molecular photoionization. (a) Measured fine-structure-resolved photoelectron spectrum of the O_2 $X^3\Sigma_g^-$ $(v = 0, N = 1) \rightarrow O_2^+$ $b^4\Sigma_g^-$ $(v^+ = 0, N^+ = 1)$ transition recorded by Palm and Merkt (reproduced from [152]). Peaks are labelled with the total neutral-state angular momentum quantum number J above and the corresponding ionic one J^+ below the assignment bars. The spectrum shows three well-separated peaks reflecting the three spin-rotation components in the neutral $X^3\Sigma_g^-$ state. These peaks are themselves composed of three partially overlapping lines associated with the spin-rotation levels in the ionic $b^4\Sigma_g^-$ state. **(b)** Stick spectrum showing the normalized intensities of individual spin-rotation-resolved transitions. The experimental intensities extracted from the spectrum in (a) are shown as blue circles. The green diamonds show a fit of our photoionization model to the measured intensities with the two BOS coefficients C_0 and C_2 treated as free parameters. Good agreement between measured and theoretically calculated intensities is observed. The red squares show the spin-rotation resolved intensities as obtained from our model when using the values of $C_0/C_2 = 0.6/0.4$ determined in [161] from intensities of a rotationally, but not fine-structure-resolved spectrum. Although, no free parameter affecting the relative intensities is left, these are well reproduced by our model. (For clarity, the sticks showing the theoretically calculated line intensities are horizontally offset by $0.06\,\mathrm{cm}^{-1}$ and $0.12\,\mathrm{cm}^{-1}$. All intensities are normalized to unity for the most intense transition.)

well. Furthermore, the ratio of the two BOS coefficients, which entails the relative line intensities,[6] obtained from our fit accounts for $C_2/C_0 = 0.3/0.7$. This result is in agreement with the values of $C_2 = 0.4 \pm 0.1$, $C_0 = 0.6 \pm 0.1$ found by Hsu et al. (Fig. 7 in [161]) in the analysis of the relative intensities of different *rotational*—instead of fine-structure—lines.

As a further test of our model, we directly substituted the BOS coefficients from [161] into equation (5.30). Though, in this way no free parameter affecting the relative intensities of the lines appears in the model and the only free parameter left is a global normalization factor, the line intensities predicted by our model (red squares in Fig. 5.2 (b)) reproduces well the measured intensities. This supports our assumption that the influence of the electron spin on transition probabilities in molecular photoionization may be described without additional free parameters, i.e., that the transition matrix element may be separated into a spin and a rovibronic factor according to angular momentum coupling theory (see also [162]).

5.2.4 Example 2: Hyperfine-structure effects in the photoionization of nitrogen

We are not aware of any hyper-fine-structure-resolved photoelectron spectrum reported in the literature that could serve as a benchmark for our photoionization model. So, in order to illustrate the implications of our model in its hfs-resolved form (equation (5.46)), we calculated the relative intensities of hfs-resolved photoionization transitions of nitrogen. In particular, we studied the hfs lines of the transition $N_2\ X^1\Sigma_g^+\ N = 2 \rightarrow N_2^+\ X^2\Sigma_g^+\ N^+ = 4$ as an illustrative example. A level scheme is shown in Fig. 5.3. As the neutral electronic ground state of N_2 is a singlet state, the total electron spin vanishes and we have $N = J$. The nuclear spin, by contrast, does not necessarily vanish and we expect hyperfine levels characterized by the total angular momentum quantum number $F = N + I, N + I - 1, \ldots, |N - I|$. According to the Pauli principle, the values $I = 0$ or 2 are possible for $N = 2$. Being interested in hyperfine-structure effects, we study the later case here. The N_2^+ ion exhibits fine and hyperfine structure as discussed in Ch. 3, i.e., the rotational levels are split by the spin-rotation interaction into two spin-rotation components labelled by the quantum number J, which may take the two values $J^+ = N^+ + 1/2$ and $J^+ = N^+ - 1/2$. The spin-rotation levels are split further into hyperfine levels associated with the quantum number F^+ with the values $F^+ = J^+ + I^+, J^+ + I^+ - 1, \ldots, |J^+ - I^+|$.

Like in the previous example of O_2, the photoelectron spectrum of N_2 is dominated by the vibronic transition matrix elements $\left\langle n^+\Lambda^+, v^+ \middle| \mathrm{T}'^k_{\Delta\Lambda} \middle| n\Lambda, v \right\rangle$ with $k = 0$ and $k = 2$. Transition matrix elements with $k > 2$ show considerable reduced magnitude [166, 167] and are neglected here. For the $N = 2 \rightarrow N^+ = 4$ transitions, we have $J = N = 2$ and $J^+ = 9/2$ or $7/2$. Since for both of these transitions we have $|\Delta J| > 1/2$, they may solely occur due to the $k = 2$ vibronic transition matrix element. Hence, the relative magnitude of the two vibronic transition matrix elements with $k = 0$ and $k = 2$ is not relevant to predict relative intensities of these hyperfine-structure transitions and their relative intensities are not subject to any free parameters.

The intensities calculated from equation (5.46) are shown in Fig. 5.4. Obviously, a propensity towards transitions obeying the relation $\Delta J = \Delta F$ is observed in these line intensities, i.e., the hyperfine-structure-resolved ionizing transitions studied here are governed by a similar propensity rule as the

[6] The values of the BOS coefficients on an absolute scale are of no significance when analyzing relative line intensities.

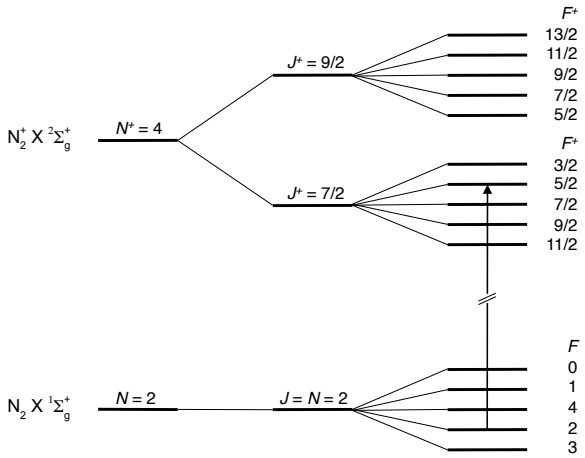

Figure 5.3. Level structure of the nitrogen molecular ion and the neutral nitrogen molecule. The $X^2\Sigma_g^+$ electronic ground state of N_2^+ exhibits fine- and hyperfine-structure levels as discussed in Ch. 3. In the $X^1\Sigma_g^+$ ground state of neutral N_2, the total electron spin vanishes and spin-rotational fine structure does not occur. Coupling of the rotational angular momentum to the nuclear spin ($I = 2$ nuclear spin manifold shown here) results in hyperfine levels denoted by $F = 1, \ldots, 4$. (The energetic order of the hyperfine levels in the neutral N_2 $^1\Sigma_g^+$ state has been estimated using electric-quadrupole coupling constants extrapolated from spectroscopic data on the neutral N_2 $A^3\Sigma_u^+$ state and from N_2 complexes [163, 164, 165].)

electric-quadrupole bound-bound transitions studied in Ch. 3. This finding reflects the similar treatment of the hyperfine structure in our models for both of these processes: in both cases the hyperfine-structure states are expressed in the tensor product basis of the fine-structure (spin-rotational) and the nuclear spin states according to angular momentum algebra. As both, the electric-quadrupole operator studied in Ch. 3, and the photoionization operator T'^k_q with $k = 2$ are second-rank spherical tensors, the same angular momentum coupling coefficients (expressed as a Wigner 6j-symbols) appear in the formulae governing the respective line intensities.

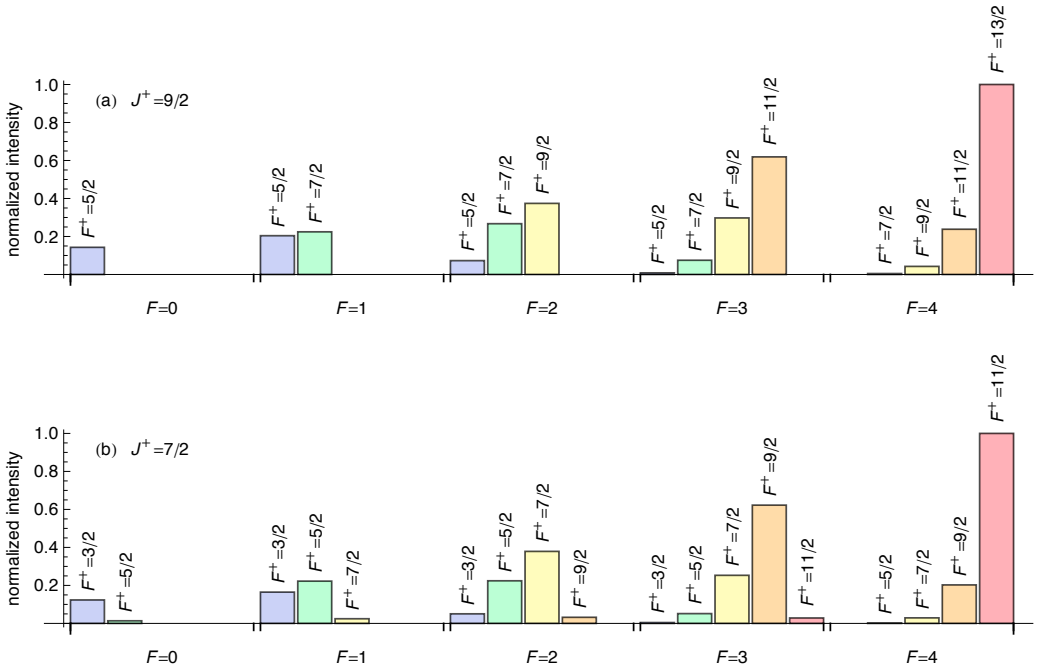

Figure 5.4. Hyperfine-structure effects in molecular photoionization shown by the example of the relative intensities of the N_2 $X^1\Sigma_g^+$ $N = 2 \rightarrow N_2^+$ $X^2\Sigma_g^+$ $N^+ = 4$ ionization transitions: chart of the relative intensities of transitions between different hyperfine levels in the neutral N_2 molecule and the N_2^+ molecular ion labelled by their total angular momentum quantum number F and F^+, respectively. **(a)** $J^+ = 9/2$ spin-rotation component, **(b)** $J^+ = 7/2$ spin-rotation component. The photoionization transitions follow the propensity rule $\Delta J = \Delta F$, similar to the propensity found for electric-quadrupole transitions between bound states discussed in Ch. 3. (For clarity, transitions with relative intensities $< 10^{-3}$ have been suppressed.)

5.3 Resonance-enhanced multiphoton ionization

5.3.1 Introduction

In the preceding section, a model for fine- and hyperfine-structure-resolved photoionization intensities has been developed. Although this model describes the one-photon ionization satisfactorily, it is not directly applicable to the [2+1'] REMPI scheme used in the experiments presented in Ch. 4 to produce N_2^+ ions.

Such a three-photon, two-colour REMPI scheme is sketched in Fig. 5.5: the neutral, diatomic molecule AB is first excited from the electronic ground state to some neutral, electronically excited state (AB*) by absorption of two photons at some (angular) frequency ω_1. Thereafter, the molecule is ionized by absorption of a third photon at a different frequency ω_2 forming the molecular ion AB^+.

Following this picture, we describe the [2+1'] REMPI scheme as a sequence of two independent processes: a transition from the electronic-ground-state molecule AB to the neutral, electronic-excited molecule AB* and a subsequent ionization of this molecule yielding the molecular ion AB^+.

For the excitation step (AB $\rightarrow$ AB*), a model for hfs-resolved two-photon transitions between bound states will be developed. With this model we may calculate the excitation rate $R(\mathrm{AB} \rightarrow \mathrm{AB}^*)$ and hence the population ρ' of excited molecules AB*. The ionization of the excited molecules is then described by our ionization model developed in the preceding section, with the excited-state population ρ' used in lieu of the thermal ground-state population (equation (5.5)) having appeared in the model for direct ionization.

The excitation of the neutral molecules AB to AB* by polarized radiation leads to an aligned population ρ', meaning that the several Zeeman states of a certain spin-rotational or hfs level in the excited state are unequally populated. Since so far isotropic populations have been implicitly assumed in our photoionization model, the model needs to be adapted for these anisotropic populations.

These two effects, hfs-resolved two-photon transitions and ionization of molecules from anisotropic populations, are first treated separately and later combined to a model for the [2+1'] REMPI process. Finally, the implications of this model are illustrated by a couple of representative examples.

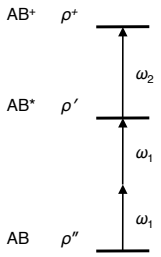

Figure 5.5. Schematic view of a [2+1'] resonance-enhanced multiphoton ionization process. The neutral, electronic-ground-state molecules AB are excited by absorption of two photons at some (angular) frequency ω_1 yielding electronic excited molecules AB*. Those are then ionized by absorption of a third photon at a different frequency ω_2, resulting in the molecular ions AB^+. The populations associated with AB, AB* and AB^+ are denoted ρ'', ρ' and ρ^+, respectively.

5.3.2 Excitation step: Hfs-resolved two-photon transitions

Two- and multiphoton transitions in diatomic molecules have been discussed in several publications, e.g., by Bray and Hochstrasser [168], Maïnos [169], Lefebvre-Brion and Field [170] or Hippler [171]. These transitions follow the so-called "Göppert-Meyer mechanism" first described by Göppert-Meyer in [172, 173]. Here, we will extend these results to cover hyperfine-structure-resolved transitions. Our treatment covers $^1\Sigma$ states as found in the [2+1'] REMPI of N_2.

In essence, in a two-photon transition following the Göppert-Meyer mechanism, ground and excited state are connected by two virtual one-photon transitions via an intermediate state. As excitation is possible via different intermediate states, the several virtual transition routes are summed, weighted by the inverse mismatch between the energy of the photons absorbed and the one-photon transition energies.

Like for one-photon transitions, the transition rate $R_{\mathrm{g}\to\mathrm{e}}$ for the excitation of the molecule from the ground state $|\mathrm{g}\rangle$ to the excited state $|\mathrm{e}\rangle$ is expressed as a factor depending on the intensity of the radiation field and a factor specific to the transition addressed, namely the two-photon line strength S_{ge} [171]:

$$R_{\mathrm{g}\to\mathrm{e}} \propto (I_0)^2 S_{\mathrm{ge}}. \tag{5.47}$$

In contrast to one-photon transitions, the *square* of the radiation intensity I_0 enters in the two-photon transition rate.

The two-photon line strength factor S_{ge} is given according to [171] as

$$S_{\mathrm{ge}} = \sum_{M_\mathrm{e},M_\mathrm{g}} \left| \sum_{\mathrm{i}} \frac{1}{\omega_{\mathrm{ig}} - \omega_1} \langle \mathrm{e} \,|\, \mathbf{e}_\sigma \cdot \hat{\boldsymbol{\mu}} \,|\, \mathrm{i} \rangle \langle \mathrm{i} \,|\, \mathbf{e}_\sigma \cdot \hat{\boldsymbol{\mu}} \,|\, \mathrm{g} \rangle \right|^2 . \tag{5.48}$$

Here, $|\mathrm{i}\rangle$ is the intermediate state of the virtual one-photon transition route with the sum over i including all accessible intermediate states. M_g and M_e label the different Zeeman states in the ground and the excited state, respectively, and $\hbar\omega_{\mathrm{ig}}$ is the energy difference between the ground and the intermediate state. Therefore, the term $\omega_{\mathrm{ig}} - \omega_1$ represents the mismatch between the ground-intermediate-state transition energy $\hbar\omega_{\mathrm{ig}}$ and the photon energy $\hbar\omega_1$ (see Fig. 5.6 (a)). Moreover, $\hat{\boldsymbol{\mu}}$ is the electric-dipole operator and $\mathbf{e}_\sigma$ the unit polarization vector of the radiation. The index σ indicates the polarization: $\sigma = 0$ stands for linear, $\sigma = \pm 1$ for circular polarization.

Assuming that all the molecular states involved may be written as a tensor product of an electronic-vibrational state (labelled "ev") and a nuclear-spin-rotational state (labelled "nsr"),

$$|\mathrm{g}\rangle = |\mathrm{g_{ev}}\rangle\,|\mathrm{g_{nsr}}\rangle = |\mathrm{g_{ev}}, \mathrm{g_{nsr}}\rangle\,, \tag{5.49a}$$

$$|\mathrm{i}\rangle = |\mathrm{i_{ev}}\rangle\,|\mathrm{i_{nsr}}\rangle = |\mathrm{i_{ev}}, \mathrm{i_{nsr}}\rangle\,, \tag{5.49b}$$

$$|\mathrm{e}\rangle = |\mathrm{e_{ev}}\rangle\,|\mathrm{e_{nsr}}\rangle = |\mathrm{e_{ev}}, \mathrm{e_{nsr}}\rangle\,, \tag{5.49c}$$

the two-photon line strength in (5.48) takes the form:

$$S_{\mathrm{ge}} = \sum_{M_\mathrm{e},M_\mathrm{g}} \left| \sum_{\mathrm{i_{ev}}} \sum_{\mathrm{i_{nsr}}} \frac{1}{\omega_{\mathrm{ig}} - \omega_1} \langle \mathrm{e_{ev}}, \mathrm{e_{nsr}} \,|\, \mathbf{e}_\sigma \cdot \hat{\boldsymbol{\mu}} \,|\, \mathrm{i_{ev}}, \mathrm{i_{nsr}} \rangle \langle \mathrm{i_{ev}}, \mathrm{i_{nsr}} \,|\, \mathbf{e}_\sigma \cdot \hat{\boldsymbol{\mu}} \,|\, \mathrm{g_{ev}}, \mathrm{g_{nsr}} \rangle \right|^2 . \tag{5.50}$$

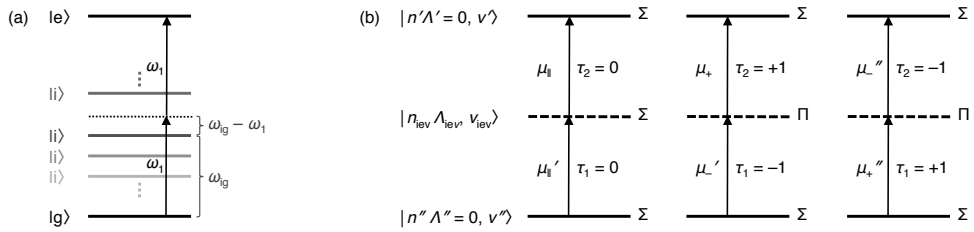

Figure 5.6. Mechanism of two-photon transitions. (a) Two-photon transitions are described by virtual one-photon transition routes connecting the ground state $|\mathrm{g}\rangle$ to an excited state $|\mathrm{e}\rangle$ via an intermediate state $|\mathrm{i}\rangle$. The two-photon line strength is given by a weighted sum of the several one-photon transition routes via different intermediate states $|\mathrm{i}\rangle$. Their weights—illustrated here by different grey tones—are determined by the inverse of the energy mismatch $\hbar(\omega_{\mathrm{ig}} - \omega_1)$ between the photon energy $\hbar\omega_1$ and the transition energy $\hbar\omega_{\mathrm{ig}}$. **(b)** Two-photon transitions between two Σ states may occur via Σ or Π intermediate states. Transition routes are labelled by the effective electric-dipole matrix element ($\mu_{||}\mu'_{||}$, $\mu_+\mu'_-$, $\mu''_-\mu''_+$, see equation (5.80)) and the relevant spherical tensor component of the electric-dipole operator in the molecule-fixed frame ($\tau_{1,2} = 0, \pm 1$).

Here the sum $\sum_{\mathrm{i}}$ over all intermediate states has been written as a sum over all electronic-vibrational intermediate states $\sum_{\mathrm{i_{ev}}}$ and all nuclear-spin-rotational intermediate states $\sum_{\mathrm{i_{nsr}}}$.

Expressing the scalar product $\mathbf{e}_\sigma \cdot \hat{\boldsymbol{\mu}}$ using spherical tensor notation and changing to the molecule-fixed frame by the aid of Wigner rotation matrices as well as factorizing the two transition matrix elements into purely angular and purely vibronic matrix element, yields

$$\begin{aligned}
&\langle \mathrm{e_{ev}}, \mathrm{e_{nsr}} \,|\, \mathbf{e}_\sigma \cdot \hat{\boldsymbol{\mu}} \,|\, \mathrm{i_{ev}}, \mathrm{i_{nsr}} \rangle \\
&= \sum_{\tau_1=-1}^{1} \left\langle \mathrm{e_{ev}}, \mathrm{e_{nsr}} \,\middle|\, \left[\hat{\mathcal{D}}^{(1)}_{\sigma\tau_1}\right]^* \mathrm{T}^1_{\tau_1}\left[\hat{\boldsymbol{\mu}}\right] \,\middle|\, \mathrm{i_{ev}}, \mathrm{i_{nsr}} \right\rangle \qquad (5.51) \\
&= \sum_{\tau_1=-1}^{1} \left\langle \mathrm{e_{ev}} \,\middle|\, \mathrm{T}^1_{\tau_1}\left[\hat{\boldsymbol{\mu}}\right] \,\middle|\, \mathrm{i_{ev}} \right\rangle \left\langle \mathrm{e_{nsr}} \,\middle|\, \left[\hat{\mathcal{D}}^{(1)}_{\sigma\tau_1}\right]^* \,\middle|\, \mathrm{i_{nsr}} \right\rangle \qquad (5.52)
\end{aligned}$$

and

$$\begin{aligned}
&\langle \mathrm{i_{ev}}, \mathrm{i_{nsr}} \,|\, \mathbf{e}_\sigma \cdot \hat{\boldsymbol{\mu}} \,|\, \mathrm{g_{ev}}, \mathrm{g_{nsr}} \rangle \\
&= \sum_{\tau_2=-1}^{1} \left\langle \mathrm{i_{ev}}, \mathrm{i_{nsr}} \,\middle|\, \left[\hat{\mathcal{D}}^{(1)}_{\sigma\tau_2}\right]^* \mathrm{T}^1_{\tau_2}\left[\hat{\boldsymbol{\mu}}\right] \,\middle|\, \mathrm{g_{ev}}, \mathrm{g_{nsr}} \right\rangle \qquad (5.53) \\
&= \sum_{\tau_2=-1}^{1} \left\langle \mathrm{i_{ev}} \,\middle|\, \mathrm{T}^1_{\tau_2}\left[\hat{\boldsymbol{\mu}}\right] \,\middle|\, \mathrm{g_{ev}} \right\rangle \left\langle \mathrm{i_{nsr}} \,\middle|\, \left[\hat{\mathcal{D}}^{(1)}_{\sigma\tau_2}\right]^* \,\middle|\, \mathrm{g_{nsr}} \right\rangle, \qquad (5.54)
\end{aligned}$$

such that we obtain:

$$\begin{aligned}
S_{\mathrm{ge}} = \sum_{M_{\mathrm{e}}, M_{\mathrm{g}}} \Bigg| \sum_{\mathrm{i_{ev}}} \sum_{\mathrm{i_{nsr}}} \frac{1}{\omega_{\mathrm{ig}} - \omega_1} \sum_{\tau_1,\tau_2} &\left\langle \mathrm{e_{ev}} \,\middle|\, \mathrm{T}^1_{\tau_1}\left[\hat{\boldsymbol{\mu}}\right] \,\middle|\, \mathrm{i_{ev}} \right\rangle \left\langle \mathrm{i_{ev}} \,\middle|\, \mathrm{T}^1_{\tau_2}\left[\hat{\boldsymbol{\mu}}\right] \,\middle|\, \mathrm{g_{ev}} \right\rangle \\
&\left\langle \mathrm{e_{nsr}} \,\middle|\, \left[\hat{\mathcal{D}}^{(1)}_{\sigma\tau_1}\right]^* \,\middle|\, \mathrm{i_{nsr}} \right\rangle \left\langle \mathrm{i_{nsr}} \,\middle|\, \left[\hat{\mathcal{D}}^{(1)}_{\sigma\tau_2}\right]^* \,\middle|\, \mathrm{g_{nsr}} \right\rangle \Bigg|^2 . \qquad (5.55)
\end{aligned}$$

The energy difference between ground and intermediate level $\hbar\omega_{\mathrm{ig}}$ depends in principle on both, the vibronic and the nuclear-spin-rotational state of the intermediate level, i.e., $\omega_{\mathrm{ig}} = \omega_{\mathrm{i_{ev}i_{nsr}g}}$. However,

since the nuclear-spin-rotational contribution to ω_{ig} is small compared to the vibronic one, we may neglect the latter and approximate the energy mismatch for far-off-resonant excitation as $\omega_{\mathrm{ig}} - \omega_1 = \omega_{\mathrm{i_{ev}i_{nsr}g}} - \omega_1 \approx \omega_{\mathrm{i_{ev}g}} - \omega_1$. Doing so, the term $1/(\omega_{\mathrm{ig}} - \omega_1) \approx 1/(\omega_{\mathrm{i_{ev}g}} - \omega_1)$ may be put in front of the sum over the nuclear-spin-rotational intermediate states ($\sum_{\mathrm{i_{nsr}}}$) and the expression for the line strength separates into a product of two independent sums, $\sum_{\mathrm{i_{ev}}}$ and $\sum_{\mathrm{i_{nsr}}}$:

$$S_{\mathrm{ge}} = \sum_{M_{\mathrm{e}},M_{\mathrm{g}}} \left| \sum_{\tau_1,\tau_2} \left(\sum_{\mathrm{i_{ev}}} \frac{1}{\omega_{\mathrm{i_{ev}g}} - \omega_1} \left\langle \mathrm{e_{ev}} \left| \, \mathrm{T}^1_{\tau_1} \left[\hat{\boldsymbol{\mu}}\right] \right| \mathrm{i_{ev}} \right\rangle \left\langle \mathrm{i_{ev}} \left| \, \mathrm{T}^1_{\tau_2} \left[\hat{\boldsymbol{\mu}}\right] \right| \mathrm{g_{ev}} \right\rangle \right) \right.$$
$$\left. \left(\sum_{\mathrm{i_{nsr}}} \left\langle \mathrm{e_{nsr}} \left| \left[\hat{\mathcal{D}}^{(1)}_{\sigma\tau_1}\right]^* \right| \mathrm{i_{nsr}} \right\rangle \left\langle \mathrm{i_{nsr}} \left| \left[\hat{\mathcal{D}}^{(1)}_{\sigma\tau_2}\right]^* \right| \mathrm{g_{nsr}} \right\rangle \right) \right|^2 . \tag{5.56}$$

Without any weighting factors, the sum over the intermediate nuclear-spin-rotational states boils down to a sum of projection operators. Since this sum includes *all* nuclear-spin-rotational states, the sum of the projection operators is equal to the identity operator for the nuclear-spin-rotational states, i.e.,

$$\sum_{\mathrm{i_{nsr}}} |\mathrm{i_{nsr}}\rangle \langle \mathrm{i_{nsr}}| = \hat{I}_{\mathrm{nsr}}, \tag{5.57}$$

such that we arrive at

$$S_{\mathrm{ge}} = \sum_{M_{\mathrm{e}},M_{\mathrm{g}}} \left| \sum_{\tau_1,\tau_2} \left\langle \mathrm{e_{nsr}} \left| \left[\hat{\mathcal{D}}^{(1)}_{\sigma\tau_1}\right]^* \left[\hat{\mathcal{D}}^{(1)}_{\sigma\tau_2}\right]^* \right| \mathrm{g_{nsr}} \right\rangle \right.$$
$$\left. \sum_{\mathrm{i_{ev}}} \frac{1}{\omega_{\mathrm{i_{ev}g}} - \omega_1} \left\langle \mathrm{e_{ev}} \left| \, \mathrm{T}^1_{\tau_1} \left[\hat{\boldsymbol{\mu}}\right] \right| \mathrm{i_{ev}} \right\rangle \left\langle \mathrm{i_{ev}} \left| \, \mathrm{T}^1_{\tau_2} \left[\hat{\boldsymbol{\mu}}\right] \right| \mathrm{g_{ev}} \right\rangle \right|^2 . \tag{5.58}$$

To proceed, we need to choose a basis for the molecular states. As we only consider $^1\Sigma$ states, Hund's case (a) or (b) basis sets are equally well suited. We chose the Hund's case (b) notation here and write the electronic-vibrational ground, intermediate and excited states as,

$$|\mathrm{g_{ev}}\rangle = \left|n''\Lambda'', v''\right\rangle , \tag{5.59a}$$
$$|\mathrm{i_{ev}}\rangle = |n_{\mathrm{i_{ev}}}\Lambda_{\mathrm{i_{ev}}}, v_{\mathrm{i_{ev}}}\rangle , \tag{5.59b}$$
$$|\mathrm{e_{ev}}\rangle = \left|n'\Lambda', v'\right\rangle . \tag{5.59c}$$

Here, n'', $n_{\mathrm{i_{ev}}}$, n' denote the electronic state in the ground, intermediate and excited level, respectively. v'', $v_{\mathrm{i_{ev}}}$, v' stand for the corresponding vibrational states and Λ'', $\Lambda_{\mathrm{i_{ev}}}$, Λ' are the projections of the total electron orbital angular momenta on the internuclear axis.

The angular part of the ground and excited state are written as

$$|\mathrm{g_{nsr}}\rangle = \left|N''\Lambda''I''F''M''_F\right\rangle , \tag{5.60a}$$
$$|\mathrm{e_{nsr}}\rangle = \left|N'\Lambda'I'F'M'_F\right\rangle , \tag{5.60b}$$

with N'' and N' the rotational quantum numbers in the ground and the excited state, I'' and I' the respective nuclear spin quantum numbers, F'' and F' the total angular momentum quantum numbers as well as M''_F, M'_F the corresponding angular momentum projection quantum numbers. (For reference,

Table 5.2. Symbols used in the model of the [2+1'] REMPI process.

Quantum number (Magnitude)	Mol.-fixed projection	Space-fixed projection	Description
n''	-	-	Electronic quantum number in the neutral ground state (AB)
v''	-	-	Vibrational quantum number in the neutral ground state
N''	Λ''	M_N''	Orbital-rotational angular momentum in the neutral ground state
I''	-	M_I''	Nuclear spin in the neutral ground state
F''	-	M_F''	Total angular momentum in the neutral ground state
$n_{\mathrm{i_{ev}}}$	-	-	Electronic quantum number in the intermediate state of the two-photon transition in the excitation step (AB → AB*)
$v_{\mathrm{i_{ev}}}$	-	-	Vibrational quantum number in the intermediate state of the two-photon transition in the excitation step
n'	-	-	Electronic quantum number in the neutral, excited state (AB*)
v'	-	-	Vibrational quantum number in the neutral, excited state
N'	Λ'	M_N'	Orbital-rotational angular momentum in the neutral, excited state
I'	-	M_I'	Nuclear spin in the neutral, excited state
F'	-	M_F'	Total angular momentum in the neutral, excited state
n^+	-	-	Electronic quantum number of the molecular ion (AB^+)
v^+	-	-	Vibrational quantum number of the molecular ion
N^+	Λ^+	M_N^+	Orbital-rotational angular momentum of the molecular ion
S^+	-	M_S^+	Electron spin of the molecular ion
J^+	-	M_J^+	Total angular momentum of the molecular ion excluding nuclear spin
I^+	-	M_I^+	Nuclear spin of the molecular ion
F^+	-	M_F^+	Total angular momentum of the molecular ion
1	τ_1 $(=\tau)$	σ	Angular momentum of the first photon in the excitation step
1	τ_2	σ	Angular momentum of the second photon in the excitation step
κ	$\tau_1+\tau_2$	2σ	Total angular momentum transferred to/from the molecule in the excitation step
1	-	μ_0	Angular momentum of the photon in the ionization step (AB* → AB^+)
l	-	m_l	Orbital angular momentum of the photoelectron
s	-	m_s	Spin of the photoelectron ($s=1/2$)
k	q	p	Total orbital angular momentum transferred to/from the molecule in the ionization step ($p=-m_l+\mu_0$)
u	-	w	Total angular momentum transferred to/from the molecule in the ionization step ($w=-m_s+p$)

important symbols used in our REMPI model are compiled in Tab. 5.2.)

As we are assuming Σ states for the ground and the excited state, we have $\Lambda''=\Lambda'=0$. For the intermediate state, also states with $\Lambda_{\mathrm{i_{ev}}}\neq 0$ need to be considered (Fig. 5.6 (b)).

In this notation, the line strength for the two-photon transition is,

$$S_{''\leftrightarrow'} = \sum_{M_F',M_F''}\left|\sum_{\tau_1,\tau_2}\left\langle N'\Lambda'I'F'M_F'\left|\left[\hat{\mathcal{D}}^{(1)}_{\sigma\tau_1}\right]^*\left[\hat{\mathcal{D}}^{(1)}_{\sigma\tau_2}\right]^*\right|N''\Lambda''I''F''M_F''\right\rangle \right.$$
$$\left.\sum_{\mathrm{i_{ev}}}\frac{1}{\omega_{\mathrm{i_{ev}g}}-\omega_1}\left\langle n'\Lambda',v'\left|\,\mathrm{T}^1_{\tau_1}\left[\hat{\boldsymbol{\mu}}\right]\right|n_{\mathrm{i_{ev}}}\Lambda_{\mathrm{i_{ev}}},v_{\mathrm{i_{ev}}}\right\rangle\left\langle n_{\mathrm{i_{ev}}}\Lambda_{\mathrm{i_{ev}}},v_{\mathrm{i_{ev}}}\left|\,\mathrm{T}^1_{\tau_2}\left[\hat{\boldsymbol{\mu}}\right]\right|n''\Lambda'',v''\right\rangle\right|^2. \tag{5.61}$$

To exploit that the nuclear spin states are not affected in rovibronic transitions, we decouple the nuclear spins from the total angular momenta in the ground and the excited state by expressing them

as,

$$\left|N''\Lambda''I''F''M_F''\right\rangle = \sum_{M_N'',M_I''} C^{F''M_F''}_{N''M_N''I''M_I''} \left|N''\Lambda''M_N'', I''M_I''\right\rangle, \tag{5.62a}$$

$$\left\langle N'\Lambda'I'F'M_F'\right| = \sum_{M_N',M_I'} C^{F'M_F'}_{N'M_N'I'M_I'} \left\langle N'\Lambda'M_N', I'M_I'\right|, \tag{5.62b}$$

with the Clebsch-Gordan coefficients $C^{F''M_F''}_{N''M_N''I''M_I''}$ and $C^{F'M_F'}_{N'M_N'I'M_I'}$.

The angular matrix element in (5.61) thus accounts for:

$$\begin{aligned}
&\left\langle N'\Lambda'I'F'M_F' \left| \left[\hat{\mathcal{D}}^{(1)}_{\sigma\tau_1}\right]^* \left[\hat{\mathcal{D}}^{(1)}_{\sigma\tau_2}\right]^* \right| N''\Lambda''I''F''M_F''\right\rangle \\
&= \sum_{M_N',M_I'} \sum_{M_N'',M_I''} C^{F'M_F'}_{N'M_N'I'M_I'} C^{F''M_F''}_{N''M_N''I''M_I''} \left\langle N'\Lambda'M_N', I'M_I' \left| \left[\hat{\mathcal{D}}^{(1)}_{\sigma\tau_1}\right]^* \left[\hat{\mathcal{D}}^{(1)}_{\sigma\tau_2}\right]^* \right| N''\Lambda''M_N'', I''M_I''\right\rangle \\
&= \sum_{M_N',M_I'} \sum_{M_N'',M_I''} C^{F'M_F'}_{N'M_N'I'M_I'} C^{F''M_F''}_{N''M_N''I''M_I''} \left\langle N'\Lambda'M_N' \left| \left[\hat{\mathcal{D}}^{(1)}_{\sigma\tau_1}\right]^* \left[\hat{\mathcal{D}}^{(1)}_{\sigma\tau_2}\right]^* \right| N''\Lambda''M_N''\right\rangle \left\langle I'M_I' \,\middle|\, I''M_I''\right\rangle \\
&= \sum_{M_N',M_I'} \sum_{M_N'',M_I''} C^{F'M_F'}_{N'M_N'I'M_I'} C^{F''M_F''}_{N''M_N''I''M_I''} \left\langle N'\Lambda'M_N' \left| \left[\hat{\mathcal{D}}^{(1)}_{\sigma\tau_1}\right]^* \left[\hat{\mathcal{D}}^{(1)}_{\sigma\tau_2}\right]^* \right| N''\Lambda''M_N''\right\rangle \delta_{I'I''}\delta_{M_I'M_I''} \\
&= \delta_{I'I''} \sum_{M_N'} \sum_{M_N'',M_I''} C^{F'M_F'}_{N'M_N'I''M_I''} C^{F''M_F''}_{N''M_N''I''M_I''} \left\langle N'\Lambda'M_N' \left| \left[\hat{\mathcal{D}}^{(1)}_{\sigma\tau_1}\right]^* \left[\hat{\mathcal{D}}^{(1)}_{\sigma\tau_2}\right]^* \right| N''\Lambda''M_N''\right\rangle \\
&= \delta_{I'I''}(-1)^{N'-I''+M_F'}(-1)^{N''-I''+M_F''}\sqrt{2F'+1}\sqrt{2F''+1} \\
&\quad \sum_{M_N',M_N''} \left\langle N'\Lambda'M_N' \left| \left[\hat{\mathcal{D}}^{(1)}_{\sigma\tau_1}\right]^* \left[\hat{\mathcal{D}}^{(1)}_{\sigma\tau_2}\right]^* \right| N''\Lambda''M_N''\right\rangle \sum_{M_I''} \begin{pmatrix} N' & I'' & F' \\ M_N' & M_I'' & -M_F' \end{pmatrix} \begin{pmatrix} N'' & I'' & F'' \\ M_N'' & M_I'' & -M_F'' \end{pmatrix}.
\end{aligned} \tag{5.63}$$

The product of the Wigner rotation matrices may be expanded in a Clebsch-Gordan series according to equation (3.116) in [61],

$$\hat{\mathcal{D}}^{(j_1)}_{m_1'm_1} \hat{\mathcal{D}}^{(j_2)}_{m_2'm_2} = \sum_{j_3=|j_1-j_2|}^{j_1+j_2} (2j_3+1) \begin{pmatrix} j_1 & j_2 & j_3 \\ m_1' & m_2' & m_3' \end{pmatrix} \begin{pmatrix} j_1 & j_2 & j_3 \\ m_1 & m_2 & m_3 \end{pmatrix} [\hat{\mathcal{D}}^{(j_3)}_{m_3'm_3}]^*. \tag{5.64}$$

Applying this relation to the product $\left[\hat{\mathcal{D}}^{(1)}_{\sigma\tau_1}\right]^* \left[\hat{\mathcal{D}}^{(1)}_{\sigma\tau_2}\right]^*$ and using the properties of the Wigner rotation matrices (equation (4.2.7) in [62]) as well as those of the Wigner 3j-symbols (equation (2.30) and (2.31) in [61]) yields,

$$\left[\hat{\mathcal{D}}^{(1)}_{\sigma\tau_1}\right]^* \left[\hat{\mathcal{D}}^{(1)}_{\sigma\tau_2}\right]^* = \sum_{\kappa=0}^{2} (2\kappa+1) \begin{pmatrix} 1 & 1 & \kappa \\ -\sigma & -\sigma & 2\sigma \end{pmatrix} \begin{pmatrix} 1 & 1 & \kappa \\ -\tau_2 & -\tau_1 & \tau_1+\tau_2 \end{pmatrix} \hat{\mathcal{D}}^{(\kappa)}_{-2\sigma,\,-\tau_1-\tau_2}. \tag{5.65}$$

The rotational matrix element in (5.63) is thus

$$\begin{aligned}
\left\langle N'\Lambda'M_N' \left| \left[\hat{\mathcal{D}}^{(1)}_{\sigma\tau_1}\right]^* \left[\hat{\mathcal{D}}^{(1)}_{\sigma\tau_2}\right]^* \right| N''\Lambda''M_N''\right\rangle = \sum_{\kappa=0}^{2} (2\kappa+1) \begin{pmatrix} 1 & 1 & \kappa \\ -\sigma & -\sigma & 2\sigma \end{pmatrix} \begin{pmatrix} 1 & 1 & \kappa \\ -\tau_2 & -\tau_1 & \tau_1+\tau_2 \end{pmatrix} \\
\left\langle N'\Lambda'M_N' \left| \hat{\mathcal{D}}^{(\kappa)}_{-2\sigma,\,-\tau_1-\tau_2} \right| N''\Lambda''M_N''\right\rangle.
\end{aligned} \tag{5.66}$$

Inserting appropriately normalized Wigner rotation matrices for the rotational states (with the three Euler angles ϕ, θ, χ),

$$\langle \phi\,\theta\,\chi | N''\Lambda'' M_N'' \rangle = \sqrt{\frac{2N''+1}{8\pi^2}} \left[\mathscr{D}^{(N'')}_{M_N''\Lambda''}(\phi,\theta,\chi) \right]^*, \tag{5.67a}$$

$$\langle N'\Lambda' M_N' | \phi\,\theta\,\chi \rangle = \sqrt{\frac{2N'+1}{8\pi^2}} \mathscr{D}^{(N')}_{M_N'\Lambda'}(\phi,\theta,\chi), \tag{5.67b}$$

we obtain for the matrix element in (5.66) an integral over three Wigner rotation matrices that may be expressed in form of 3j-symbols as

$$\left\langle N'\Lambda' M_N' \left| \hat{\mathcal{D}}^{(\kappa)}_{-2\sigma,\,-\tau_1-\tau_2} \right| N''\Lambda'' M_N'' \right\rangle = \sqrt{2N'+1}\sqrt{2N''+1}(-1)^{M_N''-\Lambda''} \begin{pmatrix} N' & \kappa & N'' \\ M_N' & -2\sigma & -M_N'' \end{pmatrix} \begin{pmatrix} N' & \kappa & N'' \\ \Lambda' & -\tau_1-\tau_2 & -\Lambda'' \end{pmatrix}, \tag{5.68}$$

where we made use of equation (4.2.7) and (4.6.2) from [62].

Substituting this expression into (5.66) yields,

$$\begin{aligned} &\left\langle N'\Lambda' M_N' \left| \left[\hat{\mathcal{D}}^{(1)}_{\sigma\tau_1}\right]^* \left[\hat{\mathcal{D}}^{(1)}_{\sigma\tau_2}\right]^* \right| N''\Lambda'' M_N'' \right\rangle \\ &\quad = \sqrt{2N'+1}\sqrt{2N''+1}(-1)^{M_N''-\Lambda''} \sum_{\kappa=0}^{2}(2\kappa+1) \begin{pmatrix} 1 & 1 & \kappa \\ -\sigma & -\sigma & 2\sigma \end{pmatrix} \begin{pmatrix} 1 & 1 & \kappa \\ -\tau_2 & -\tau_1 & \tau_1+\tau_2 \end{pmatrix} \\ &\qquad \begin{pmatrix} N' & \kappa & N'' \\ M_N' & -2\sigma & -M_N'' \end{pmatrix} \begin{pmatrix} N' & \kappa & N'' \\ \Lambda' & -\tau_1-\tau_2 & -\Lambda'' \end{pmatrix}, \end{aligned} \tag{5.69}$$

and subsequent substitution into (5.63) gives

$$\begin{aligned} &\left\langle N'\Lambda' I' F' M_F' \left| \left[\hat{\mathcal{D}}^{(1)}_{\sigma\tau_1}\right]^* \left[\hat{\mathcal{D}}^{(1)}_{\sigma\tau_2}\right]^* \right| N''\Lambda'' I'' F'' M_F'' \right\rangle \\ &\quad = \delta_{I'I''}(-1)^{N'-I''+M_F'}(-1)^{N''-I''+M_F''}(-1)^{-\Lambda''}\sqrt{2F'+1}\sqrt{2F''+1}\sqrt{2N'+1}\sqrt{2N''+1} \\ &\qquad \sum_{\kappa=0}^{2}(2\kappa+1) \begin{pmatrix} 1 & 1 & \kappa \\ -\sigma & -\sigma & 2\sigma \end{pmatrix} \begin{pmatrix} 1 & 1 & \kappa \\ -\tau_2 & -\tau_1 & \tau_1+\tau_2 \end{pmatrix} \begin{pmatrix} N' & \kappa & N'' \\ \Lambda' & -\tau_1-\tau_2 & -\Lambda'' \end{pmatrix} \\ &\qquad \sum_{M_N',M_N'',M_I''} (-1)^{M_N''} \begin{pmatrix} N' & \kappa & N'' \\ M_N' & -2\sigma & -M_N'' \end{pmatrix} \begin{pmatrix} N' & I'' & F' \\ M_N' & M_I'' & -M_F' \end{pmatrix} \begin{pmatrix} N'' & I'' & F'' \\ M_N'' & M_I'' & -M_F'' \end{pmatrix}. \end{aligned} \tag{5.70}$$

To simplify the matrix element in equation (5.70), we seek for a more compact form for the terms on its last line using a Wigner 6j-symbol. With the properties of the 3j-symbols, these terms may be

expressed as follows:

$$\sum_{M'_N,M''_N,M''_I} (-1)^{M''_N} \begin{pmatrix} N' & \kappa & N'' \\ M'_N & -2\sigma & -M''_N \end{pmatrix} \begin{pmatrix} N' & I'' & F' \\ M'_N & M''_I & -M'_F \end{pmatrix} \begin{pmatrix} N'' & I'' & F'' \\ M''_N & M''_I & -M''_F \end{pmatrix}$$

$$= (-1)^{N'+\kappa+N''+M''_F} \sum_{M'_N,M''_N,M''_I} (-1)^{-M''_I} \begin{pmatrix} N' & \kappa & N'' \\ -M'_N & 2\sigma & M''_N \end{pmatrix} \begin{pmatrix} N' & I'' & F' \\ M'_N & M''_I & -M'_F \end{pmatrix} \begin{pmatrix} N'' & I'' & F'' \\ M''_N & M''_I & -M''_F \end{pmatrix} \tag{5.71}$$

$$= (-1)^{M''_F-I''-F'-F''} \begin{Bmatrix} \kappa & N'' & N' \\ I'' & F' & F'' \end{Bmatrix} \begin{pmatrix} F' & \kappa & F'' \\ -M'_F & 2\sigma & M''_F \end{pmatrix}, \tag{5.72}$$

where equation (C.2) from Appendix C.1 has been used to derive the last equation.

Substituting into (5.70) yields for the matrix element,

$$\begin{aligned} &\left\langle N'\Lambda'I'F'M'_F \middle| \left[\hat{\mathcal{D}}^{(1)}_{\sigma\tau_1}\right]^* \left[\hat{\mathcal{D}}^{(1)}_{\sigma\tau_2}\right]^* \middle| N''\Lambda''I''F''M''_F \right\rangle \\ &\quad = \delta_{I'I''}(-1)^{N'+N''-\Lambda''-3I''-F'-F''+M'_F+2M''_F} \sqrt{2F'+1}\sqrt{2F''+1}\sqrt{2N'+1}\sqrt{2N''+1} \\ &\quad \sum_{\kappa=0}^{2}(2\kappa+1) \begin{pmatrix} 1 & 1 & \kappa \\ -\sigma & -\sigma & 2\sigma \end{pmatrix} \begin{pmatrix} 1 & 1 & \kappa \\ -\tau_2 & -\tau_1 & \tau_1+\tau_2 \end{pmatrix} \begin{pmatrix} N' & \kappa & N'' \\ \Lambda' & -\tau_1-\tau_2 & -\Lambda'' \end{pmatrix} \\ &\quad \begin{Bmatrix} \kappa & N'' & N' \\ I'' & F' & F'' \end{Bmatrix} \begin{pmatrix} F' & \kappa & F'' \\ -M'_F & 2\sigma & M''_F \end{pmatrix}. \end{aligned} \tag{5.73}$$

The two-photon line strength from (5.61) thus accounts for:

$$\begin{aligned} S_{''\leftrightarrow'} = (2F'+1)(2F''+1)(2N'+1)(2N''+1)\delta_{I'I''} &\sum_{M'_F,M''_F} \left| \sum_{\kappa=0}^{2}(2\kappa+1) \begin{pmatrix} 1 & 1 & \kappa \\ -\sigma & -\sigma & 2\sigma \end{pmatrix} \right. \\ &\begin{Bmatrix} \kappa & N'' & N' \\ I'' & F' & F'' \end{Bmatrix} \begin{pmatrix} F' & \kappa & F'' \\ -M'_F & 2\sigma & M''_F \end{pmatrix} \sum_{\tau_1,\tau_2} \begin{pmatrix} 1 & 1 & \kappa \\ -\tau_2 & -\tau_1 & \tau_1+\tau_2 \end{pmatrix} \begin{pmatrix} N' & \kappa & N'' \\ \Lambda' & -\tau_1-\tau_2 & -\Lambda'' \end{pmatrix} \\ &\left. \sum_{\mathrm{i_{ev}}} \frac{1}{\omega_{\mathrm{i_{ev}g}} - \omega_1} \left\langle n'\Lambda', v' \middle| \mathrm{T}^1_{\tau_1}[\hat{\boldsymbol{\mu}}] \middle| n_{\mathrm{i_{ev}}}\Lambda_{\mathrm{i_{ev}}}, v_{\mathrm{i_{ev}}} \right\rangle \left\langle n_{\mathrm{i_{ev}}}\Lambda_{\mathrm{i_{ev}}}, v_{\mathrm{i_{ev}}} \middle| \mathrm{T}^1_{\tau_2}[\hat{\boldsymbol{\mu}}] \middle| n''\Lambda'', v'' \right\rangle \right|^2. \end{aligned} \tag{5.74}$$

The first 3j-symbol vanishes for $\kappa = 1$ and we may thus omit the $\kappa = 1$ term in the sum over κ. By writing the sum over κ explicitly, it may be shown that the cross terms (appearing when expanding the absolute magnitude) vanish when summed over all values for M'_F and M''_F because of the orthogonality properties of the 3j-symbols.

Moreover, the terms in the double sum over τ_1, τ_2 not fulfilling the relation $\tau_1 + \tau_2 = \Lambda' - \Lambda''$ vanish. As we consider transitions between Σ states, we have $\Lambda' = \Lambda'' = 0$ and hence $\tau_2 = -\tau_1$. Skipping the subscript $_1$ on τ_1 by setting $\tau = \tau_1$, we thus obtain,

$$\begin{aligned} S_{''\leftrightarrow'} = (2F'+1)(2F''+1)(2N'+1)(2N''+1)\delta_{I'I''} &\sum_{\kappa=0,2}(2\kappa+1) \begin{pmatrix} 1 & 1 & \kappa \\ -\sigma & -\sigma & 2\sigma \end{pmatrix}^2 \\ &\begin{Bmatrix} \kappa & N'' & N' \\ I'' & F' & F'' \end{Bmatrix}^2 \begin{pmatrix} N' & \kappa & N'' \\ 0 & 0 & 0 \end{pmatrix}^2 U(\kappa), \end{aligned} \tag{5.75}$$

with

$$U(\kappa) = \Bigg| \sum_{\tau=-1}^{1} \begin{pmatrix} 1 & 1 & \kappa \\ \tau & -\tau & 0 \end{pmatrix} \sum_{\mathrm{i_{ev}}} \frac{1}{\omega_{\mathrm{i_{ev}g}} - \omega_1} \left\langle n'\,\Lambda' = 0, v' \,\middle|\, \mathrm{T}^1_\tau\left[\hat{\boldsymbol{\mu}}\right] \,\middle|\, n_{\mathrm{i_{ev}}}\Lambda_{\mathrm{i_{ev}}}, v_{\mathrm{i_{ev}}} \right\rangle \left\langle n_{\mathrm{i_{ev}}}\Lambda_{\mathrm{i_{ev}}}, v_{\mathrm{i_{ev}}} \,\middle|\, \mathrm{T}^1_{-\tau}\left[\hat{\boldsymbol{\mu}}\right] \,\middle|\, n''\,\Lambda'' = 0, v'' \right\rangle \Bigg|^2 . \tag{5.76}$$

We study the expression $U(\kappa)$ separately for $\kappa = 0$ and $\kappa = 2$. For $\kappa = 0$, evaluation of the 3j-symbol yields

$$\begin{aligned} U(0) =& \Bigg| \sum_{\tau=-1}^{1} \begin{pmatrix} 1 & 1 & 0 \\ \tau & -\tau & 0 \end{pmatrix} \sum_{\mathrm{i_{ev}}} \frac{1}{\omega_{\mathrm{i_{ev}g}} - \omega_1} \left\langle n'\Lambda', v' \,\middle|\, \mathrm{T}^1_\tau\left[\hat{\boldsymbol{\mu}}\right] \,\middle|\, n_{\mathrm{i_{ev}}}\Lambda_{\mathrm{i_{ev}}}, v_{\mathrm{i_{ev}}} \right\rangle \\ & \left\langle n_{\mathrm{i_{ev}}}\Lambda_{\mathrm{i_{ev}}}, v_{\mathrm{i_{ev}}} \,\middle|\, \mathrm{T}^1_{-\tau}\left[\hat{\boldsymbol{\mu}}\right] \,\middle|\, n''\Lambda'', v'' \right\rangle \Bigg|^2 && (5.77) \\ =& \frac{1}{3} \left| \mu_{||}\mu'_{||} - \mu_+\mu'_- - \mu''_-\mu''_+ \right|^2 && (5.78) \\ =& \frac{1}{3}\mu_{\mathrm{I}}^2, && (5.79) \end{aligned}$$

with the abbreviations [168, 105][7]

$$\mu_{||}\mu'_{||} = \sum_{\mathrm{i_{ev}}} \frac{1}{\omega_{\mathrm{i_{ev}g}} - \omega_1} \left\langle n'\Lambda', v' \,\middle|\, \mathrm{T}^1_0\left[\hat{\boldsymbol{\mu}}\right] \,\middle|\, n_{\mathrm{i_{ev}}}\Lambda_{\mathrm{i_{ev}}}, v_{\mathrm{i_{ev}}} \right\rangle \left\langle n_{\mathrm{i_{ev}}}\Lambda_{\mathrm{i_{ev}}}, v_{\mathrm{i_{ev}}} \,\middle|\, \mathrm{T}^1_0\left[\hat{\boldsymbol{\mu}}\right] \,\middle|\, n''\Lambda'', v'' \right\rangle , \tag{5.80a}$$

$$\mu_+\mu'_- = \sum_{\mathrm{i_{ev}}} \frac{1}{\omega_{\mathrm{i_{ev}g}} - \omega_1} \left\langle n'\Lambda', v' \,\middle|\, \mathrm{T}^1_{+1}\left[\hat{\boldsymbol{\mu}}\right] \,\middle|\, n_{\mathrm{i_{ev}}}\Lambda_{\mathrm{i_{ev}}}, v_{\mathrm{i_{ev}}} \right\rangle \left\langle n_{\mathrm{i_{ev}}}\Lambda_{\mathrm{i_{ev}}}, v_{\mathrm{i_{ev}}} \,\middle|\, \mathrm{T}^1_{-1}\left[\hat{\boldsymbol{\mu}}\right] \,\middle|\, n''\Lambda'', v'' \right\rangle , \tag{5.80b}$$

$$\mu''_-\mu''_+ = \sum_{\mathrm{i_{ev}}} \frac{1}{\omega_{\mathrm{i_{ev}g}} - \omega_1} \left\langle n'\Lambda', v' \,\middle|\, \mathrm{T}^1_{-1}\left[\hat{\boldsymbol{\mu}}\right] \,\middle|\, n_{\mathrm{i_{ev}}}\Lambda_{\mathrm{i_{ev}}}, v_{\mathrm{i_{ev}}} \right\rangle \left\langle n_{\mathrm{i_{ev}}}\Lambda_{\mathrm{i_{ev}}}, v_{\mathrm{i_{ev}}} \,\middle|\, \mathrm{T}^1_{+1}\left[\hat{\boldsymbol{\mu}}\right] \,\middle|\, n''\Lambda'', v'' \right\rangle , \tag{5.80c}$$

and

$$\mu_{\mathrm{I}}^2 = \left| \mu_{||}\mu'_{||} - \mu_+\mu'_- - \mu''_-\mu''_+ \right|^2 . \tag{5.81}$$

For $\kappa = 2$, we obtain similarly

$$U(2) = \frac{1}{30} \left| 2\mu_{||}\mu'_{||} + \mu_+\mu'_- + \mu''_-\mu''_+ \right|^2 = \frac{1}{30}\mu_{\mathrm{S}}^2, \tag{5.82}$$

where we have set $\mu_{\mathrm{S}}^2 = \left| 2\mu_{||}\mu'_{||} + \mu_+\mu'_- + \mu''_-\mu''_+ \right|^2$.

The hfs-resolved two-photon line strength between $^1\Sigma$ states is thus:

$$\begin{aligned} S_{''\leftrightarrow'} =& (2F'+1)(2F''+1)(2N'+1)(2N''+1)\delta_{I'I''} \\ & \left[\frac{1}{3}\frac{1}{2N''+1} \begin{pmatrix} 1 & 1 & 0 \\ -\sigma & -\sigma & 2\sigma \end{pmatrix}^2 \begin{Bmatrix} 0 & N'' & N' \\ I'' & F' & F'' \end{Bmatrix}^2 \mu_{\mathrm{I}}^2 \right. \\ & \left. + \frac{1}{6} \begin{pmatrix} N' & 2 & N'' \\ 0 & 0 & 0 \end{pmatrix}^2 \begin{pmatrix} 1 & 1 & 2 \\ -\sigma & -\sigma & 2\sigma \end{pmatrix}^2 \begin{Bmatrix} 2 & N'' & N' \\ I'' & F' & F'' \end{Bmatrix}^2 \mu_{\mathrm{S}}^2 \right] . \end{aligned} \tag{5.83}$$

[7] For the signs of $\mu_+\mu'_-$ and $\mu''_-\mu''_+$ different conventions are found in the literature. Here, the same sign convention as in [105] has been chosen, differing from the one used in [168].

For circular polarized radiation, we have $\sigma = \pm 1$. As σ denotes the projection associated with κ on the space-fixed z-axis, we must have $\kappa \geq \sigma$. Hence, the term with $\kappa = 0$ in (5.75), i.e., the first summand in the brackets in (5.83), does not apply for circular polarization. With the last 3j-symbol accounting for 1/5, we thus obtain:

$$S^{(\mathrm{circ})}_{N'' \leftrightarrow N'} = \frac{1}{30}(2F'+1)(2F''+1)(2N'+1)(2N''+1)\delta_{I'I''} \begin{pmatrix} N' & 2 & N'' \\ 0 & 0 & 0 \end{pmatrix}^2 \begin{Bmatrix} 2 & N'' & N' \\ I'' & F' & F'' \end{Bmatrix}^2 \mu_{\mathrm{S}}^2. \quad (5.84)$$

For linear polarization, we have $\sigma = 0$ for a suitable chosen space-fixed frame of reference. The two squared 3j-symbols involving σ then account for 1/3 and 2/15, respectively, and the line strength is

$$\begin{aligned} S^{(\mathrm{lin})}_{N'' \leftrightarrow N'} = {} & (2F'+1)(2F''+1)(2N'+1)(2N''+1)\delta_{I'I''} \\ & \left[\frac{1}{9} \frac{1}{2N''+1} \begin{Bmatrix} 0 & N'' & N' \\ I'' & F' & F'' \end{Bmatrix}^2 \mu_{\mathrm{I}}^2 + \frac{1}{45} \begin{pmatrix} N' & 2 & N'' \\ 0 & 0 & 0 \end{pmatrix}^2 \begin{Bmatrix} 2 & N'' & N' \\ I'' & F' & F'' \end{Bmatrix}^2 \mu_{\mathrm{S}}^2 \right]. \end{aligned} \quad (5.85)$$

In order to validate these results, the total line strength for all hfs-resolved transitions belonging to the same rotational line,

$$S^{(\mathrm{circ,\ tot})}_{N'' \leftrightarrow N'} = \sum_{F'=|N'-I'|}^{N'+I'} \sum_{F''=|N''-I''|}^{N''+I''} S^{(\mathrm{circ})}_{N'' \leftrightarrow N'} \quad (5.86)$$

and

$$S^{(\mathrm{lin,\ tot})}_{N'' \leftrightarrow N'} = \sum_{F'=|N'-I'|}^{N'+I'} \sum_{F''=|N''-I''|}^{N''+I''} S^{(\mathrm{lin})}_{N'' \leftrightarrow N'} \quad (5.87)$$

are considered. Evaluating these sums, using the symmetry and orthogonality properties of the 6j-symbols (equation 9.8(3) in [77]) yields,

$$S^{(\mathrm{circ,\ tot})}_{N'' \leftrightarrow N'} = \frac{1}{30}(2N'+1)(2N''+1)(2I''+1)\delta_{I'I''} \begin{pmatrix} N' & 2 & N'' \\ 0 & 0 & 0 \end{pmatrix}^2 \mu_{\mathrm{S}}^2 \quad (5.88)$$

and

$$S^{(\mathrm{lin,\ tot})}_{N'' \leftrightarrow N'} = (2N'+1)(2N''+1)(2I''+1)\delta_{I'I''} \left[\frac{1}{9}\delta_{N'N''} \frac{1}{2N''+1} \mu_{\mathrm{I}}^2 + \frac{1}{45} \begin{pmatrix} N' & 2 & N'' \\ 0 & 0 & 0 \end{pmatrix}^2 \mu_{\mathrm{S}}^2 \right]. \quad (5.89)$$

Apart from the factor $2I''+1$, reflecting the degeneracy due to the nuclear spin, these are exactly the expressions given in Tab. 3 of [168] (for $\Omega = 0$). Hence, our expressions for hfs-resolved two-photon line strengths correctly reproduce the results for the rotationally resolved two-photon line strength derived in [168].

So far, the line strength associated with the *total* population in a (N', I', F') level has been considered. This is the quantity usually of interest for transitions between bound states. For our particular purpose, namely to describe the REMPI process, the population in a certain Zeeman state $|N', I', F', M'_F\rangle$ is

needed. The relevant quantity is thus:[8]

$$S_{\mathrm{ge}}(M_{\mathrm{e}}) = \sum_{M_{\mathrm{g}}} \left| \sum_{\mathrm{i}} \frac{1}{\omega_{\mathrm{ig}} - \omega_1} \langle \mathrm{e}|\mathbf{e}_\sigma \cdot \hat{\boldsymbol{\mu}}|\mathrm{i}\rangle \langle \mathrm{i}|\mathbf{e}_\sigma \cdot \hat{\boldsymbol{\mu}}|\mathrm{g}\rangle \right|^2 . \tag{5.90}$$

For hfs-resolved transitions, this quantity is written in our notation as

$$\begin{aligned} S(F'', F', M_F') = \sum_{M_F''} \Bigg| \sum_{\tau_1,\tau_2} \left\langle N'\Lambda' I' F' M_F' \left| \left[\hat{\mathcal{D}}^{(1)}_{\sigma\tau_1}\right]^* \left[\hat{\mathcal{D}}^{(1)}_{\sigma\tau_2}\right]^* \right| N''\Lambda'' I'' F'' M_F'' \right\rangle \\ \sum_{\mathrm{i_{ev}}} \frac{1}{\omega_{\mathrm{i_{ev}g}} - \omega_1} \left\langle n'\Lambda', v' \left| \mathrm{T}^1_{\tau_1}[\hat{\boldsymbol{\mu}}] \right| n_{\mathrm{i_{ev}}}\Lambda_{\mathrm{i_{ev}}}, v_{\mathrm{i_{ev}}} \right\rangle \left\langle n_{\mathrm{i_{ev}}}\Lambda_{\mathrm{i_{ev}}}, v_{\mathrm{i_{ev}}} \left| \mathrm{T}^1_{\tau_2}[\hat{\boldsymbol{\mu}}] \right| n''\Lambda'', v'' \right\rangle \Bigg|^2 , \end{aligned} \tag{5.91}$$

where, as before, the nuclear-spin-rotational contribution to the energy mismatch has been neglected.

Substituting the angular transition matrix element from (5.73) and applying the above-mentioned restrictions and substitutions for τ_1, τ_2 yields for Σ-Σ transitions:

$$\begin{aligned} S(F'', F', M_F') = (2F'+1)(2F''+1)(2N'+1)(2N''+1)\delta_{I'I''} \sum_{M_F''} \Bigg| \sum_{\kappa=0,2} (2\kappa+1) \\ \begin{pmatrix} N' & \kappa & N'' \\ 0 & 0 & 0 \end{pmatrix} \begin{pmatrix} 1 & 1 & \kappa \\ -\sigma & -\sigma & 2\sigma \end{pmatrix} \begin{Bmatrix} \kappa & N'' & N' \\ I'' & F' & F'' \end{Bmatrix} \begin{pmatrix} F' & \kappa & F'' \\ -M_F' & 2\sigma & M_F'' \end{pmatrix} \\ \sum_{\tau} \begin{pmatrix} 1 & 1 & \kappa \\ \tau & -\tau & 0 \end{pmatrix} \sum_{\mathrm{i_{ev}}} \frac{1}{\omega_{\mathrm{i_{ev}g}} - \omega_1} \left\langle n'\,\Lambda' = 0, v' \left| \mathrm{T}^1_{\tau}[\hat{\boldsymbol{\mu}}] \right| n_{\mathrm{i_{ev}}}\Lambda_{\mathrm{i_{ev}}}, v_{\mathrm{i_{ev}}} \right\rangle \\ \left\langle n_{\mathrm{i_{ev}}}\Lambda_{\mathrm{i_{ev}}}, v_{\mathrm{i_{ev}}} \left| \mathrm{T}^1_{-\tau}[\hat{\boldsymbol{\mu}}] \right| n''\,\Lambda'' = 0, v'' \right\rangle \Bigg|^2 . \end{aligned} \tag{5.92}$$

In contrast to the total line strength considered before, the above expression does not include a sum over the excited-state projection angular momentum quantum number M_F'. As a consequence, the orthogonality of the 3j-symbols may not be used to get rid of the cross terms. Hence, evaluating (5.92) is in general only possible when knowing both, the magnitude and the *phase* of the vibronic transition matrix elements. If the phases are unknown, angular terms may not be separated from vibronic ones and relative nuclear-spin-rotational intensities may not be determined.

Fortunately, the schemes commonly used for state-selective preparation of molecular ions (as discussed in Ch. 4 of this thesis and in the literature [106, 108, 109]) are based on O or S lines in the excitation

[8] The quantity $S(M_{\mathrm{e}})$ defined in (5.90) does not fully comply with the usual definition of a line strength, which involves sums over all degenerate states of the initial and the final level. $S(M_{\mathrm{e}})$ is rather just a quantity proportional to the excitation rate populating a certain M_{e}-Zeeman state and hence to the population in this state after a given excitation period. Nonetheless, the symbol S is used for this quantity here as well.

step. As those exhibit $|\Delta N| = 2$, only the $\kappa = 2$ term in (5.92) is relevant for them and we obtain:

$$S_{\mathrm{S,\,O}}(F'', F', M'_F) = \frac{5}{6}(2F'+1)(2F''+1)(2N'+1)(2N''+1)\delta_{I'I''} \begin{pmatrix} 1 & 1 & 2 \\ -\sigma & -\sigma & 2\sigma \end{pmatrix}^2 \begin{Bmatrix} 2 & N'' & N' \\ I'' & F' & F'' \end{Bmatrix}^2 \sum_{M''_F} \begin{pmatrix} F' & 2 & F'' \\ -M'_F & 2\sigma & M''_F \end{pmatrix}^2 \begin{pmatrix} N' & 2 & N'' \\ 0 & 0 & 0 \end{pmatrix}^2 \mu_{\mathrm{S}}^2, \tag{5.93}$$

with μ_{S}^2 as in (5.82).

In the case of linearly polarized radiation ($\sigma = 0$), this results in

$$S^{(\mathrm{lin})}_{\mathrm{S,\,O}}(F'', F', M'_F) = \frac{1}{9}(2F'+1)(2F''+1)(2N'+1)(2N''+1)\delta_{I'I''} \begin{Bmatrix} 2 & N'' & N' \\ I'' & F' & F'' \end{Bmatrix}^2 \begin{pmatrix} F' & 2 & F'' \\ -M'_F & 0 & M'_F \end{pmatrix}^2 \begin{pmatrix} N' & 2 & N'' \\ 0 & 0 & 0 \end{pmatrix}^2 \mu_{\mathrm{S}}^2. \tag{5.94}$$

5.3.3 Ionization step: Effects of anisotropic populations

Having developed a model for the excitation step AB → AB* of the [2+1'] REMPI process, we will now consider the ionization step AB* → AB^+. The population of the excited molecules AB* produced by the two-photon excitation is in general anisotropic, i.e., different Zeeman states of the spin-rotational or hfs levels are unequally populated.

This effect is illustrated in Fig. 5.7 with hyperfine structure and fine structure in the neutral molecule omitted for clarity: diatomic molecules AB in the neutral ground state are excited by absorption of electromagnetic radiation at an (angular) frequency ω_1 yielding a population ρ' of neutral, excited molecules AB*. These excited molecules AB* are then ionized by electromagnetic radiation at another frequency ω_2 forming the molecular ions AB^+. In the case of excitation with linearly, z-polarized radiation, only transitions without change in the projection angular momentum quantum number, i.e., with $M'_N = M''_N$, are allowed. Therefore, the entire excited-state population ρ' is confined to the $M'_N = 0$ Zeeman state. As a consequence, ionization may only occur from this particular Zeeman state and the strengths of ionization transitions from other Zeeman states of the excited level do not contribute to the ionization process.

For other polarizations or more complicated level schemes (fine and hyperfine structure), this effect is similar: the population ρ' of the neutral, excited molecules AB* to be ionized is subject to the polarization of the radiation in the excitation step and thus in general anisotropic. Therefore, the strength of the ionization transitions addressing particular Zeeman states must be weighted by the population in these states. In the following, we develop a model for ionization of anisotropically populated states based on this weighting. First, we only consider spin-rotational fine structure, next, the model is extended to cover hyperfine structure.

Denoting the population of excited molecules AB* in a certain Zeeman state by $\rho'(J', M'_J)$, the quantity $P(J', J^+)$, proportional to the photoionization transition probability between fine-structure levels, is

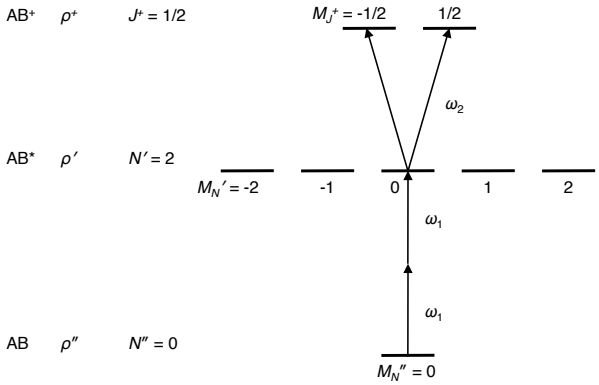

Figure 5.7. Anisotropic population in the excited state of REMPI. Example of the $N'' = 0 \rightarrow N' = 2 \rightarrow N^+ = 0$ REMPI scheme with linear polarization for excitation: because of the selection rule $M'_N = M''_N$ only the $M'_N = 0$ Zeeman state of the neutral, excited level is populated. Ionization may thus only occur from this particular Zeeman state.

given by

$$P(J', J^+) = \sum_l \sum_{m_l} \sum_{m_s} \sum_{M'_J, M_J^+} \rho'(J', M'_J) \left| \left\langle n^+\Lambda^+, v^+, N^+\Lambda^+ S^+ J^+ M_J^+ \right| \langle s, m_s | \langle l, m_l | \, \hat{\boldsymbol{\mu}} \right. \\ \left. \left| n'\Lambda', v', N'\Lambda' S' J' M'_J \right\rangle \right|^2 . \qquad (5.95)$$

For a normalized, isotropic population, this expression is identical to equation (5.7) of Sec. 5.2.1.

Substituting the matrix element from (5.27), we obtain

$$P(J', J^+) = (2N'+1)(2N^+ + 1)(2S'+1)(2J'+1)(2J^+ + 1) \sum_l \sum_{m_l} \sum_{m_s} \sum_{M'_J, M_J^+} \rho'(J', M'_J) \\ \left| \sum_{k=l\pm 1} (-1)^k \sqrt{2k+1} \begin{pmatrix} l & 1 & k \\ -m_l & \mu_0 & -p \end{pmatrix} \left\langle n^+\Lambda^+, v^+ \left| \, \mathrm{T}'^k_{\Delta\Lambda} \, \right| n'\Lambda', v' \right\rangle \begin{pmatrix} N^+ & k & N' \\ -\Lambda^+ & \Delta\Lambda & \Lambda' \end{pmatrix} \right. \\ \left. \sum_{u=|k-s|}^{k+s} (2u+1) \begin{pmatrix} J^+ & u & J' \\ -M_J^+ & w & M_J \end{pmatrix} \begin{pmatrix} u & k & s \\ w & -p & m_s \end{pmatrix} \begin{Bmatrix} J^+ & u & J' \\ N^+ & k & N' \\ S^+ & s & S' \end{Bmatrix} \right|^2 \qquad (5.96)$$

As the terms in the sum over M'_J are weighted by the populations $\rho'(J', M'_J)$, we may not use the orthogonality properties of the Wigner 3j-symbols to get rid of the cross terms in the above expression. Hence, the vibronic transition matrix elements $\left\langle n^+\Lambda^+, v^+ \left| \, \mathrm{T}'^k_{\Delta\Lambda} \, \right| n\Lambda, v \right\rangle$ may not be isolated from the other terms in (5.96) and, since these matrix elements are in general complex quantities, the transition probability may not be calculated unless the magnitudes and the *phases* of these matrix elements are known. In other words, for ionization of an anisotropic level, interference effects between different vibronic transition matrix elements become important.

In order to illustrate this effect, we study the transition probability for a $^1\Sigma \rightarrow {}^2\Sigma$ ionization process for the spin-rotation levels $N' = J' = 2 \rightarrow N^+ = 2$, $J^+ = 3/2$ and $N' = J' = 2 \rightarrow N^+ = 2$, $J^+ = 5/2$ under the assumption of a population in the $J' = 2$ level confined to the $M'_J = 0$ Zeeman state (i.e., $\rho'(J' = 2, M'_J = 0) = 1$ and $\rho'(J' = 2, M'_J \neq 0) = 0$) as it results from two-photon excitation from the

rovibronic ground state with linearly polarized radiation. When writing the vibronic transition matrix elements as complex numbers in polar form,[9]

$$\left\langle n^+\Lambda^+ = 0, v^+ \middle| \mathrm{T}'^{k=0}_0 \middle| n'\Lambda' = 0, v' \right\rangle = \sqrt{C_0}\exp(i\phi_0), \tag{5.97a}$$

$$\left\langle n^+\Lambda^+ = 0, v^+ \middle| \mathrm{T}'^{k=2}_0 \middle| n'\Lambda' = 0, v' \right\rangle = \sqrt{C_2}\exp(i\phi_2), \tag{5.97b}$$

with $C_0, C_2 \in \mathbb{R}, C_0, C_2 \geq 0$ and $\phi_0, \phi_2 \in [0, 2\pi)$ and assuming the matrix elements with $k > 2$ to vanish, evaluation of (5.96) yields

$$P(J' = 2, J^+ = 3/2) = 0.13\,C_0 + 0.07\,C_2 - 0.11\sqrt{C_0 C_2}\cos(\phi_0 - \phi_2) \tag{5.98}$$

and

$$P(J' = 2, J^+ = 5/2) = 0.20\,C_0 + 0.10\,C_2 - 0.16\sqrt{C_0 C_2}\cos(\phi_0 - \phi_2). \tag{5.99}$$

The transition probability for ionization of an anisotropic populated level thus clearly depends not only on the magnitude, but also on the relative phase $\phi_0 - \phi_2$ of the vibronic transition matrix elements (unless the ionization process is dominated by only one of these matrix elements, i.e. $C_0 \gg C_2$ or vice versa). This effect is illustrated in Fig. 5.8. The relative strength of the ionization transitions may therefore in general not be calculated without information about the relative phases of the vibronic transition matrix elements. Despite rendering the description of intensities in the REMPI process complicated, this effect, on the other hand, means that measuring REMPI intensities could in principle provide a probe, not only for the magnitude, but also for the phase of these matrix elements.

Besides the above mentioned transitions with $N' = 2 \rightarrow N^+ = 2$, Fig. 5.8 also shows the strength of the $N' = J' = 2 \rightarrow N^+ = 0$, $J^+ = 1/2$ transition. Since this transition exhibits $|\Delta N| = 2$, the $k = 0$ term in (5.96) vanishes and it occurs entirely due to the $k = 2$ term in equation (5.96). Hence, interference effects are not present and a dependency on the phase of the matrix elements is not observed.

To describe the state-selective preparation of molecular ions with REMPI, we may once more exploit that usually S and O lines (i.e., $|\Delta N| = 2$) are employed in these ionization schemes such that interference effects, as in the example above, are not an issue. We will therefore focus on these lines in the following.

The transition probability for such lines between Σ states may be simplified to:

$$\begin{aligned} P^{(\mathrm{S,\,O})}(J', J^+) = {} & 5(2N'+1)(2N^+ + 1)(2S'+1)(2J'+1)(2J^+ + 1) \sum_l \sum_{m_l} \sum_{m_s} \sum_{M'_J, M_J^+} \rho'(J', M'_J) \\ & \left| \left\langle n^+\Lambda^+ = 0, v^+ \middle| \mathrm{T}'^{k=2}_0 \middle| n'\Lambda' = 0, v' \right\rangle \right|^2 \begin{pmatrix} l & 1 & 2 \\ -m_l & \mu_0 & -p \end{pmatrix}^2 \begin{pmatrix} N^+ & 2 & N' \\ 0 & 0 & 0 \end{pmatrix}^2 \\ & \left| \sum_{u=3/2}^{5/2} (2u+1) \begin{pmatrix} J^+ & u & J' \\ -M_J^+ & w & M_J \end{pmatrix} \begin{pmatrix} u & 2 & 1/2 \\ w & -p & m_s \end{pmatrix} \begin{Bmatrix} J^+ & u & J' \\ N^+ & 2 & N' \\ S^+ & 1/2 & S' \end{Bmatrix} \right|^2 . \end{aligned} \tag{5.100}$$

[9] The square root in the magnitude of the vibronic transition matrix element has been introduced in order that the relation $C_k = \left| \left\langle n^+\Lambda^+, v^+ \middle| \mathrm{T}'^{k}_{\Delta\Lambda} \middle| n'\Lambda', v' \right\rangle \right|^2$ still holds.

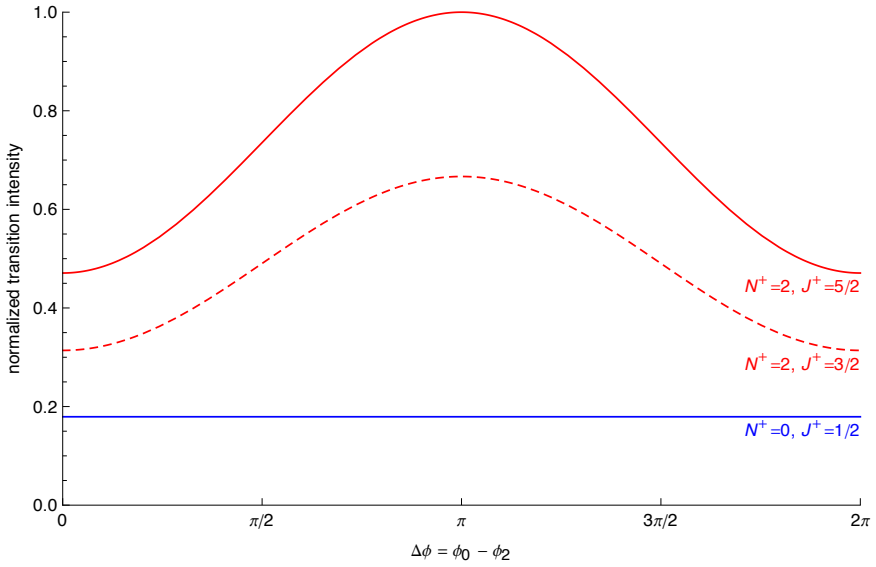

Figure 5.8. Interference effects in photoionization of anisotropically populated states. When ionizing a neutral molecule from an anisotropically populated level, interference effects between different vibronic transition matrix elements may occur. The intensity of different ionization transitions may then not only depend on the magnitude of the vibronic transition matrix element (i.e., the BOS coefficients), but also on their relative phase. Here, this effect is shown for the $N' = 2 \rightarrow N^+ = 2, J^+ = 5/2$ (solid, red line) and the $N' = 2 \rightarrow N^+ = 2, J^+ = 3/2$ (dashed, red line) transitions, when assuming the entire neutral population being confined to the $N' = 2, M'_N = 0$ Zeeman state. Because of the interference of the vibronic matrix elements with $k = 0$ and $k = 2$, the transition probability depends on the relative phase $\Delta\phi$ between these matrix elements. For the $N' = 2 \rightarrow N^+ = 0, J^+ = 1/2$ transition (solid, blue line), on the contrary, no interference effects are observed, as this transition may only occur due to the $k = 2$ vibronic transition matrix element. (For the values shown, the BOS coefficients have been assumed as $C_0 = 0.8$, $C_2 = 0.2$ and all other BOS coefficients are supposed to vanish.)

The effects discussed so far for spin-rotation-resolved transitions are analogously found in hfs-resolved lines. Particularly, interference effects may occur when ionizing a molecule from a hfs level with anisotropically populated Zeeman states. As a consequence, transition probabilities may in general only be calculated when knowing both, the magnitude and the phase, of the vibronic transition matrix elements.

The transition probability for photoionization of excited molecules with populations $\rho'(F', M'_F)$ of the Zeeman states of the hfs levels is given by:

$$P(J', F', J^+, F^+) = \sum_l \sum_{m_l} \sum_{m_s} \sum_{M'_F, M_F^+} \rho'(F', M'_F) \left| \left\langle n^+\Lambda^+, v^+, N^+\Lambda^+ S^+ J^+ I^+ F^+ M_F^+ \right| \langle s, m_s | \langle l, m_l | \right.$$
$$\left. \hat{\boldsymbol{\mu}} \left| n'\Lambda', v', N'\Lambda' S' J' I' F' M'_F \right\rangle \right|^2. \tag{5.101}$$

When substituting the matrix element from (5.43), we obtain (with $\Delta\Lambda = \Lambda^+ - \Lambda'$),

$$P(J', F', J^+, F^+) = (2N'+1)(2N^+ + 1)(2S'+1)(2J'+1)(2J^+ + 1)(2F'+1)(2F^+ + 1)\delta_{I'I^+}$$
$$\sum_l \sum_{m_l} \sum_{m_s} \sum_{M'_F, M_F^+} \rho'(F', M'_F) \left| \sum_{k=l\pm 1} (-1)^k \sqrt{2k+1} \begin{pmatrix} l & 1 & k \\ -m_l & \mu_0 & -p \end{pmatrix} \right.$$
$$\left\langle n^+\Lambda^+, v^+ \left| \, \mathrm{T}'^k_{\Delta\Lambda} \, \right| n'\Lambda', v' \right\rangle \begin{pmatrix} N^+ & k & N' \\ -\Lambda^+ & \Delta\Lambda & \Lambda' \end{pmatrix} \sum_{u=|k-s|}^{k+s} (-1)^{-u}(2u+1)$$
$$\left. \begin{pmatrix} u & k & s \\ w & -p & m_s \end{pmatrix} \begin{Bmatrix} J^+ & u & J' \\ N^+ & k & N' \\ S^+ & s & S' \end{Bmatrix} \begin{Bmatrix} u & J' & J^+ \\ I' & F^+ & F' \end{Bmatrix} \begin{pmatrix} F^+ & u & F' \\ -M_F^+ & w & M'_F \end{pmatrix} \right|^2. \tag{5.102}$$

Again, interference effects do not occur for transitions with $|\Delta N| = 2$ under the assumption that all vibronic transition matrix elements with $k > 2$ essentially vanish. In this case, equation (5.102) simplifies to:

$$P_{\mathrm{S,\,O}}(J', F', J^+, F^+) = 5(2N'+1)(2N^+ + 1)(2S'+1)(2J'+1)(2J^+ + 1)(2F'+1)(2F^+ + 1)\delta_{I'I^+}$$
$$\left| \left\langle n^+\Lambda^+ = 0, v^+ \left| \, \mathrm{T}'^{k=2}_0 \, \right| n'\Lambda' = 0, v' \right\rangle \right|^2 \begin{pmatrix} N^+ & 2 & N' \\ 0 & 0 & 0 \end{pmatrix}^2$$
$$\sum_{l=1,3} \sum_{m_l} \sum_{m_s} \sum_{M'_F, M_F^+} \rho'(F', M'_F) \begin{pmatrix} l & 1 & 2 \\ -m_l & \mu_0 & -p \end{pmatrix}^2 \left| \sum_{u=3/2}^{5/2} (-1)^{-u}(2u+1) \right.$$
$$\left. \begin{pmatrix} u & 2 & 1/2 \\ w & -p & m_s \end{pmatrix} \begin{Bmatrix} J^+ & u & J' \\ N^+ & 2 & N' \\ S^+ & 1/2 & S' \end{Bmatrix} \begin{Bmatrix} u & J' & J^+ \\ I' & F^+ & F' \end{Bmatrix} \begin{pmatrix} F^+ & u & F' \\ -M_F^+ & w & M'_F \end{pmatrix} \right|^2. \tag{5.103}$$

If the neutral, excited molecules AB* are in a singlet state (such as for N_2 in the $a''\,{}^1\Sigma_g^+$ state), we have $S' = 0$ and $J' = N'$. The 9j-symbol may then be substituted by a 6j-symbol and equation (5.103)

takes the form,

$$P_{\mathrm{S,\,O}}^{(S'=0,\mathrm{lin})}(N',F',J^+,F^+) = \frac{5}{2}(2N^+ + 1)(2N' + 1)(2J^+ + 1)(2F^+ + 1)(2F' + 1)\delta_{I'I^+}$$
$$\begin{pmatrix} N^+ & 2 & N' \\ 0 & 0 & 0 \end{pmatrix}^2 \left|\left\langle n^+\Lambda^+ = 0, v^+ \left| \mathrm{T}_0'^{k=2} \right| n'\Lambda' = 0, v' \right\rangle\right|^2$$
$$\sum_{l=1,3}\sum_{m_l}\sum_{m_s}\sum_{M_F',M_F^+} \rho'(F',M_F') \begin{pmatrix} l & 1 & 2 \\ -m_l & 0 & m_l \end{pmatrix}^2 \left| \sum_{u=3/2}^{5/2} (2u+1) \right.$$
$$\begin{pmatrix} u & 2 & 1/2 \\ -m_l - m_s & m_l & m_s \end{pmatrix} \begin{Bmatrix} J^+ & u & N' \\ 2 & N^+ & 1/2 \end{Bmatrix} \begin{Bmatrix} u & N' & J^+ \\ I' & F^+ & F' \end{Bmatrix}$$
$$\left. \begin{pmatrix} F^+ & u & F' \\ -M_F^+ & -m_l - m_s & M_F' \end{pmatrix} \right|^2 . \tag{5.104}$$

Here, linear polarization ($\mu_0 = 0$, i.e., $p = -m_l$ and $w = -m_l - m_s$) has been assumed.

When including the mixing of the pure Hund's case (b_{β_J}) basis states by the hfs Hamiltonian occurring in low rotational states of N_2^+ as discussed in Sec. 3.3, the ionic states are expressed as

$$\langle n^+\Lambda^+, v^+, N^+\Lambda^+S^+\widetilde{J^+}I^+F^+M_F^+| = \sum_{J^+=|N^+-S^+|}^{N^++S^+} c_{\widetilde{J^+},J^+,F^+} \langle n^+\Lambda^+, v^+, N^+\Lambda^+S^+J^+I^+F^+M_F^+| . \tag{5.105}$$

The transition probability then becomes:

$$P_{\mathrm{S,\,O}}^{(S'=0,\mathrm{lin})}(N',F',\widetilde{J^+},F^+) = \frac{5}{2}(2N^+ + 1)(2N' + 1)(2F^+ + 1)(2F' + 1)\delta_{I'I^+}$$
$$\begin{pmatrix} N^+ & 2 & N' \\ 0 & 0 & 0 \end{pmatrix}^2 \left|\left\langle n^+\Lambda^+ = 0, v^+ \left| \mathrm{T}_0'^{k=2} \right| n'\Lambda' = 0, v' \right\rangle\right|^2$$
$$\sum_{l=1,3}\sum_{m_l} \begin{pmatrix} l & 1 & 2 \\ -m_l & 0 & m_l \end{pmatrix}^2 \sum_{M_F'} \rho'(F',M_F') \sum_{M_F^+}\sum_{m_s} \left| \sum_{J^+=|N^+-S^+|}^{N^++S^+} c_{\widetilde{J^+},J^+,F^+} \right.$$
$$\sqrt{2J^+ + 1}(-1)^{2J^+} \sum_{u=3/2}^{5/2} (2u+1) \begin{pmatrix} u & 2 & 1/2 \\ -m_l - m_s & m_l & m_s \end{pmatrix}$$
$$\left. \begin{Bmatrix} J^+ & u & N' \\ 2 & N^+ & 1/2 \end{Bmatrix} \begin{Bmatrix} u & N' & J^+ \\ I' & F^+ & F' \end{Bmatrix} \begin{pmatrix} F^+ & u & F' \\ -M_F^+ & -m_l - m_s & M_F' \end{pmatrix} \right|^2 . \tag{5.106}$$

5.3.4 A Model for the [2+1'] REMPI process

Having discussed the ionization of anisotropically populated levels as well as derived the line strength of hyperfine-structure-resolved two-photon transitions, we may now combine these results to a model for the [2+1'] REMPI process. This model then may be used to calculate the relative hfs populations of N_2^+ ions produced by the [2+1'] REMPI scheme described in Ch. 4.

The populations of the hfs levels of the neutral, electronically excited molecules AB* in the REMPI process ($\mathrm{a}''\,^1\Sigma_\mathrm{g}^+$ state in the case of N_2^+) are proportional to the excitation rates of the transitions

populating these levels multiplied with the populations of the relevant levels of the electronic ground state:

$$\rho'(F', M'_F) \propto \sum_{F''=|J''-I''|}^{J''+I''} R_{F''\to F', M'_F}\, \rho''(F''). \tag{5.107}$$

Here, the sum over all the ground-state hfs levels has been included since hyperfine structure is supposed to be unresolved in the two-photon excitation step. The electronic-ground-state populations are given by a Boltzmann distribution according to the relevant thermal energies $k_\mathrm{B}T$,

$$\rho''(F'') = g_{F''} \exp\left(-E_{F''}/k_\mathrm{B}T\right), \tag{5.108}$$

with $E_{F''}$ the energy of the level F'' and $g_{F''}$ its degeneracy. Since the hfs splittings are usually small compared to the thermal energies ($\Delta E_\mathrm{hfs} \ll k_\mathrm{B}T$), the energies $E_{F''}$ are almost equal for all hfs levels belonging to the same rotational level and the above exponential factor is nearly constant for them. The relative hfs populations within the same rotational level are thus approximately given by the degeneracy of the hfs levels: $\rho''(F'') \propto g_{F''}$. The excitation rate $R_{F''\to F', M'_F}$, on the other hand, is proportional[10] to the line strength $S^{(\mathrm{lin})}_{\mathrm{S,\,O}}(F'', F', M'_F)$ of this transition multiplied with $1/g_{F''}$. Thus, these degeneracy factors cancel and the populations in the electronically excited state are proportional to the line strength of the transitions populating these levels:

$$\rho'(F', M'_F) \propto \sum_{F''=|J''-I''|}^{J''+I''} S^{(\mathrm{lin})}_{\mathrm{S,\,O}}(F'', F', M'_F), \tag{5.109}$$

where $S^{(\mathrm{lin})}_{\mathrm{S,\,O}}(F'', F', M'_F)$ is the line strength of the two-photon transition in the excitation step given by equation (5.94) of Sec. 5.3.2.

To obtain the relative populations $\rho^+(J^+, F^+)$ of the molecular ions AB^+ we are finally interested in, we may thus substitute the neutral, excited-state populations $\rho'(F', M'_F)$ appearing in our ionization model for anisotropic populations (equation (5.104) of Sec. 5.3.3) by the total two-photon excitation line strength from (5.109) and (5.94). With this substitution, the relative populations in the ionic hfs levels are given by:

$$\begin{aligned}
\rho^+_{F'}(J^+, F^+) \propto\ & (2N^+ + 1)(2N' + 1)^2(2N'' + 1)(2J^+ + 1)(2F^+ + 1)(2F' + 1)^2 \\
& \begin{pmatrix} N^+ & 2 & N' \\ 0 & 0 & 0 \end{pmatrix}^2 \begin{pmatrix} N' & 2 & N'' \\ 0 & 0 & 0 \end{pmatrix}^2 \left| \left\langle n^+\Lambda^+ = 0, v^+ \middle| \mathrm{T}'^{k=2}_0 \middle| n'\Lambda' = 0, v' \right\rangle \right|^2 \mu_\mathrm{S}^2 \\
& \sum_{F''=|J''-I''|}^{J''+I''} (2F'' + 1) \begin{Bmatrix} 2 & N'' & N' \\ I'' & F' & F'' \end{Bmatrix}^2 \sum_{M'_F} \begin{pmatrix} F' & 2 & F'' \\ -M'_F & 0 & M'_F \end{pmatrix}^2 \\
& \sum_{l=1,3} \sum_{m_l} \begin{pmatrix} l & 1 & 2 \\ -m_l & 0 & m_l \end{pmatrix}^2 \sum_{m_s} \sum_{M^+_F} \left| \sum_{u=3/2}^{5/2} (2u + 1) \begin{pmatrix} u & 2 & 1/2 \\ -m_l - m_s & m_l & m_s \end{pmatrix} \right. \\
& \left. \begin{Bmatrix} J^+ & u & N' \\ 2 & N^+ & 1/2 \end{Bmatrix} \begin{Bmatrix} u & N' & J^+ \\ I'' & F^+ & F' \end{Bmatrix} \begin{pmatrix} F^+ & u & F' \\ -M^+_F & -m_l - m_s & M'_F \end{pmatrix} \right|^2 .
\end{aligned} \tag{5.110}$$

As these populations are calculated for ionization via a particular hfs level of the neutral, excited

[10] See remarks to equation (5.4) on p. 89.

state, the subscript $_{F'}$ has been added.

If the polarization vectors of the radiation used for excitation and ionization are not parallel, but tilted by some angle α relative to each other, we need to take into account that the projection quantum numbers used in the excitation and the ionization step are not referring to the same frame of reference.[11] This is achieved by multiplying the populations calculated in the excitation frame (labelled below by projection quantum numbers $\overline{M}'_F$ as arguments) with a squared Wigner rotation matrix $\mathscr{D}^{F'}_{\overline{M}'_F M'_F}(0,\alpha,0)$ and summing over the projection quantum numbers in the excitation frame $\overline{M}'_F$ (see [150, 174]):

$$\rho'_\alpha(F', M'_F) = \sum_{\overline{M}'_F=-F'}^{F'} \left[\mathscr{D}^{F'}_{\overline{M}'_F M'_F}(0,\alpha,0)\right]^2 \rho'(F', \overline{M}'_F) \tag{5.111}$$

$$\propto \sum_{\overline{M}'_F=-F'}^{F'} \left[\mathscr{D}^{F'}_{\overline{M}'_F M'_F}(0,\alpha,0)\right]^2 \sum_{F''=|J''-I''|}^{J''+I''} S^{(\text{lin. pol.})}_{\text{S, O}}(F'', F', \overline{M}'_F) \tag{5.112}$$

Substituting this expression into (5.104) and again using (5.94) for the two-photon excitation yields the following result for the ionic populations:

$$\begin{aligned}
\rho^+_{F'\alpha}(J^+, F^+) \propto\ & (2N^+ + 1)(2N' + 1)^2(2N'' + 1)(2J^+ + 1)(2F^+ + 1)(2F' + 1)^2 \\
& \begin{pmatrix} N^+ & 2 & N' \\ 0 & 0 & 0 \end{pmatrix}^2 \begin{pmatrix} N' & 2 & N'' \\ 0 & 0 & 0 \end{pmatrix}^2 \left|\left\langle n^+\Lambda^+ = 0, v^+ \,\middle|\, \mathrm{T}'^{k=2}_0 \,\middle|\, n'\Lambda' = 0, v' \right\rangle\right|^2 \mu_{\text{S}}^2 \\
& \sum_{F''=|J''-I''|}^{J''+I''} (2F'' + 1) \begin{Bmatrix} 2 & N'' & N' \\ I'' & F' & F'' \end{Bmatrix}^2 \sum_{\overline{M}'_F} \begin{pmatrix} F' & 2 & F'' \\ -\overline{M}'_F & 0 & \overline{M}'_F \end{pmatrix}^2 \sum_{M'_F} \left[\mathscr{D}^{F'}_{\overline{M}'_F M'_F}(0,\alpha,0)\right]^2 \\
& \sum_{l=1,3} \sum_{m_l} \begin{pmatrix} l & 1 & 2 \\ -m_l & 0 & m_l \end{pmatrix}^2 \sum_{m_s} \sum_{M^+_F} \left| \sum_{u=3/2}^{5/2} (2u + 1) \begin{pmatrix} u & 2 & 1/2 \\ -m_l - m_s & m_l & m_s \end{pmatrix} \right. \\
& \left. \begin{Bmatrix} J^+ & u & N' \\ 2 & N^+ & 1/2 \end{Bmatrix} \begin{Bmatrix} u & N' & J^+ \\ I'' & F^+ & F' \end{Bmatrix} \begin{pmatrix} F^+ & u & F' \\ -M^+_F & -m_l - m_s & M'_F \end{pmatrix} \right|^2 .
\end{aligned} \tag{5.113}$$

[11] For both, the excitation and the ionization step, the polarization of the radiation has been assumed parallel to the z-axis of the space-fixed frame. Allowing for an angle between the two polarization vectors thus implies that the calculations for these two steps refer to two different space-fixed frames.

Mixing between Hund's case (b_{β_J}) basis states is taken into account when substituting the excited-state populations from (5.112) into (5.106) and results in:

$$\begin{aligned}\rho^+_{F'\,\alpha}(\widetilde{J^+},F^+) \propto\ & (2N^+ +1)(2N'+1)^2(2N''+1)(2F^+ +1)(2F'+1)^2 \\ & \begin{pmatrix} N^+ & 2 & N' \\ 0 & 0 & 0 \end{pmatrix}^2 \begin{pmatrix} N' & 2 & N'' \\ 0 & 0 & 0 \end{pmatrix}^2 \left|\left\langle n^+\Lambda^+ = 0, v^+ \,\middle|\, \mathrm{T}'^{k=2}_0 \,\middle|\, n'\Lambda' = 0, v' \right\rangle\right|^2 \mu_{\mathrm{S}}^2 \\ & \sum_{F''=|J''-I''|}^{J''+I''} (2F''+1) \begin{Bmatrix} 2 & N'' & N' \\ I'' & F' & F'' \end{Bmatrix}^2 \sum_{\overline{M'_F}} \begin{pmatrix} F' & 2 & F'' \\ -\overline{M'_F} & 0 & \overline{M'_F} \end{pmatrix}^2 \sum_{M'_F} \left[\mathscr{D}^{F'}_{\overline{M'}_F M'_F}(0,\alpha,0)\right]^2 \\ & \sum_{l=1,3}\sum_{m_l} \begin{pmatrix} l & 1 & 2 \\ -m_l & 0 & m_l \end{pmatrix}^2 \sum_{m_s}\sum_{M_F^+} \left| \sum_{J^+=|N^+-S^+|}^{N^++S^+} c_{\widetilde{J^+},J^+,F^+} \right. \\ & \left. \sqrt{2J^+ +1}(-1)^{2J^+} \sum_{u=3/2}^{5/2} (2u+1) \begin{pmatrix} u & 2 & 1/2 \\ -m_l - m_s & m_l & m_s \end{pmatrix} \begin{Bmatrix} J^+ & u & N' \\ 2 & N^+ & 1/2 \end{Bmatrix} \right. \\ & \left. \begin{Bmatrix} u & N' & J^+ \\ I'' & F^+ & F' \end{Bmatrix} \begin{pmatrix} F^+ & u & F' \\ -M_F^+ & -m_l - m_s & M'_F \end{pmatrix} \right|^2 . \end{aligned} \tag{5.114}$$

Below, the implications of our model are shown by a couple of representative examples for the [2+1'] REMPI scheme of nitrogen with the N_2 $a''\,^1\Sigma_g^+$ as the neutral, excited state, i.e., for the scheme discussed in Ch. 4. First, we apply our model to study the relative populations in different hfs levels when not resolving the hyperfine structure in the ionization step. This means, the contributions owing to all the transitions from the several hfs levels in the neutral, excited $a''\,^1\Sigma_g^+$ state leading to the same hfs level in the ion are summed. In other words, the total ionic populations given by

$$\rho^+_{\mathrm{tot}}(J^+,F^+) = \sum_{F'} \rho^+_{F'}(J^+,F^+), \tag{5.115}$$

$$\rho^+_{\mathrm{tot}\,\alpha}(J^+,F^+) = \sum_{F'} \rho^+_{F'\,\alpha}(J^+,F^+), \tag{5.116}$$

$$\rho^+_{\mathrm{tot}\,\alpha}(\widetilde{J^+},F^+) = \sum_{F'} \rho^+_{F'\,\alpha}(\widetilde{J^+},F^+), \tag{5.117}$$

for parallel or tilted polarization vectors when neglecting mixing of Hund's case (b_{β_J}) states, as well as with this mixing taken into account, are studied.

This treatment reflects the current state of the experiment described in Ch. 4: since the bandwidth of the ionization laser is too large to resolve individual hfs transitions between the N_2 $a''\,^1\Sigma_g^+$ and the N_2^+ $X^2\Sigma_g^+$ state, all of them contribute to the population of a certain hfs level in the ion. Only after ionization, these populations are probed in a hfs-resolved way by vibrational spectroscopy of the N_2^+ ion.

Thereafter, the populations obtained when only addressing particular hfs transitions between the N_2 $a''\,^1\Sigma_g^+$ and the N_2^+ $X^2\Sigma_g^+$ state are shown. This scenario may not be realized at present with our experimental setup because of the bandwidth of the pulsed dye laser used for ionization, but might become feasible when employing a spectrally narrower radiation source for ionization.

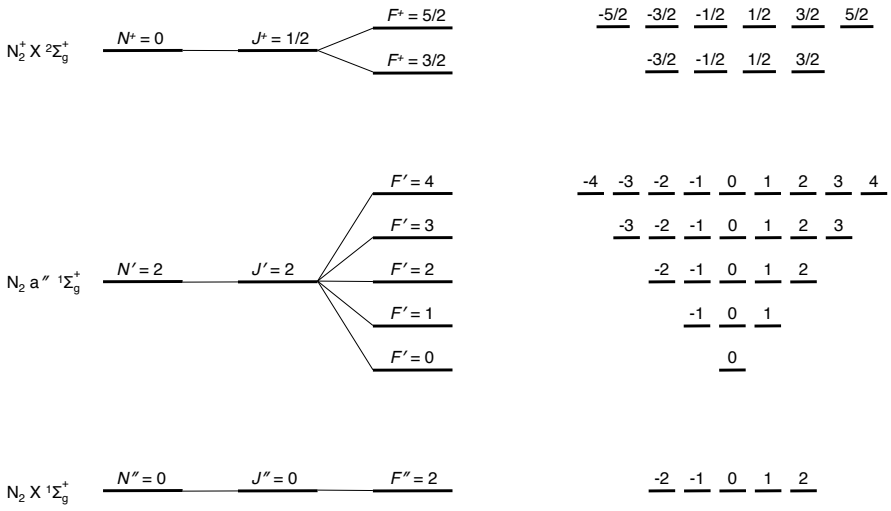

Figure 5.9. Level diagram for the S(0)-O(2) REMPI of nitrogen showing the relevant fs and hfs levels as well as the Zeeman states for the REMPI sequence $N'' = 0 \rightarrow N' = 2 \rightarrow N^+ = 0$ of the $I = 2$ nuclear spin manifold of N_2/N_2^+. (As the exact hyperfine structure of the $a''\,^1\Sigma_g^+$ state is unknown, levels of this state are ordered by their degeneracy.)

5.3.5 Non-hfs-resolved photoionization of molecular nitrogen

S(0)-O(2) REMPI sequence As a first application of our model, the ionization scheme presented in Ch. 4 to produce N_2^+ ions state-selectively in the rovibrational ground state, i.e., the REMPI sequence $N'' = 0 \rightarrow N' = 2 \rightarrow N^+ = 0$ for the $I = 2$ nuclear spin manifold of N_2/N_2^+ is studied. The hyperfine structure is supposed to be unresolved in both, the excitation and the ionization step, as it is currently the case in our experiment. The energy levels and corresponding Zeeman states involved are shown in Fig. 5.9. As evident from this diagram, quite a few hfs levels and Zeeman states are involved even in this relatively simple case. This complexity is reflected in the calculation of the ionic hfs populations with our model.

The results obtained are shown in Fig. 5.10 and 5.11. Fig. 5.10 shows the populations in the neutral, excited N_2 $a''\,^1\Sigma_g^+$ state. In the left column, these populations are shown with reference to the excitation frame, in the right one, the corresponding values after transformation to the ionization frame are given. The effect that only a subset of the Zeeman states may be populated by excitation with linearly polarized radiation is clearly visible in the left column of Fig. 5.10: Zeeman states with $\overline{M}'_F > 2$ are not populated due to the selection rule $\overline{M}'_F = M''_F$ for excitation with linearly polarized radiation (polarization vector parallel to quantization axis).

For the right column of Fig. 5.10, an angle of $\alpha = 90°$ between the two polarization vectors of excitation and ionization has been assumed. Such an angle may result when using a frequency *tripled* laser for excitation and a frequency *doubled* one for ionization. The frame transformation described by equation (5.111) leads to a redistribution of the population such that previously unpopulated Zeeman states are populated, when regarded with respect to this frame of reference.

The relative populations in the different hfs levels of the N_2^+ ions produced in this REMPI process are shown in Fig. 5.11 as blue and red bars for parallel ($\alpha = 0°$) and perpendicular ($\alpha = 90°$) polarization vectors, respectively.

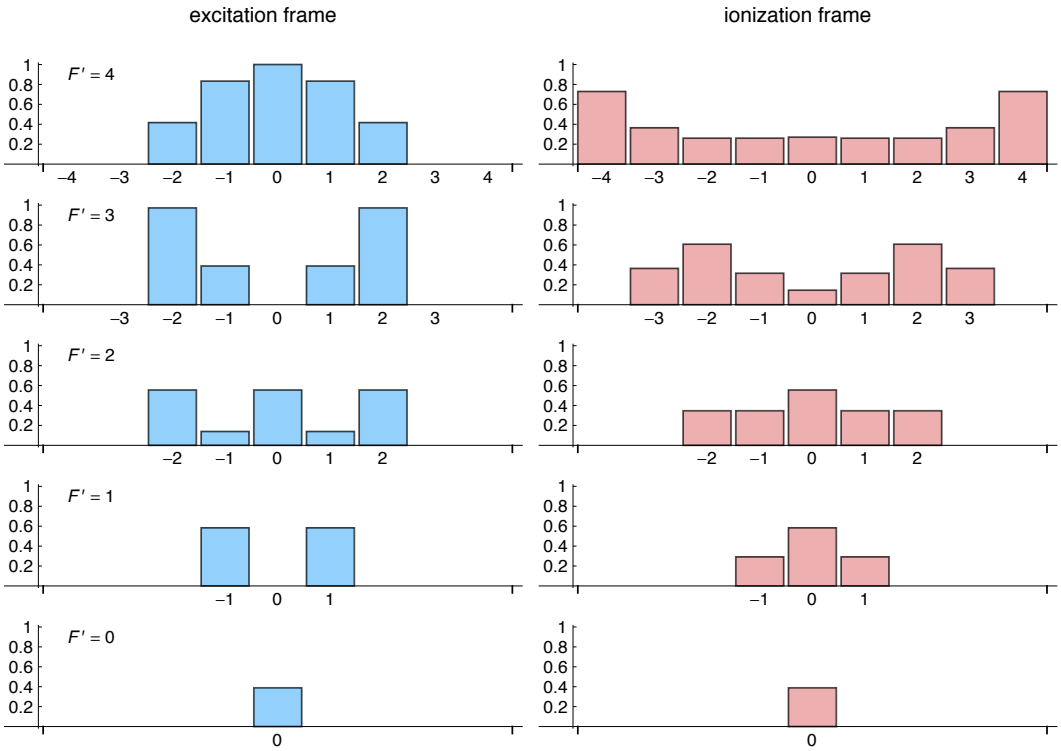

Figure 5.10. Populations in the neutral, excited state of the S(0)-O(2) REMPI scheme of nitrogen. Bar charts of the relative populations in the $a'' \, ^1\Sigma_g^+$ state for the REMPI sequence $N'' = 0 \rightarrow N' = 2 \rightarrow N^+ = 0$ of N_2. The charts in the left column show the relative populations in the Zeeman states of the hfs levels with $F' = 4$ to 0 (top to bottom) with respect to the excitation frame of reference. In the right column, the same populations are shown in the ionization frame of reference, when assuming an angle of $\alpha = 90°$ between the polarization vectors of excitation and ionization. The bars are labelled by the projection angular momentum quantum numbers below the horizontal axis.

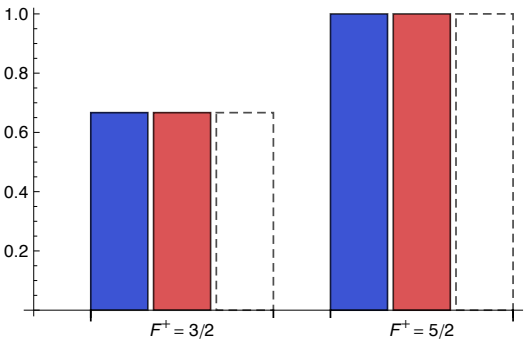

Figure 5.11. Populations in the rovibrational ground state of N_2^+ produced by S(0)-O(2) REMPI. Relative populations of the two hfs levels of N_2^+ ions produced by the REMPI sequence $N'' = 0 \rightarrow N' = 2 \rightarrow N^+ = 0$. The blue bars show the populations as obtained for parallel polarization vectors for excitation and ionization ($\alpha = 0°$), for the red ones an angle of $\alpha = 90°$ between the two polarization vectors has been assumed. For reference, the populations expected from the "pseudo-thermal" model (see text) are indicated by the white, dash-edged bars. For the example shown, our REMPI model predicts the same relative populations for parallel and perpendicular polarization vectors. Moreover, identical relative populations are also obtained by the "pseudo-thermal" model. These coincidences, however, do in general not occur, as illustrated in Fig. 5.14. (Values are normalized to yield equal total populations for parallel and perpendicular polarization, as well as for the "pseudo-thermal" model, then normalized to unity for the highest value.)

For reference, the white, dash-edged bars show the relative populations when assuming them to be proportional to the degeneracy of the levels. We refer to them as the "pseudo-thermal" populations, since these are the relative hfs populations of a thermal ensemble in the limit of the thermal energy $k_{\mathrm{B}}T$ large compared to the hfs splittings.

Surprisingly, the pseudo-thermal model yields identical results as our ionization model. As a consequence, the deviations from the expected relative line intensities observed in the electric-quadrupole spectrum of N_2^+ in Ch. 4 may not be explained by the relative populations of the hfs levels of the ionic rovibrational ground state prior to vibrational excitation, but rather seem to be caused by the same effects the total intensity deviations are attributed to (see Sec. 4.3.4).

However, as shown below, this coincidence is particular for the S(0)-O(2) ionization sequence and does in general not occur for other ionic rotational levels.

S(2)-O(4) REMPI sequence As an example with a richer structure, the ionization sequence $N'' = 2 \rightarrow N' = 4 \rightarrow N^+ = 2$ in the same system as before is analyzed. The relevant energy levels and Zeeman states are depicted in Fig. 5.12. Compared to the previous example, even more levels and Zeeman states are involved.

The populations in the neutral, excited N_2 $a''\,^1\Sigma_g^+$ and the ionic N_2^+ $X^2\Sigma_g^+$ state are shown in Fig. 5.13 and Fig. 5.14, respectively. Like in the previous example, the left column of Fig. 5.13 shows the populations in the Zeeman states belonging to the hfs levels of the $a''\,^1\Sigma_g^+$ state with respect to the excitation frame of reference, whereas the right column shows them with respect to the ionization frame. As before, an angle of $\alpha = 90°$ is assumed between the two polarization vectors. The effect of diminished populations in Zeeman states with high absolute values for the projection angular momentum quantum number due to the selection rules for the excitation step is observed once more. Also observed again is the redistribution of population in course of the frame transformation described by equation (5.111). The relative hfs populations in the $J^+ = 3/2$ and $J^+ = 5/2$ spin-rotational levels are shown in Fig. 5.14 (a) and 5.14 (b), respectively. Here, pure Hund's case (b_{β_J}) states are assumed and the mixing among them is neglected. The populations are shown for both, parallel (blue bars) and perpendicular (red bars) polarization vectors for ionization and excitation. For comparison, also the pseudo-thermal populations are indicated (white, dash-edged bars). In the lower row of Fig. 5.14 (panels (c) and (d)), the corresponding values are shown, when taking into account the mixing of the Hund's case (b_{β_J}) states with the mixing coefficients given in Tab. 5.3.

In contrast to the previous example, the relative hfs populations obtained by our REMPI model now deviate from the pseudo-thermal populations. The deviations, however, are rather small and might only have a minor influence on experiments with molecular ions produced by REMPI. The differences between the values calculated for pure Hund's case (b_{β_J}) states to those obtained when taking into account the mixing of the two spin-rotation components by the hfs Hamiltonian are as small as they are hardly noticeable in Fig. 5.14.

5.3.6 Hfs-resolved photoionization of molecular nitrogen

So far, we have analyzed hfs-state populations of N_2^+ ions generated by hfs-*un*resolved photoionization. This means, ions were assumed as being produced in a REMPI process, in which the hyperfine structure

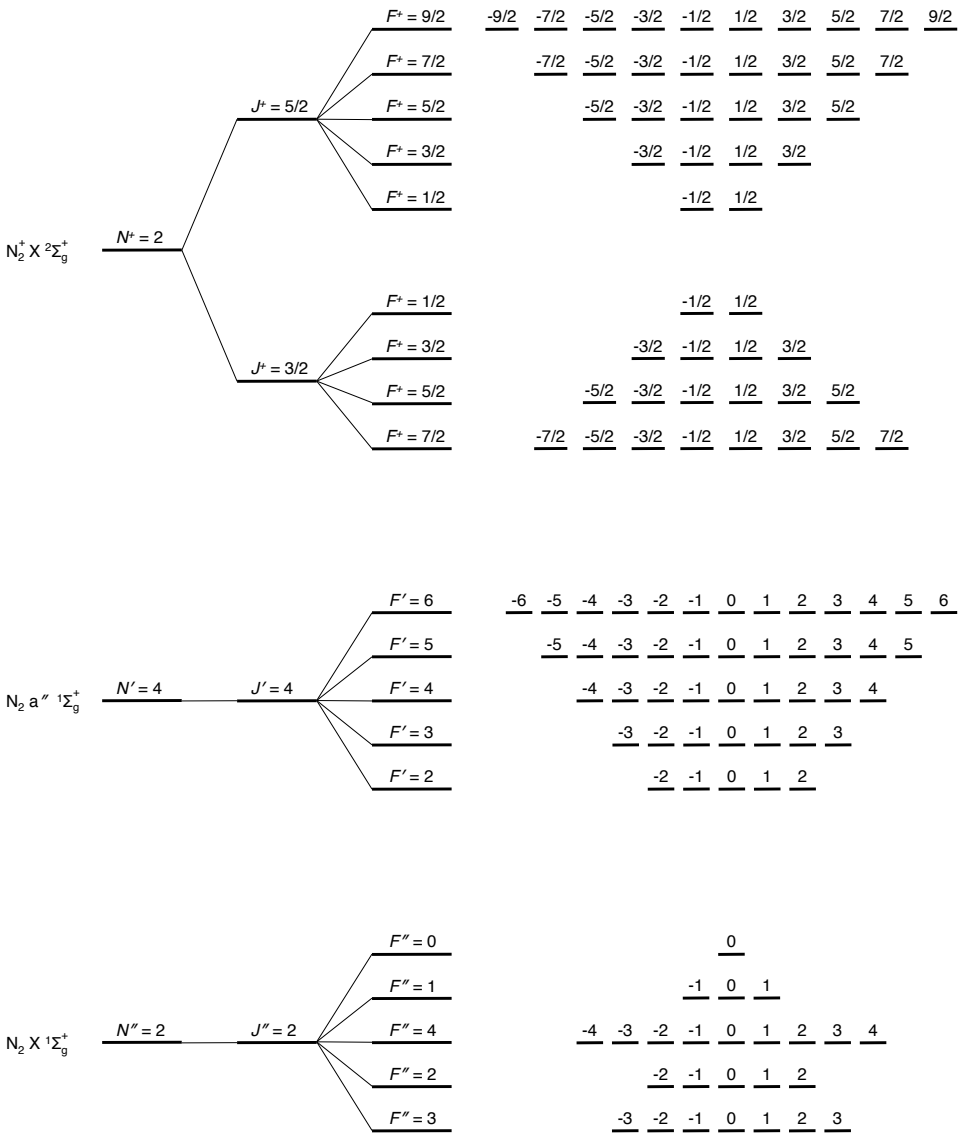

Figure 5.12. Level diagram for the S(2)-O(4) REMPI of nitrogen showing the relevant fs and hfs levels as well as the Zeeman states for the REMPI sequence $N'' = 2 \rightarrow N' = 4 \rightarrow N^+ = 2$ of the $I = 2$ nuclear spin manifold of N_2/N_2^+. (For details on the hfs of neutral N_2, see Fig. 5.3 and 5.9.)

Table 5.3. Expansion coefficients for the eigenstates of the hfs Hamiltonian of $^{14}N_2^+$ $(v^+ = 0, N^+ = 2)$ in the Hund's case (b_{β_J}) basis.

State		Coefficients	
$\widetilde{J^+}$	F^+	$c_{\widetilde{J^+},J^+=3/2,F^+}$	$c_{\widetilde{J^+},J^+=5/2,F^+}$
5/2	9/2	0.0000	1.0000
5/2	7/2	0.1756	0.9845
3/2	7/2	-0.9845	0.1756
5/2	5/2	0.2003	0.9797
3/2	5/2	-0.9797	0.2003
5/2	3/2	0.1752	0.9845
3/2	3/2	-0.9845	0.1752
5/2	1/2	0.1046	0.9945
3/2	1/2	-0.9945	0.1046

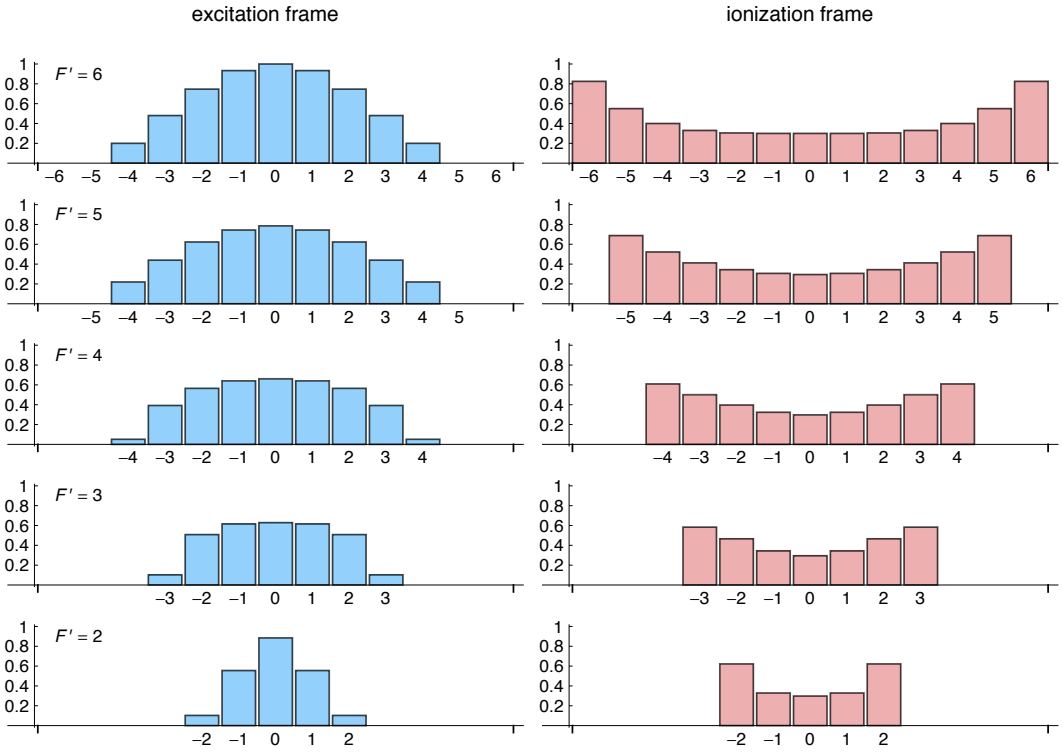

Figure 5.13. Populations in the neutral, excited state of the S(2)-O(4) REMPI scheme of nitrogen. Bar charts of the relative populations in the $a''\,^1\Sigma_g^+$ state for the REMPI sequence $N'' = 2 \rightarrow N' = 4 \rightarrow N^+ = 2$ of N_2. The charts in the left column show the relative populations in the Zeeman states of the hfs levels with $F' = 6$ to 2 (top to bottom) with respect to the excitation frame of reference. In the right column, the same populations are shown in the ionization frame of reference, when assuming an angle of $\alpha = 90°$ between the polarization vectors of excitation and ionization. The bars are labelled by the projection angular momentum quantum numbers below the horizontal axis.

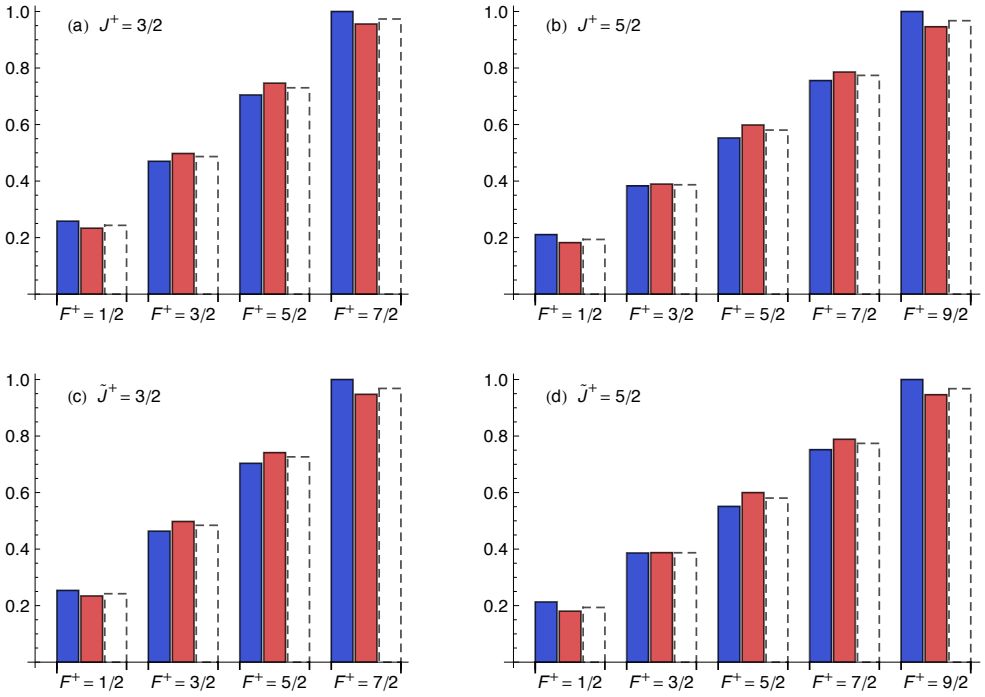

Figure 5.14. Ionic populations due to S(2)-O(4) REMPI of nitrogen. Relative populations of the fs and hfs levels of the $N^+ = 2$ rotational state of N_2^+ produced by the REMPI sequence $N'' = 2 \rightarrow N' = 4 \rightarrow N^+ = 2$. **Upper row:** values for the $J^+ = 3/2$ (panel (a)) and $J^+ = 5/2$ (panel (b)) spin-rotation component when assuming pure Hund's case (b_{β_J}) states. The blue bars show the populations obtained for parallel polarization vectors for excitation and ionization ($\alpha = 0°$), for the red ones an angle of $\alpha = 90°$ between the two polarization vectors is assumed. For reference, the populations expected from the pseudo-thermal model (see text) are indicated by the white, dash-edged bars. **Lower row:** corresponding values, when taking into account the mixing of the Hund's case (b_{β_J}) states. (Values are normalized to yield equal total populations for parallel and perpendicular polarization, as well as for the "pseudo-thermal" model, then normalized to unity for the highest value in each diagram.)

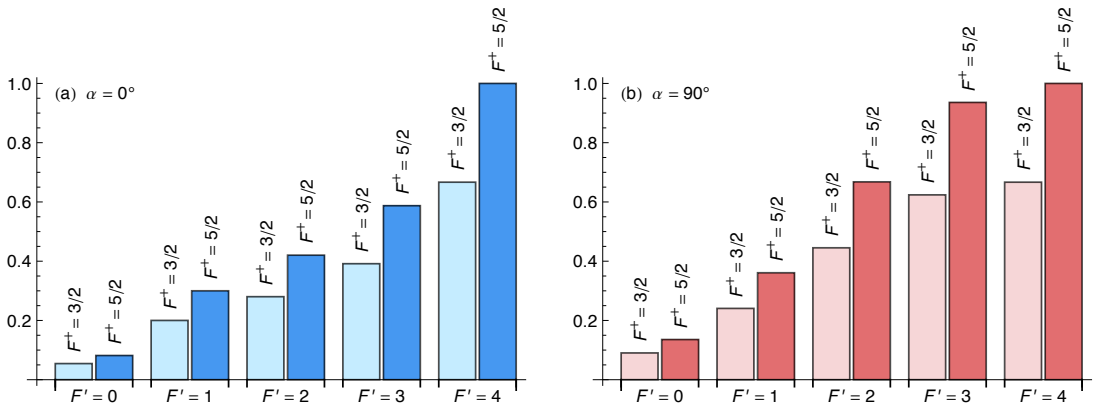

Figure 5.15. Populations in the rovibrational ground state of N_2^+ due to S(0)-O(2) REMPI for specific ionizing hfs transitions. Relative contributions to the two ionic hfs populations $F^+ = 3/2$ and $F^+ = 5/2$ from individual hfs levels of the neutral $a''\,^1\Sigma_g^+$ state ($F' = 0, ..., 4$) for parallel **(a)** and perpendicular **(b)** polarization vectors. Ionization from all neutral hfs levels populates both ionic hfs states, no clear propensity is observed.

is not resolved, but the ionic populations were then supposed to be *probed* in a hfs-*resolved* manner, e.g., by hfs-resolved vibrational spectroscopy as discussed in Ch. 4.

Having achieved control over the vibronic and spin-rotational degrees of freedom [108, 109], extending state-selectivity to the hfs domain, i.e., producing molecular ions also in a hfs-state-selective manner, is appealing. Particularly, for future non-destructive and coherent spectroscopic techniques [42] hfs-state-selective preparation might become important. As mentioned above, such a hfs-state-selective production is not achievable with our current setup, because of the limits imposed by the bandwidth of the dye lasers used for REMPI. This limitation could be overcome by using a spectrally narrower radiation source for the ionization step of the REMPI sequence, e.g., a cw-seeded pulsed dye amplifier (see, e.g., [175]) or a pulsed titanium:sapphire oscillator-amplifier system (see, e.g., [176]).

Here, we study the implications of our REMPI model for such a hfs-state-selective preparation scheme by analyzing the relative populations of N_2^+ ions for hfs-resolved ionization transitions. This means, we suppose the same neutral, excited populations as before (Fig. 5.10 and 5.13), but calculate the relative ionic populations for particular $F' \rightarrow F^+$ transitions. We are interested, if certain propensity rules for these hfs-resolved ionization transitions exist. Such propensity rules could help achieving considerable state-selectivity, even with the hyperfine structure not entirely resolved in the ionization step.

The results obtained for the S(0)-O(2) REMPI sequence are shown in Fig. 5.15. As seen from this figure, ionization from all hfs levels of the neutral, excited N_2 $a''\,^1\Sigma_g^+$ state leads to ionic populations in both hfs levels of the rovibronic ground state of N_2^+. In other words, no clear propensity is observed.

Hfs-state-selective production of N_2^+ in the rovibronic ground state hence would have to be achieved almost entirely by spectroscopic addressing. If this is possible, depends on the bandwidth of the radiation used for ionization and the hfs splitting in the N_2 $a''\,^1\Sigma_g^+$ state. On the latter, no information seems available, as the spectroscopic investigation of this state [177, 104, 103, 178] has not yet achieved the resolution needed to resolve the hyperfine structure.

The hfs-resolved results from our model for the S(2)-O(4) REMPI scheme are shown in Fig. 5.16 and 5.17 with and without considering the mixing of Hund's case (b_{β_J}) basis states, respectively. For the

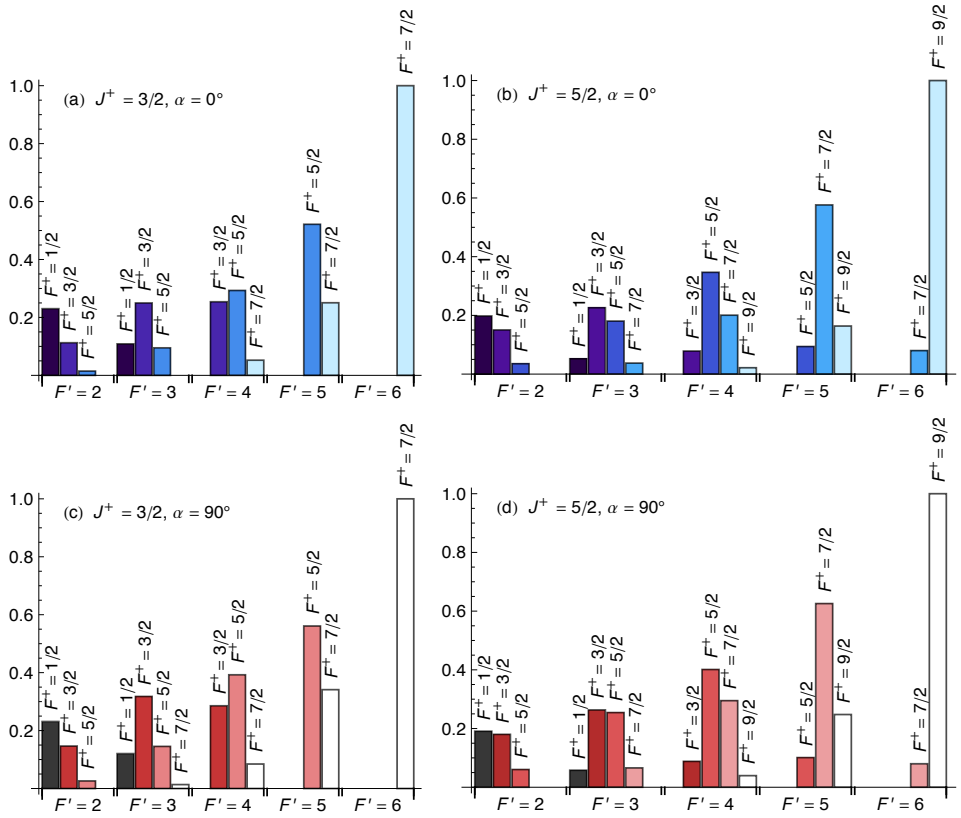

Figure 5.16. Ionic populations due to S(2)-O(4) REMPI of nitrogen for specific ionization hfs transitions. Upper row: contributions to the relative hfs populations of N_2^+ ions for the $J^+ = 3/2$ (panel (a)) and $J^+ = 5/2$ (panel (b)) spin-rotation components from individual hfs levels of the neutral $a'' \, ^1\Sigma_g^+$ state assuming parallel polarization vectors of excitation and ionization ($\alpha = 0°$). **Lower row:** corresponding values for perpendicular polarization vectors ($\alpha = 90°$). For most transitions, a distinct propensity is observed: ionization from a particular neutral hfs level ($F' = 2, ..., 4$) preferentially results in a population in only one, eventually two, ionic hfs levels. For all ionic states, pure Hund's case (b_{β_J}) coupling has been assumed, mixing of the two spin-rotational states has been neglected. Values $< 10^{-2}$ have been suppressed for clarity.

$N^+ = 2$ state produced in this scheme, the relative populations exhibit a pattern remarkably different from that seen in the previous example. Certain hfs levels of the neutral, excited $a'' \, ^1\Sigma_g^+$ state populate almost exclusively certain particular hfs levels in the N_2^+ ion. In other words, a clear propensity is observed. For the majority of the transitions, this characteristics is summarized by the propensity rule $\Delta J = \Delta F$ (with $\Delta J = J^+ - N'$ and $\Delta F = F^+ - F'$). Deviations from this rule are observed for $J^+ = 3/2$ at low values of F'.

As a consequence of this propensity, reasonable hfs-state-selectivity might be achieved even without full spectroscopic addressing of individual hfs transitions.

5.4 Summary and Conclusion

In this chapter, a model for fine- and hyperfine-structure effects in molecular photoionization has been developed. With this model, relative populations of fine- and hyperfine-structure levels of molecular ions produced either by direct, one-photon ionization or by resonance-enhanced multiphoton ionization

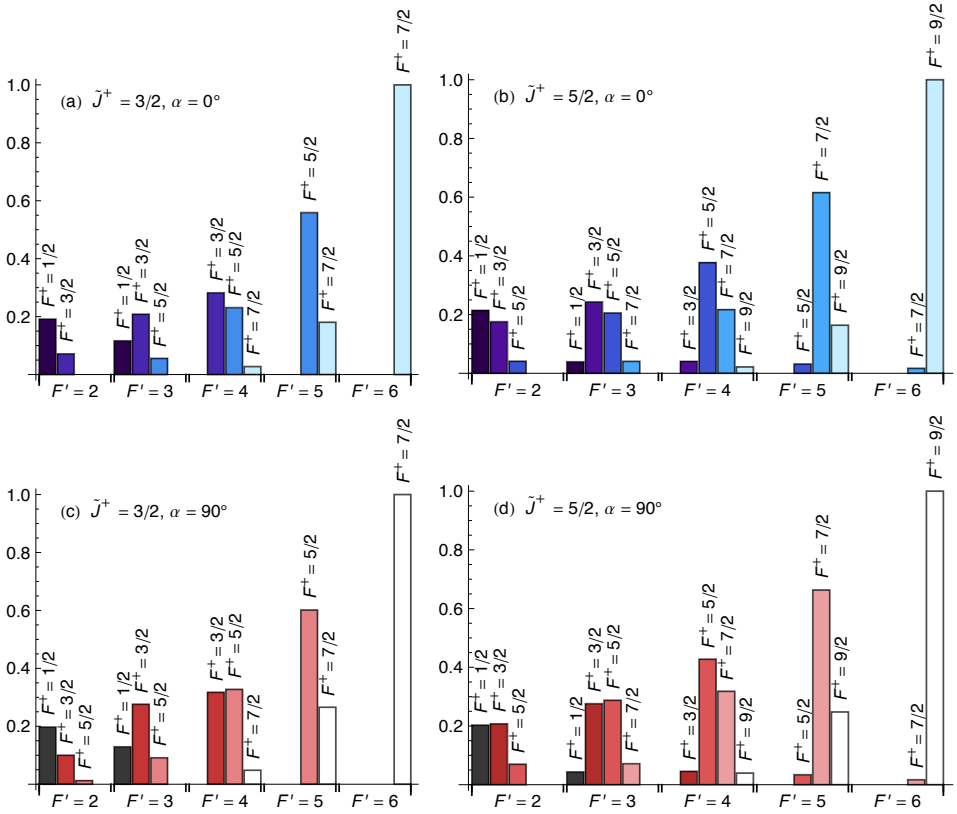

Figure 5.17. Ionic populations due to S(2)-O(4) REMPI of nitrogen for specific ionization hfs transitions including spin-rotation mixing. Same contributions to the relative hfs populations of N_2^+ for the two spin-rotation levels $\widetilde{J^+} = 3/2$ (panel (a) and (c)) and $\widetilde{J^+} = 5/2$ (panel (b) and (d)) as in Fig. 5.16, but with the mixing of the two spin-rotation components by the hfs Hamiltonian taken into account. Charts in the upper (lower) row apply for parallel (perpendicular) polarization vectors of ionization and excitation. Values $< 10^{-2}$ have been suppressed for clarity.

may be estimated. Our model has been successfully applied to describe and interpret the fine-structure-resolved photoelectron spectrum of oxygen recorded by Palm and Merkt [152]. Furthermore, it has been employed to calculate the relative populations of N_2^+ ions produced by the [2+1'] REMPI scheme used in experiments with rovibrational state-selected nitrogen ions, such as the one described in Ch. 4 of this thesis or in the literature [108, 109, 133]. Finally, the implications of our model for future ionization schemes to produce hfs-state-selected molecular ions have been studied.

Regarding the present non-hfs-resolved production of N_2^+, the relative populations of the hfs levels deviate only slightly from those expected on the basis of the degeneracy of these levels ("pseudo-thermal" populations). For future hfs-state-selective ionization schemes, the propensity rule $\Delta J = \Delta F$ has been found, which might be exploited to achieve reasonable state-selectivity even without fully resolving the hyperfine structure in the ionization process.

Our photoionization model involves several approximations. In particular, the model is based on the separation of the quantum states of the molecular ion and its neutral precursor into a vibronic and an angular state. Moreover, the angular state is expressed as a tensor product of a rotational, an electron spin and a nuclear spin state according to angular momentum algebra. In the case of REMPI, we describe the [2+1'] REMPI process as two independent steps: an excitation step providing electronically excited, neutral molecules, which is described as a two-photon bound-bound transition, and a subsequent ionization step, in which these excited molecules are ionized.

The separation of the molecular quantum state is validated by the successful description of the measured fine-structure-resolved photoelectron spectrum of oxygen. In the case of nitrogen, applicability of this approximation is assumed to be correct, as spectra between bound states in N_2 and N_2^+ do not show substantial rotational-vibronic interactions. The description of the REMPI process as a two-step sequence has proved correct before [150, 149, 179] and therefore is assumed to be applicable for the [2+1'] REMPI of nitrogen as well. However, to prove the veracity of our model, validating its predictions by comparison with experimental data is desirable. Measurements for such a validation are in preparation at the time of this writing.

Chapter 6

Non-destructive state detection and quantum logic spectroscopy

6.1 Introduction

A challenge in high-precision experiments with molecular ions is quantum-state detection. As molecular ions do in general not exhibit closed optical cycling transitions, their quantum state is usually detected either by state-dependent photodissociation [180, 181, 182, 18] or—as described in Ch. 4 of this thesis—by a state-dependent reaction. Both of these methods are destructive: as soon as the quantum state of an ion has been detected, the ion is lost. Repeated measurements on the same ion are not possible.

Destructive detection limits experimental efficiency and requires reloading of the ion trap after each measurement, potentially impairing the well-controlled, isolated environment of trapped ions. Moreover, to compensate for the limited efficiency, destructive measurements are performed on ensembles of several dozens to hundreds of ions. This averaging of measured quantities might imply an increased measurement uncertainty due to inhomogeneities in the environment of the ions such as electromagnetic stray fields or blackbody radiation.

To get around these limitations, a non-destructive quantum-state-detection technique to be employed in an experiment with just a single molecular ion would be ideal. Such a technique allows repeated measurements of the same ion without these disturbances.

Molecular ions exhibit a remarkable potential advantage towards this goal over neutral molecules thanks to their Coulomb interaction. The Coulomb interaction couples the motion of several ions trapped in the same ion trap. This coupling may be used to circumvent the lack of optical cycling transitions in molecules. Exploiting it, we may realize an experiment for repeated, non-destructive interrogation of a single molecular ion by use of a hybrid two-ion system: a single molecular ion, which is of spectroscopic interest—referred to as the "spectroscopy ion"—and a cotrapped atomic ion—denoted the "logic ion"—used for state detection. When perturbing the motional state of the spectroscopy ion, that one of the logic ion is perturbed as well. If such a perturbation is made dependent on the internal—say electronic or rotational-vibrational—state of the spectroscopy ion, the motional state of the logic ion becomes dependent on the internal quantum state for the spectroscopy ion as

well. This change in the motional state may be mapped on the internal state of the logic ion, which finally can be detected via a closed optical cycling transition.

Such a scheme—known as "quantum logic spectroscopy", since techniques from trapped-ion quantum information processing are borrowed—has first been demonstrated by Schmidt et al. [39] with two atomic ions. In that experiment, the quantum state of the spectroscopically favorable Al^+ ion was mapped on a Be^+ ion for detection. That way, the lack of accessible optical cycling transitions in Al^+ was circumvented. This and similar methods were subsequently used in ultrahigh-precision experiments with atomic ions [183, 184, 185, 186].

Several schemes have been proposed [187, 40, 188, 189, 41, 190, 42, 43]—and one recently realized [44]—to employ similar techniques for detecting the quantum state of a molecular ion by means of an atomic ion. Here, we discuss a scheme originally proposed by Mur-Petit et al. [42]. This scheme is based on "geometric quantum phases" rendering it largely independent of the ion temperature and resilient to certain ambient disturbances. In the language of quantum information processing, it consists of a "controlled phase gate" [191, 192, 193, 194] controlled by the spectroscopy ion and acting on the logic ion. In combination with a Ramsey type interferometric measurement, such a phase gate may be used to map the state of the molecular ion onto the atomic ion and hence to detect it.

This chapter is structured as follows: in the next section, we explain the general theory of our state-detection method. We begin with an overview on the state-detection protocol. Then, the dynamics and in particular the quantum phases of trapped ions subject to transient forces are derived. They are first discussed for a single ion modeled as a forced harmonic oscillator. Subsequently, the theory is extended to two ions. We will see that a controlled phase gate may be realized with time-dependent forces acting on the two-ion system and we will calculate the relevant contribution to the phase of such a system. In the penultimate section, we discuss a concrete implementation of the proposed scheme for N_2^+ and Ca^+ as a spectroscopy and a logic ion, respectively, driven by optical dipole forces induced with Gaussian laser beams. Experimental parameters, such as beam intensities, beam radii and laser frequency detunings are estimated. Moreover, effects of experimental imperfections and disturbances are qualitatively discussed. The chapter finishes with a concluding summary.

6.2 Theory

6.2.1 State-detection protocol

An overview on the proposed state-detection method may be obtained from Fig. 6.1. The two ions, a molecular N_2^+ ion as a spectroscopy ion and an atomic Ca^+ ion as a logic ion, are trapped in a linear rf ion trap. Two focused Gaussian laser beams are inserted perpendicular to the trap axis. Each of them addresses a strong, electric-dipole transition in one of the two ions. They induce a shift of the ionic energy levels known as "light shift" or "ac Stark shift". With the ions located in the flank of the beams, the light intensity and hence the energy shift is inhomogeneous. Thus, a force is exerted on each ion, known as "optical dipole force". These forces are used to manipulate the motion of the ions along the trap axis.

The relevant level schemes are shown in Fig. 6.2. The transition ultimately of interest is the $X^2\Sigma_g^+, v = 0 - X^2\Sigma_g^+, v = 1$ electric-quadrupole vibrational transition in N_2^+ (v is the vibrational

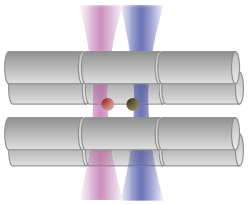

Figure 6.1. Experimental setup for molecular quantum logic spectroscopy. Sketch of the experimental setup for detection of the quantum state of a molecular ion via an atomic ion through quantum logic operations. Both ions are trapped in the same linear quadrupole trap. Their motion along the trap axis is manipulated with optical dipole forces exerted by Gaussian laser beams. The coupling of the motion of the ions is used to map the quantum state of the molecular "spectroscopy ion" on the atomic "logic ion", from where it may be readout.

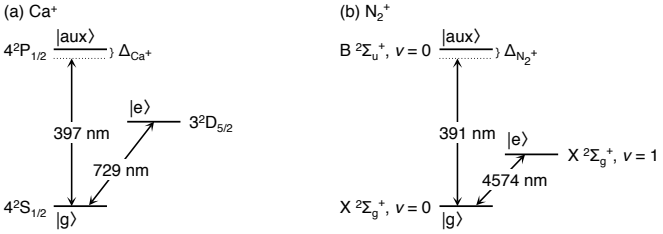

Figure 6.2. Energy level scheme for the proposed quantum logic spectroscopy experiment. **(a)** Ca^+ ion, **(b)** N_2^+ ion. Both ions exhibit a weak, electric-quadrupole transition between the ground state $|g\rangle$ and a metastable state $|e\rangle$ as well as a strong, electric-dipole transition connecting the ground state to an auxiliary excited state $|aux\rangle$.

quantum number). We assume a spectroscopic experiment addressing this transition has been made prior to employing the state-detection method. Our goal is to determine the quantum state of the N_2^+ ion after this experiment with respect to that vibrational transition. To exert the optical dipole force needed for state detection, the strong, electric-dipole $X^2\Sigma_g^+, v = 0 - B^2\Sigma_u^+, v = 0$ transition is used. This electronic and the aforementioned vibrational transition originate from the common N_2^+ ground state and form a V-shaped three-level system.

In the Ca^+ ion, a similar V-shaped system is formed by the electric-quadrupole transition connecting the $4^2S_{1/2}$ ground to the metastable $3^2D_{5/2}$ state (lifetime $\approx 1\,s$, see [195], p. 146) together with the strong, electric-dipole $4^2S_{1/2} - 4^2P_{1/2}$ transition.

We will refer to the ground state of either ion as $|g\rangle$, the excited (metastable) state of the quadrupole transition as $|e\rangle$ and the upper state of the dipole transition, which serves as an auxiliary state, as $|aux\rangle$.[1]

In short, the proposed state-detection method works by mapping the population ratio of the $|g\rangle - |e\rangle$ system in the spectroscopy ion to the $|g\rangle - |e\rangle$ system in the logic ion and to then probe this population ratio by observing the fluorescence through optical cycling on the $|g\rangle - |aux\rangle$ transition in Ca^+.

To this end, the motion of the ions along the trap axis is controlled with optical dipole forces exerted by the Gaussian laser beams, which address the dipole-allowed $|g\rangle - |aux\rangle$ transitions. They are detuned from resonance to (largely) avoid excitation.

[1] The $|g\rangle$, $|e\rangle$ and $|aux\rangle$ states are of course different ones for the logic and the spectroscopy ion. Emphasizing their corresponding roles, we use the same symbols for both of them here. From context it will always be clear, which state we are actually referring to.

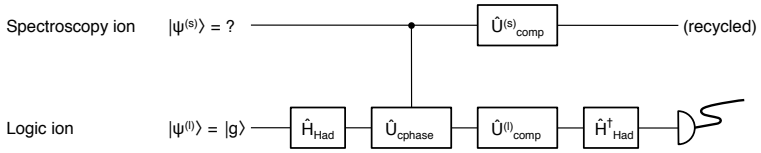

Figure 6.3. State-detection protocol visualized as a circuit diagram. After having initialized the logic ion in the ground state $|\mathrm{g}\rangle$, a superposition of the $|\mathrm{g}\rangle$ and the $|\mathrm{e}\rangle$ state is generated by the Hadamard transformation $\hat{H}_{\mathrm{Had}} = e^{-i\sigma_y^{(\mathrm{l})}\pi/4}$. A controlled phase gate $\hat{U}_{\mathrm{cphase}}$ acting on the ground state of the logic ion senses the state of the spectroscopy ion. Neglecting single-particles phases, the effect of this controlled phase gate may be written as $\hat{U}_{\mathrm{cphase}} = \hat{P}_{\mathrm{g}}^{(\mathrm{s})}(\hat{P}_{\mathrm{g}}^{(\mathrm{l})}e^{i\phi} + \hat{P}_{\mathrm{e}}^{(\mathrm{l})}) + \hat{P}_{\mathrm{e}}^{(\mathrm{s})}\hat{I}^{(\mathrm{l})}$. The former can be compensated by appropriate single-particle operations $\hat{U}_{\mathrm{comp}}^{(\mathrm{l,s})}$. Thereafter, the Hadamard transformation is reversed to translate the phase into a population difference that is finally measured. Here, $\hat{P}_{\mathrm{g}}^{(\cdot)} = |\mathrm{g}\rangle\langle\mathrm{g}|$ and $\hat{P}_{\mathrm{e}}^{(\cdot)} = |\mathrm{e}\rangle\langle\mathrm{e}|$ are the projectors on the ground and the excited state of the logic $^{(\mathrm{l})}$ and the spectroscopy $^{(\mathrm{s})}$ ion. $\hat{I}^{(\mathrm{l})}$ and $\sigma_y^{(\mathrm{l})} = i(|\mathrm{e}\rangle\langle\mathrm{g}| - |\mathrm{g}\rangle\langle\mathrm{e}|)$ are the identity operator and the Pauli y matrix of the logic ion, respectively.

The forces exerted on the ions give rise to a non-trivial phase in the quantum state of the two-ion system. For properly tailored forces, a controlled phase gate may be realized. This controlled phase gate is used together with single-particle manipulations for the above-mentioned mapping.

In detail, the proposed state-detection protocol consists of the following steps (see Fig. 6.3):

1. The logic ion is initialized to the $|\mathrm{g}\rangle$ state by optical pumping.
2. A "$\pi/2$" laser pulse on the $|\mathrm{g}\rangle - |\mathrm{e}\rangle$ transition of the logic ion generates an equal superposition state of the $|\mathrm{g}\rangle$ and the $|\mathrm{e}\rangle$ state.
3. Gaussian laser beams addressing the $|\mathrm{g}\rangle - |\mathrm{aux}\rangle$ transitions of the logic and the spectroscopy ion are employed to exert optical dipole forces on both ions. The forces give rise to a non-trivial phase acquired by the two-ion system. This phase includes a contribution due to the Coulomb interaction of the two ions.
4. With appropriate individual manipulations on both ions, spurious single-particle phases induced in the previous step are canceled.
5. Using another laser pulse addressing the $|\mathrm{g}\rangle - |\mathrm{e}\rangle$ transition of the logic ion, the transformation of step 2 is reversed.
6. The state of the logic ion is measured by probing the population in its $|\mathrm{g}\rangle$ state on the $|\mathrm{g}\rangle - |\mathrm{aux}\rangle$ transition.

In step 1, the internal quantum state of the logic ion $|\psi^{(\mathrm{l})}\rangle$ is initialized to the ground state: $|\psi^{(\mathrm{l})}\rangle = |\mathrm{g}\rangle$. The spectroscopy ion is assumed to be in a superposition state of its ground and excited state as a result of the spectroscopic experiment done prior to state detection. Its internal quantum state $|\psi^{(\mathrm{s})}\rangle$ hence is: $|\psi^{(\mathrm{s})}\rangle = a\,|\mathrm{g}\rangle + b\,|\mathrm{e}\rangle$ with unknown coefficients a and b (normalized such that: $|a|^2 + |b|^2 = 1$).

In step 2, the logic ion is taken to the superposition state $\psi^{(\mathrm{l})} = \frac{1}{\sqrt{2}}(|\mathrm{g}\rangle + |\mathrm{e}\rangle)$. The transformation done in this step is known as a "Hadamard gate" in the context of quantum information processing [196]. It distributes the population in the logic ion equally between the ground state $|\mathrm{g}\rangle$ and the excited state $|\mathrm{e}\rangle$. As the optical dipole force in the following step only acts on the ground state $|\mathrm{g}\rangle$, the excited state $|\mathrm{e}\rangle$ provides a phase reference for the subsequent measurement of the ground-state quantum phase.

Step 3 represents the actual controlled phase gate. The force on the logic ion results in a phase acquired by its $|\mathrm{g}\rangle$ state relative to the $|\mathrm{e}\rangle$ state. This phase is altered by a force acting simultaneously on the spectroscopy ion owing to the coupling of the motion of both ions via their Coulomb interaction. The phase therefore depends on the quantum state of the spectroscopy ion.

In step 4, the single-ion phases induced in the previous step are compensated, such that the total phase acquired in the gate operation only consists of the contribution caused by the interaction of the two ions.

In step 5, depending on the relative phase between the $|\mathrm{g}\rangle$ and the $|\mathrm{e}\rangle$ state of the logic ion, a different fraction of the logic-ion population is transferred to the ground state. Hence, the phase difference is translated into a population difference.

Finally, in step 6, the population in the $|\mathrm{g}\rangle$ state of the logic ion is measured. As the $|\mathrm{g}\rangle - |\mathrm{aux}\rangle$ system of the logic ion forms a (nearly) closed cycling transition, the population may be probed by repeated laser-excitation-spontaneous-decay cycles while observing the fluorescence. A bright logic ion indicates population in the $|\mathrm{g}\rangle$ state, a dark one a populated $|\mathrm{e}\rangle$ state. In other words, the two-ion wavefunction collapses and the previously unknown coefficients in the state of the spectroscopy ion are obtained as either $(|a|, |b|) = (1, 0)$ or $(|a|, |b|) = (0, 1)$.

The crucial point is the change of the phase acquired in step 3, as a consequence of a force acting simultaneously on the spectroscopy ion while the one on the logic ion is exerted. Since the force on the spectroscopy ion only acts, when it is in the ground state $|\mathrm{g}\rangle$ and does not occur in the excited state $|\mathrm{e}\rangle$, there is a contribution to the relative phase between the $|\mathrm{g}\rangle$ and $|\mathrm{e}\rangle$ state of the logic ion dependent on the state of the spectroscopy ion. For suitably chosen forces, the state of the spectroscopy ion is mapped on the logic ion, where it is detected.

By analogy with the "electron shelving" method used for atomic ions, we may refer to the method proposed here as "vibrational shelving spectroscopy", since it is based on the screening of the spectroscopy ion from the optical dipole force dependent on its vibrational state.

6.2.2 Dynamics of a trapped ion subject to a time-dependent force

We begin the quantitative discussion of our proposed state-detection method by studying the dynamics of a single ion in a linear rf ion trap subject to a time-dependent force. We assume that the confining potential is weakest along the symmetry axis of the trap and considerably stronger perpendicularly. The ion is supposed to be as cold as no relevant motion perpendicular to the symmetry axis occurs. Furthermore, the axial trapping potential is assumed to be harmonic.

We may then describe the motional degrees of freedom of the ion in essence by a one-dimensional harmonic oscillator. For an ion of mass m, confined in a potential characterized by the angular frequency ω, the relevant Hamiltonian is:

$$\hat{H}_{\mathrm{HO}} = \frac{\hat{p}^2}{2m} + \frac{m\omega^2\hat{x}^2}{2}, \tag{6.1}$$

with $\hat{x}$ and $\hat{p}$ the position and momentum operator, respectively.[2]

[2] In accordance with the usual terminology of the one-dimensional harmonic oscillator, we use the symbol $\hat{x}$ for the operator of the ion position along the symmetry axis of the trap. In the context of charged particle trapping, this axis is usually chosen as the z-axis. As no other directions than the axial one are relevant here, no confusion should arise.

With an additional time-dependent force $F(t)$ acting along the trap axis, the Hamiltonian becomes,

$$\hat{H}(t) = \frac{\hat{p}^2}{2m} + \frac{m\omega^2\hat{x}^2}{2} - F(t)\hat{x}. \tag{6.2}$$

Using the dimensionless operators $\tilde{x} = \beta\hat{x}$ and $\tilde{p} = \frac{1}{\hbar\beta}\hat{p}$ with[3] $\beta = \sqrt{\frac{m\omega}{\hbar}}$ as well as expressing the force in units of energy as $f(t) = \frac{1}{\beta}F(t)$, this Hamiltonian equals to:

$$\hat{H}(t) = \frac{\hbar\omega}{2}\left(\tilde{p}^2 + \tilde{x}^2\right) - f(t)\tilde{x}. \tag{6.3}$$

In terms of the ladder operators, $\hat{a} = \frac{1}{\sqrt{2}}\left(\tilde{x} + i\tilde{p}\right)$ and $\hat{a}^\dagger = \frac{1}{\sqrt{2}}\left(\tilde{x} - i\tilde{p}\right)$, it is written as,

$$\hat{H}(t) = \hbar\omega\left(\hat{a}^\dagger\hat{a} + \frac{1}{2}\right) - \frac{f(t)}{\sqrt{2}}\left(\hat{a}^\dagger + \hat{a}\right), \tag{6.4}$$

or when ignoring zero-point energy as,

$$\hat{H}'(t) = \hbar\omega\hat{a}^\dagger\hat{a} - \frac{f(t)}{\sqrt{2}}\left(\hat{a}^\dagger + \hat{a}\right). \tag{6.5}$$

To solve the time-dependent Schrödinger equation,

$$i\hbar\frac{\partial}{\partial t}\left|\psi_{\mathrm{m}}(t)\right\rangle = H'(t)\left|\psi_{\mathrm{m}}(t)\right\rangle, \tag{6.6}$$

for the motional state $|\psi_{\mathrm{m}}(t)\rangle$ of the ion, it is convenient to use the "quasi-classical" or "coherent" states $|z\rangle$ (see, e.g., [197] or [72] pp. 509 ff.). These states are defined in terms of the phonon-number states $|n\rangle$ as

$$|z\rangle = e^{-|z|^2/2}\sum_{n=0}^{\infty}\frac{z^n}{\sqrt{n!}}|n\rangle \tag{6.7}$$

and are eigenstates of the lowering operator $\hat{a}$ with complex eigenvalue z. They form a "complete set" meaning that any state of the relevant Hilbert space can be written as a (continuous) expansion of them. Restricting our discussion to quasi-classical states therefore does not imply any loss of generality.

The quasi-classical states exhibit a remarkable time evolution in a purely harmonic potential: for $f(t) = 0$ in (6.5), a quasi-classical state $|z_0\rangle$ characterized by the complex parameter z_0 at time $t = 0$, remains a quasi-classical state $|z(t)\rangle$ with the parameter $z(t)$ evolving on a circle in the complex plane:

$$z(t) = z_0 e^{-i\omega t}. \tag{6.8}$$

The real and the imaginary part of z are proportional to the expectation value of the position and momentum operator, respectively. Hence, z is often written as $z = X + iP$ with $X, P \in \mathbb{R}$. Due to the evolution of $z(t)$ according to (6.8), these expectation values oscillate sinusoidally with time—exactly as for a classical harmonic oscillator—while the position-momentum uncertainty product is minimal. Moreover, the curve in the complex plane described by $z(t)$ corresponds to the classical phase portrait.

[3] The quantity $1/\beta$ is the "characteristic length" of the harmonic oscillator.

If an additional time-dependent force is applied ($f(t) \neq 0$ in (6.5)), a solution of (6.6) is found in the form of a quasi-classical state with an additional time-dependent phase factor,[4]

$$|\psi_{\mathrm{m}}(t)\rangle = e^{i\phi(t)}\,|z(t)\rangle\,, \tag{6.9}$$

where the parameter $z(t)$ and the phase $\phi(t)$ follow the equations [194]:

$$\frac{\mathrm{d}z(t)}{\mathrm{d}t} = -i\omega z(t) + i\frac{1}{\sqrt{2}\hbar}f(t), \tag{6.10}$$

$$\frac{\mathrm{d}\phi(t)}{\mathrm{d}t} = \frac{1}{2\sqrt{2}\hbar}f(t)(z(t)+z(t)^*). \tag{6.11}$$

Equation (6.10) is solved by [194]:

$$z(t) = e^{-i\omega t}\left(z_0 + \frac{i}{\sqrt{2}\hbar}\int_0^t e^{i\omega\tau}f(\tau)\,\mathrm{d}\tau\right). \tag{6.12}$$

The first factor on the right-hand side above is due to the evolution of the harmonic oscillator without an additional force (cf. equation (6.8)). We may get rid of this factor when regarding $z(t)$ with respect to a corotating frame in phase space by defining $z_{\mathrm{r}}(t) = e^{i\omega t}z(t)$. Equation (6.10) then becomes,

$$\frac{\mathrm{d}z_r}{\mathrm{d}t} = \frac{i}{\sqrt{2}\hbar}e^{i\omega t}f(t), \tag{6.13}$$

and the phase $\phi(t)$ evolves according to,

$$\frac{\mathrm{d}\phi(t)}{\mathrm{d}t} = \mathrm{Im}\left[\frac{\mathrm{d}z_r(t)}{\mathrm{d}t}z_r(t)^*\right], \tag{6.14}$$

with Im[ ] denoting the imaginary part of the term in brackets.

Integrating this expression, we obtain the phase at time t as,

$$\phi(t) = \mathrm{Im}\left[\frac{iz_0^*}{\sqrt{2}\hbar}\int_0^t e^{i\omega\tau}f(\tau)\,\mathrm{d}\tau + \frac{1}{2\hbar^2}\int_0^t\int_0^{\tau_1} e^{i\omega(\tau_1-\tau_2)}f(\tau_1)f(\tau_2)\,\mathrm{d}\tau_2\mathrm{d}\tau_1\right], \tag{6.15}$$

for a state initially given as $|z_0\rangle$ at time $t = 0$.

Further below, we will use state-dependent forces to generate a phase depending on the internal state of the ion. In order to neither entangle the internal and the motional degrees of freedom, nor to permanently affect the motional state, we require the force to cease after some fixed point in time t_{fin} and to fulfill the condition:

$$\int_0^{t_{\mathrm{fin}}} e^{i\omega\tau}f(\tau)\,\mathrm{d}\tau = 0. \tag{6.16}$$

The quasi-classical state then arrives at t_{fin} at the same phase-space position, as it had without the force $f(t)$, as may be seen when substituting (6.16) into (6.12) and comparing with (6.8).

[4]The phase factor $e^{i\phi(t)}$ appearing in the quantum mechanical treatment of the forced harmonic oscillator is not to be confused with the constant of integration, called "phase" too, appearing in the solution of the classical equation of motion of a harmonic oscillator, such as $x(t) = x_0\cos(\omega t+\theta)$. This "classical phase" θ corresponds here to the argument of the complex parameter z characterizing the quasi-classical state $|z\rangle$.

The phase accumulated up to then is independent of z_0 and accounts for,

$$\phi(t_{\mathrm{fin}}) = \frac{1}{2\hbar^2}\mathrm{Im}\int_0^{t_{\mathrm{fin}}}\int_0^{\tau_1} e^{i\omega(\tau_1-\tau_2)} f(\tau_1)f(\tau_2)\,\mathrm{d}\tau_2\mathrm{d}\tau_1, \tag{6.17}$$

as obtained when substituting (6.16) into (6.15).

The independence of the acquired phase from the initial phase-space position z_0 is crucial for our state-detection technique being resilient to experimental imperfections and environmental disturbances. Moreover, it ensures that an ion in any initial motional state, not only in a quasi-classical state, acquires the same phase. In particular, for an ion in a thermal state, the phase acquired is independent of the ion-temperature owing to this independence.

Being independent of z_0, equation (6.17) may easily be adapted for the more general case of a transient force acting in the interval from t_{init} to t_{fin} (and vanishing otherwise), which fulfills the condition,

$$\int_{t_{\mathrm{init}}}^{t_{\mathrm{fin}}} e^{i\omega\tau} f(\tau)\,\mathrm{d}\tau = 0. \tag{6.18}$$

We obtain the phase acquired upon such a force has been exerted as,

$$\phi(t_{\mathrm{fin}}) = \frac{1}{2\hbar^2}\mathrm{Im}\int_{t_{\mathrm{init}}}^{t_{\mathrm{fin}}}\int_{t_{\mathrm{init}}}^{\tau_1} e^{i\omega(\tau_1-\tau_2)} f(\tau_1)f(\tau_2)\,\mathrm{d}\tau_2\mathrm{d}\tau_1. \tag{6.19}$$

This phase is interpreted in a neat way when regarding the curve described by $z_{\mathrm{r}}(t)$ in phase space with respect to the rotating frame introduced above. Since the quasi-classical state returns at $t = t_{\mathrm{fin}}$ to the initial phase-space position, $z_{\mathrm{r}}(t)$ describes a closed curve: $z_{\mathrm{r}}(t_{\mathrm{init}}) = z_{\mathrm{r}}(t_{\mathrm{fin}})$. Writing equation (6.14) in terms of the real and the imaginary part of $z_r = X_r + iP_r$, we get:

$$\dot{\phi}(t) = \mathrm{Im}\left[\dot{z}_r(t)z_r(t)^*\right] = \dot{P}_r(t)X_r(t) - P_r(t)\dot{X}_r(t), \tag{6.20}$$

where the dots ($\dot{}$) indicate time-derivatives. Integrating this equation over the closed curve $z_{\mathrm{r}}(t)$ for $t \in [t_{\mathrm{init}}, t_{\mathrm{fin}}]$, we obtain the phase as:

$$\phi_{\mathrm{init}\to\mathrm{fin}} = \oint_{t_{\mathrm{init}}}^{t_{\mathrm{fin}}} \dot{P}_r(t)X_r(t) - P_r(t)\dot{X}_r(t)\,\mathrm{d}t = 2A. \tag{6.21}$$

By means of "Leibniz's sector formula" (see, e.g., [198], pp. 246ff.), we can understand the above integral as twice the area A enclosed by the curve of $z_{\mathrm{r}}(t)$ in phase space. Fig. 6.4 shows an example for the evolution of a quasi-classical state in phase space subject to a transient force fulfilling (6.18).

Regarding the experimental realization, a convenient time-dependence for the force is a Gaussian time-profile:

$$f(t) = f^{(0)}e^{-(2t/T)^2}. \tag{6.22}$$

For such a Gaussian "force pulse", the condition (6.18) is not exactly fulfilled. However, for times long before and long after the peak value of the force (compared to the pulse duration T), i.e., in the limit $t_{\mathrm{init}} \to -\infty$, $t_{\mathrm{fin}} \to +\infty$, this condition is approximately met for a pulse duration considerably longer than the harmonic-oscillator period. Mur-Petit et al. [42] found the lower limit $T \geq 5\pi/\omega$. The phase

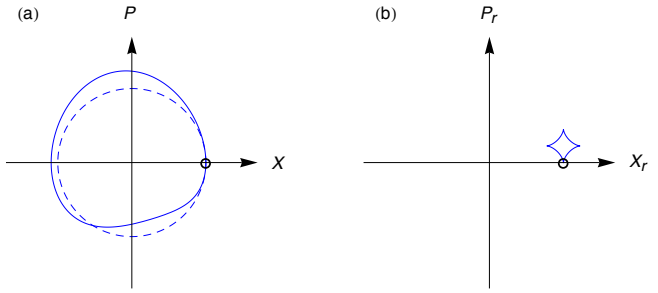

Figure 6.4. Phase portrait of a forced harmonic oscillator. (a) Evolution of a quasi-classical harmonic-oscillator state in position-momentum phase space subject to a force $F(t) \propto \sin(2\omega t)$ (solid trace) as opposed to unperturbed, pure harmonic evolution (dashed trace). The force complies to the condition (6.18) and the oscillator returns to the initial phase-space position (small, black circle). **(b)** Evolution with respect to a rotating frame. The curve described by the forced oscillator is closed and the quantum mechanical phase acquired due to forcing equals twice the area enclosed by this curve. (Adapted from [194].)

acquired in this asymptotic limit[5] is obtained as,

$$\phi_{\text{fin}} = \frac{1}{2}\left(\frac{f^{(0)}}{\hbar}\right)^2 \text{Im}\int_{-\infty}^{\infty}\int_{-\infty}^{\tau_1} e^{i\omega(\tau_1-\tau_2)} e^{-(2\tau_1/T)^2} e^{-(2\tau_2/T)^2}\,\mathrm{d}\tau_2\mathrm{d}\tau_1. \tag{6.23}$$

This integral may be given in analytical form within the "adiabatic approximation". Here, this approximation implies that the pulse is sufficiently long, and hence "smooth", that the condition $\frac{1}{\hbar\omega}\frac{\mathrm{d}f(t)}{\mathrm{d}t} \approx 0$ is met [194]. Integration by parts then yields,

$$\phi_{\text{fin}} = \sqrt{\frac{\pi}{2}}\frac{T}{4\omega}\left(\frac{f^{(0)}}{\hbar}\right)^2 = \sqrt{\frac{\pi}{2}}\frac{T}{4\omega}\left(\frac{F^{(0)}}{\hbar\beta}\right)^2, \tag{6.24}$$

with $F^{(0)} = f^{(0)}\beta$.

Forces with an arbitrary time profile may be treated by numerical integration of equation (6.18) and (6.19).

6.2.3 Two ions: Normal mode decomposition

If there are two ions in the same ion trap, they both localize on the trap axis when being cooled for suitably chosen experimental parameters, i.e., they form a Coulomb crystal in form of an ion string. Thus, we may still treat their motion as a one-dimensional problem. The motion of both ions, however, is coupled and in order to apply the theory developed above, we need to decouple it using the concept of "normal modes" [200, 201, 202, 203]. Below, this normal mode decomposition is first presented for the classical motion of two ions in a pure harmonic potential, i.e., without additional forces. Thereafter, the problem is treated quantum mechanically and the effect of additional forces on the two-ion quantum state is studied.

[5]Here, the analogy of the problem of a harmonic oscillator with a transient force to a scattering problem becomes evident—a point nicely worked out by Carruthers and Nieto [199], who solved it using the Green's function formalism.

The classical Lagrangian for two ions with masses m_1, m_2 and charge Q at positions x_1, x_2 reads,

$$\mathcal{L}(x_1, \dot{x}_1, x_2, \dot{x}_2) = \frac{1}{2} m_1 \dot{x}_1^2 + \frac{1}{2} m_2 \dot{x}_2^2 - V(x_1, x_2), \tag{6.25}$$

with the potential energy,

$$V(x_1, x_2) = \frac{1}{2} m_1 \omega_1^2 x_1^2 + \frac{1}{2} m_2 \omega_2^2 x_2^2 + \frac{Q^2}{4\pi\varepsilon_0 |x_1 - x_2|}, \tag{6.26}$$

and $\dot{x}_1$, $\dot{x}_2$ the temporal derivatives of x_1 and x_2, respectively, as well as ε_0 the vacuum permittivity.

Obviously, the equations of motion for x_1 and x_2,

$$\frac{\mathrm{d}}{\mathrm{d}t} \frac{\partial \mathcal{L}}{\partial \dot{x}_1} = \frac{\partial \mathcal{L}}{\partial x_1}, \tag{6.27a}$$

$$\frac{\mathrm{d}}{\mathrm{d}t} \frac{\partial \mathcal{L}}{\partial \dot{x}_2} = \frac{\partial \mathcal{L}}{\partial x_2}, \tag{6.27b}$$

are coupled by the Coulomb interaction term in the potential $V(x_1, x_2)$. In the following, we will show that decoupled equations of motion may be obtained under certain conditions.

As both ions are trapped by the same external potential, we have $m_1\omega_1^2 = m_2\omega_2^2$ and hence,

$$V(x_1, x_2) = \frac{1}{2} m_1 \omega_1^2 \left(x_1^2 + x_2^2\right) + \frac{Q^2}{4\pi\varepsilon_0 |x_1 - x_2|}. \tag{6.28}$$

Without loss of generality, we assume $m_1 \geq m_2$ and define the mass ratio $\mu = m_1/m_2 \geq 1$. Dropping the index 1, we then write $m = m_1$ and $m_2 = m/\mu$ as well as $\omega = \omega_1$.

When the two ions are cooled to a sufficiently low temperature, they form a Coulomb crystal and locate at the minima of the potential energy, namely at the positions:

$$x_1^{(0)} = -\left(\frac{Q^2}{16\pi\varepsilon_0 m\omega^2}\right)^{1/3}, \tag{6.29a}$$

$$x_2^{(0)} = \left(\frac{Q^2}{16\pi\varepsilon_0 m\omega^2}\right)^{1/3}. \tag{6.29b}$$

Assuming the ions to only exhibit small excursions from these equilibrium positions, we may approximate the potential energy in their vicinity by a Taylor expansion up to second order in the displacements $\bar{x}_1 = x_1 - x_1^{(0)}$ and $\bar{x}_2 = x_2 - x_2^{(0)}$:

$$\begin{aligned} V(x_1, x_2) \approx{}& V\left(x_1^{(0)}, x_2^{(0)}\right) + \left.\frac{\partial V}{\partial x_1}\right|_{\left(x_1^{(0)}, x_2^{(0)}\right)} \bar{x}_1 + \left.\frac{\partial V}{\partial x_2}\right|_{\left(x_1^{(0)}, x_2^{(0)}\right)} \bar{x}_2 \\ &+ \frac{1}{2} \left.\frac{\partial^2 V}{\partial x_1^2}\right|_{\left(x_1^{(0)}, x_2^{(0)}\right)} \bar{x}_1^2 + \frac{1}{2} \left.\frac{\partial^2 V}{\partial x_2^2}\right|_{\left(x_1^{(0)}, x_2^{(0)}\right)} \bar{x}_2^2 + \left.\frac{\partial^2 V}{\partial x_1 \partial x_2}\right|_{\left(x_1^{(0)}, x_2^{(0)}\right)} \bar{x}_1 \bar{x}_2 \end{aligned} \tag{6.30}$$

$$= V\left(x_1^{(0)}, x_2^{(0)}\right) + m\omega^2 \bar{x}_1^2 + m\omega^2 \bar{x}_2^2 - m\omega^2 \bar{x}_1 \bar{x}_2, \tag{6.31}$$

where we have used that the first derivatives of the potential vanish at the minima.

Using matrix notation, we may write this expression for the potential energy as,

$$V(\bar{x}_1, \bar{x}_2) = V_0 + \frac{1}{2}\begin{pmatrix}\bar{x}_1 & \bar{x}_2\end{pmatrix}\begin{pmatrix}2m\omega^2 & -m\omega^2 \\ -m\omega^2 & 2m\omega^2\end{pmatrix}\begin{pmatrix}\bar{x}_1 \\ \bar{x}_2\end{pmatrix}, \tag{6.32}$$

with the constant term $V_0 = V\left(x_1^{(0)}, x_2^{(0)}\right)$.

Defining the mass-weighted displacements,

$$q_1 = \sqrt{m_1}\bar{x}_1 = \sqrt{m}\bar{x}_1, \tag{6.33a}$$

$$q_2 = \sqrt{m_2}\bar{x}_2 = \sqrt{\frac{m}{\mu}}\bar{x}_2, \tag{6.33b}$$

we may furthermore write (6.32) as,

$$V(q_1, q_2) = V_0 + \frac{1}{2}\begin{pmatrix}q_1 & q_2\end{pmatrix}\begin{pmatrix}2\omega^2 & -\sqrt{\mu}\omega^2 \\ -\sqrt{\mu}\omega^2 & 2\mu\omega^2\end{pmatrix}\begin{pmatrix}q_1 \\ q_2\end{pmatrix}. \tag{6.34}$$

Ignoring constant terms, the Lagrangian in these new coordinates q_1, q_2 is given as

$$\mathcal{L}(q_1, \dot{q}_1, q_2, \dot{q}_2) = \frac{1}{2}\dot{q}_1^2 + \frac{1}{2}\dot{q}_2^2 - V(q_1, q_2), \tag{6.35}$$

where as before the dots indicate time derivatives.

Decoupling the equations of motion for q_1 and q_2 hence boils down to diagonalizing the matrix in (6.34). This matrix is diagonalized when using the coordinates q_{IP} and q_{OP} defined as

$$q_{\mathrm{IP}} = uq_2 + vq_1, \tag{6.36a}$$

$$q_{\mathrm{OP}} = vq_2 - uq_1 \tag{6.36b}$$

with

$$u = \left(1 + \frac{\left(1 - \mu - \sqrt{1 - \mu + \mu^2}\right)^2}{\mu}\right)^{-1/2}, \tag{6.37a}$$

$$v = (1 - u^2)^{1/2}. \tag{6.37b}$$

The potential energy then becomes,

$$V(q_{\mathrm{IP}}, q_{\mathrm{OP}}) = V_0 + \frac{1}{2}\begin{pmatrix}q_{\mathrm{IP}} & q_{\mathrm{OP}}\end{pmatrix}\begin{pmatrix}\omega_{\mathrm{IP}}^2 & 0 \\ 0 & \omega_{\mathrm{OP}}^2\end{pmatrix}\begin{pmatrix}q_{\mathrm{IP}} \\ q_{\mathrm{OP}}\end{pmatrix} \tag{6.38}$$

with

$$\omega_{\mathrm{IP}} = \omega\sqrt{1 + \mu - \sqrt{1 - \mu + \mu^2}}, \tag{6.39a}$$

$$\omega_{\mathrm{OP}} = \omega\sqrt{1 + \mu + \sqrt{1 - \mu + \mu^2}}. \tag{6.39b}$$

The Lagrangian in these "normal coordinates" is thus,

$$\mathcal{L}(q_{\mathrm{IP}}, \dot{q}_{\mathrm{IP}}, q_{\mathrm{OP}}, \dot{q}_{\mathrm{OP}}) = \frac{1}{2}\dot{q}_{\mathrm{IP}}^2 + \frac{1}{2}\dot{q}_{\mathrm{OP}}^2 - \frac{1}{2}\omega_{\mathrm{IP}}^2 q_{\mathrm{IP}}^2 - \frac{1}{2}\omega_{\mathrm{OP}}^2 q_{\mathrm{OP}}^2, \tag{6.40}$$

and the equations of motion for q_{IP} and q_{OP} are decoupled. Furthermore, they are both solved by the usual harmonic-oscillator ansatz.

The two coordinates q_{IP} and q_{OP} correspond to the two normal modes of oscillation, the "in-phase mode" and the "out-of-phase mode". If, e.g., the initial conditions at time $t = 0$ are $q_{\mathrm{IP}}(t = 0) \neq 0$ and $q_{\mathrm{OP}}(t = 0) = 0$, the two ions oscillate in phase at angular frequency ω_{IP}. In the case, $q_{\mathrm{OP}}(t = 0) \neq 0$ and $q_{\mathrm{IP}}(t = 0) = 0$, they oscillate out of phase at angular frequency ω_{OP}. For arbitrary initial conditions, a solution of the equations of motion is found as a combination of these two normal modes.

In order to work with quantities of familiar dimension, we define the variables $x_{\mathrm{IP}} = q_{\mathrm{IP}}/\sqrt{m}$ and $x_{\mathrm{OP}} = q_{\mathrm{OP}}/\sqrt{m}$. The Lagrangian then takes the form

$$\mathcal{L}(x_{\mathrm{IP}}, \dot{x}_{\mathrm{IP}}, x_{\mathrm{OP}}, \dot{x}_{\mathrm{OP}}) = \frac{1}{2}m\dot{x}_{\mathrm{IP}}^2 + \frac{1}{2}m\dot{x}_{\mathrm{OP}}^2 - \frac{1}{2}m\omega_{\mathrm{IP}}^2 x_{\mathrm{IP}}^2 - \frac{1}{2}m\omega_{\mathrm{OP}}^2 x_{\mathrm{OP}}^2. \tag{6.41}$$

In view of the quantum mechanical problem, we now switch from the Lagrangian to the Hamilton formalism. The classical Hamiltonian function is given as the Legendre transform of the Lagrangian, which yields:

$$\mathcal{H}(x_{\mathrm{IP}}, p_{\mathrm{IP}}, x_{\mathrm{OP}}, p_{\mathrm{OP}}) = \frac{p_{\mathrm{IP}}^2}{2m} + \frac{p_{\mathrm{OP}}^2}{2m} + \frac{m\omega_{\mathrm{IP}}^2 x_{\mathrm{IP}}^2}{2} + \frac{m\omega_{\mathrm{OP}}^2 x_{\mathrm{OP}}^2}{2}, \tag{6.42}$$

with the momenta $p_{\mathrm{IP}} = \frac{\partial \mathcal{L}}{\partial \dot{x}_{\mathrm{IP}}} = m\dot{x}_{\mathrm{IP}}$ and $p_{\mathrm{OP}} = \frac{\partial \mathcal{L}}{\partial \dot{x}_{\mathrm{OP}}} = m\dot{x}_{\mathrm{OP}}$.

The quantum mechanical Hamiltonian operator is obtained by substituting the position and momentum variables in the classical Hamiltonian function (6.42) by the corresponding quantum mechanical operators $\hat{x}_{\mathrm{IP}}$, $\hat{x}_{\mathrm{OP}}$ and $\hat{p}_{\mathrm{IP}}$, $\hat{p}_{\mathrm{OP}}$:

$$\hat{H} = \frac{\hat{p}_{\mathrm{IP}}^2}{2m} + \frac{\hat{p}_{\mathrm{OP}}^2}{2m} + \frac{m\omega_{\mathrm{IP}}^2 \hat{x}_{\mathrm{IP}}^2}{2} + \frac{m\omega_{\mathrm{OP}}^2 \hat{x}_{\mathrm{OP}}^2}{2}. \tag{6.43}$$

This Hamiltonian is the sum of the Hamiltonians of two harmonic oscillators. Therefore, we may apply the well-known formalism of the quantum mechanical harmonic oscillator. In particular, we may define the dimensionless operators,

$$\tilde{x}_{\mathrm{IP,\,OP}} = \beta_{\mathrm{IP,\,OP}} \hat{x}_{\mathrm{IP,\,OP}}, \tag{6.44a}$$

$$\tilde{p}_{\mathrm{IP,\,OP}} = \frac{1}{\hbar\beta_{\mathrm{IP,\,OP}}} \hat{p}_{\mathrm{IP,\,OP}}, \tag{6.44b}$$

with $\beta_{\mathrm{IP,\,OP}} = \sqrt{\frac{m\omega_{\mathrm{IP,\,OP}}}{\hbar}}$ as well as the ladder operators,

$$\hat{a}_{\mathrm{IP,\,OP}} = \frac{1}{\sqrt{2}} \left(\tilde{x}_{\mathrm{IP,\,OP}} + i\tilde{p}_{\mathrm{IP,\,OP}} \right), \tag{6.45a}$$

$$\hat{a}_{\mathrm{IP,\,OP}}^{\dagger} = \frac{1}{\sqrt{2}} \left(\tilde{x}_{\mathrm{IP,\,OP}} - i\tilde{p}_{\mathrm{IP,\,OP}} \right), \tag{6.45b}$$

to bring the Hamiltonian in the standard form,

$$\hat{H} = \hbar\omega_{\mathrm{IP}}\left(\hat{a}_{\mathrm{IP}}^{\dagger}\hat{a}_{\mathrm{IP}} + \frac{1}{2}\right) + \hbar\omega_{\mathrm{OP}}\left(\hat{a}_{\mathrm{OP}}^{\dagger}\hat{a}_{\mathrm{OP}} + \frac{1}{2}\right), \tag{6.46}$$

which, when ignoring the zero-point energy, is equivalent to:

$$\hat{H}' = \hbar\omega_{\mathrm{IP}}\hat{a}_{\mathrm{IP}}^{\dagger}\hat{a}_{\mathrm{IP}} + \hbar\omega_{\mathrm{OP}}\hat{a}_{\mathrm{OP}}^{\dagger}\hat{a}_{\mathrm{OP}}. \tag{6.47}$$

6.2.4 Two ions: Effect of time-dependent forces

Having discussed the problem of two ions in a pure harmonic potential, we now include additional time-dependent forces acting on the ions. As before, we start with the classical Lagrangian that reads in this case,

$$\mathcal{L}(x_1, \dot{x}_1, x_2, \dot{x}_2) = \frac{1}{2}m_1\dot{x}_1^2 + \frac{1}{2}m_2\dot{x}_2^2 - V(x_1, x_2) + F_1(t)x_1 + F_2(t)x_2, \tag{6.48}$$

with $F_1(t)$ and $F_2(t)$ the forces acting on ion 1 and 2, respectively, and $V(x_1, x_2)$ defined in (6.26). Applying the same "small-displacement approximation" as above and ignoring constant terms, we see that this expression corresponds to:

$$\mathcal{L}(\bar{x}_1, \dot{\bar{x}}_1, \bar{x}_2, \dot{\bar{x}}_2) = \frac{1}{2}m_1\dot{\bar{x}}_1^2 + \frac{1}{2}m_2\dot{\bar{x}}_2^2 - V(\bar{x}_1, \bar{x}_2) + F_1(t)\bar{x}_1 + F_2(t)\bar{x}_2. \tag{6.49}$$

The terms in this Lagrangian not involving the forces $F_1(t)$, $F_2(t)$ may be treated by exactly the same normal mode decomposition as above. The quantities $\bar{x}_1$ and $\bar{x}_2$ in the force terms are expressed by inverting equation (6.33) and (6.36) as $\bar{x}_1 = vx_{\mathrm{IP}} - ux_{\mathrm{OP}}$ and $\bar{x}_2 = \sqrt{\mu}\,(ux_{\mathrm{IP}} + vx_{\mathrm{OP}})$. In that way, we obtain the Lagrangian:

$$\begin{aligned}\mathcal{L}(x_{\mathrm{IP}}, \dot{x}_{\mathrm{IP}}, x_{\mathrm{OP}}, \dot{x}_{\mathrm{OP}}) = {} & \frac{1}{2}m\dot{x}_{\mathrm{IP}}^2 + \frac{1}{2}m\dot{x}_{\mathrm{OP}}^2 - \frac{1}{2}m\omega_{\mathrm{IP}}^2x_{\mathrm{IP}}^2 - \frac{1}{2}m\omega_{\mathrm{OP}}^2x_{\mathrm{OP}}^2 \\ & + F_1(t)\,(vx_{\mathrm{IP}} - ux_{\mathrm{OP}}) + F_2(t)\sqrt{\mu}\,(ux_{\mathrm{IP}} + vx_{\mathrm{OP}})\,.\end{aligned} \tag{6.50}$$

As in the previous section, the two equations of motion for x_{IP} and x_{OP} have thus been separated. However, a force acting on only one of the two ions affects both normal modes and hence also both ions. It is exactly this coupling that lies at the heart of the phase gate described here.

The Legendre transform of the Lagrangian (6.50) yields the classical Hamiltonian function as:

$$\begin{aligned}\mathcal{H}(x_{\mathrm{IP}}, p_{\mathrm{IP}}, x_{\mathrm{OP}}, p_{\mathrm{OP}}) = {} & \frac{p_{\mathrm{IP}}^2}{2m} + \frac{p_{\mathrm{OP}}^2}{2m} + \frac{m\omega_{\mathrm{IP}}^2x_{\mathrm{IP}}^2}{2} + \frac{m\omega_{\mathrm{OP}}^2x_{\mathrm{OP}}^2}{2} \\ & - F_1(t)\,(vx_{\mathrm{IP}} - ux_{\mathrm{OP}}) - F_2(t)\sqrt{\mu}\,(ux_{\mathrm{IP}} + vx_{\mathrm{OP}})\,.\end{aligned} \tag{6.51}$$

For a quantum mechanical description, the Hamiltonian operator is again obtained by substituting the position and momentum variables by the corresponding operators, i.e.,

$$\hat{H} = \frac{\hat{p}_{\mathrm{IP}}^2}{2m} + \frac{\hat{p}_{\mathrm{OP}}^2}{2m} + \frac{m\omega_{\mathrm{IP}}^2\hat{x}_{\mathrm{IP}}^2}{2} + \frac{m\omega_{\mathrm{OP}}^2\hat{x}_{\mathrm{OP}}^2}{2} - F_1(t)\,(v\hat{x}_{\mathrm{IP}} - u\hat{x}_{\mathrm{OP}}) - F_2(t)\sqrt{\mu}\,(u\hat{x}_{\mathrm{IP}} + v\hat{x}_{\mathrm{OP}})\,. \tag{6.52}$$

Rearranging terms and switching to the dimensionless operators defined in (6.44) and then to the

ladder operators from (6.45), the Hamiltonian becomes:

$$\begin{aligned}\hat{H} &= \frac{1}{2}\hbar\omega_{\mathrm{IP}}\left(\tilde{p}_{\mathrm{IP}}^2+\tilde{x}_{\mathrm{IP}}^2\right)+\frac{1}{2}\hbar\omega_{\mathrm{OP}}\left(\tilde{p}_{\mathrm{OP}}^2+\tilde{x}_{\mathrm{OP}}^2\right)\\ &\quad-\Big(F_1(t)v+F_2(t)\sqrt{\mu}u\Big)\frac{\tilde{x}_{\mathrm{IP}}}{\beta_{\mathrm{IP}}}+\Big(F_1(t)u-F_2(t)\sqrt{\mu}v\Big)\frac{\tilde{x}_{\mathrm{OP}}}{\beta_{\mathrm{OP}}} \qquad (6.53)\\ &= \hbar\omega_{\mathrm{IP}}\left(\hat{a}_{\mathrm{IP}}^\dagger\hat{a}_{\mathrm{IP}}+\frac{1}{2}\right)+\hbar\omega_{\mathrm{OP}}\left(\hat{a}_{\mathrm{OP}}^\dagger\hat{a}_{\mathrm{OP}}+\frac{1}{2}\right)\\ &\quad-\frac{1}{\sqrt{2}\beta_{\mathrm{IP}}}\Big(F_1(t)v+F_2(t)\sqrt{\mu}u\Big)\left(\hat{a}_{\mathrm{IP}}+\hat{a}_{\mathrm{IP}}^\dagger\right)\\ &\quad+\frac{1}{\sqrt{2}\beta_{\mathrm{OP}}}\Big(F_1(t)u-F_2(t)\sqrt{\mu}v\Big)\left(\hat{a}_{\mathrm{OP}}+\hat{a}_{\mathrm{OP}}^\dagger\right). \qquad (6.54)\end{aligned}$$

Neglecting zero-point energy, we realize that this Hamiltonian has the form of a sum of two single-particle, forced-harmonic-oscillator Hamiltonians, $\hat{H}_{\mathrm{IP}}$ and $\hat{H}_{\mathrm{OP}}$, discussed in Sec. 6.2.2 (cf. equation (6.5)),

$$\begin{aligned}\hat{H}' &= \hbar\omega_{\mathrm{IP}}\hat{a}_{\mathrm{IP}}^\dagger\hat{a}_{\mathrm{IP}}-\frac{f_{\mathrm{IP}}(t)}{\sqrt{2}}\left(\hat{a}_{\mathrm{IP}}+\hat{a}_{\mathrm{IP}}^\dagger\right)+\hbar\omega_{\mathrm{OP}}\hat{a}_{\mathrm{OP}}^\dagger\hat{a}_{\mathrm{OP}}-\frac{f_{\mathrm{OP}}(t)}{\sqrt{2}}\left(\hat{a}_{\mathrm{OP}}+\hat{a}_{\mathrm{OP}}^\dagger\right) \qquad (6.55)\\ &= \hat{H}_{\mathrm{IP}}+\hat{H}_{\mathrm{OP}}, \qquad (6.56)\end{aligned}$$

when setting

$$f_{\mathrm{IP}}(t) = \frac{1}{\beta_{\mathrm{IP}}}\left(F_1(t)v+F_2(t)\sqrt{\mu}u\right), \qquad (6.57a)$$

$$f_{\mathrm{OP}}(t) = \frac{1}{\beta_{\mathrm{OP}}}\left(F_2(t)\sqrt{\mu}v-F_1(t)u\right). \qquad (6.57b)$$

The time-dependent Schrödinger equation associated with the Hamiltonian (6.55) can thus be solved by a tensor product ansatz for the motional state $|\psi_{\mathrm{m}}(t)\rangle = |\psi_{\mathrm{IP}}(t)\rangle\,|\psi_{\mathrm{OP}}(t)\rangle$ with $|\psi_{\mathrm{IP}}(t)\rangle$ only evolving according to $\hat{H}_{\mathrm{IP}}$ and $|\psi_{\mathrm{OP}}(t)\rangle$ only according to $\hat{H}_{\mathrm{OP}}$.

Moreover, when using the complete set of quasi-classical states, we may find a solution of the Schrödinger equation as,

$$|\psi_{\mathrm{m}}(t)\rangle = e^{i\phi_{\mathrm{IP}}(t)}e^{i\phi_{\mathrm{OP}}(t)}\,|z_{\mathrm{IP}}(t)\rangle\,|z_{\mathrm{OP}}(t)\rangle, \qquad (6.58)$$

with the parameter $z_{\mathrm{IP}}(t)$ evolving according to equation (6.10) and the phase $\phi_{\mathrm{IP}}(t)$ according to (6.11), when substituting $f(t)$ therein by $f_{\mathrm{IP}}(t)$ from (6.57a). Equivalently, $z_{\mathrm{OP}}(t)$ and $\phi_{\mathrm{OP}}(t)$ evolve according to (6.10) and (6.11), respectively, when using $f_{\mathrm{OP}}(t)$ from (6.57b).

For transient forces, satisfying the two criteria,

$$\int_{t_{\mathrm{init}}}^{t_{\mathrm{fin}}} e^{i\omega_{\mathrm{IP}}\tau}f_{\mathrm{IP}}(\tau)\,\mathrm{d}\tau = 0, \qquad (6.59a)$$

$$\int_{t_{\mathrm{init}}}^{t_{\mathrm{fin}}} e^{i\omega_{\mathrm{OP}}\tau}f_{\mathrm{OP}}(\tau)\,\mathrm{d}\tau = 0, \qquad (6.59b)$$

the quasi-classical states return to their initial phase-space positions at t_{fin}: $z_{\mathrm{IP,OP}}(t_{\mathrm{init}}) = z_{\mathrm{IP,OP}}(t_{\mathrm{fin}})$,

and the phases accumulated are:

$$\phi_{\mathrm{IP,OP}}(t_{\mathrm{fin}}) = \frac{1}{2\hbar^2}\mathrm{Im}\int_{t_{\mathrm{init}}}^{t_{\mathrm{fin}}}\int_{t_{\mathrm{init}}}^{\tau_1} e^{i\omega_{\mathrm{IP,OP}}(\tau_1-\tau_2)} f_{\mathrm{IP,OP}}(\tau_1) f_{\mathrm{IP,OP}}(\tau_2)\,\mathrm{d}\tau_2\mathrm{d}\tau_1. \tag{6.60}$$

When we express the acquired phase in terms of a single phase factor, according to

$$|\psi_{\mathrm{m}}(t)\rangle = e^{i\phi_{\mathrm{tot}}(t)}\,|z_{\mathrm{IP}}(t)\rangle\,|z_{\mathrm{OP}}(t)\rangle\,, \tag{6.61}$$

with $\phi_{\mathrm{tot}} = \phi_{\mathrm{IP}}(t) + \phi_{\mathrm{OP}}(t)$, this total phase is given as,

$$\begin{aligned}\phi_{\mathrm{tot}}(t_{\mathrm{fin}}) = \frac{1}{2\hbar^2}\mathrm{Im}\int_{t_{\mathrm{init}}}^{t_{\mathrm{fin}}}\int_{t_{\mathrm{init}}}^{\tau_1} & e^{i\omega_{\mathrm{IP}}(\tau_1-\tau_2)} f_{\mathrm{IP}}(\tau_1) f_{\mathrm{IP}}(\tau_2) \\ & + e^{i\omega_{\mathrm{OP}}(\tau_1-\tau_2)} f_{\mathrm{OP}}(\tau_1) f_{\mathrm{OP}}(\tau_2)\,\mathrm{d}\tau_2\mathrm{d}\tau_1.\end{aligned} \tag{6.62}$$

6.2.5 State-dependent forces

In the previous two sections, we have only discussed the motional degrees of freedom of the ions. Primarily of interest, however, are the internal degrees of freedom. As outlined in Sec. 6.2.1, the internal degrees of freedom may be treated effectively as a two-level system. The internal states of ion 1 and 2 are thus given as,

$$|\psi_{\mathrm{int}}^{(1)}\rangle = c_{\mathrm{e}}^{(1)}\,|\mathrm{e}\rangle + c_{\mathrm{g}}^{(1)}\,|\mathrm{g}\rangle\,, \tag{6.63a}$$

$$|\psi_{\mathrm{int}}^{(2)}\rangle = c_{\mathrm{e}}^{(2)}\,|\mathrm{e}\rangle + c_{\mathrm{g}}^{(2)}\,|\mathrm{g}\rangle\,, \tag{6.63b}$$

with coefficients $c_{\mathrm{e}}^{(j)}, c_{\mathrm{g}}^{(j)} \in \mathbb{C}$ fulfilling $|c_{\mathrm{g}}^{(j)}|^2 + |c_{\mathrm{e}}^{(j)}|^2 = 1$ $(j = 1, 2)$ and $|\mathrm{g}\rangle$, $|\mathrm{e}\rangle$ the ground and excited state of the respective ion. The complete effective quantum state of the two-ion system is thus formed as a tensor product of the motional and the internal states: $|\psi_{\mathrm{tot}}\rangle = |\psi_{\mathrm{m}}\rangle\,|\psi_{\mathrm{int}}^{(1)}\rangle\,|\psi_{\mathrm{int}}^{(2)}\rangle$.

Expressing the motional state in terms of normal modes and using the complete set of quasi-classical states, we may write the effective total quantum state as:

$$|\psi_{\mathrm{tot}}\rangle = |z_{\mathrm{IP}}\rangle\,|z_{\mathrm{OP}}\rangle\,|\psi_{\mathrm{int}}^{(1)}\rangle\,|\psi_{\mathrm{int}}^{(2)}\rangle\,. \tag{6.64}$$

As explained in Sec. 6.2.1, the forces only act on the ions, when these are in their ground state and vanish in the excited state. Mathematically, this state dependence is expressed by multiplying the forces with the projection operators $\hat{P}_{\mathrm{g}}^{(1,2)} = |\mathrm{g}\rangle\langle\mathrm{g}|$, which are 1, if the respective ion is in the ground state $|\mathrm{g}\rangle$, and 0, if it is in the excited state $|\mathrm{e}\rangle$, i.e, by the substitutions:[6]

$$F_1(t) \to \hat{P}_{\mathrm{g}}^{(1)} F_1(t), \tag{6.65a}$$

$$F_2(t) \to \hat{P}_{\mathrm{g}}^{(2)} F_2(t). \tag{6.65b}$$

The quantum mechanical Hamiltonian for the two-ion system with state-dependent forces hence

[6] As before, we use the same symbols for the ground and the excited state of both ions. The corresponding states are to be understood in the definitions of the projection operators.

is:

$$\hat{H} = \frac{\hat{p}_1^2}{2m_1} + \frac{\hat{p}_2^2}{2m_2} + V(\hat{x}_1, \hat{x}_2) - \hat{P}_{\mathrm{g}}^{(1)} F_1(t)\hat{x}_1 - \hat{P}_{\mathrm{g}}^{(2)} F_2(t)\hat{x}_2. \tag{6.66}$$

By means of normal mode decomposition, we may bring this Hamiltonian in the form of (6.55), but with $f_{\mathrm{IP}}(t)$ and $f_{\mathrm{OP}}(t)$ therein substituted by:

$$\hat{f}_{\mathrm{IP}}(t) = \frac{1}{\beta_{\mathrm{IP}}} \left(\hat{P}_{\mathrm{g}}^{(1)} F_1(t) v + \hat{P}_{\mathrm{g}}^{(2)} F_2(t) \sqrt{\mu} u \right), \tag{6.67a}$$

$$\hat{f}_{\mathrm{OP}}(t) = \frac{1}{\beta_{\mathrm{OP}}} \left(\hat{P}_{\mathrm{g}}^{(2)} F_2(t) \sqrt{\mu} v - \hat{P}_{\mathrm{g}}^{(1)} F_1(t) u \right). \tag{6.67b}$$

Provided the conditions (6.59) are met, the motional quantum state returns at t_{fin} to the initial one, except for an additional phase. This phase $\phi_{\mathrm{tot}}(t_{\mathrm{fin}})$ is, as before, given by (6.62), but with $f_{\mathrm{IP}}(t)$ and $f_{\mathrm{OP}}(t)$ therein substituted by their counterparts from (6.67). The phase thus involves the projection operators.

Realizing that the projectors acting on different ions commute ($\hat{P}_{\mathrm{g}}^{(1)} \hat{P}_{\mathrm{g}}^{(2)} = \hat{P}_{\mathrm{g}}^{(2)} \hat{P}_{\mathrm{g}}^{(1)}$) and that they are idempotent ($\hat{P}_{\mathrm{g}}^{(1,2)} \hat{P}_{\mathrm{g}}^{(1,2)} = \hat{P}_{\mathrm{g}}^{(1,2)}$), we see that the phase $\phi_{\mathrm{tot}}(t_{\mathrm{fin}})$ decomposes into a sum of three terms according to:

$$\hat{\phi}_{\mathrm{tot}}(t_{\mathrm{fin}}) = \phi_1 \hat{P}_{\mathrm{g}}^{(1)} + \phi_2 \hat{P}_{\mathrm{g}}^{(2)} + \phi_{12} \hat{P}_{\mathrm{g}}^{(1)} \hat{P}_{\mathrm{g}}^{(2)}. \tag{6.68}$$

Here, we are first of all interested in the term ϕ_{12}. This is the contribution to the phase relevant for a controlled phase gate. To clarify this point, we may rewrite the phase factor using the above-mentioned properties of projection operators to simplify the matrix exponential as,

$$e^{i\phi_{12} \hat{P}_{\mathrm{g}}^{(1)} \hat{P}_{\mathrm{g}}^{(2)}} = \hat{P}_{\mathrm{g}}^{(2)} \left[\hat{P}_{\mathrm{g}}^{(1)} e^{i\phi_{12}} + \hat{P}_{\mathrm{e}}^{(1)} \right] + \hat{P}_{\mathrm{e}}^{(2)} \hat{I}^{(1)}, \tag{6.69}$$

with $\hat{P}_{\mathrm{e}}^{(1,2)} = |\mathrm{e}\rangle\langle\mathrm{e}|$ the projectors on the excited state of ion 1 and 2, respectively, and $\hat{I}^{(1)}$ the identity operator belonging to ion 1.[7] The term in brackets in (6.69) gives rise to a phase shift of the ground state of ion 1 (the logic ion) relative to its excited state, i.e., it describes a phase gate. The projector $\hat{P}_{\mathrm{g}}^{(2)}$ constrains the phase gate operation to the case where ion 2 (the spectroscopy ion) is in the ground state. Thus, the overall effect on the two-ion system is that of a controlled phase gate.

From (6.62) and (6.67) we obtain the relevant phase ϕ_{12} for given forces $F_1(t)$ and $F_2(t)$ as,

$$\phi_{12} = \frac{uv\sqrt{\mu}}{2\hbar^2} \mathrm{Im} \int_{t_{\mathrm{init}}}^{t_{\mathrm{fin}}} \int_{t_{\mathrm{init}}}^{\tau_1} \left(\frac{e^{i\omega_{\mathrm{IP}}(\tau_1 - \tau_2)}}{\beta_{\mathrm{IP}}^2} - \frac{e^{i\omega_{\mathrm{OP}}(\tau_1 - \tau_2)}}{\beta_{\mathrm{OP}}^2} \right) \big(F_1(\tau_1) F_2(\tau_2) + F_1(\tau_2) F_2(\tau_1) \big) \, \mathrm{d}\tau_2 \mathrm{d}\tau_1. \tag{6.70}$$

For forces following a Gaussian time profile,

$$F_1(t) = F_1^{(0)} e^{-(2t/T)^2}, \tag{6.71a}$$

$$F_2(t) = F_2^{(0)} e^{-(2t/T)^2}, \tag{6.71b}$$

the conditions (6.59) are approximately met for $T \geq 5\pi/\omega_{\mathrm{IP}}$.[8] Within the adiabatic approximation, the

[7] The identity operator of one part of a tensor product Hilbert space is of course the identity operator of the whole space and hence could be omitted. For clarity, it is explicitly written in (6.69).

[8] If so, the analogous criterion for ω_{OP} is met as well, since $\omega_{\mathrm{OP}} > \omega_{\mathrm{IP}}$.

integral in (6.70) can then be given analytically for the asymptotic limit $t_{\mathrm{init}} = -\infty$, $t_{\mathrm{fin}} = +\infty$:

$$\phi_{12} = \frac{uv\sqrt{\mu}}{2\hbar^2}\sqrt{\frac{\pi}{2}}F_1^{(0)}F_2^{(0)}T\left(\frac{1}{\beta_{\mathrm{IP}}^2\omega_{\mathrm{IP}}} - \frac{1}{\beta_{\mathrm{OP}}^2\omega_{\mathrm{OP}}}\right). \tag{6.72}$$

Using the definitions of β_{IP} and β_{OP} together with the relation,

$$uv\sqrt{\mu} = \left(3\omega^2\left(\frac{1}{\omega_{\mathrm{IP}}^2} - \frac{1}{\omega_{\mathrm{OP}}^2}\right)\right)^{-1}, \tag{6.73}$$

we may express the quantity ϕ_{12} in terms of the single-particle axial trapping frequency ω and the mass m of ion 1 as:

$$\phi_{12} = \sqrt{\frac{\pi}{2}}\frac{F_1^{(0)}F_2^{(0)}T}{6\hbar\omega^2 m}. \tag{6.74}$$

6.3 Implementation

6.3.1 Optical dipole force

Having studied the dynamics of a two-ion system subject to state-dependent, transient forces, we may now turn to the implementation of our state-detection method based on optical dipole forces as outlined in Sec. 6.2.1, i.e., forces induced by off-resonant Gaussian laser beams addressing the $|\mathrm{g}\rangle - |\mathrm{aux}\rangle$ transitions in the two ions.

In general, the optical dipole force is given as ([128], p. 199):

$$\mathbf{F}(\mathbf{r}) = -\frac{\hbar\Delta}{2}\frac{\Omega(\mathbf{r})}{\Delta^2 + \Omega(\mathbf{r})^2/2 + \Gamma^2/4}\nabla\Omega(\mathbf{r}). \tag{6.75}$$

Here, Δ is the detuning of the laser frequency from the $|\mathrm{g}\rangle - |\mathrm{aux}\rangle$ transition, Γ the natural linewidth of this transition, $\Omega(\mathbf{r})$ the Rabi frequency and $\nabla\Omega(\mathbf{r})$ its gradient at position $\mathbf{r}$, respectively.

The Rabi frequency—a quantity usually encountered in the context of the coherent evolution of two-level systems—serves here as a measure for the laser intensity with the same dimension as the detuning.[9] The squared Rabi frequency is proportional to the laser intensity $I(\mathbf{r})$ and hence to the total laser beam power P_{tot} divided by the squared beam radius w:

$$\Omega(\mathbf{r})^2 \propto I(\mathbf{r}) \propto \frac{P_{\mathrm{tot}}}{w^2}. \tag{6.76}$$

Typical Rabi frequencies for the $|\mathrm{g}\rangle - |\mathrm{aux}\rangle$ transition in the Ca^+ and N_2^+ ion as a function of the laser beam radius are shown in Fig. 6.5 for a number of beam powers.

For detunings large compared to the Rabi frequency ($|\Delta| \gg \Omega$) and the latter also large relative to

[9] When studying the dynamics of two-level systems perturbed by electromagnetic radiation, as we have done in Ch. 2, but for nearly monochromatic instead of broadband radiation, the population is found to oscillate between the two levels. The Rabi frequency corresponds to the frequency of this oscillation for a radiation field in resonance with the two-level transition. Here, we study off-resonant radiation, almost not exciting any population. The Rabi frequency just serves as a convenient measure for the radiation intensity.

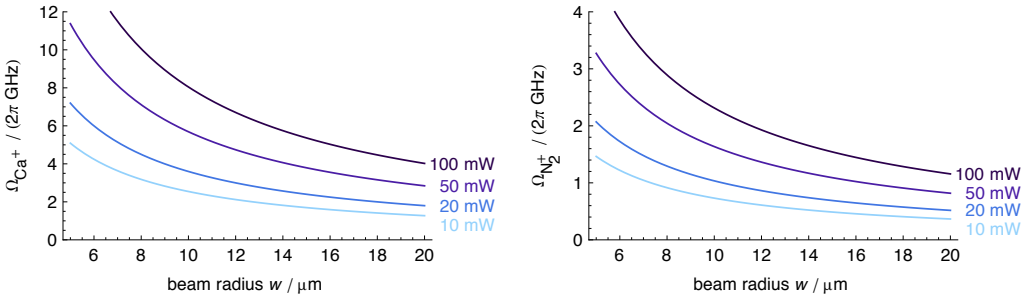

Figure 6.5. Typical Rabi frequencies. Rabi frequencies for the $4^2S_{1/2} - 4^2P_{1/2}$ transition in Ca^+ (left panel) and the $X^2\Sigma_g^+ \; v = 0, N = 0 - B^2\Sigma_u^+ \; v = 0, N = 1$ transition in N_2^+ (right panel) as a function of the $1/e^2$ beam radius w for a total beam power of 10, 20, 50, and 100 mW at the position of maximum intensity gradient. (v and N denote the vibrational and the rotational quantum number, respectively. See Appendix D for the calculation of the values shown.)

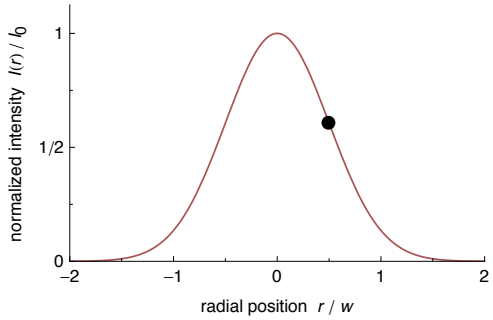

Figure 6.6. Transverse intensity profile of a Gaussian laser beam. Normalized intensity $I(r)/I_0$ as a function of the radial position in units of the $1/e^2$ beam radius w. The intensity follows the relation $I(r) = I_0 \exp(-2r^2/w^2)$ with I_0 the intensity at the beam centreline and r the radial distance from the centreline. At $r = \pm w/2$ the intensity gradient is maximal, resulting in a maximum optical dipole force.

the natural linewidth ($\Omega \gg \Gamma$), the dipole force may be approximated as,

$$\mathbf{F}(\mathbf{r}) = -\frac{\hbar}{4\Delta}\nabla\Omega(\mathbf{r})^2. \tag{6.77}$$

In our proposed setup, the intensity gradient is formed by the transverse beam profile of a Gaussian laser beam (see Fig. 6.6). For the ions being in the plane of the beam waist of a Gaussian laser beam, the tangential and the axial derivative of $\Omega(\mathbf{r})$ vanish due to symmetry reasons. The optical dipole force hence only exhibits a component radial to the beam,[10] which is given by,

$$F_{\mathrm{rad}}(r) = -\frac{\hbar}{4\Delta}\frac{\partial}{\partial r}\Omega(r)^2. \tag{6.78}$$

The Rabi frequency of an ion in a Gaussian laser beam, same as the intensity, follows a Gaussian profile,

$$\Omega(r) = \Omega_0 e^{-\frac{r^2}{w^2}}, \tag{6.79}$$

[10] If the ion is not exactly in the plane of the beam waist, the optical dipole force also acts in direction of the beam. The radial component, however, still dominates and the present treatment is a fairly good approximation. Moreover, the beam radius w that corresponds to the "waist size" (hence the symbol w) in the plane of the beam waist, increases with increasing distance from this plane and the intensity is lowered accordingly.

where Ω_0 is the Rabi frequency at the beam centre and r the radial distance from the beam centre-line.

The radial component of the gradient of the squared Rabi frequency at the position of maximum intensity gradient ($r = \pm w/2$) hence is,

$$\frac{\partial}{\partial r}\Omega(r)^2\bigg|_{r=\pm w/2} = \mp\frac{2\Omega_0^2}{w}e^{-\frac{1}{2}} = \mp\frac{2\Omega'^2}{w}, \tag{6.80}$$

with $\Omega' = \Omega(r = w/2) = \Omega_0 e^{-\frac{1}{4}}$ the Rabi frequency at this position. Substituting these results into (6.78), we obtain the magnitude of the optical dipole force at maximum intensity gradient of a Gaussian beam as,

$$|F_{\mathrm{rad}}(r = \pm w/2)| = \frac{\hbar\Omega'^2}{2w\Delta}. \tag{6.81}$$

With the Rabi frequencies of the Ca^+ and N_2^+ ions at these positions denoted as Ω_{Ca^+} and $\Omega_{N_2^+}$ as well as the respective detunings and beam radii as Δ_{Ca^+}, $\Delta_{N_2^+}$ and w_{Ca^+}, $w_{N_2^+}$, the magnitude of the optical dipole forces exerted on the ions are:

$$F_{Ca^+} = \frac{\hbar\Omega_{Ca^+}^2}{2w_{Ca^+}\Delta_{Ca^+}}, \tag{6.82a}$$

$$F_{N_2^+} = \frac{\hbar\Omega_{N_2^+}^2}{2w_{N_2^+}\Delta_{N_2^+}}. \tag{6.82b}$$

For the phase-gate operation discussed in the previous section, we want the forces to follow a Gaussian time-profile according to (6.71). To this end, the laser intensities are attenuated appropriately, e.g., by means of an acousto-optic modulator (see [58], pp. 804ff.). The quantities F_{Ca^+} and $F_{N_2^+}$ from (6.82) then correspond to the time-independent coefficients $F_1^{(0)}$ and $F_2^{(0)}$ in (6.74), respectively.[11]

Substituting them into (6.74), we obtain the relevant contribution to the phase of the two-ion system as,

$$\phi_{12} = \sqrt{\frac{\pi}{2}}\frac{\hbar T}{24m\omega^2}\frac{\Omega_{Ca^+}^2\Omega_{N_2^+}^2}{\Delta_{Ca^+}\Delta_{N_2^+}}\frac{1}{w_{Ca^+}w_{N_2^+}}. \tag{6.83}$$

Here, m and ω and are the mass and the single-particle axial secular trapping frequency of the Ca^+ ion, respectively.

6.3.2 Photon scattering

An issue with optical dipole forces is photon scattering. If photons from the laser beams exerting these forces are absorbed by the ions through excitation of the $|g\rangle - |aux\rangle$ transition, their coherent evolution is disturbed. Therefore, photon scattering must be avoided.

Scattering events of photons from a coherent light source follow a Poisson distribution [204]. The probability that at most n scattering events occur during a period T is given by the cumulative

[11] Because of the choice $m_1 \geq m_2$ in Sec. 6.2.3, quantities with index 1 from the previous section correspond to the Ca^+ ion, those with index 2 to the N_2^+ ion.

distribution function,

$$P(n) = e^{-\bar{n}} \sum_{k=0}^{n} \frac{\bar{n}^k}{k!}, \tag{6.84}$$

with $\bar{n}$ the mean number of scattering events during this period T. The probability of no photons being scattered during this period thus is: $P(n=0) = e^{-\bar{n}}$.

The mean number of photons scattered is the product of the scattering rate R_{sc} and the duration of laser irradiation T: $\bar{n} = R_{\mathrm{sc}}T$. [12] The scattering rate is given by ([128], p. 180),

$$R_{\mathrm{sc}} = \frac{\Gamma}{2} \frac{\Omega'^2/2}{\Delta^2 + \Omega'^2/2 + \Gamma^2/4} \approx \frac{\Gamma}{4} \left(\frac{\Omega'}{\Delta}\right)^2, \tag{6.85}$$

where, as before, the approximation $|\Delta| \gg \Omega \gg \Gamma$ has been used.

The probability that no photon is scattered within T is thus:

$$P(n=0) = e^{-T\frac{\Gamma}{4}\left(\frac{\Omega'}{\Delta}\right)^2}. \tag{6.86}$$

As we want this probability to be near unity, the opposite probability ϵ of scattering at least one photon while exerting the optical dipole force is close to zero and may be approximated as,

$$\epsilon = 1 - P(n=0) \approx \frac{\Gamma T}{4} \left(\frac{\Omega'}{\Delta}\right)^2. \tag{6.87}$$

With the values $\Gamma_{\mathrm{Ca}^+} = 132 \times 10^6\,\mathrm{s}^{-1}$ and $\Gamma_{\mathrm{N}_2^+} = 3.80 \times 10^6\,\mathrm{s}^{-1}$ from Appendix D, we may calculate this scattering probability for both ions for any given Rabi frequency and detuning Ω_{Ca^+}, Δ_{Ca^+} or $\Omega_{\mathrm{N}_2^+}$, $\Delta_{\mathrm{N}_2^+}$ and irradiation time T. Vice versa, we may work out the mutual dependencies of these quantities for a given scattering probability ϵ.

6.3.3 Parameter estimation and feasibility

Having worked out the relevant formulae for our state-detection scheme with optical dipole forces, we may now estimate the parameters relevant for an experimental implementation and asses feasibility of our method. The stage is set by the equations (6.83) and (6.87) that yield the phase ϕ_{12} and the scattering probability ϵ, respectively, as well as (6.76) that relates the Rabi frequencies to the experimentally accessible quantities of beam power and beam radius.

There are in total eight parameters, we need to choose such that the required phase is obtained, the scattering probability ϵ is acceptable and technical limitations are not exceeded: the laser pulse duration T, the axial secular trapping frequency ω, the Rabi frequencies Ω_{Ca^+}, $\Omega_{\mathrm{N}_2^+}$, the detunings Δ_{Ca^+}, $\Delta_{\mathrm{N}_2^+}$ and the beam radii w_{Ca^+}, $w_{\mathrm{N}_2^+}$.

Before calculating actual values, we shortly analyze the mutual dependencies and the scaling behaviour of these parameters. For the two-ion system to accumulate the geometric phase needed, the optical dipole force must be high enough, while the scattering rate must be kept low. As the inverse detuning

[12] Here, we assume the laser intensity to be constant during the period T. For the Gaussian time profile of equation (6.71), this is not the case. In an exact calculation, the value of ϵ is reduced by a factor $\sqrt{\pi}/2 \approx 0.89$ for otherwise identical parameters. This factor being close to unity, we neglect it for simplicity in the order-of-magnitude estimation done here.

appears linear in the force (see equation (6.81)), but squared in the scattering probability (see equation (6.87)), while the Rabi frequency appears squared in both of them, a force sufficiently large as well as a low scattering probability, may be achieved by a large Rabi frequency together with a large detuning.

A large Rabi frequency may be either achieved with a high beam intensity or a small beam radius. Both of these quantities are constrained by technical limitations such as available laser power, quality of focusing and beam shaping optics and beam pointing stability. Therefore, a trade-off between these conflicting requirements must be found. The beam radius is a particularly crucial parameter as it affects both, the Rabi frequency at the position of the ions as well as its gradient.

For a quantitative analysis, we need to reduce the number of parameters. We proceed as follows:

- We chose the secular trapping frequency as $\omega = 2\pi \times 100\,\mathrm{kHz}$, a typical value for our trap, corresponding to $\omega_{\mathrm{IP}} = 2\pi \times 108\,\mathrm{kHz}$ for the Ca^+-N_2^+-system.
- We chose a value for the scattering probability ϵ. Here, the values $\epsilon = 0.1$ and $\epsilon = 0.01$ are studied. Together with the pulse duration T, the ratio of the Rabi frequency Ω_{Ca^+} ($\Omega_{N_2^+}$) to the detuning Δ_{Ca^+} ($\Delta_{N_2^+}$) then is fixed by equation (6.87) and we may eliminate the detunings from equation (6.83).
- We assume the radii of the two beams addressing the Ca^+ and the N_2^+ ion to be equal, $w_{Ca^+} = w_{N_2^+} =: w$, as these two beams are to be focused by the same optics and their wavelengths differ by less than two percent.
- As the phase ϕ_{12} depends only on the product of the two Rabi frequencies Ω_{Ca^+} and $\Omega_{N_2^+}$, rather then on their individual values, we substitute them by the mean Rabi frequency $\overline{\Omega}$ defined as the geometric mean of the Rabi frequencies of the Ca^+ and the N_2^+ ion: $\overline{\Omega} = \sqrt{\Omega_{Ca^+}\Omega_{N_2^+}}$

In so doing, we have eliminated all but the two parameters w and $\overline{\Omega}$ from the right-hand side of equation (6.83). In particular, we have eliminated the pulse duration T, meaning that our results will be independent of T. Hence, we may use the shortest pulse allowed by the condition in Sec. 6.2.5, namely $T = 5\pi/\omega_{\mathrm{IP}} = 23.2\,\mu\mathrm{s}$, in order to minimize the requirement for the coherence time and thus the sensitivity to magnetic field fluctuations.[13] We set $\phi_{12} = \pi$, as needed for a population inversion in the Ca^+ ion depending on the N_2^+ quantum state, and solve the equation obtained from the parameter reduction to get the mean Rabi frequency $\overline{\Omega}$ as a function of the beam radius w.

As can be seen from the red curves in Fig. 6.7, a linear dependence of the mean Rabi frequency $\overline{\Omega}$ on the beam radius w is obtained. Along with this *required* mean Rabi frequency, we also show in Fig. 6.7 the *achievable* mean Rabi frequency (blue curves), i.e., the mean Rabi frequency achieved for a given beam radius at a certain beam power as obtained from the values shown in Fig. 6.5.

For a point on one of the blue curves to the left of the intersection with a chosen red one, the required Rabi frequency is lower than the one achievable for the respective beam power. Hence, realization is possible under these conditions. On the contrary, for points to the right of this intersection, the

[13] From equation (6.83), the reader might be tempted to infer that the same phase could be achieved with a lower Rabi frequency (and hence lower beam power) when increasing the pulse duration T. However, since the ions then are exposed to radiation for a longer period of time, the ratio of the detuning to the Rabi frequency must be increased as well in order to keep the scattering probability ϵ at a given value. Therefore, no reduction in the Rabi frequency is accomplished.

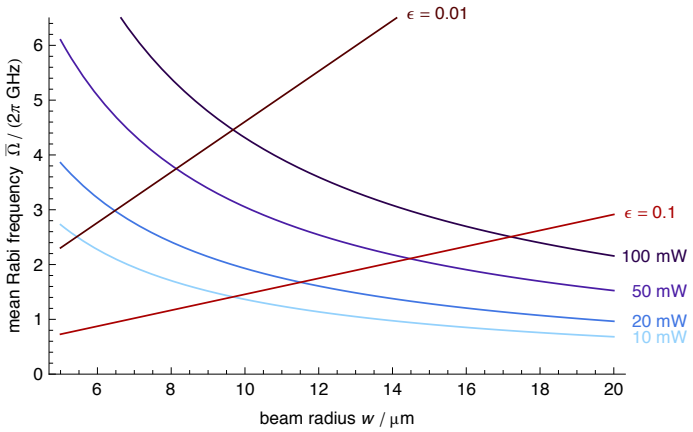

Figure 6.7. Mean Rabi frequencies as a function of the beam radius. The two red lines show the mean Rabi frequency $\overline{\Omega}$ needed to accumulate a phase of $\phi_{12} = \pi$ as a function of the beam radius w ($= w_{Ca^+} = w_{N_2^+}$) for a scattering probability of $\epsilon = 0.1$ and $\epsilon = 0.01$, respectively. As the intensity gradient—and hence the optical dipole force—decreases with increasing beam radius, the Rabi frequency required for the given phase increases with the beam radius. The blue curves show the mean Rabi frequencies obtained as a function of the beam radius for the given laser beam power. A beam radius smaller than at the intersection of a red with a blue curve indicates that the Rabi frequency is high enough to realize the geometric phase gate for the respective beam power and the scattering probability. For a beam radius larger than this limiting value, the achievable Rabi frequency is too low for the two-ion system to accumulate the phase needed without exceeding the chosen scattering probability, i.e., realization is not possible for the given parameters.

required mean Rabi frequency exceeds the one achievable with the given beam power, i.e., the proposed phase gate cannot be realized under these conditions.

For an eligible beam radius and beam power, the mean Rabi frequency $\overline{\Omega}$ needed, can be realized with various individual Rabi frequencies for the two ions and these are associated with different detunings. As two representative examples, we study here the laser beam powers of 50 mW and 100 mW at $\epsilon = 0.01$. The maximum possible beam radii for these values are 8.1 μm and 9.7 μm, respectively. These values lie in a regime feasible when using frequency doubled, amplified diode lasers and common optical components for beam shaping and focusing. The mean Rabi frequencies at these maximum beam radii are $\overline{\Omega} = 3.75$ GHz and $\overline{\Omega} = 4.46$ GHz, for 50 mW and 100 mW, respectively. These mean Rabi frequencies may be achieved by any combination of individual Rabi frequencies Ω_{Ca^+} and $\Omega_{N_2^+}$ obeying $\Omega_{Ca^+}\Omega_{N_2^+} = \overline{\Omega}^2$. This mutual inverse-proportional dependence of the two Rabi frequencies is shown in Fig. 6.8.

Having chosen suitable Rabi frequencies, appropriate detunings Δ_{Ca^+}, $\Delta_{N_2^+}$ are to be determined. Owing to equation (6.87), the detunings of both ions depend linearly on the respective Rabi frequencies for a chosen scattering probability ϵ: $\Delta_{Ca^+} \propto \Omega_{Ca^+}$, $\Delta_{N_2^+} \propto \Omega_{N_2^+}$. However, since the Rabi frequencies of the two ions are inversely proportional to each other, the same is true for the detunings: $\Delta_{Ca^+} \propto 1/\Delta_{N_2^+}$. These dependencies are depicted in Fig. 6.9 showing the detuning for the Ca^+ ion (left vertical axis) with respect to the Rabi frequency for that ion (bottom horizontal axis) together with the respective quantities for the N_2^+ ion on the non-linear top and right axis.[14]

[14]Here, the detunings are assumed to be positive. As seen from equation (6.83), a change in the sign of one of the two detunings results in a sign change of the acquired phase ϕ_{12}, which is of no relevance. Hence, our discussion is also valid for negative detunings, when the figures given are understood as absolute values. In an actual implementation, detunings are to be chosen such that the coupling to levels beside those described by the two-level model are minimized.

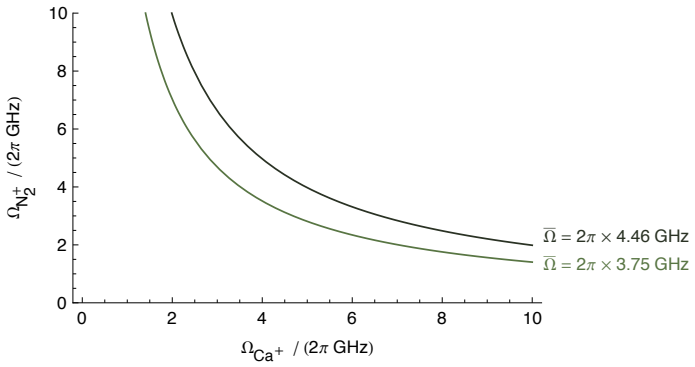

Figure 6.8. Individual Rabi frequencies of the logic and the spectroscopy ion. A given mean Rabi frequency $\overline{\Omega}$ may be achieved with different individual Rabi frequencies Ω_{Ca^+}, $\Omega_{\mathrm{N}_2^+}$ depending inversely proportional on each other. Here, this dependence is shown for the two beam radii of $w = 8.1\,\mu\mathrm{m}$ and $w = 9.7\,\mu\mathrm{m}$, the maximum values for beam powers of 50 mW and 100 mW, respectively, corresponding to $\overline{\Omega} = 2\pi \times 3.75\,\mathrm{GHz}$ (lower trace) and $\overline{\Omega} = 2\pi \times 4.46\,\mathrm{GHz}$ (upper trace).

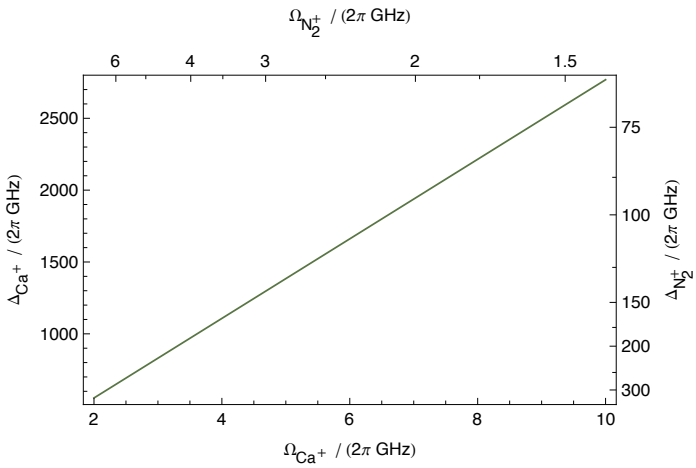

Figure 6.9. Detunings for the logic and the spectroscopy ion as a function of Rabi frequencies. The detuning for the Ca^+ ion is proportional to the Rabi frequency of that ion, as shown here by the bottom and the left axis. The same holds for the N_2^+ ion, as seen from the top and right axis. The Rabi frequency and the detuning of the N_2^+ ion, however, are inversely proportional to the respective quantities of the Ca^+ ion, as may be seen by the non-linear top and right axis. Values shown apply for $\overline{\Omega} = 2\pi \times 3.75\,\mathrm{GHz}$.

Finally, we may analyze the scaling of the experimental parameters with the secular axial trapping frequency ω. As may be derived from equation (6.83) and the definition of $\overline{\Omega}$, the mean Rabi frequency $\overline{\Omega}$ scales linearly with ω (and so do Ω_{Ca^+}, $\Omega_{\mathrm{N}_2^+}$, Δ_{Ca^+} and $\Delta_{\mathrm{N}_2^+}$). Therefore, the above results may be easily adapted for different axial trapping frequencies. By reducing ω, the required Rabi frequencies—and so the beam powers needed—could be decreased. However, as the value used above is already at the lower end of the typical range ion traps are operated with, a further reduction might affect stable trapping and laser cooling. Also, the wave packet size of the ions at a given temperature increases for less tight trapping, rendering them prone to spatial inhomogeneities of optical dipole forces induced by Gaussian laser beams (see below).

6.3.4 Experimental imperfections

So far we have studied our proposed state-detection method by means of one-dimensional harmonic oscillators, quasi-classical states and spatially constant forces. In reality, the ions move in three-dimensional space and are trapped by time-varying electric fields that only on time-average result in a (nearly) harmonic effective potential. Moreover, following Doppler laser cooling, motional degrees of freedom of the ions are described by a thermal density operator rather than by quasi-classical states [205]. We will shortly discuss these experimental imperfections, namely finite-temperature and micromotion effects, in a qualitative way.

In principle, ions in thermal states evolve in our state-detection scheme as shown here for quasi-classical states, as can be shown by expressing the thermal states in terms of quasi-classical states and exploiting the independence of the acquired phase from the initial phase-space position. Therefore, our state-detection technique is temperature-independent. This reasoning, however, only applies for spatially constant forces. The optical dipole forces exerted by Gaussian laser beams are only (approximately) constant within a region around $r = \pm w/2$ small compared to the beam radius w (see Fig. 6.6).[15] So, for our model to be applicable, the spread of the ion wave packets must be small compared to the beam radii. For a thermal state, this wave packet size increases with temperature. At the Doppler cooling limit of Ca^+ (0.5 mK), the root-mean-square wave packet size is roughly half a micrometer.[16] Therefore, this limit is met for the beam radii studied above.[17] Insensitivity to ion temperature might be improved by using less tightly focused laser beams—at the expense of a higher beam power needed.

As explained in Ch. 4, ions are trapped in an rf ion trap by oscillating electric fields creating on time average a confining effective potential. Ions trapped that way always oscillate at the rf drive frequency except if they are exactly at the rf null line. In other words, they exhibit "micromotion". In case of parasitic electric fields (known as "patch potentials" [206]) or spurious phase shifts between rf voltages on different trap electrodes, the equilibrium positions of the ions might be offset from the rf null line resulting in "excess micromotion". Unless such effects are perfectly canceled [123], the ions in practice steadily exhibit a non-vanishing micromotion amplitude. In our state-detection scheme, micromotion results in a modulation of the forces exerted on the ions—and hence of the phase acquired—at the rf frequency. Since the rf period is short compared to the laser pulse duration and since the laser intensity is continuously increased and decreased, the total accumulated phase is averaged over many micromotion cycles, reducing the effect of micromotion on the accumulated phase.

Concluding, we see that the simplified discussion of our proposed state-detection method given here describes the relevant effects adequately. Deviations from this simplified model should not pose any serious issues for an actual implementation.

[15] Since the second derivative of the intensity vanishes at the point of maximum intensity gradient, this position is not only optimal in terms of the magnitude of the force, but also regarding its spatial homogeneity.

[16] The root-mean-square wave packet size of a harmonic oscillator with angular frequency ω and mass m in thermal equilibrium at absolute temperature T_{abs} is ([72], p. 577),

$$\sqrt{\langle \hat{x}^2 \rangle} = \sqrt{\frac{\hbar}{2m\omega} \coth \frac{\hbar\omega}{2k_{\mathrm{B}}T_{\mathrm{abs}}}},$$

with k_{B} the Boltzmann constant.

[17] An analogous criterion applies for the wave packet size in direction of the laser beam. Here, the relevant beam parameter is the Rayleigh range ([58], pp. 76 f.), which accounts for a few hundred micrometers for the parameters studied above, and hence results in an even less restrictive limit than the radial criterion.

6.4 Summary and conclusion

In this chapter, a non-destructive state-detection technique for trapped molecular ions has been studied. The proposed method is based on geometric quantum phases induced by transient, state-dependent forces. Non-destructive state detection is essential for future high-precision experiments with trapped molecular ions, as it allows efficient detection of their quantum state, eliminates the need for trap reloading and renders single-ion experiments possible.

Implementation of the proposed scheme with optical dipole forces induced by off-resonant, focused Gaussian laser beams has been found feasible. Effects of finite ion temperature and micromotion amplitude have been qualitatively discussed. As far as may be judged from this discussion, they do not seem to pose serious difficulties for an actual realization.

Our proposed state-detection technique competes with other proposed [187, 40, 188, 189, 41, 190, 42, 43] or even already realized [44] non-destructive state-detection methods for molecular ions. Future developments will tell, which of these turn out to be most suitable for actual high-precision experiments with molecular ions.

Chapter 7

Conclusion and Outlook

In this thesis, electric-dipole-forbidden rotation-vibration transitions in homonuclear diatomic molecular ions have been studied. As these transitions are very weak, their observation is challenging. On the other hand, they exhibit extremely low natural linewidths and, correspondingly, long lifetimes of excited states. Therefore, they are of interest to precision spectroscopy and studying fundamental scientific questions, most prominently a possible variation of the proton-to-electron mass ratio.

We have started our discussion of forbidden transitions with their underlying physical mechanism. Based on quantum mechanical perturbation theory, we have discussed the physics of electric-quadrupole transitions in a clear and consistent way. We have compiled knowledge distributed in the atomic and molecular spectroscopy literature and rigorously derived results usually only found without derivation. Moreover, we have given a description of rotation-vibration transitions in terms of the multipole moments of the molecular charge distribution—a description without an analogue in atomic spectroscopy and hence not found in common textbook explanations of forbidden transitions.

Concerning fine and hyperfine structure in electric-quadrupole rotation-vibration spectra, we have calculated the relative intensities of fine- and hyperfine-resolved lines. These calculations are based on the separability of angular and vibronic coordinates and the treatment of the former by spherical tensor algebra.

At the heart of this thesis lies the observation of electric-quadrupole rotation-vibration transitions in the homonuclear molecular nitrogen cation N_2^+—to our knowledge the first observation of a dipole-forbidden vibrational transition in a molecular ion. This observation has been achieved by combining a number of advanced techniques from atomic and molecular physics, such as trapping, sympathetic cooling and state-selective production of molecular ions, use of a frequency-stabilized quantum cascade laser for rotational-vibrational excitation as well as of a highly sensitive charge transfer reaction for detection of vibrationally excited ions.

By analyzing the measured spectrum with the known fine- and hyperfine-structure Hamiltonian of N_2^+ and spectroscopic constants from the literature [96, 102], we were able to assign the observed spectral features and thus to prove observation of electric-quadrupole rotation-vibration transitions.

Therefore, we may conclude that the extremely weak electric-quadrupole rotation-vibration transitions in trapped and cooled homonuclear diatomic molecular ions may be addressed with our experimental approach.

The intensity of the lines remains an open issue. The measured spectrum shows deviations in the line intensities from theoretical expectations, both in absolute as well as relative terms. An in-depth analysis has revealed possible reasons for this discrepancy, first and foremost rotationally inelastic N_2^+-Ar collisions prior to excitation. However, further investigation is needed to draw a definitive conclusion on this issue.

Spectra of molecular ions produced by photoionization, such as the N_2^+ electric-quadrupole rotation-vibration spectrum presented here, depend on the ionic fine and hyperfine ground-state population, i.e., on the ion production method. We have developed a model to predict these populations for ions produced by molecular photoionization. This model is based on incorporation of fine- and hyperfine-structure effects in the model for rotationally resolved photoionization from Buckingham, Orr and Sichel [148]. Concerning its physical content, our model capitalizes on the separability of electron and nuclear spin states from the vibronic photoionization matrix element.

We have first developed our ionization model for direct, one-photon, ionization. In that form it has been successfully applied to the fine-structure-resolved photoelectron spectrum of oxygen from Palm and Merkt [152]. Thereafter, we have extended our model to the [2+1'] resonance-enhanced multiphoton ionization (REMPI) of nitrogen used in our experiment. In the particular case of N_2^+ produced in the rotational ground state with the present non-hfs-resolved ionization scheme, we found an identical distribution of the N_2^+ population on the ionic hfs-levels as for a thermal ion population. For other ionic rotational states, we found propensities for preferential formation of ions in certain hfs levels for ionization from particular hfs levels of the neutral electronically excited state utilized in REMPI. Employing spectrally narrower lasers for REMPI, we might be able to exploit these propensities for preparation of N_2^+ ions in selected ionic hyperfine levels.

Finally, we have studied a novel, non-destructive state-detection technique for repeated interrogation of a single molecular ion by a cotrapped atomic ion. This technique is based on geometric quantum phases induced by optical dipole forces acting on the hybrid atomic-molecular two-ion system. With tailored forces, the quantum state of the molecular ion is mapped onto the atomic one. From the latter, the state is detected through probing a closed optical cycling transition.

By estimating the relevant experimental parameters, such as laser powers, laser beam radii and laser frequency detunings, we have assessed feasibility of the proposed method. Moreover, we have qualitatively discussed experimental imperfections, in particular finite-temperature and micromotion effects, and found them not to impose serious issues for an experimental implementation.

The path to follow for future experiments is as obvious as it is challenging: with spectrally narrower mid-IR radiation sources, the exceptionally small natural linewidth of electric-quadrupole vibrational transitions might be exploited. By means of a non-destructive state-detection method, repeated measurements of such a transition in a single molecular ion should be within reach. Ultimately, we could then become able to achieve the accuracy and precision needed to investigate effects of interest to fundamental physics, such as a possible variation of the proton-to-electron mass ratio, through measurement of electric-dipole-forbidden rotation-vibration transitions in a trapped, cooled molecular ion. Obviously, this is a project for years, if not decades, and represents a formidable challenge—but one worth the effort.

Appendix A

Definitions of and units for the electric-quadrupole moment

A.1 Definitions

There are several different definitions for the Cartesian electric-quadrupole moment tensor used in the literature. They differ by constant factors and whether or not they are given in traceless form. Furthermore, different authors either use the form for a set of discrete, pointlike charges or for a continues charge distribution. The following three definitions are among the most often used ones. They are given here for a tuple of N pointlike particles with charges q_j $(j = 1, ..., N)$ and position vectors $\mathbf{r}_j$ with Cartesian components $r_{j,\alpha}, r_{j,\beta}$, $(\alpha, \beta = x, y, z)$:

$$Q^{(\mathrm{I})}_{\alpha\beta} = \sum_{j=1}^{N} q_j \left(r_{j,\alpha} r_{j,\beta} - \delta_{\alpha\beta} \frac{r_j^2}{3} \right), \tag{A.1}$$

$$Q^{(\mathrm{II})}_{\alpha\beta} = \frac{1}{2} \sum_{j=1}^{N} q_j \left(3 r_{j,\alpha} r_{j,\beta} - \delta_{\alpha\beta} r_j^2 \right), \tag{A.2}$$

$$Q^{(\mathrm{III})}_{\alpha\beta} = \sum_{j=1}^{N} q_j \left(3 r_{j,\alpha} r_{j,\beta} - \delta_{\alpha\beta} r_j^2 \right). \tag{A.3}$$

Definition (I) is used by Bunker and Jensen [67][1] and Condon and Shortly [49][2]. This definition has been adopted for this text. Definition (II) is also used frequently in the spectroscopic literature, such as in [80, 75]. Definition (III) is found in general textbooks on electromagnetism [207].

These definitions are related to each other according to:

$$Q^{(\mathrm{I})}_{\alpha\beta} = \frac{2}{3} Q^{(\mathrm{II})}_{\alpha\beta} = \frac{1}{3} Q^{(\mathrm{III})}_{\alpha\beta}. \tag{A.4}$$

Apart from different definitions used, the value of the molecular quadrupole moment might also depend

[1] In the definition of the quadrupole moment in [67] (equation (14-108) on p. 460) the charge is squared, which obviously is a misprint.

[2] In [49] the quadrupole moment is first defined in a non-traceless form ([49], p. 85). Later the traceless form is adopted for the calculation of spectroscopic transitions ([49], pp. 94 ff.).

on the origin of coordinates the calculation refers to, since only the lowest-order non-vanishing moment of a multipole expansion is independent of the point of origin. The quadrupole moment thus depends on the origin chosen, if the molecule posses a monopole (as for a molecular ion) or a dipole moment. For the calculation of vibrational line strengths, the origin should be chosen at the molecular centre of mass, as this is the origin resulting from the separation of the translational motion of the molecule (see [67], p. 416). Nonetheless, molecular multipole moments are sometimes calculated with respect to the geometrical centre of the molecule (e.g. in [75]). In the case of N_2^+, these two possible points of origin coincide for symmetry reasons.

A.2 Units

The SI unit for an electric-quadrupole moment is $1\,\mathrm{C\,m^2}$. As typical molecular quadrupole moments are many orders of magnitude smaller than this unit, they are usually reported in atomic units, i.e., in multiples of ea_0^2 (e: elementary charge, a_0: Bohr radius). Another unit used for electric-quadrupole moments is $1\,\mathrm{D\mathring{A}}$ (1 Debye Ångström), also known as "one Buckingham" ($1\,\mathrm{B}$).

Expressed in SI units, these units account for:

$$1\,ea_0^2 = 4.487 \times 10^{-40}\,\mathrm{C\,m^2}, \tag{A.5}$$

$$1\,\mathrm{D\mathring{A}} = 0.7435\,ea_0^2 = 3.336 \times 10^{-40}\,\mathrm{C\,m^2}. \tag{A.6}$$

Appendix B

Excitation rate calculation

In the following, the electric-quadrupole excitation rate for the IR fundamental S(0) transition[1] $F'' = 3/2 \rightarrow \widetilde{J}' = 5/2, F' = 7/2$ in N_2^+ and the lifetime of the excited $v' = 1, \widetilde{J}' = 5/2, F' = 7/2$ state is calculated.

Numerical evaluation of equation (3.74) for this transition using the coefficients from Tab. 3.3 yields

$$S_{F''=3/2,\widetilde{J}'=5/2,F'=7/2} = 0.3186 \left| \left\langle \mathrm{X}, v' = 1 \left| \, \mathrm{T}_0^2 \left[\hat{\mathrm{Q}}^{(\mathrm{m})} \right] \right| \mathrm{X}, v'' = 0 \right\rangle \right|^2 . \tag{B.1}$$

The vibrational transition matrix element in Cartesian tensor notation (see equation (3.34)) is given by

$$\left\langle \mathrm{X}, v' = 1 \left| \, \mathrm{T}_0^2 \left[\hat{\mathrm{Q}}^{(\mathrm{m})} \right] \right| \mathrm{X}, v'' = 0 \right\rangle = \sqrt{\frac{3}{2}} \left\langle v' = 1 \left| \, \hat{Q}^{(\mathrm{m})}_{\mathrm{X},zz} \right| v'' = 0 \right\rangle . \tag{B.2}$$

According to equation (2.237) the above matrix element is evaluated in the double-harmonic approximation as

$$\left\langle v' = 1 \left| \, \hat{Q}^{(\mathrm{m})}_{\mathrm{X},zz} \right| v'' = 0 \right\rangle = \left. \frac{\mathrm{d}Q^{(\mathrm{m})}_{\mathrm{X},zz}}{\mathrm{d}R} \right|_{R=R_\mathrm{e}} R_\mathrm{e} \sqrt{\frac{\widetilde{B}_\mathrm{e}}{\widetilde{\omega}_\mathrm{e}}} . \tag{B.3}$$

Since we are not aware of any experimental data for the derivative of the electric quadrupole moment in N_2^+, we used the value from the theoretical study by Bruna and Grein [45]. They reported a value of $\mathrm{d}Q^{(\mathrm{m,\ B\&G})}_{\mathrm{X},zz}/\mathrm{d}R|_{R_\mathrm{e}} = 2.63\, ea_0$ (p. 73 in [45]). Unfortunately, it is not clearly stated which definition (see Appendix A.1) for the molecular quadrupole moment has been used in [45]. By comparing the values for the quadrupole moment of *neutral* N_2 also given in [45] with those reported in [80], it may be inferred that the same definition has been used in these two studies, namely Def. (II) in Appendix A.1. When converted to the definition used in Ch. 2 (Def. (I) in Appendix A.1), this value corresponds to $\mathrm{d}Q^{(\mathrm{m})}_{\mathrm{X},zz}/\mathrm{d}R|_{R_\mathrm{e}} = 1.75\, ea_0$.

Using this value together with the quantities $R_\mathrm{e} = 2.13\, a_0$, $\widetilde{\omega}_\mathrm{e} = 2140\,\mathrm{cm}^{-1}$ (from Tab. 1 in [45]) and $\widetilde{B}_\mathrm{e} = 1.93\,\mathrm{cm}^{-1}$ (from [98]), we obtain

$$\left\langle v' = 1 \left| \, \hat{Q}^{(\mathrm{m})}_{\mathrm{X},zz} \right| v'' = 0 \right\rangle = 0.112\, ea_0^2 . \tag{B.4}$$

[1] To keep the notation simple, the $^+$ superscript is omitted in this section. As no states of neutral N_2 are considered, no confusion should occur.

The line strength for the $F'' = 3/2 \leftrightarrow \widetilde{J}' = 5/2, F' = 7/2$ transition thus accounts for

$$S_{F''=3/2,\widetilde{J}'=5/2,F'=7/2} = 6.01 \times 10^{-3}\, e^2 a_0^4 = 1.21 \times 10^{-81}\,\mathrm{C^2 m^4}. \tag{B.5}$$

The Einstein A-coefficient is given by the line strength according to equation (2.131) as

$$A_{\widetilde{J}',F'\to F''} = \frac{8\pi^5}{5\varepsilon_0 h\lambda^5}\frac{1}{g'} S_{F'',\widetilde{J}',F'}, \tag{B.6}$$

and the Einstein $B^{(\nu)}_{F''\to\widetilde{J}',F'}$-coefficient[2] is calculated from the Einstein $A_{\widetilde{J}',F'\to F''}$-coefficient according to

$$B^{(\nu)}_{F''\to\widetilde{J}',F'} = \frac{g'}{g''}\frac{\lambda^3}{8\pi h} A_{\widetilde{J}',F'\to F''}. \tag{B.7}$$

Here, g' and g'' denote the degeneracy in the upper and lower level, respectively. For the transition studied, we have $\lambda = 1/(2186.1804\,\mathrm{cm^{-1}}) = 4574\,\mathrm{nm}$, $g' = 2F'+1 = 8$ and $g'' = 2F''+1 = 4$ resulting in

$$A_{\widetilde{J}'=5/2,F'=7/2\to F''=3/2} = 6.30 \times 10^{-9}\,\mathrm{s^{-1}} \tag{B.8}$$

and

$$B^{(\nu)}_{F''=3/2\to\widetilde{J}'=5/2,F'=7/2} = 7.24 \times 10^{7}\,\mathrm{s^{-1}(Jm^{-3}Hz^{-1})^{-1}}. \tag{B.9}$$

The vibrational excitation rate $R_{F''\to\widetilde{J}',F'}$ per ion is given by the Einstein B-coefficient multiplied with the spatial and spectral energy density $\rho^{(\nu)}$:

$$R_{F''\to\widetilde{J}',F'} = B_{F''\to\widetilde{J}',F'}\rho^{(\nu)}. \tag{B.10}$$

As mentioned in Sec. 4.2.5, the effective IR beam power of 170 mW at a FWHM beam diameter of 140 µm yields an irradiance of $7.7 \times 10^6\,\mathrm{W\,m^{-2}}$ at the beam centre. Assuming a Gaussian spectral profile with a FWHM bandwidth of 19 MHz (as obtained from the measured spectrum) this translates into a spectral irradiance of $0.38\,\mathrm{W\,m^{-2}\,Hz^{-1}}$ or, when divided by the speed of light, to a spectral and spatial energy density[3] of $\rho^{(\nu)} = 1.3 \times 10^{-9}\,\mathrm{J\,m^{-3}\,Hz^{-1}}$.

Substituting this value into (B.10) yields an excitation rate for the electric-quadrupole S(0), $v'' = 0, F'' = 3/2 \to v' = 1, \widetilde{J}' = 5/2, F' = 7/2$ transition of

$$R_{F''=3/2\to\widetilde{J}'=5/2,F'=7/2} = 9.14 \times 10^{-2}\,\mathrm{s^{-1}} \tag{B.11}$$

per ion.

In order to estimate the natural linewidth and the lifetime of the excited $F' = 7/2, \widetilde{J}' = 5/2$ state, the total decay rate, including the decay to both hyperfine components of the ground state, has to be considered. This results in a life time of $\tau_{F'=7/2,\widetilde{J}'=5/2} = 3.16 \times 10^7\,\mathrm{s}$ or 366 days, corresponding to a natural linewidth of 5.03 nHz FWHM.

[2] Contrary to Ch. 2, the Einstein B-coefficient used here is defined with respect to the energy density per frequency interval instead for per *angular* frequency interval. This is indicated by the superscript $^{(\nu)}$. Denoting the coefficient used in Ch. 2 as $B^{(\omega)}$ and using the equations $B^{(\nu)}\rho^{(\nu)} = B^{(\omega)}\rho^{(\omega)}$ and $\rho^{(\omega)}\mathrm{d}\omega = \rho^{(\nu)}\mathrm{d}\nu$ (with ρ the spatial and spectral energy density and $\omega = 2\pi\nu$), the relation $B^{(\nu)} = B^{(\omega)}/(2\pi)$ is found.

[3] In accordance with the Einstein B-coefficient, the energy density is given per frequency interval and not per *angular* frequency interval, as indicated by the superscript $^{(\nu)}$.

Appendix C

Relations from tensor algebra

C.1 Relations for the Wigner 6j-symbol

Based on the definition of the 6j-symbol, one may show the relation (see equation (4.15) in [61]):

$$\begin{Bmatrix} j_1 & j_2 & j_3 \\ j_4 & j_5 & j_6 \end{Bmatrix} \begin{pmatrix} j_5 & j_1 & j_6 \\ m_5 & m_1 & m_6 \end{pmatrix} = \sum_{m_2,m_3,m_4} (-1)^{j_1+j_2-j_3+j_4+j_5+j_6-m_1-m_4} \begin{pmatrix} j_1 & j_2 & j_3 \\ m_1 & m_2 & -m_3 \end{pmatrix} \begin{pmatrix} j_4 & j_5 & j_3 \\ m_4 & m_5 & m_3 \end{pmatrix} \begin{pmatrix} j_2 & j_4 & j_6 \\ m_2 & m_4 & -m_6 \end{pmatrix}. \tag{C.1}$$

Using the symmetries of the 3j-symbols the following expression is derived:

$$\begin{Bmatrix} j_1 & j_2 & j_3 \\ j_4 & j_5 & j_6 \end{Bmatrix} \begin{pmatrix} j_5 & j_1 & j_6 \\ m_5 & m_1 & m_6 \end{pmatrix} (-1)^{-j_1-j_2+j_3-j_4-j_5-j_6+m_1} = \sum_{m_2,m_3,m_4} (-1)^{-m_4} \begin{pmatrix} j_3 & j_1 & j_2 \\ -m_3 & m_1 & m_2 \end{pmatrix} \begin{pmatrix} j_3 & j_4 & j_5 \\ m_3 & m_4 & m_5 \end{pmatrix} \begin{pmatrix} j_2 & j_4 & j_6 \\ m_2 & m_4 & -m_6 \end{pmatrix}. \tag{C.2}$$

C.2 Relation for the Wigner 9j-symbol

According to [76], p. 144, the following relation holds for the 9j-symbol:

$$\sum_{m_6,m_9,m_4,m_7} \begin{pmatrix} j_3 & j_6 & j_9 \\ m_3 & m_6 & m_9 \end{pmatrix} \begin{pmatrix} j_1 & j_4 & j_7 \\ m_1 & m_4 & m_7 \end{pmatrix} \begin{pmatrix} j_4 & j_5 & j_6 \\ m_4 & m_5 & m_6 \end{pmatrix} \begin{pmatrix} j_7 & j_8 & j_9 \\ m_7 & m_8 & m_9 \end{pmatrix} = \sum_{j_2} (2j_2+1) \begin{pmatrix} j_1 & j_2 & j_3 \\ m_1 & m_2 & m_3 \end{pmatrix} \begin{pmatrix} j_2 & j_5 & j_8 \\ m_2 & m_5 & m_8 \end{pmatrix} \begin{Bmatrix} j_1 & j_2 & j_3 \\ j_4 & j_5 & j_6 \\ j_7 & j_8 & j_9 \end{Bmatrix}. \tag{C.3}$$

Appendix D

Calculation of Rabi frequencies

D.1 Definition

Regarding a quantum mechanical two-level system with lower state $|\mathrm{a}\rangle$ and upper state $|\mathrm{b}\rangle$ that couples via the electric-dipole operator $\hat{\boldsymbol{\mu}}$ to an electric field $\mathbf{E}(t) = E_0 \mathbf{e}_0 \cos(\omega t)$ oscillating as a function of time t at angular frequency ω with amplitude $E_0 > 0$ and unit polarization vector $\mathbf{e}_0$, we define the Rabi frequency [200, 208, 128] as:

$$\Omega = \left| \frac{E_0}{\hbar} \langle \mathrm{b} \,|\, \hat{\boldsymbol{\mu}} \cdot \mathbf{e}_0 \,|\, \mathrm{a} \rangle \right| . \tag{D.1}$$

Assuming linearly, z-polarized radiation, i.e., $\mathbf{e}_0 = (0, 0, 1)$, we have $\hat{\boldsymbol{\mu}} \cdot \mathbf{e}_0 = \hat{\mu}_z = \mathrm{T}^1_0[\hat{\boldsymbol{\mu}}]$ with $\mathrm{T}^1_0[\hat{\boldsymbol{\mu}}]$ the zero component of the space-fixed electric-dipole operator understood as a first-rank spherical tensor operator.

The Rabi frequency hence is:

$$\Omega = \frac{E_0}{\hbar} \left| \langle \mathrm{b} \,|\, \mathrm{T}^1_0[\hat{\boldsymbol{\mu}}] \,|\, \mathrm{a} \rangle \right| . \tag{D.2}$$

In the context of the state-detection method discussed in Ch. 6, the state $|\mathrm{a}\rangle$ corresponds to the ground state $|\mathrm{g}\rangle$ and the state $|\mathrm{b}\rangle$ to the auxiliary excited state $|\mathrm{aux}\rangle$.

Usually the upper and lower level are degenerate and particular states of these levels are characterized by the space-fixed projections m' and m'' belonging to the upper and lower angular momentum quantum numbers j' and j'', respectively. The Rabi frequency may then be written as,

$$\Omega = \frac{E_0}{\hbar} \left| \langle j' m' \,|\, \mathrm{T}^1_0[\hat{\boldsymbol{\mu}}] \,|\, j'' m'' \rangle \right| . \tag{D.3}$$

In this notation, angular momentum and spherical tensor algebra may be used to derive the electric-dipole operator matrix elements from tabulated quantities such as Einstein A-coefficients or pure vibronic dipole-operator matrix elements.

As the Rabi frequency scales linearly with the electric field amplitude E_0, we will below calculate the quantity Ω/E_0 corresponding to the Rabi frequency at unit electric field amplitude. Thereafter, we derive the field amplitude at a certain position in a Gaussian laser beam and get the actual Rabi frequency as the product of these two quantities.

D.2 Calcium ion

The optical dipole force exerted on the Ca^+ ion is (mainly) induced through the coupling of the ground level $4^2S_{1/2}$ by the electromagnetic radiation to the excited $4^2P_{1/2}$ level.[1] Hence, the states $|j''m''\rangle$ and $|j'm'\rangle$ in (D.3) are Zeeman states of these two levels. The magnitude of the dipole matrix elements between them is obtained from the known Einstein A-coefficient as follows: the matrix elements appearing in (D.3) for different projection quantum numbers are related among each other by the Wigner-Eckart theorem [61],

$$\left\langle j'm' \left| \mathrm{T}^1_p\left[\hat{\boldsymbol{\mu}}\right] \right| j''m'' \right\rangle = (-1)^{j'-m'} \begin{pmatrix} j' & 1 & j'' \\ -m' & p & m'' \end{pmatrix} \left\langle j' \left\| \mathrm{T}^1_{\cdot}\left[\hat{\boldsymbol{\mu}}\right] \right\| j'' \right\rangle, \tag{D.4}$$

with $\left\langle j' \left\| \mathrm{T}^1_{\cdot}\left[\hat{\boldsymbol{\mu}}\right] \right\| j'' \right\rangle$ the "reduced matrix element".

From the definition of the Einstein A-coefficient,

$$A_{j'\to j''} = \frac{8\pi^2}{3\varepsilon_0 \hbar \lambda^3} \sum_{p=-1}^{1} \sum_{m''=-j''}^{j''} \left| \left\langle j'm' \left| \mathrm{T}^1_p\left[\hat{\boldsymbol{\mu}}\right] \right| j''m'' \right\rangle \right|^2, \tag{D.5}$$

together with the Wigner-Eckart theorem and the properties of the Wigner 3j-symbols [61], the magnitude of the reduced matrix element may be expressed as:

$$\left| \left\langle j' \left\| \mathrm{T}^1_{\cdot}\left[\hat{\boldsymbol{\mu}}\right] \right\| j'' \right\rangle \right|^2 = \frac{3\varepsilon_0 \hbar \lambda^3}{8\pi^2} (2j'+1) A_{j'\to j''}. \tag{D.6}$$

Here, λ is the wavelength of the transition and ε_0 the vacuum permittivity.

Substituting these results into (D.3), we obtain the Rabi frequency for linearly polarized radiation (and hence $m' = m''$) as,

$$\Omega = E_0 \left| \begin{pmatrix} j' & 1 & j'' \\ -m'' & 0 & m'' \end{pmatrix} \right| \sqrt{\frac{3\varepsilon_0 \lambda^3}{8\pi^2 \hbar} (2j'+1) A_{j'\to j''}}. \tag{D.7}$$

For the $4^2S_{1/2} - 4^2P_{1/2}$ transition, we have $j' = j'' = 1/2$ and $m'' = \pm 1/2$. Since the magnitude of the 3j-symbol in (D.7) is invariant under a change of the lower-row signs (see equation (2.31) in [61]), we may chose without loss of generality $m'' = 1/2$.

Using the values $\lambda = 396.958\,65\,\mathrm{nm}$ and $A_{4^2P_{1/2}\to 4^2S_{1/2}} = 132 \times 10^6\,\mathrm{s}^{-1}$ from [195], p. 146, we obtain the Rabi frequency at unit electric field amplitude as,

$$\frac{\Omega_{Ca^+}}{E_0} = 9.4 \times 10^4\,\mathrm{s}^{-1}(\mathrm{Vm}^{-1})^{-1}. \tag{D.8}$$

[1] We neglect here the optical dipole force due to the coupling of the ground level to the $4^2P_{3/2}$ level. The relative contribution to the total optical dipole force due to that transition increases with the (blue) detuning and accounts for roughly 10 to 20 % of the total force for the parameters used in Sec. 6.3. Given the uncertainty of the Einstein A-coefficient our calculation is based on of 10 % [195], this approximation seems reasonable.

D.3 Nitrogen ion

The dipole force exerted on the N_2^+ ion is induced by the coupling of the rovibronic ground level $X^2\Sigma_g^+$, $v''=0, N''=0$ to the auxiliary excited level $B^2\Sigma_u^+, v'=1, N'=1$. Here, v'' and N'' (v' and N') are the vibrational and rotational quantum number in the ground (auxiliary excited) state.

The excited level is split into two spin-rotation components with total angular momenta $J'=1/2$ and $J'=3/2$. Since the optical dipole force is induced with electromagnetic radiation far detuned from resonance, we may add the forces created by the coupling to both spin-rotation components. We will do so by first working out the Rabi frequency of both components separately and later combining them into an effective Rabi frequency to describe the total force.

The electric-dipole operator matrix elements of the $X^2\Sigma_g^+, v''=0 - B^2\Sigma_u^+, v'=1$ transition are calculated in a similar way as shown for electric-quadrupole transitions in Ch. 3. Their squared absolute magnitude is:

$$\begin{aligned}
&\left|\left\langle B^2\Sigma_u^+, v'=1, N', J', M_J' \left| \mathrm{T}_p^1\left[\hat{\boldsymbol{\mu}}^{(\mathrm{s})}\right] \right| X^2\Sigma_g^+, v''=0, N'', J'', M_J'' \right\rangle\right|^2 \\
&\quad = (2N'+1)(2N''+1)(2J'+1)(2J''+1) \begin{pmatrix} N' & 1 & N'' \\ 0 & 0 & 0 \end{pmatrix}^2 \begin{pmatrix} J' & 1 & J'' \\ -M_J' & p & -M_J'' \end{pmatrix}^2 \\
&\qquad \begin{Bmatrix} N' & J' & 1/2 \\ J'' & N'' & 1 \end{Bmatrix}^2 \left|\left\langle B^2\Sigma_u^+, v'=1 \left| \mathrm{T}_0^1\left[\hat{\boldsymbol{\mu}}^{(\mathrm{m})}\right] \right| X^2\Sigma_g^+, v''=0 \right\rangle\right|^2 .
\end{aligned} \tag{D.9}$$

Here, $\mathrm{T}_0^1\left[\hat{\boldsymbol{\mu}}^{(\mathrm{s})}\right]$ and $\mathrm{T}_0^1\left[\hat{\boldsymbol{\mu}}^{(\mathrm{m})}\right]$ are the zero component of the electric-dipole operator in spherical tensor notation with respect to the space-fixed and the molecule-fixed frame, respectively. J'' and J' are the quantum numbers of the total angular momenta without nuclear spin in the ground and the auxiliary excited state and M_J', M_J'' the quantum numbers of the respective space-fixed projections.

The angular factors in (D.9) account for 1/9 for the transition $J''=1/2 \rightarrow J'=1/2$ and for 2/9 for the transition $J''=1/2 \rightarrow J'=3/2$.

The absolute magnitude of the vibronic matrix element is obtained in the "r-centroid approximation" [95] as,

$$\left|\left\langle B^2\Sigma_u^+, v' \left| \mathrm{T}_0^1\left[\hat{\boldsymbol{\mu}}^{(\mathrm{m})}\right] \right| X^2\Sigma_g^+, v'' \right\rangle\right|^2 = q_{v',v''} \left|R_e(\overline{r}_{v',v''})\right|^2 , \tag{D.10}$$

with the Franck-Condon factor $q_{v',v''}$ and the electronic transition moment $R_e(\overline{r}_{v',v''})$. Using the values from [95] (Tab. 15, p. 1072), we obtain:

$$\left|\left\langle B^2\Sigma_u^+, v'=0 \left| \mathrm{T}_0^1\left[\hat{\boldsymbol{\mu}}^{(\mathrm{m})}\right] \right| X^2\Sigma_g^+, v''=0 \right\rangle\right|^2 = 0.337 e^2 a_0^2. \tag{D.11}$$

The Rabi frequency at unit field amplitude for the two relevant transitions hence are,

$$\frac{\Omega_{J'=1/2}}{E_0} = 0.194 \frac{e a_0}{\hbar}, \tag{D.12a}$$

$$\frac{\Omega_{J'=3/2}}{E_0} = 0.274 \frac{e a_0}{\hbar}. \tag{D.12b}$$

The effective Rabi frequency for the N_2^+ ion defined as $\Omega_{N_2^+} = \sqrt{\Omega^2_{J'=1/2} + \Omega^2_{J'=3/2}}$ thus is:

$$\frac{\Omega_{N_2^+}}{E_0} = 0.335\frac{ea_0}{\hbar} = 2.7 \times 10^4\,\mathrm{s}^{-1}(\mathrm{Vm}^{-1})^{-1}. \tag{D.13}$$

The same result is obtained when entirely ignoring the electron spin and treating the transition as if it occurred between two $^1\Sigma$ states. Following the same argument, the effective Rabi frequency at a large detuning also is equal whether or not hyperfine structure is overlying spin-rotational structure.

Along the same lines as shown above for the Rabi frequency, the line strength and hence the natural linewidth of the transitions in the N_2^+ ion may be calculated. Using the value of $\lambda = 1/\tilde{\nu} = 1/(25\,564.7\,\mathrm{cm}^{-1})$ for the transition wavelength from [95], we obtain $\Gamma_{N_2^+} = 3.80 \times 10^6\,\mathrm{s}^{-1}$.

D.4 Electric field amplitude in a Gaussian laser beam

The electric field amplitude E_0 at a certain position of an electromagnetic wave is related to the intensity I at that position via,

$$I = \frac{1}{2}\varepsilon_0 c E_0^2. \tag{D.14}$$

For a Gaussian laser beam, the intensity within the beam profile is given by ([58], p. 79):

$$I(r) = \frac{2P_{\mathrm{tot}}}{\pi w^2} e^{-\frac{2r^2}{w^2}}, \tag{D.15}$$

with r the distance from the beam centreline, P_{tot} the total beam power and w the $1/e^2$ beam radius (the distance from the beam centreline, at which the intensity is reduced by a factor of $1/e^2$ from the value at the centreline).

The ions are assumed to be at the positions of maximum intensity gradient, $r = \pm w/2$, of the two beams. The intensity at these positions is,

$$I\left(r = \pm\frac{w}{2}\right) = \frac{2P_{\mathrm{tot}}}{\pi w^2} e^{-\frac{1}{2}}, \tag{D.16}$$

corresponding to an the electric field amplitude of

$$E_0\left(r = \pm\frac{w}{2}\right) = \frac{2}{w}\sqrt{\frac{P_{\mathrm{tot}}}{\pi\varepsilon_0 c}} e^{-\frac{1}{4}}. \tag{D.17}$$

Multiplying equations (D.8) and (D.13) by this value, we get the Rabi frequency for both, the Ca^+ and N_2^+ ion, for a given beam power P_{tot} and beam radius w.

Bibliography

[1] J. Bleck-Neuhaus, *Elementare Teilchen*, Springer, Berlin, 2013.

[2] A. Zee, *Einstein Gravity in a Nutshell*, Princeton University Press, Princeton, 2013.

[3] L. Bergström, *Ann. Phys.* **524**, 479 (2012).

[4] P. J. E. Peebles and B. Ratra, *Rev. Mod. Phys.* **75**, 559 (2003).

[5] A. Strominger, *Nucl. Phys. B, Proc. Suppl.* **192–193**, 119 (2009).

[6] J.-Ph. Uzan, *Rev. Mod. Phys.* **75**, 403 (2003).

[7] S. G. Karshenboim and E. Peik., *Astrophysics, Clocks and Fundamental Constants*, volume 648 of *Lecture Notes in Physics*, Springer, Berlin, 2004.

[8] J.-Ph. Uzan, *Living Rev. Relativity* **14** (2011).

[9] M. S. Safronova, *Physics* **7**, 117 (2014).

[10] E. Reinhold, R. Buning, U. Hollenstein, A. Ivanchik, P. Petitjean, and W. Ubachs, *Phys. Rev. Lett.* **96**, 151101 (2006).

[11] N. Huntemann, B. Lipphardt, C. Tamm, V. Gerginov, S. Weyers, and E. Peik, *Phys. Rev. Lett.* **113**, 210802 (2014).

[12] R. M. Godun, P. B. R. Nisbet-Jones, J. M. Jones, S. A. King, L. A. M. Johnson, H. S. Margolis, K. Szymaniec, S. N. Lea, K. Bongs, and P. Gill, *Phys. Rev. Lett.* **113**, 210801 (2014).

[13] R. I. Thompson, *Astrophys. Lett.* **16**, 3 (1975).

[14] N. Kanekar, W. Ubachs, K. M. Menten, J. Bagdonaite, A. Brunthaler, C. Henkel, S. Muller, H. L. Bethlem, and M. Daprà, *Mon. Not. R. Astron. Soc.: Lett.* **448**, L104 (2015).

[15] J. Bagdonaite, W. Ubachs, M. T. Murphy, and J. B. Whitmore, *Phys. Rev. Lett.* **114**, 071301 (2015).

[16] M. Kajita, G. Gopakumar, M. Abe, M. Hada, and M. Keller, *Phys. Rev. A* **89**, 032509 (2014).

[17] M. Kajita, G. Gopakumar, M. Abe, and M. Hada, *J. Mol. Spectrosc.* **300**, 99 (2014).

[18] J. Biesheuvel, J.-Ph. Karr, L. Hilico, K. S. E. Eikema, W. Ubachs, and J. C. J. Koelemeij, *Nat. Commun.* **7**, 10385 (2016).

[19] P. Jansen, H. L. Bethlem, and W. Ubachs, *J. Chem. Phys.* **140**, 010901 (2014).

[20] E. J. Salumbides, J. C. J. Koelemeij, J. Komasa, K. Pachucki, K. S. E. Eikema, and W. Ubachs, *Phys. Rev. D* **87**, 112008 (2013).

[21] E. J. Salumbides, W. Ubachs, and V. I. Korobov, *J. Mol. Spectrosc.* **300**, 65 (2014).

[22] J. J. Hudson, B. E. Sauer, M. R. Tarbutt, and E. A. Hinds, *Phys. Rev. Lett.* **89**, 023003 (2002).

[23] J. J. Hudson, D. M. Kara, I. J. Sallman, B. E. Sauer, M. R. Tarbutt, and E. A. Hinds, *Nature* **473**, 493 (2011).

[24] J. Baron, W. C. Campbell, D. DeMille, J. M. Doyle, G. Gabrielse, Y. V. Gurevich, P. W. Hess, N. R. Hutzler, E. Kirilov, I. Kozyryev, B. R. O'Leary, C. D. Panda, M. F. Parsons, E. S. Petrik, B. Spaun, A. C. Vutha, and A. D. West, *Science* **343**, 269 (2014).

[25] M. Quack, J. Stohner, and M. Willeke, *Annu. Rev. Phys. Chem.* **59**, 741 (2008).

[26] C. S. Wu, E. Ambler, R. W. Hayward, D. D. Hoppes, and R. P. Hudson, *Phys. Rev.* **105**, 1413 (1957).

[27] R. L. Garwin, L. M. Lederman, and M. Weinrich, *Phys. Rev.* **105**, 1415 (1957).

[28] M. Quack, *Angew. Chem. Int. Ed.* **41**, 4618 (2002).

[29] G. Herzberg, *Molecular Spectra and Molecular Structure, Volume I, Spectra of Diatomic Molecules*, Krieger, Malabar, Florida, reprinted 2nd edition, 1989.

[30] P. W. Atkins and R. Friedman, *Molecular Quantum Mechanics*, Oxford University Press, Oxford, 4th edition, 2008.

[31] G. Herzberg, *Nature* **163**, 170 (1949).

[32] J. Reid, R. L. Sinclair, A. M. Robinson, and A. R. W. McKellar, *Phys. Rev. A* **24**, 1944 (1981).

[33] D. Reuter, D. E. Jennings, and J. W. Brault, *J. Mol. Spectrosc.* **115**, 294 (1986).

[34] A. Campargue, S. Kassi, K. Pachucki, and J. Komasa, *Phys. Chem. Chem. Phys.* **14**, 802 (2012).

[35] S.-M. Hu, H. Pan, C.-F. Cheng, Y. R. Sun, X.-F. Li, J. Wang, A. Campargue, and A.-W. Liu, *Astrophys. J.* **749**, 76 (2012).

[36] S. Kassi, A. Campargue, K. Pachucki, and J. Komasa, *J. Chem. Phys.* **136**, 184309 (2012).

[37] S. Kassi and A. Campargue, *J. Mol. Spectrosc.* **300**, 55 (2014).

[38] Y. Tan, J. Wang, C. F. Cheng, X. Q. Zhao, A. W. Liu, and S. M. Hu, *J. Mol. Spectrosc.* **300**, 60 (2014).

[39] P. O. Schmidt, T. Rosenband, C. Langer, W. M. Itano, J. C. Bergquist, and D. J. Wineland, *Science* **309**, 749 (2005).

[40] P. O. Schmidt, T. Rosenband, J. C. J. Koelemeij, D. B. Hume, W. M. Itano, J. C. Bergquist, and D. J. Wineland, Spectroscopy of atomic and molecular ions using quantum logic, in *AIP Conference Proceedings*, volume CP862, p. 305, 2006.

[41] D. B. Hume, C. W. Chou, D. R. Leibrandt, M. J. Thorpe, D. J. Wineland, and T. Rosenband, *Phys. Rev. Lett.* **107**, 243902 (2011).

[42] J. Mur-Petit, J. J. García-Ripoll, J. Pérez-Ríos, J. Campos-Martínez, M. I. Hernández, and S. Willitsch, *Phys. Rev. A* **85**, 022308 (2012).

[43] M. Shi, P. F. Herskind, M. Drewsen, and I. L. Chuang, *New J. Phys.* **15**, 113019 (2013).

[44] F. Wolf, Y. Wan, J. C. Heip, F. Gebert, C. Shi, and P. O. Schmidt, *Nature* **530**, 457 (2016).

[45] P. J. Bruna and F. Grein, *J. Mol. Spectrosc.* **227**, 67 (2004).

[46] J.-Ph. Karr, *J. Mol. Spectrosc.* **300**, 37 (2014).

[47] S. Schiller, D. Bakalov, and V. I. Korobov, *Phys. Rev. Lett.* **113**, 023004 (2014).

[48] M. Kajita, *Phys. Rev. A* **92**, 043423 (2015).

[49] E. U. Condon and G. H. Shortley, *The Theory of Atomic Spectra*, Cambridge University Press, Cambridge, repr. edition, 1979.

[50] M. Mizushima, *Quantum Mechanics of Atomic Spectra and Atomic Structure*, W. A. Benjamin, New York, 1970.

[51] B. W. Shore and D. H. Menzel, *Principles of atomic spectra*, John Wiley & Sons, New York, 1968.

[52] D. Papoušek, *Collect. Czech. Chem. Commun.* **54**, 2555 (1989).

[53] Y.-N. Chiu, *J. Chem. Phys.* **42**, 2671 (1965).

[54] H. M. James and A. S. Coolidge, *Astrophys. J.* **87**, 438 (1938).

[55] D. J. Griffiths, *Quantenmechanik*, Pearson, München, 2nd edition, 2012.

[56] D. A. Park, *Introduction to the Quantum Theory*, McGraw-Hill, New York, 3rd edition, 1992.

[57] B. H. Bransden and C. J. Joachain, *Physics of Atoms and Molecules*, Prentice Hall, Harlow, 2nd edition, 2003.

[58] B. E. A. Saleh and M. C. Teich, *Fundamentals of Photonics*, John Wiley & Sons, New York, 2007.

[59] J. D. Macomber, *The Dynamics of Spectroscopic Transitions*, John Wiley & Sons, New York, 1976.

[60] J. M. Brown and A. Carrington, *Rotational Spectroscopy of Diatomic Molecules*, Cambridge University Press, Cambridge, 2003.

[61] R. N. Zare, *Angular Momentum*, John Wiley & Sons, New York, 1988.

[62] A. R. Edmonds, *Drehimpulse in der Quantenmechanik*, Bibliographisches Institut, Mannheim, 1964.

[63] R. A. Horn and C. R. Johnson, *Matrix Analysis*, Cambridge University Press, Cambridge, 2nd edition, 2013.

[64] A. Einstein, *Mitteilungen der Physikalischen Gesellschaft Zürich* **18**, 47 (1916).

[65] R. C. Hilborn, *arXiv*, physics/0202029 (2002).

[66] J. B. Tatum, *Astrophys. J.* **14**, 21 (1967).

[67] P. R. Bunker and P. Jensen, *Molecular Symmetry and Spectroscopy*, NRC Research Press, Ottawa, 2nd edition, 2006.

[68] P. R. Bunker, *Molecular Symmetry and Spectroscopy*, Academic Press, Inc., London, 1979.

[69] M. Mizushima, *The Theory of Rotating Diatomic Molecules*, John Wiley & Sons, New York, 1975.

[70] I. N. Levine, *Molecular Spectroscopy*, A Wiley-Interscience publication, John Wiley & Sons, New York, 1975.

[71] M. Born and R. Oppenheimer, *Ann. Phys.* **84**, 457 (1927).

[72] C. Cohen-Tannoudji, B. Diu, and F. Laloë, *Quantenmechanik*, volume 1, de Gruyter, Berlin, 4th edition, 2009.

[73] A. Postnikov, Lectures on the Density Functional Theory, www.home.uni-osnabrueck.de/apostnik/Lectures/DFT-1.pdf, 2009.

[74] E. K. U. Gross, E. Runge, and O. Heinonen, *Many-Particle Theory*, Adam Hilger, Bristol, 1991.

[75] J. Kobus, D. Moncrieff, and S. Wilson, *Phys. Rev. A* **62**, 062503 (2000).

[76] D. M. Brink and G. R. Satchler, *Angular Momentum*, Clarendon Press, Oxford, 3rd edition, 1993.

[77] D. A. Varshalovich, A. N. Moskalev, and V. K. Khersonskii, *Quantum Theory of Angular Momentum*, World Scientific, Singapore, 1989.

[78] W. B. Person and G. Zerbi, *Vibrational intensities in infrared and Raman spectroscopy*, volume 20 of *Studies in physical and theoretical chemistry*, Elsevier, Amsterdam, 1982.

[79] P. F. Bernath, *Spectra of Atoms and Molecules*, Oxford University Press, New York, 2nd edition, 2005.

[80] D. B. Lawson and J. F. Harrison, *J. Phys. Chem. A* **101**, 4781 (1997).

[81] D. C. Cartwright and T. H. Dunning, *J. Phys. B* **7**, 1776 (1974).

[82] G. Karl and J. D. Poll, *J. Chem. Phys.* **46**, 2944 (1967).

[83] C. Camy-Peyret, J.-M. Flaud, L. Delbouille, G. Roland, J. W. Brault, and L. Testerman, *J. Phys., Lett.* **42**, L279 (1981).

[84] A. Goldman, R. H. Tipping, Q. Ma, C. D. Boone, P. F. Bernath, P. Demoulin, F. Hase, M. Schneider, J. W. Hannigan, M. T. Coffey, and C. P. Rinsland, *J. Quant. Spectrosc. Radiat. Transfer* **103**, 168 (2007).

[85] M. Germann and S. Willitsch, *Mol. Phys.* **114**, 769 (2016).

[86] M. Fassbender, *Z. Phys.* **30**, 73 (1924).

[87] D. Coster and H. H. Brons, *Z. Phys.* **70**, 492 (1931).

[88] W. H. J. Childs, *Proc. R. Soc. London, Ser. A* **137**, 641 (1932).

[89] L. Klynning and P. Pages, *Phys. Scr.* **25**, 543 (1982).

[90] K. Harada, T. Wada, and T. Tanaka, *J. Mol. Spectrosc.* **163**, 436 (1994).

[91] S. D. Rosner, T. D. Gaily, and R. A. Holt, *Phys. Rev. A* **26**, 697 (1982).

[92] F. Michaud, F. Roux, S. P. Davis, and A.-D. Nguyen, *Appl. Opt.* **35**, 2867 (1996).

[93] F. Michaud, F. Roux, S. P. Davis, A.-D. Nguyen, and C. O. Laux, *J. Mol. Spectrosc.* **203**, 1 (2000).

[94] A. Lofthus and P. H. Krupenie, *J. Phys. Chem. Ref. Data* **6**, 113 (1977).

[95] F. R. Gilmore, R. R. Laher, and P. J. Espy, *J. Phys. Chem. Ref. Data* **21**, 1005 (1992).

[96] N. Berrah Mansour, C. Kurtz, T. C. Steimle, G. L. Goodman, L. Young, T. J. Scholl, S. D. Rosner, and R. A. Holt, *Phys. Rev. A* **44**, 4418 (1991).

[97] T. A. Miller, T. Suzuki, and E. Hirota, *J. Chem. Phys.* **80**, 4671 (1984).

[98] D. W. Ferguson, K. N. Rao, P. A. Martin, and G. Guelachvili, *J. Mol. Spectrosc.* **153**, 599 (1992).

[99] K. A. Dick, W. Benesch, H. M. Crosswhite, S. G. Tilford, R. A. Gottscho, and R. W. Field, *J. Mol. Spectrosc.* **69**, 95 (1978).

[100] R. A. Gottscho, R. W. Field, K. A. Dick, and W. Benesch, *J. Mol. Spectrosc.* **74**, 435 (1979).

[101] S. D. Rosner, T. D. Gaily, and R. A. Holt, *J. Mol. Spectrosc.* **109**, 73 (1985).

[102] T. J. Scholl, R. A. Holt, and S. D. Rosner, *J. Mol. Spectrosc.* **192**, 424 (1998).

[103] M. J. J. Vrakking, A. S. Bracker, and Y. T. Lee, *J. Chem. Phys.* **96**, 7195 (1992).

[104] K. R. Lykke and B. D. Kay, *J. Chem. Phys.* **95**, 2252 (1991).

[105] T. F. Hanisco and A. C. Kummel, *J. Phys. Chem.* **95**, 8565 (1991).

[106] S. R. Mackenzie, F. Merkt, E. J. Halse, and T. P. Softley, *Mol. Phys.* **86**, 1283 (1995).

[107] R. Seiler, U. Hollenstein, G. M. Greetham, and F. Merkt, *Chem. Phys. Lett.* **346**, 201 (2001).

[108] X. Tong, A. H. Winney, and S. Willitsch, *Phys. Rev. Lett.* **105**, 143001 (2010).

[109] X. Tong, D. Wild, and S. Willitsch, *Phys. Rev. A* **83**, 023415 (2011).

[110] S. Schlemmer, T. Kuhn, E. Lescop, and D. Gerlich, *Int. J. Mass Spectrom.* **185**, 589 (1999).

[111] R. A. Frosch and H. M. Foley, *Phys. Rev.* **88**, 1337 (1952).

[112] T. M. Dunn, Nuclear Hyperfine Structure in the Electronic Spectra of Diatomic Molecules, in *Molecular Spectroscopy: Modern Research*, edited by K. Narahari Rao and C. Weldon Mathews, Academic Press, New York, 1972.

[113] D. R. Farley and R. J. Cattolica, *J. Quant. Spectrosc. Radiat. Transfer* **56**, 753 (1996).

[114] M. Germann, X. Tong, and S. Willitsch, *Nat. Phys.* **10**, 820 (2014).

[115] M. Germann, X. Tong, and S. Willitsch, *Chimia* **69**, 213 (2015).

[116] J. Faist, *Quantum Cascade Lasers*, Oxford University Press, Oxford, 2013.

[117] S. Earnshaw, *Trans. Cambridge Philos. Soc.* **7**, 97 (1842).

[118] W. Paul, *Rev. Mod. Phys.* **62**, 531 (1990).

[119] P. K. Ghosh, *Ion Traps*, Clarendon Press, Oxford, 1995.

[120] F. G. Major, V. N. Gheorghe, and G. Werth, *Charged Particle Traps*, Springer, Berlin, 2005.

[121] R. E. March and J. F. J. Todd, *Quadrupole Ion Trap Mass Spectrometry*, John Wiley & Sons, Hoboken, 2nd edition, 2005.

[122] D. Gerlich, Inhomogeneous RF Fields: A Versatile Tool for the Study of Processes with Slow Ions, in *State-Selected and State-to-State Ion-Molecule Reaction Dynamics, Part 1: Experiment*, edited by C.-Y. Ng and M. Baer, volume 82 of *Advances in Chemical Physics*, John Wiley & Sons, New York, 1992.

[123] D. J. Berkeland, J. D. Miller, J. C. Bergquist, W. M. Itano, and D. J. Wineland, *J. Appl. Phys.* **83**, 5025 (1998).

[124] M. Drewsen and A. Brøner, *Phys. Rev. A* **62**, 045401 (2000).

[125] D. Leibfried, R. Blatt, C. Monroe, and D. Wineland, *Rev. Mod. Phys.* **75**, 281 (2003).

[126] S. Willitsch, M. T. Bell, A. D. Gingell, and T. P. Softley, *Phys. Chem. Chem. Phys.* **10**, 7200 (2008).

[127] H. J. Metcalf and P. van der Straten, *Laser Cooling and Trapping*, Springer, New York, 1999.

[128] C. J. Foot, *Atomic Physics*, Oxford University Press, Oxford, 2005.

[129] E. S. Shuman, J. F. Barry, D. R. Glenn, and D. DeMille, *Phys. Rev. Lett.* **103**, 223001 (2009).

[130] E. S. Shuman, J. F. Barry, and D. DeMille, *Nature* **467**, 820 (2010).

[131] J. Xie and R. N. Zare, *J. Chem. Phys.* **93**, 3033 (1990).

[132] J. Xie and R. N. Zare, *J. Chem. Phys.* **97**, 2891 (1992).

[133] X. Tong, T. Nagy, J. Yosa Reyes, M. Germann, M. Meuwly, and S. Willitsch, *Chem. Phys. Lett.* **547**, 1 (2012).

[134] Daylight Solutions, Inc., San Diego, CA, USA, *Tunable Mid-IR External Cavity Laser System, User Manual*, 2010.

[135] L. S. Rothman, D. Jacquemart, A. Barbe, D. Chris Benner, M. Birk, L. R. Brown, M. R. Carleer, C. Chackerian Jr., K. Chance, L. H. Coudert, V. Dana, V. M. Devi, J.-M. Flaud, R. R. Gamache, A. Goldman, J.-M. Hartmann, K. W. Jucks, A. G. Maki, J.-Y. Mandin, S. T. Massie, J. Orphal, A. Perrin, C. P. Rinsland, M. A. H. Smith, J. Tennyson, R. N. Tolchenov, R. A. Toth, J. Vander Auwera, P. Varanasi, and G. Wagner, *J. Quant. Spectrosc. Radiat. Transfer* **96**, 139 (2005).

[136] C. B. Zhang, D. Offenberg, B. Roth, M. A. Wilson, and S. Schiller, *Phys. Rev. A* **76**, 012719 (2007).

[137] T. Matthey, T. Cickovski, S. Hampton, A. Ko, Q. Ma, M. Nyerges, T. Raeder, T. Slabach, and J. A. Izaguirre, *ACM Trans. Math. Softw.* **30**, 237 (2004).

[138] S. Kato, M. J. Frost, V. M. Bierbaum, and S. R. Leone, *Can. J. Chem.* **72**, 625 (1994).

[139] M. Meuwly, private communication, 2016.

[140] G. Villares, A. Hugi, S. Blaser, and J. Faist, *Nat. Commun.* **5**, 5192 (2014).

[141] M. G. Hansen, E. Magoulakis, Q.-F. Chen, I. Ernsting, and S. Schiller, *Opt. Lett.* **40**, 2289 (2015).

[142] B. Argence, B. Chanteau, O. Lopez, D. Nicolodi, M. Abgrall, C. Chardonnet, C. Daussy, B. Darquié, Y. Le Coq, and A. Amy-Klein, *Nat. Photonics* **9**, 456 (2015).

[143] S. Willitsch and F. Merkt, *Int. J. Mass Spectrom.* **245**, 14 (2005).

[144] W. Demtröder, *Molecular Physics*, Wiley-VCH, Weinheim, 2005.

[145] D. W. Turner, C. Baker, A. D. Baker, and C. R. Brundle, *Molecular Photoelectron Spectroscopy*, Wiley-Interscience, London, 1970.

[146] F. Merkt, S. Willitsch, and U. Hollenstein, High-resolution Photoelectron Spectroscopy, in *Handbook of High-resolution Spectroscopy*, edited by M. Quack and F. Merkt, volume 3, p. 1617, John Wiley & Sons, Hoboken, 2011.

[147] A. M. Ellis, M. Feher, and T. G. Wright, *Electronic and Photoelectron Spectroscopy*, Cambridge University Press, Cambridge, 2005.

[148] A. D. Buckingham, B. J. Orr, and J. M. Sichel, *Philos. Trans. R. Soc., A* **268**, 147 (1970).

[149] S. N. Dixit and V. McKoy, *J. Chem. Phys.* **82**, 3546 (1985).

[150] S. W. Allendorf, D. J. Leahy, D. C. Jacobs, and R. N. Zare, *J. Chem. Phys.* **91**, 2216 (1989).

[151] K. Wang and V. McKoy, *J. Chem. Phys.* **95**, 4977 (1991).

[152] H. Palm and F. Merkt, *Phys. Rev. Lett.* **81**, 1385 (1998).

[153] F. Merkt, R. Signorell, H. Palm, A. Osterwalder, and M. Sommavilla, *Mol. Phys.* **95**, 1045 (1998).

[154] H. J. Wörner, U. Hollenstein, and F. Merkt, *Phys. Rev. A* **68**, 032510 (2003).

[155] A. Osterwalder, A. Wüest, F. Merkt, and Ch. Jungen, *J. Chem. Phys.* **121**, 11810 (2004).

[156] H. A. Cruse, Ch. Jungen, and F. Merkt, *Phys. Rev. A* **77**, 042502 (2008).

[157] D. Sprecher, Ch. Jungen, and F. Merkt, *J. Chem. Phys.* **140**, 104303 (2014).

[158] Ch. Jungen, Elements of Quantum Defect Theory, in *Handbook of High-resolution Spectroscopy*, edited by M. Quack and F. Merkt, volume 1, p. 471, John Wiley & Sons, Hoboken, 2011.

[159] S. N. Dixit, D. L. Lynch, V. McKoy, and W. M. Huo, *Phys. Rev. A* **32**, 1267 (1985).

[160] F. Merkt and T. P. Softley, *Int. Rev. Phys. Chem.* **12**, 205 (1993).

[161] C.-W. Hsu, M. Evans, S. Stimson, C. Y. Ng, and P. Heimann, *Chem. Phys.* **231**, 121 (1998).

[162] R. Signorell and F. Merkt, *Mol. Phys.* **92**, 793 (1997).

[163] R. S. Freund, T. A. Miller, D. De Santis, and A. Lurio, *J. Chem. Phys.* **53**, 2290 (1970).

[164] D. De Santis, A. Lurio, T. A. Miller, and R. S. Freund, *J. Chem. Phys.* **58**, 4625 (1973).

[165] A. C. Legon and P. W. Fowler, *Z. Naturforsch.* **47a**, 367 (1992).

[166] P. Baltzer, L. Karlsson, and B. Wannberg, *Phys. Rev. A* **46**, 315 (1992).

[167] G. Öhrwall, P. Baltzer, and J. Bozek, *Phys. Rev. A* **59**, 1903 (1999).

[168] R. G. Bray and R. M. Hochstrasser, *Mol. Phys.* **31**, 1199 (1976).

[169] C. Maïnos, *Phys. Rev. A* **33**, 3983 (1986).

[170] H. Lefebvre-Brion and R. W. Field, *The Spectra and Dynamics of Diatomic Molecules*, Elsevier, Amsterdam, 2004.

[171] M. Hippler, *Mol. Phys.* **97**, 105 (1999).

[172] M. Göppert, *Naturwissenschaften* **17**, 932 (1929).

[173] M. Göppert-Mayer, *Ann. Phys.* **401**, 273 (1931).

[174] K. L. Reid, D. J. Leahy, and R. N. Zare, *J. Chem. Phys.* **95**, 1746 (1991).

[175] U. Hollenstein, H. Palm, and F. Merkt, *Rev. Sci. Instrum.* **71**, 4023 (2000).

[176] S. Hannemann, E.-J. van Duijn, and W. Ubachs, *Rev. Sci. Instrum.* **78**, 103102 (2007).

[177] A. W. Kam and F. M. Pipkin, *Phys. Rev. A* **43**, 3279 (1991).

[178] E. J. Salumbides, A. Khramov, and W. Ubachs, *J. Phys. Chem. A* **113**, 2383 (2009).

[179] S. N. Dixit and P. Lambropoulos, *Phys. Rev. A* **27**, 861 (1983).

[180] B. Roth, J. C. J. Koelemeij, H. Daerr, and S. Schiller, *Phys. Rev. A* **74**, 040501 (2006).

[181] J. C. J. Koelemeij, B. Roth, A. Wicht, I. Ernsting, and S. Schiller, *Phys. Rev. Lett.* **98**, 173002 (2007).

[182] K. Højbjerre, A. K. Hansen, P. S. Skyt, P. F. Staanum, and M. Drewsen, *New J. Phys.* **11**, 055026 (2009).

[183] T. Rosenband, D. B. Hume, P. O. Schmidt, C. W. Chou, A. Brusch, L. Lorini, W. H. Oskay, R. E. Drullinger, T. M. Fortier, J. E. Stalnaker, S. A. Diddams, W. C. Swann, N. R. Newbury, W. M. Itano, D. J. Wineland, and J. C. Bergquist, *Science* **319**, 1808 (2008).

[184] C. W. Chou, D. B. Hume, J. C. J. Koelemeij, D. J. Wineland, and T. Rosenband, *Phys. Rev. Lett.* **104**, 070802 (2010).

[185] C. W. Chou, D. B. Hume, T. Rosenband, and D. J. Wineland, *Science* **329**, 1630 (2010).

[186] D. J. Wineland, *Rev. Mod. Phys.* **85**, 1103 (2013).

[187] S. Schiller and V. Korobov, *Phys. Rev. A* **71**, 032505 (2005).

[188] I. S. Vogelius, L. B. Madsen, and M. Drewsen, *J. Phys. B* **39**, S1259 (2006).

[189] J. C. J. Koelemeij, B. Roth, and S. Schiller, *Phys. Rev. A* **76**, 023413 (2007).

[190] S. Ding and D. N. Matsukevich, *New J. Phys.* **14**, 023028 (2012).

[191] J. I. Cirac and P. Zoller, *Nature* **404**, 579 (2000).

[192] D. Leibfried, B. DeMarco, V. Meyer, D. Lucas, M. Barrett, J. Britton, W. M. Itano, B. Jelenković, C. Langer, T. Rosenband, and D. J. Wineland, *Nature* **422**, 412 (2003).

[193] M. Šašura and A. M. Steane, *Phys. Rev. A* **67**, 062318 (2003).

[194] J. J. García-Ripoll, P. Zoller, and J. I. Cirac, *Phys. Rev. A* **71**, 062309 (2005).

[195] C. Donald, *Development of an Ion Trap Quantum Information Processor*, PhD thesis, University of Oxford (Hertford College), 2000.

[196] N. David Mermin, *Quantum Computer Science*, Cambridge University Press, Cambridge, 2007.

[197] R. J. Glauber, *Phys. Rev.* **131**, 2766 (1963).

[198] K. Königsberger, *Analysis 1*, Springer, Berlin, 6th edition, 2004.

[199] P. Carruthers and M. M. Nieto, *Am. J. Phys.* **33**, 537 (1965).

[200] D. F. V. James, *Appl. Phys. B* **66**, 181 (1998).

[201] D. Kielpinski, B. E. King, C. J. Myatt, C. A. Sackett, Q. A. Turchette, W. M. Itano, C. Monroe, D. J. Wineland, and W. H. Zurek, *Phys. Rev. A* **61**, 032310 (2000).

[202] G. Morigi and H. Walther, *Eur. Phys. J. D* **13**, 261 (2001).

[203] D. Leibfried, *New J. Phys.* **14**, 023029 (2012).

[204] M. Fox, *Quantum Optics*, Oxford University Press, Oxford, 2006.

[205] D. Leibfried, D. M. Meekhof, B. E. King, C. Monroe, W. M. Itano, and D. J. Wineland, *Phys. Rev. Lett.* **77**, 4281 (1996).

[206] G. H. Low, P. F. Herskind, and I. L. Chuang, *Phys. Rev. A* **84**, 053425 (2011).

[207] J. D. Jackson, *Classical Electrodynamics*, John Wiley & Sons, New York, 3rd edition, 1999.

[208] B. E. King, *arXiv*, 0804.4528 (2008).

Acknowledgements

As usual for a project of that scope, this thesis was only possible with the help, advice and support from a number of persons.

First, I would like to thank Professor Stefan Willitsch for giving me the opportunity to perform the research for this thesis in his research group at the University of Basel, for his advice and supervision, particularly for carefully revising also the lengthiest of my calculations. Then, I would like to thank Professor Frédéric Merkt from ETH Zürich for assessing this thesis as a co-examiner. Moreover, I would like to thank Professor Stefan Antusch from the University of Basel for reviewing my introduction from the point of view of elementary particle physics and cosmology.

Regarding the experimental work, my biggest thank goes to Dr. Xin Tong, who introduced me to the experimental techniques used for measuring the electric-quadrupole rotation-vibration spectrum of N_2^+ and with whom I have recorded this spectrum. Furthermore, I would like to thank Philipp Knöpfel, Grischa Martin and Dieter Wild from the mechanical workshop at our department for their assistance, especially for constructing the instruments and the experimental setup, without which these experiments never had been possible. Moreover, I would like to thank Georg Holderied for assistance with laboratory electronics and Dr. Anatoly Johnson for help with electronics and lasers.

Concerning the theoretical work about non-destructive state detection and quantum logic spectroscopy, I would like to thank Dr. Juan José García-Ripoll and Dr. Jordi Mur-Petit from CSIC Madrid. Thank you for your hospitality during my visit at CSIC and for taking your time to introduce me to these concepts. In this context, I would also like to thank Dr. Roman Schmied from the University of Basel for his advice and for helpful discussions.

Furthermore, I would like to thank all my colleagues from our research group, who have all assisted and supported me—be it with valuable hints or with a helping hand in the lab, with inspiring and helpful discussions or just by contributing to a nice working atmosphere with an encouraging word, a good joke, etc. Thanks a lot to all of you! Particularly, I would like to thank Ian Rouse for his advice in numerous questions about correct English wording and Kaveh Najafian for carefully revising my introduction and conclusions chapter.

I would like to acknowledge financial support from the University of Basel, from the Swiss National Science Foundation (Schweizerischer Nationalfonds zur Förderung der wissenschaftlichen Forschung) that supported this thesis as part of the National Centre of Competence in Research NCCR-QSIT – Quantum Science & Technology (Nationaler Forschungsschwerpunkt QSIT – Quantenwissenschaften und -technologie), as well as from the European COST network that funded my visit at CSIC Madrid as a Short-Term Scientific Mission (STSM) within the COST scientific program on Ion Traps for Tomorrow's Applications.

An essential prerequisite for successful work—and life in general—is always for me the personal and emotional support from the people around me. Therefore, I would like to say thank you to everyone who supported me during the time of working at this thesis, especially my family and my friends.

Finally, a remark about the aids used for this thesis: as usual for a scientific thesis, a number of sources and aids have been used in the process of performing experiments for, compiling the material of and writing this thesis: scientific articles, textbooks, reference works, websites, discussions with coworkers and colleagues from other research groups, software packages, laboratory appliances, tools, etc., etc. Although greatest care has been taken to list all relevant sources and aids appropriately, it is neither common, nor possible to list all of them explicitly.

Understanding the causes behind things always makes me feel lucky—many thanks to all of you for having made that possible for me!